Cranfield University

C. S. KANG

VANED RECESS ANTI-STALL FOR AXIAL FLOW FANS AND COMPRESSORS

School of Mechanical Engineering

Ph.D Thesis

Cranfield University
School of Mechanical Engineering

Ph.D THESIS

1995/1996

C. S. KANG

VANED RECESS ANTI-STALL FOR AXIAL-FLOW FANS AND COMPRESSORS

Supervisors: Dr. A. B. McKenzie
Prof. R. L. Elder

February 1996

This thesis is submitted for the degree of PhD

Dedicated to My Beloved

Motherland

People's Republic of China

ABSTRACT

The study of anti-stall techniques for fans and compressors has never been more significant, since the potential applications were recognised in gas turbines, tunnel ventilation (jet fans) and industrial process where fans/compressors would benefit from the devices. This thesis will discuss the techniques achieving competitiveness by modifying the conventional casing design of the fan and compressor, which is referred to as casing treatments, taking into account the change of maximum efficiency and flow range.

An experimental investigation to examine the influence of the vaned recess casing treatment on stall margin, operating efficiency and flow field of a low speed axial flow fan with aerospace type blade loading is presented. Different geometrical designs of the vaned passages were examined and more than 65% of stall margin improvements and over twice pressure rise with insignificant peak efficiency change were obtained.

Experiments to examine the effect of casing treatments on the flow field were carried out using the same fan rig with a tip clearance of 1.2% of the blade height. A high frequency data acquisition system including both hardware and software was developed and the 3-D flow measurements with a slanted hot-wire were undertaken. The first detailed results of flow measurements associated with the vaned recess casing treatment are presented, including both time-averaged and ensemble-averaged measurement results. The flow features in both the solid casing and treated casing builds are captured and comparison between the builds presented. The results revealed that the stall margin improvement due to the casing treatment was not achieved by reducing the incidence nor by increasing the total pressure in the tip region. It appeared that the combined functions of elimination of the whirling flow, the removal of the randomness of the inlet flow and modification of the tip clearance flow are salient features associated with the mechanism of the treatment.

The steady flow field of the test fan with various tip clearances has also been simulated in the rotating frame with computational fluid dynamics (CFD) to investigate the clearance effect on the end-wall flow development and to elucidate the behaviour of the tip leakage flow, and hopefully shed more light onto the flow phenomena involved.

ACKNOWLEDGEMENTS

I would like to express my sincere gratitude to my supervisors Dr. A. B. McKenzie and Prof. R. L. Elder for their expert supervision, advice, encouragement and caring attitude throughout this doctoral study. It is really a pleasure to work with them.

Big thanks are due to Dr. A. Tourlidakis for providing his TURBO-3D CFD code and for his guidance on the numerical work.

The author feels indebted to all my friends and colleagues who have offered all kinds of help and encouragement. In particular, thanks must go to Mr. Ian Bennett and Mr. Stephen Hill for an impartial proof reading. Thanks must also go to the technicians in the Test Houses, in particular Mr. Bernard Charnley, ... for their help in the experimental phase of this study.

The author also wishes to thank the Committee of Vice Chancellor's and Principals of the United Kingdom (CVCP) for granting ORS award, and the Department of Turbomachinery and Engineering Mechanics, SME, Cranfield University for the grant awarded.

Last but not least, I would like to thank all my family particularly my parents and my wife for all their support and the sacrifices they had to make.

Chang Shou KANG

February 1996

Cranfield University

CONTENTS

LIST OF FIGURES

NOMENCLATURE

C_a rotor axial chord (mm)

Ce rotor axial chord exposure (mm)

C_p specific heat of air at constant pressure)J/kg. K)

M mass flow rate (kg/s)

N rotor speed (rpm)

P_S static pressure

U blade speed (m/s)

U_m mid span blade speed (m/s)

V_0, V_3 absolute inlet and outlet velocity (m/s)

V_1, V_2 relative inlet and outlet velocity (m/s)

V_a axial velocity (m/s)

V_t circumferential velocity (m/s)

V_r radial velocity (m/s)

ϕ flow coefficient, $\phi=V_a/U_m$

$\Delta\phi$ stall margin improvement (%), $\Delta\phi=1-\phi_{ts}/\phi_{ss}$

ΔH stage enthalpy rise

τ measured torque (Nm)

η total to total efficiency (%)

η_{sm} peak efficiency for solid casing (%)

η_{tm} peak efficiency for treated casing (%)

$\Delta\eta_m$ peak efficiency loss (%)

ρ air density (kg/m^3)

ψ total to static pressure rise coefficient

$\psi=(P_{s2} - P_{t1})/(0.5\rho U_m^2)$

ϕ_{ss} flow coefficient at stall point for solid casing

ϕ_{ts} flow coefficient at stall point for treated casing

ψ_{sm} peak pressure rise coefficient for solid casing

ψ_{tm} peak pressure rise coefficient for treated casing

$\Delta\psi$ pressure rise improvement (%), $\Delta\psi=\psi_{tm}/\psi_{sm}-1$

CHAPTER 1 INTRODUCTION

1.1 GENERAL INTRODUCTION

The fan/compressor market becomes more and more competitive internationally and sensitive to high performance (particularly high operational efficiency and broad operating range) and low manufacturing cost. However, an operational constraint on flow range which often limits the pressure-rise capability of the compressor is the occurrence of rotating stall and/or surge.

It is well known that rotating stall is a disturbance of the rotor region of the compressor, which may trigger surge to occur. Because of the large scale pressure fluctuations involved, the phenomena may cause a large fall in pressure rise with aerodynamic instability, blade vibration, noise and even mechanical failure as a result of the periodic loading and unloading of blades. The occurrence of surge therefore causes plant shutdown leading to a loss in production and possibly costly damage when used in a process environment. Safety is the key word for road and rail tunnel ventilation and the fans used in ventilation systems must be economical in routine operation and effective in non-routine operation (like fire and other emergency conditions). Jet fans located in restricted rail tunnels can experience considerable pressure pulses due to the passage of trains. The breakdowns may be caused by the influence of abrupt changes in cross-sectional area of a railway tunnel on the propagation of pressure waves caused by passing trains. This necessitates that the fan can be operated in such arduous conditions free from the risk of stalling. In a gas turbine engine, rotating stall will seriously restrict the flow into the combustion chamber resulting in overheating and deceleration of the engine. Restarting of the stalled engine is then often not possible until the stall cell has been cleared and normal flow conditions restored. This usually requires an

almost complete shutdown of the engine.

Considerable effort has been expended in the past to understand and control the phenomenon. A large number of conventional stall control techniques employ the basic concept of restricting the operation of the compressor to the "right" of the stall limit by a predetermined safety margin. This can prevent operation at maximum efficiency which may lie at or close to the stall line, and also limits the operating range. The alternative is to delay the stall inception allowing operation at normally stalled flow rate. There are basically two approaches to achieve this: Active Stall Control and Passive Stall Control. Active stall control achieves its purpose by introducing further dynamics into the compression process to dissipate any tendency for an instability to develop. The additional dynamics introduced into the system is usually that of bleed ports controlled by fast acting valves or variable guide vanes, which is not to be discussed further here. The passive stall control technique usually involves modifying the design of the compressor, particularly the outer casing of the compressor. This would provide an extended continuous increasing pressure characteristic which peaks at a much lower flow rate with a comparatively small efficiency penalty. Such an anti-stall device would also reduce the operational and maintenance costs, reduce or remove cumulative fatigue damage that fan blades often suffer, and increase the level of safety of operation. Although an additional production cost may be involved, it could often be recovered by the potential gains in performance and reduced need for variable anti-surge devices such as bleed valves and variable stagger stators.

The study of anti-stall techniques has never been more significant since many fan/compressor producers realised the potential applications in gas turbine engines, tunnel ventilation fans and industrial process applications, such as boiler plant where the selected fan is required to operate at several duties. The anti-stall devices developed provide a broad operating range, high reliability, tolerance to flow distortion, long life span

and low operational cost, enabling the fan and compressor industries to be more competitive in the word wide market.

1.2 BACKGROUND

The concept of stall delay techniques began in the early 1960's and the application of casing treatments to compressors and fans remains a significant topic. Since 1970, many investigators have revealed that the application of groove or slot type casing treatments over the tips of the rotor blades or to the rotating drum beneath the stator has a marked effect on stall margin improvement of aero-engine type axial compressors and fans. Among all slot type treatments the so-called 'axial skewed groove' has been demonstrated to be the most successful. It has been examined by many investigators, most notably **Smith** and **Cumpsty** (1984), **Takata** and **Tsukuda** (1977) and **Fujita** and **Takata** (1974). The technique can lead to a limited but valuable stall margin improvement (around 20%) and significant pressure rise, though, depending upon the individual design, some are more effective than others. Unfortunately the efficiency penalties are usually equivalent to 2-4% of stage efficiency, which is the main reason for their limited use in practice.

An alternative, more successful kind of casing treatment called *vaned recess casing treatment* has recently shown a remarkable effect on the stall margin and pressure rise of industrial fans. The concept goes back to the patent work of **Ivanov** et al. (1984) and further research conducted by **Miyake** et al. (1987). More recently **Bard** (1984, 1993) reported a stabilising device integrated into the casing of axial fans which completely eliminated the stalling cycle without affecting the peak efficiency. Generally, the higher blade loading (higher blade setting angle), the more abrupt the characteristic is, and the more difficult to achieve a continuous type characteristics. Since aero-engine type fans generally have much higher blade loading than industrial fans, different behaviour and more difficulties are expected when this treatment is applied to an aero-engine

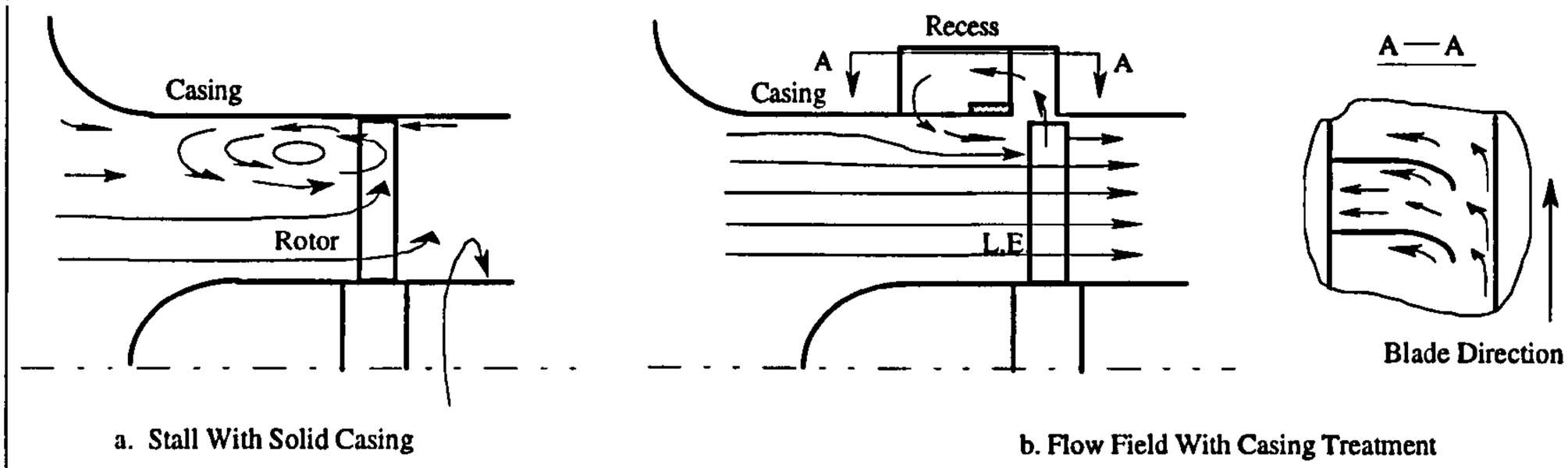

a. Stall With Solid Casing

b. Flow Field With Casing Treatment

Fig. 1 Sketch of the Operation Of the Casing Treatment

fan or compressor. The effect of the vaned recess casing treatment on a fan with a typical aero-engine loading was studied and reported by **Azimian** et al. (1989) who demonstrated very encouraging results, indicating much larger improvements of stall margin and less efficiency sacrifice than the conventional slot type treatments. **Ziabasharhagh** et al. (1992) conducted detailed experiments on high hub/tip ratio (0.7 and 0.9) and demonstrated that the device is capable of increasing stall margin on a range of machines and tolerance to inlet flow distortion.

There have been a number of papers about the mechanism of slot type casing treatments, e.g. by **Takata** et al. (1977), **Smith** et al. and **Crook** et al. (1993). Various hypotheses have been proposed but none of them explain the phenomenon observed in recessed treatment satisfactorily, since the operation of these two types of casing treatments is not identical, though there may be many common points. The working mechanism of the recess vaned treatment has not been fully understood yet but the flow process seems physically identified. **Ziabasharhagh** et al. (1992), based on the 'wool tuft' flow study, provided a hypothesis of the operation from which the following physical description of the flow may be deduced as sketched in **Fig.1-1**. As the flow rate is reduced below the normal stall point, the low momentum fluid associated with stalling flow on the rotor blades is centrifuged towards the blade tip and then recirculates axially, as shown in **Fig.1a,** and also circumferentially in the untreated fan. Without the anti-

stall device, the centrifuged flow reaching the casing must be deflected forward or rearward or both by the casing as well as being entrained by the mainstream. When the treatment is applied, this tip flow passes radially into the treatment recess where the tangential flow component of the flow is removed by the stationary cambered vanes, then discharges out of the recess into the main flow as illustrated in **Fig.1b**. By this means the rotor is enabled to continue pumping to higher pressures at lower flows. This description for the physical process of the flow is however insufficient to fully understand why and how the device works.

To date, the treatment has been mainly designed on a trial-and-error basis with a particular case in mind and details obviously differ between machines. The findings in a particular machine cannot be straightforwardly transferred to others. For example, **Bard**(1993) achieved his best result by positioning the anti-stall device just upstream of the rotor (no rotor chord was exposed), while **Azimian** et al. (1989) got no improvement by this arrangement and the best result was achieved when about 2/3 of the rotor axial chord was exposed to the treatment. For this reason, the number of experiments which may be conceived is limitless. It is highly desirable to enhance an aerodynamic understanding of the operation of the treatments by further study and possibly the application of Computational Fluid Dynamics (which has shown promise in a variety of flow analysis problems) so that optimum configuration can be more readily defined. Because of the complexities, it is not surprising to find that CFD on this aspect has been neglected by casing treatment researchers. The only two references available are published by **Crook** et al. (1993) for the slotted type hub treatment and **Hall** et al. (1994) for both slotted type and vaned recess casing treatments.

In summary, much work remains to be done before the anti-stall device can be widely used in practice and adopted as a standard item by designers. There is still the challenge of finding the most effective and cheapest stall suppression method or device that is able to substantially extend the

operation range without sacrificing much in terms of efficiency. What is required is a detailed study of the treatment design and flow phenomena involved in the casing treatment in both experimental and numerical ways.

1.3 PRESENT STUDY

Taking into account all the above incentives, this present work continues the casing treatment studies for fans and low speed compressors with the following objectives:

- further studying the effectiveness of the device to obtain additional information regarding the potential gain in stall margin available from optimum treatment configurations;
- gaining a better understanding of the mechanism by studying the flow phenomena involved.
- providing some guide lines for recess vaned casing treatment design.

To achieve these objectives, both experimental investigation and numerical approaches were necessary, (although the latter has just scratched the surface of the problem). Based on knowledge gained from the previous work in the area, three configurations with different geometry were designed and tested. These varied in vane number, inner ring cross-section, vane shape (including camber and recess vane-chord overlap). Using a 508mm test fan these designs were extensively tested and the effectiveness of stall margin and pressure rise improvement were assessed. More than 65% of stall margin improvements and over twice the pressure rise with insignificant peak efficiency penalty were obtained. The study also involved the detailed flow measurements in the rotor region and inside casing treatments with a slanted hot-wire, and the salient features of the flow phenomena associated with the stall and anti-stall device are identified, providing some insight to the operation of the device. Computer simulation of the 3-D flow in the test fan (solid wall build) and analysis of the tip leakage flow with CFD method has been made. The results revealed that the stall margin improvement due to the casing treatment was not

achieved by reducing the incidence nor by increasing the total pressure in the tip region. It appeared that the elimination of the whirl flow, inward radial flow from the recess to the main stream, the removal of the randomness of the inlet flow and tip pressure equalisation are salient features associated with the mechanism. Combining these functions resulted in a substantial stall margin improvement with no significant efficiency change.

1.4 STRUCTURE OF THE THESIS

After this introduction, a literature review of the work is given in **Chapter Two**. To the author's knowledge, most of the important work and observations in this field are briefly reviewed, including almost all the work on slotted type of casing treatment and vaned recess anti-stall devices. **Chapter Three** provides a description of the test rigs, the design of the vaned recess casing treatment, instrumentation and measurement techniques in which the three dimensional flow measurement technique with a single hot-wire probe is detailed. Detailed performance test results and examination of the effectiveness of the casing treatment and some critical design points are presented and discussed in **Chapter Four**. The results of the detailed flow measurements in the rotor region and inside the casing treatment recess and discussion can be found in **Chapter Five**, in which both time-averaged and ensemble-averaged measurement results are included. **Chapter Six** provides the 3-D flow analysis of the test fan with CFD method, in which the flow at design and off design condition was predicted and the tip leakage flow effects on the fan performance was examined. In **Chapter Seven**, after a general discussion of the mechanism and applications of the anti-stall device, conclusions from the present work are drawn and proposals for possible future research are made.

CHAPTER 2 REVIEW OF PREVIOUS WORK

Stall in compressors can be associated with the initiation of several types of aerodynamic instabilities which limit the performance. Considerable efforts to predict the stall inception, delay the stall and improve the stall margin have been made since rotating stall was first discovered in 1938 (reported by **Cheshire** in 1945). The continuing trend in aero-engines toward increasing compressor pressure ratio per stage has stimulated renewed interest in compressor instabilities. As knowledge increased in this area, novel ideas emerged for suppressing stall as much as possible. This has been driven by the obvious motivation to increase the operating range of the compressor. This chapter outlines briefly the development in stall control and delay and reviews some of the previous casing treatment research which is related to the present work.

2.1 HISTORIC DEVELOPMENT IN STALL INCEPTION RESEARCH

In 1938, rotating stall was first observed when **Sir Frank Whittle**'s group was developing the first British jet engine. They constructed a low-speed research rig with an observation window to study the flow pattern at the diffuser entrance of a centrifugal compressor with wool tufts. A ten-vane diffuser system discharging to a common reservoir was brought to the surging condition by closing the throttle, and one channel would first break down (indicated by wool tufts), then the next one, the first one regaining normal flow. This reversal travelled round the system at about one-sixth of the rotational speed of the impeller in the direction of rotation (**Cheshire** 1945), and is the first recorded example of the phenomenon now known as "rotating stall".

This important observation, however, attracted little attention at that time and no further reference to it has been found.

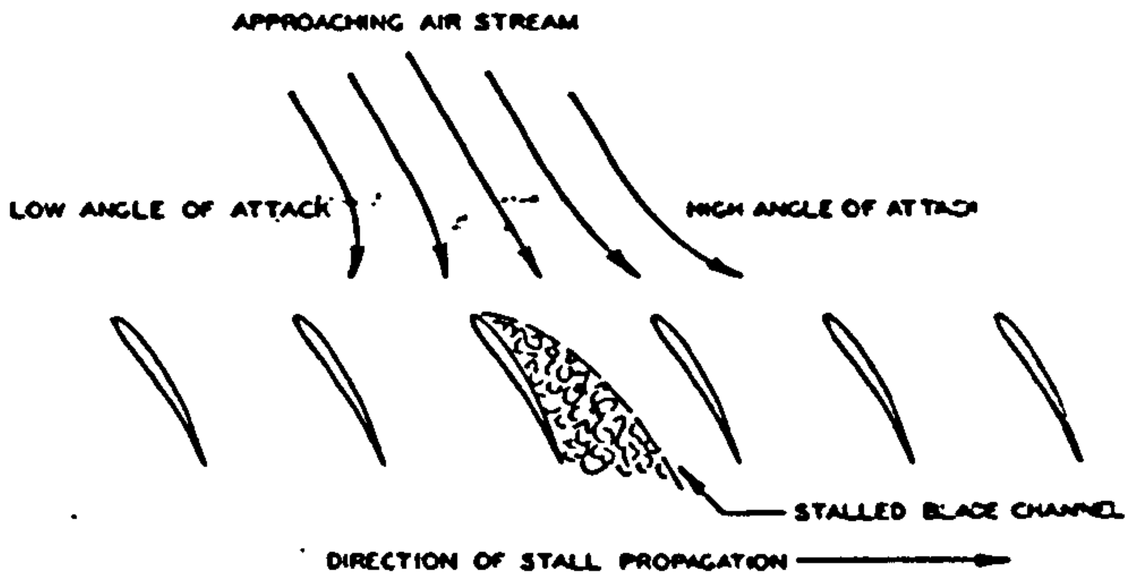

FIG. 1 STALL PROPAGATION IN A CASCADE

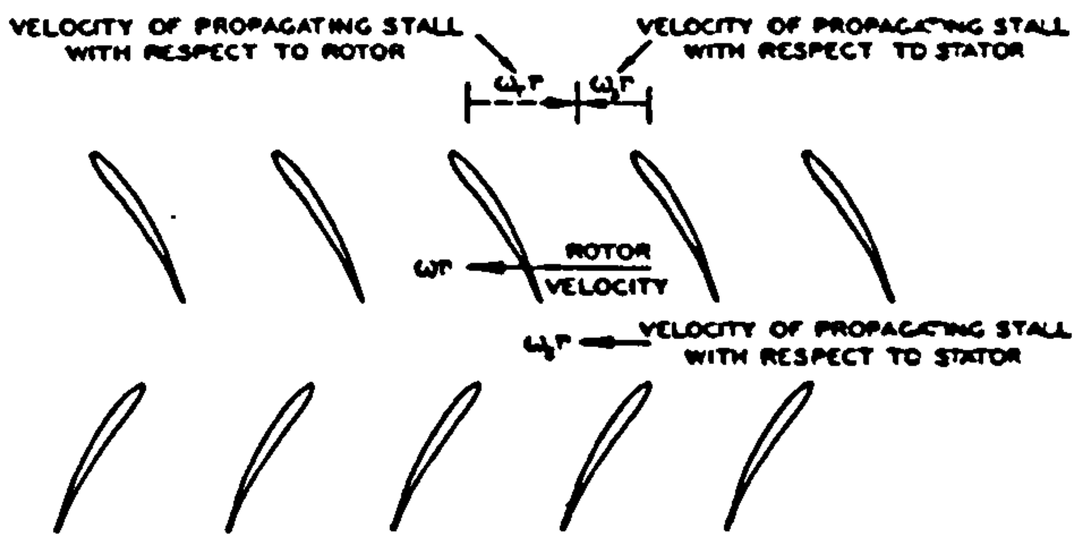

Fig.2-1 Stall Inception (Iura and Rannie, 1954)

About ten years later, at a time when rotating stall was the main cause of compressor blade failures and the major problem in the development of an axial-flow turbojet engine, rotating stall was rediscovered. **Shultze** et al. (1950) reported the occurrence of an asymmetric flow pattern detected by the means of wool tufts in an axial flow compressor. The labelling of this flow phenomena as propagating stall was first used by **Grant** (1951) in a study of the stalling characteristics of an axial flow compressor. Rotating stall patterns were detected by the use of high frequency response hot wire anemometers. The first detailed study was made by the research group under the direction of **Emmons** et al. (1955). They investigated the flow conditions in an axial compressor using hot-wire technique and found that, when the compressor was throttled, low velocity regions appeared, travelling around the annulus in the direction of rotor rotation at a lower speed, and can result in a large loss of compressor performance. They show that for the most part stalling occurs in well defined regions over the

compressor annulus. Two principal types of rotating stall were observed, one with two or more stall cells over part of the blade height and others with a single stall cell over the full range of blade height.

Marble (1953), **Huppert** and **Benser** (1953), **Iura** and **Rannie** (1954) are also amongst the earliest researchers who reported experimental investigations of propagating stall phenomena. The propagating stall was first explained qualitatively as a successive unstalling and stalling of blades in a cascade (**Fig.2-1**). In a row of highly loaded blades, a minor physical irregularity, or flow non-uniformity, can result in momentary overloading and separation. This separation or blockage will restrict the flow through the blade passage and will therefore tend to divert the incoming flow. The incidence angle is reduced to the left of the stalled blades and increased to the right. This tends to stall the next blade on the right and unstall the last stalled blade on the left. This explanation can be derived from the sketch in literature by **Iura** et al. (1954) and **Emmons** et al. (1955).

Several theories of rotating stall in compressor appear in the literature, none of which can be used to predict propagation rates with any appreciable degree of reliability. However, these theories are useful in evaluating the significance of parameters pertinent to the stall propagation mechanism and thus in planning experimental research programs.

2.2 ANTI-STALL DEVICES

Although the concept of stall delay technique began in the early 1960's, the application of casing treatment to aero-engine type compressors or fans has really only become significant since around 1970. Since then, many investigations have revealed that in tip critical machines (i.e. stall initiates at the tip region), the inception of stall can be controlled even suppressed by some modification of the outer casing near the tip of the rotor blades, called casing treatment, and many attainments of stall delay and suppression with this kind of device have been achieved. On the scale of the treatment relative to the blade dimensions, there are small casing treatment and large

casing treatment. The former usually refers to porous or slot type casing treatment and the latter the vaned recess casing treatment.

2.2.1 Slot Type Casing Treatments

The casing treatment initially developed in the 1970's was a small scale treatment which consisted of porous or slotted casings over the tip of the rotor (covering 70%--100% of the blade chord) in an axial compressor or on the shroud near the impeller tip of a centrifugal compressor. The slot type treatment has been the most common type used in multistage axial compressors and adopted in aircraft design. A similar technique called hub treatment has been used in hub critical machines. In this technique, the stall margin improvement is achieved not directly by reducing the blade incidence but by the suppression of the onset of rotating stall. The concept goes back to the outer casing blowing or bleeding technique which was initiated in the 1960's and discussed in the following sections.

Casing Treatment in Axial Machine

Lewis Research Center, NASA (National Aeronautics and Space Administration) was the pioneer group in the development of small scale casing treatment technique for axial flow compressors. In 1964, the research of NASA involved studies on blowing and bleeding at the tip of an isolated high-aspect-ratio rotor and both were found to improve the stall line significantly, with the maximum benefits coming at or near the maximum blow/bleed flow rates. There was a substantial stall line improvement compared to the smooth casing even when no air was being blown or bled. This finding in 1967 led NASA to initiate extensive research on casing treatment (**Smith** 1994). Detailed tests are described by **Koch** and **Smith** (1968) and **Koch** (1969, 1970).

Further tests were carried out on the same rig to evaluate the effects of blocking off some of the blow holes, extending the honeycomb forward, reducing the size of the chamber, adding circumferential or axial baffles etc.. The results are reported by **Bailey** and **Voit** (1970). The casing

treatment configurations included tapered holes set at a compound angle (see **Fig.2-2**), honeycomb with passages inclined at a 70° angle to the radial direction (see **Fig.2-3**) and radial drilled holes (see **Fig.2-4**). In each case, the temperature in the casing plenum, efficiency, total pressure rise ratio and other overall performance parameters were measured. *Results indicate that both skewed tapered hole and honeycomb configurations have a substantial stall margin improvement with some efficiency penalties, but radial hole configurations gave no improvement at all. The plenum volume around the honeycomb could be made quite small with no change in the stall line improvement, but when the plenum volume was zero, no improvement was obtained.*

Osborn, et al. (1971) conducted a series of test to evaluate the effect of geometrically different porous casings on the performance of a transonic, tip critical, rotor only axial-flow compressor and provided extensive information about the effects of the casing treatments. In this study, thirteen porous casings were tested, including perforated casing, honeycomb, circumferentially grooved, axially slotted, blade angle slotted and skewed slotted casing treatments. *Of them all, skewed slot open to a chamber was found to give the greatest improvement on stall margin but with a measurable efficiency penalty.*

Moore et al. (1971) tested an axial flow compressor rotor with six different casing treatments such as skewed slot casing, a circumferentially grooved casing and blade angle slot casing. Radial surveys of pressure, temperature, and flow angle were taken at several equivalent weight flow for each casing treatment. It was found that *the performance over the entire radial span of the blade is affected by the casing treatment and all the casing treatments tested improved the stall margin and enlarged the losses of the compressor*. This would indicate that the phenomena associated with casing treatment is one of stabilising the flow rather than one of reducing losses. They also concluded that casing treatment slots should not extent pass the trailing or leading edges of the blade if both high efficiency and pressure ratio are to be achieved.

Beiley (1972) examined the number, depth, and location of the circumferential grooves in the casing over the rotor blade tip to study the effect on stage stall margin and efficiency. *All but one of the circumferential groove configurations improved stall margin with no significant reduction in efficiency. The deepest grooves showed the best stall margin improvement.* Noted that stall margin improvement was the best when the forward or rear grooves were not used, therefore the mid chord of the blade is proposed as the critical part with respect to the occurrence of rotating stall.

A study by Prince et al. (1975) at General Electric tested circumferential slots, skewed axial slots and blade angled slots on a 1.5m diameter low speed compressor. This work attempted to investigate the mechanism of stall margin improvement by the means of casing treatment. The more detailed review can be found in later section in which the mechanism of the casing treatment is concerned.

Work to examine the effect of several types of casing treatments including a teardrop casing on the performance of a axial-flow transonic fan stage was conducted by **Osborn** and **Moore** (1977) also in NASA. In this study, a teardrop casing and eight variations of skewed slot casing (see **Fig.2-5**) were evaluated. The stall margin for the open, forward, long, skewed slot casing was 21%, while the solid casing had a stall margin of 15%. *The short, mid, open slot configuration had the best stall margin of 23.5%.* It appeared that *the teardrop casing would not let the forward portion of the blade load up as the flow decreased and no benefit resulted from it.*

The research mentioned above is only for transonic and low supersonic machines with high aspect ratio blades. Investigation of a supersonic (tip Mach number 0.7 to 2) annular cascade with a tangentially grooved outer casing has been undertaken by **Fabri** and **Reboux** (1975) at ONERA and has shown that there remains a marked gain in performance even in the higher supersonic range and also for low aspect blades. The study conducted on a compressor with unusually low aspect ratio(1/6) blades has shown that by using deep grooved casing, the stall margin of the compressor improved

by 20% at low speeds and by more than 40% at high speeds, meanwhile the pressure was increased by approximately 10% at high speed.

It was supposed that the effect of casing treatment in low-speed compressors might be different from that in high-speed compressors in which compressibility of the fluid may play an important role. **Takata** and **Tsukuda** (1977) reported their investigations of the casing treatment effect on the stall margin of a low-speed axial flow compressor. The configuration of the treatments were determined by referring to the NASA reports but with distinctions. The results show that both shallow skewed slotted casing (with back chamber) and the deep skewed sloted casing (without back chamber) remarkably improved stall margin. This indicates that the existence of the back chamber is not essential for the mechanism being sought, which is contrary to the observations of NASA in high-speed machines. Research at Cambridge University (**Smith** and **Cumpsty**, 1984) has also revealed that skewed slot casing treatment can provide a substantial stall margin improvement for a low-speed compressor.

Casing Treatment in Centrifugal Machine

The concept of rotating stall in centrifugal compressors was developed in parallel with axial machines but in fact, not very much of the current work on anti-stall devices has been done in centrifugal machines. According to **Amann** et al. (1975), the casing treatment applied to a small centrifugal compressor was a subject of investigation in General Motors Research Laboratories, the concept being successfully applied in the GT-309 engine in 1963. However, no published literature before 1975 on the subject has been found by the author.

It appears that the first published work using small grooves over a limited region of the impeller was undertaken by **Jones** (US Patent 3893787) in 1975, *providing modest flow range and efficiency benefits,* see **Fig.2-6**. In the same year, **Amann** et. al. (1975) reported a more successful achievement by placing a casing treatment near the blade trailing edges of a centrifugal compressor in an automotive gas turbine engine. A

circumferential slot, connected to an annular chamber (**Fig.2-7**) was effective in delaying stall. A more uniform pressure distribution with lower pulsation levels was observed with this treatment. *Casing treatment at impeller exit and vaned diffuser casing treatment gave unsatisfactory results in terms of stall margin improvement but the flow rate at choking was markedly increased.* In a patent by **Wiggins and Waltz** (1977), *the circular grooves at the inlet of the impeller also proved successful*. Further studies of such casing treatment were undertaken by **Janson** and co-workers (1980) whose investigations involved three types of treatment configurations (**Fig.2-8**). *Casing treatment near the trailing edge of the impeller and vaned diffuser casing treatment with radial slots in the external hub section gave unsatisfactory results in terms of stall margin improvement but the impeller wall treatment with inclined axial grooves were very effective to increase the stall margin.* More recently, **MacDougal** and **Elder** (1982) applied grooved treatment and slotted treatment (**Fig.2-9**) to a turbo-charger type centrifugal compressor operating with radial and backswept impellers and about *28% of flow range increase with grooved casing was obtained.*

More successful development has been achieved with bleed port in the shroud which are either enclosed or open to the ambient. The idea probably goes back to early casing treatment studies by **Koch** and **Smith** (1968) as discussed before. The Map Width Enhancer (MWE) proposed by **Fisher** (1988) is typical of work in the subject. In this design, the bleed was not to the ambient but internal to the compressor flow which significantly improved flow range and choke flow with negligible reduction in efficiency. MWE works at surge by de-coupling the inducer from the pressure created by the volute and allowing recirculation through the slot. At choke, air enters the impeller through the slot downstream of the inducer throat, giving extra choke capacity (**Fig.2-10**).

Casing Treatment In Multistage Axial-Flow Machine

As early as 1971, **Tesch** (1971) reported an investigation of casing treatment for a four stage fan. **Snyder** et al. (1972) reported the results of a

simulation study of the effects of casing treatment on a multistage compressor. It was noted that the treatment of the rear stages was needed to improve the GE J85 8-stage compressor. Casing treatment of the front stages improves only the low-speed operation of the compressor.

An investigation of the effect of casing treatment for a multistage compressor at low speed was conducted by **Wenzel** et al. (1975) and shows a almost negative result. Their study was carried out on a J85-GE-13 engine with a compressor which allowed a change to the casing wall over the rotor tip of six(1-3, 6-8) out of eight stages. Blade angle slotted and circumferential grooved casing insert were employed. The result suggested that casing treatments would have little or no effect on extending stall margin and increasing individual stage pressure rise and temperature coefficients. **Moss** (1976) reported a similar negative result for the same engine(J85-GE-13). The engine appeared to be hub critical rather than tip critical, therefore, tip treatment had no beneficial effect on stall margin.

However, **Urasek** et al. (1976) reported a successful attempt when an inlet stage of a transonic compressor was tested with three tip casing treatments. There were blade angle slots, circumferential grooves, and axial skewed slots. The bottom of the slots were closed to avoid slot to slot air recirculation. Significant increases in both rotor and stage total pressure ratio, efficiency and flow range were obtained. The greatest improvement in performance was achieved with axial skewed slots. A circumferential grooved casing applied to a two-stage high-pressure-ratio fan, reported by **Urasek** (1979), was another successful example. An investigation into the effect of small scale casing treatments for a multistage compressor undertaken by **Li** (1980) and **Gao** and **Li** (1982) also shows a positive result. To increase the inlet distortion tolerance and improve stall margin of a multistage compressor at low and medium speed, a small scale casing treatment was applied to the inlet stage of the fan and compressor by **Li** and successful results were obtained. **Gao** and **Li** applied the circumferential grooved casing treatment over the tip section of the last three stages of a nine stage compressor and results show that the rear stage

casing treatment was very effective on stall margin improvement of compressors at high speed, and in solving the problem of the in-flight shutdown which happened to some engines during lighting of the afterburner at high altitude. A usual method to extend the stable operating range of a compressor in multistage compressor design is to reduce rear stage loading, consequently increasing the stage number, size and weight of the compressor. Potentially the application of casing treatments may overcome such shortcomings.

Hub Treatment

Similar techniques applied to hub critical machines (called hub treatment) have provided beneficial effects in most cases. However an experimental investigation undertaken by **Wisler** and **Hilvers** (1974) was unsuccessful even though extensive tuft probing showed that the test rig was indeed hub critical. This fan configuration was modified by removing the stator hub shrouds and replacing them with rotating hub spool, which incorporated stator hub treatment. The performance data, obtained for the baseline and the two treatment configurations, showed that stator hub treatment did not delay the stall point nor did it modify performance of the compressor in any discernible fashion.

However many other investigators have demonstrated that hub treatment is as effective as casing treatment and it is supposed that hub treatment and casing treatment have the same working mechanism. In order to examine the effect of a discharged jet on the main stream, **Takata** and **Tsukuda** (1977) applied axial slot treatment to the hub (a rotating drum under the stator which can be driven at any speed independent of the rotor speed, **Fig.2-11)**. Compared with the drum result, the flow condition near the inner wall becomes worse when the treatment wall is stationary while the flow condition is improved remarkably when the treated wall is moving. Investigations at Massachusetts Inst. of Technology directed by **Greitzer** and **Tan** have also shown a successful result (**Prell** 1981, **Cheng** et al. 1984 and **Johnson** et al. 1987). The hub treatment (**Fig.2-12, Cheng**

et al. 1984) consisted of axial slots skewed at a 60° angle to the radial direction rotating beneath an axial compressor stator row. The slot spacing was such that the slotted area is twice that of the solid area. The slot aspect ratio (axial length/tangential width) was 2.0. It was found that the hub treatment was very effective in delaying the onset of stator stall and increasing the peak stator static pressure rise. More recently, an experimental study of the axial skewed slot hub and casing treatment undertaken by **Johnson** and **Greitzer** (1987) also showed a very successful result. This investigation was focused on the flow phenomena which will be discussed latter.

2.2.2 Vaned Recess Casing Treatment

A relatively new kind of casing treatment called *vaned recess casing treatment* has shown a remarkable effect on stall margin improvement and pressure rise. Compared to the slot type treatment, the scale of the vaned recess treatment relative to the blade dimensions is much larger (dimensions of the treatment are of the same order as the blade), hence it is called a large scale casing treatment. There is very limited literature available on the subject.

The patent work by **Ivanov** et al. (1984) could be regarded as one of the earliest documents describing recessed vaned casing treatment, **Fig.2-13**. Work was done on an axial flow ventilation fan and different results for a range of setting angles of vanes were obtained. The geometrical design guide line provided is of great interest to all the investigators although it seems to be rather arbitrary. No details, however, were given on its working mechanism. The patent work by **Russell** et al. (1984) was principally similar apart from the radially rotatable extended vanes at inlet.

The investigation conducted by **Miyake** et al. (1987) also showed that a remarkable improvement by an "air-separator" (**Fig.2-15**) over a fairly wide range of setting angle, and more recently **Fujita** et al. (1984) revealed that an "air-separator" could eliminate the unstable characteristics of an axial flow fan even for a build which originally exhibited a heavy rotating

stall.

Bard (1984) reported a stabilising device, **Fig.2-14**, integrated into the casing of axial fans. Noted that this device completely eliminates the stalling cycle without affecting the peak efficiency. The study paid much attention to the flow behaviour related to the working mechanism by which the anti-stall device works. This type of technique has been applied in industrial application with much success, one of which for tunnel ventilation is also reported by **Bard** (1993), and provided fully stable performance characteristics without stall. The most interesting thing is that the treated casing was arranged just upstream of, and not over the tips of the rotor blades. The fan performance in the working flow range above the previous stall limit was not affected, therefore no efficiency loss was involved. This arrangement differs from that proposed by **Ivanov**'s sketch and that of **Azimian** et al. (1989) and **Ziabasharhagh** et al. (1992), which will be discussed latter.

Generally speaking, the aero-engine type compressor or fan has much higher blade loading in terms of the work coefficient $\Delta H/U^2$ than the industrial fan does. The effect of the large casing treatment technique on the aero-engine type compressor or fan is naturally an interesting subject. **Azimian** et al. (1989) reported an encouraging result in this field. In their study, a large casing treatment was applied to a low speed axial fan with a typical aerospace type loading and more than 50% of stall margin improvement with insignificant efficiency penalties was obtained. A great number of experiments with up to 40 builds were made to examine the effect of the percentage of the rotor axial chord exposed to the casing recess, and the effect of vanes on stall margin improvement. The results clearly show that the percentage of the rotor axial chord exposed to the recess is a very critical parameter and more than 50% is required. The best results were achieved when the percentage was 67.

It is interesting to note that no benefit was obtained when the casing treatment was arranged in such a way that the axial chord exposed to the recess was equal to zero or negative. On the contrary, **Bard** (1993) obtained

the best result when the anti-stall device was just upstream the rotor. This indicates that the optimum portion of axial chord exposed to the casing recess might have something to do with the blade loading.

Azimian found that the casing treatment gave a much smaller stall margin improvement for the stage (rotor + stator) builds (build 1 to 10) than for rotor only. For low hub/tip radio stages, the stator hub is most often the first section to stall, and the rotor tip at a lower flow. Perhaps both rotor casing and stator hub treatment should be combined for the maximum effect.

The geometrical design, **Fig.2-16**, drawn broadly on the lines of a sketch appearing in a UK patent (1984) but redrafted by **Azimian** et al (1989) is of particular interest. In this design, the length of the vane in the recess was used as a basic dimension, the reason for which is not explained. The 48 vane builds showed a much better result than vaneless builds. The author thought that 24 vane builds gave a further improvement, but this was an ambiguous conclusion as in the study, not only the number of vanes was changed but also other geometrical parameters were significantly changed. This made it difficult to simply conclude which modification was the major contributor. The "airfoil section" build (with its function of reducing the diffusion within the recess vane passage and forming a 'core' for the recirculating flow) appeared to be a most successful build. This naturally raises the question, is an airfoil section inner ring essential for the best result? Because the flow in the casing recess suffered serious separation, the benefit from the airfoil section inner ring was a reduction of the flow diffusion or separation rather than anything else. In other words, a simpler inner ring might well do the same. Clearly this needs testing to verify.

The compressors used in aircraft engines have to operate over a wide range of flight conditions and are required not only to be capable of stable operation with a wide flow range but also to be capable of tolerance toward the condition of distorted flow into the engine. The treated casing seems capable of increasing both stall margin and tolerance to distortion.

Ziabasharhagh et al. (1992) reported the results of such experiments and positive results were obtained.

2.2.3 Summary of The Observations on Casing Treatments

To summarise the above research, the main observations were:

1. Various types of small casing treatments are effective in delaying stall for tip critical compressors, both axial and centrifugal. Hub treatments for hub critical machines have similar effects. The experiments for a 0.5 hub/tip ratio fan found that the casing treatment gave a much smaller stall margin improvement for rotor with stator builds than for rotor only. For low hub/tip radio stages, the stator hub is most often the first section to stall, and the rotor tip at a lower flow. Perhaps both rotor casing and stator hub treatment should be combined for the maximum effect.
2. The stall margin improvements by these treatments are of the order of 4%-28% with some peak efficiency penalties usually equivalent to 2-4%. Circumferential grooves provided a moderate improvement in stall margin without significant decrease in efficiency. Skewed slot configurations were found to give the greatest improvement on stall margin but with a measurable efficiency penalty.
3. The small scale casing treatment technique has been applied to both low speed and supersonic flow compressors with basically the same success. It seems clear that the flow Mach number is not critical to the behaviour of the casing treatment.
4. Although **Prince** (1975), **Takata** et al. (1977) and **Greitzer** (1980) all suggested the concept of radial flow through the casing and analysis using this concept in models for predicting rotating stall onset have shown the possibility of the stabilising influence of these radial flows, the radial-hole inserts gave no improvement at all. No benefit was received from the teardrop configuration either.
5. The backchamber (plenum) around the tapered-hole or slot casing was useful in stall margin improvement, but it appeared to be not essential

(**Urasek** et al. 1976, **Takata** and **Tsukada**, 1977).

6. Generally speaking, a large casing treatment provides better improvement on stall margin than a small one but causes problems in structure and cost in some applications. The trade-off between stall margin improvement and cost, structural difficulty and efficiency penalty must be evaluated to find an optimum solution for the application.
7. Despite the effectiveness of the casing treatment in extending the stable operating range, it has found fairly limited application. The main reason for this is that in most cases, the stall margin improvement is at the cost of efficiency, and that there can be mechanical and manufacturing difficulties associated with casing treatment usage. It should be realised that much work remains to be done before it can be widely applied industrially and adopted as a standard item by designers.

2.3 WORKING MECHANISM OF THE CASING TREATMENT

Casing treatments of various kinds have been shown to be valuable for stall margin improvement and increasing rotor and stage pressure at the stalling flow rate of the untreated stage. There was, however, little knowledge about the working mechanism, and the geometric designs of the casing treatment were somewhat arbitrary and empirical rather than scientific or fluid dynamic. Most of the many past tests on treatments placed emphasis on the effect on stall margin improvement without further investigating the flow phenomena occurring in and just above the treatment. A few though, notably **Prince** et al. (1975), **Camarata** and **Greitzer** (1975), **Takata** and **Tsukuda** (1977), **Greitzer** et al. (1979), **Smith** and **Cumpsty** (1984), **Johnson** and **Greitzer** (1987), and more recently, **Hall** et al. (1994) did examine the flow inside the slots or grooves of the treatment that allowed some interpretation of the processes involved. This section will outline the main observations.

2.3.1 Experimental Study of Casing Treatment Flow Phenomena

Bailey and **Voit** (1970) described some observations about flow phenomena associated with the casing treatment. Recirculation appeared to be necessary to improve stall margin with the tapered hole configuration and the amount of improvement was directly related to the recirculation. For the honeycomb casing treatment, the equalisation of the static pressure in the tip region seemed to be the controlling factor. In fact, the function of equalisation of the static pressure existed in the tapered hole configuration although the author did not mention it. The porous casing surrounded by a plenum presents paths for both recirculation and flow interchange between main flow and plenum. If a stall cell forms in the tip region of a rotor, a circumferential variation in static pressure must exist around the rotor. The porous casing may permit the equalisation of the unbalanced pressure and therefore delay the formation of a rotating stall cell.

General Electric (GE) firstly proposed a research program employing its large 60-in-dia low speed research compressor under the support of NASA. **Prince** (1975) reported their investigation into the possible mechanism by which the casing treatment works. In this study, analytical modelling of the flow patterns in casing treatment cavities was carried out in conjunction with the experimental investigation that included a detailed tuft survey and quantitative measurements of the flow within the treatment cavities (circumferential grooves and axial-skewed slots). This study suggested that interaction of cavity flow with main stream flow, and compliant wall absorption of pressure disturbances are the most important features of the casing treatment effects although some aspects of the experimental results do not seem to correlate. The beneficial effect of casing treatment is not dependent on high Mach number or cavity resonance. Pressure on the surface pressure side of the rotor blade close to the tip is substantially higher in the presence of axial-skewed slot or blade angle slot treatments than in the baseline configuration, and can be higher than the free stream relative total pressure. But **Smith** et al. (1984) found that there was no significant total pressure change in their case.

Some investigations have suggested the concept of a radial flow through the porous casing, and analysis carried out incorporating this idea in basic models for predicting rotating stall onset have shown the possibility of the stabilising influence of these radial flows (**Takata** et al., 1977 and **Greitzer** 1980). However, it cannot explain the phenomena that using a closed groove configuration at low speed, where there is a large fraction of circumferential flow rather than radial flow into the casing, has been found very effective in increasing stall margin. Thus the idea of "radial flow relief" does not seem to be one of the most critical features.

In order to understand the mechanism, **Takata** et al. (1977) measured the unsteady flow within the slots or grooves of the casing treatment in a low-speed axial-flow compressor. They also arranged a measurement in the stator blade row to see the effect of the discharged jet from the hub treatment on the main stream. This approach greatly simplifies the instrumentation for a minor sacrifice in flow realism. Based on the results, two models, the momentum interchange model and the mass interchange model were proposed. The former was thought more important as far as the slot type treatment configuration are concerned. However neither of them can explain the success of the bleeding application. They pointed out that in general, the casing treatment does not alter the radial distribution of the inlet axial velocity, but it has great influence on the outlet axial velocity. The fact that the deep skewed (without backchamber) and shallow skewed (with backchamber) slotted casing gave almost the same margin improvement indicate that the backchamber is not essential for the mechanism being sought.

Greitzer et al. [1979] conducted a carefully thought-out experiment based on the hypothesis that stall could be initiated either near a wall or a mid-blade region. Based on the finding by **Greitzer** and others, there seems no doubt that casing treatment is effective only in the case in which a wall stall exists. **McDougall** (1988) made a similar conclusion.

Smith et al. (1984) investigated an axial skewed slot casing treatment over the tips of an isolated low-speed rotor and described measurements

taken behind the rotor, inside the slots, and between the moving blades. From this base, most of the flow process occurring was determined, but there are aspects of the flow behaviour which are not understood. The tentative conclusion was that unsteady effects in the slot were of secondary importance. Of primary importance was the selective removal of high absolute swirl, high loss fluid from the endwall near the trailing edge of the pressure surface of the blade, and reintroduction of this, with absolute swirl direction reversed, near the blade leading edge. It is worthy to note that of all the slot type treatment, the axial skewed slot treatment is the most effective. The essential feature of this design is the inclination of the slot (for example 30° with respect to circumferential direction) from which the similar conclusion that removal of high absolute swirl is an important feature may be drawn. Considering the plot of axial velocity, the treatment had the effect of increasing the through flow (decreasing blockage) in the tip region, but decreasing it elsewhere. **Ziabasharhagh**'s results of overall performance for 0.9 hub/tip ratio builds shows that the casing treatments tends to decrease overall mass flow in most cases.

The results of the measurements by **Johnson** et al. (1987) have shown that suction of the high-blockage fluid at the rear of the passage is also important. An additional mechanism for operation of the slotted hub might therefore be that the jet somehow suppresses the tip leakage flow that occurs with the solid wall. The level of blockage in the rotor passage being greatly decreased by the casing treatment may be thought of as a result rather than a cause. What we are more interested in is why and how it can occur.

Little work has been done on the recessed casing, but the wool tuft flow study by **Azimian** et al. (1989) and **Ziabasharhagh** et al. (1992) provided a description of the flow. The mode of operation of these passive anti-stall devices seems to be that the reverse flow, thrown forward from the rotor blade tip as stall is approached, is centrifuged into the casing recess instead of displacing the incoming flow towards the hub. By means of turning vanes, the vaned recess casing treatment eliminates the swirling element

which becomes more significant as the flow is throttled, and returns the flow into the main flow, thereby creating a stable, continuously rising performance characteristic.

2.3.2 Numerical Simulation of Casing Treatment Flow

Theoretical study of the mechanism involved are very desirable as little work have been done in this field.

Snyder et al. (1972) reported the results of a simulation study of the effects of casing treatment on a multistage compressor. The simulation model is based on individual stage-by-stage steady-state characteristics. It was assumed that steady-state stage maps would be valid during surge or stall, and the casing treatment would affect only the stage map of the treated stage and would not cause flow-profile changes which would wash downstream to the next stage. It was pointed out that the rear stages casing must have been treated to improve the GE J85 8-stage compressor. Casing treatment of the front stages could improve only the low-speed operation of the compressor. It should be pointed that this is not a global(general) conclusion, and many others have demonstrated that inlet stage treatments are effective (**Urasek** et al., 1976).

Following a review of flow instabilities observed in a centrifugal compressor, **Amann** et al. (1975) employed a simplified two-dimensional analytical model of the flow at the rotor-diffuser interface, and found that flow relief in the third dimension should delay the onset of surge.

Computational fluid analysis has been very active in the prediction of various flow phenomena in turbomachinery in recent years. It is promising as a tool to aid in understanding the complexities of the phenomena associated with casing treatments. Previous attempts with CFD on the subject are few in number due to the complexities. **Crook** et al. (1993) first reported their attempt of the simulation of a grooved hub treatment flow with a three-dimensional steady viscous flow model. Hub or casing treatments have an area of flow removal over the downstream portion, and an area of flow injection over the upstream portion, of the treatment area.

This combination of flow removal and injection was simulated numerically by modelling the treatment area as a second inlet/exit to the flow field domain. The computations show that there are two main actions of hub or casing treatment on the leakage flow: (1) suction of the low total pressure fluid at the rear of the passage, and (2) suppression of the blockage in the core of the leakage vortex due to the energising of the leakage flow by high velocity injection at the front of the passage. Further research of a time dependent treatment/rotor aerodynamic interaction analysis was performed by **Hall** et al. (1994) for a modern fan rotor with a recessed vane casing treatment. Although it did not give a detailed description of the final result, it was a big step forward in the numerical solution of the flow in casing treatment.

2.3.3 Summary of the Review on the Mechanism

It seems that the mechanism by which the stall margin is improved by casing treatments is not yet fully elucidated. Various hypotheses have been proposed but none of them are able to explain all the observed phenomenon satisfactorily. However some important observations mentioned above, such as removal of whirl component, interaction between casing treatment flow and main flow, appeared to be closely related to the mechanism being sought.

CHAPTER 3. EXPERIMENTAL FACILITIES AND TECHNIQUES

This chapter describes the experimental fan rig, instrumentation and measuring techniques used in this investigation. Detailed information about the fan rig is provided, including the geometry of the rotor blades, the structure of the casing treatment section and design of various casing treatment configurations. The instrumentation used in time-averaged measurement and the data acquisition system for phase-lock unsteady flow measurements are detailed. The principle, calibration and measuring techniques of three-dimensional flow measurement with a slanted hot-wire are also presented.

3.1 EXPERIMENTAL FACILITIES

Details of the Test Fan Rig

The test rig used for the present investigation is similar to that of **Azimian** et al. (1989) with the exception of a new computerised data acquisition system. Tuft exploration and overall performance measurements had shown that the compressor was susceptible to tip stall and is therefore considered a good vehicle for the present casing treatment studies.

The test fan (C134, **Fig.3-1**) is a single stage (rotor only) axial flow fan with a design tip speed of 39m/s, tip diameter of 508mm, hub to tip ratio of 0.5 and near unity blade loading ($\Delta H/U^2$) at the hub. The rotor is equipped with 27 C_4 (circular arc profiles) rotor blades mounted by means of a "sandwich arrangement", which permits the tip clearance to be easily modified. The rotor is directly driven by a variable speed, 3.7kw AC motor.

Table 3-1 Blade Geometry

Radius (mm)	129.54	158.242	185.42	190.50	216.154	246.38
Inlet Blade Angle	35.4°	40.9°	45.7°	46.1°	49.9°	53.5°
Outlet Blade Angle	-16.9°	2.2°	16.1°	17.5°	26.6°	36.6°
Stagger Angle	9.2°	21.6°	30.9°	31.8°	38.3°	45.0°
Camber angle	52.4°	38.6°	29.6°	28.6°	23.3°	17.0°
S/C	0.623	0.761	0.898	0.917	1.04	1.18

maximum thickness/chord	12%
tip clearance/blade height	1.2%

The motor case is made in a way that it is a part of the dynamometer type torque meter which can float on bearings. The design speed of the rig is 1500rpm at which all the experiments were carried out. The rig has a short inlet section without Inlet Guide Vanes (IGV). The stator blades were fixed in the casing by means of a liner ring which makes it easy to construct a compressor without stator (see **Fig. 3-2**). It is built in two main parts. The front part comprises the compressor and driving system and the other part comprises a 508mm (20") inside diameter duct containing a conical body that constitutes a diffuser with the duct. Blade design geometry is given in **Table3-1**.

Test Fan Rig Modification

In the existing test rig, the vaned recessed casing treatment can be easily located partly over and upstream of the rotor blade tip. The axial position of the casing treatment in relation to the rotor could be modified by use of spacer rings positioned upstream and downstream of the recess. However, there is little flexibility available to move the recess further backward when it is located such that 2/3 of the rotor axial chord is exposed to the recess. To meet the demand for optimising the length between the inner ring and leading edge of the rotor, an inlet spacer ring (26mm thick)

with 4 static pressure tapping was designed and mounted far upstream of the rotor (**Fig.3-2**).

3.2 DESIGN OF CASING TREATMENTS

A vaned recess casing treatment is to replace the original solid wall casing with a recess casing which is incorporated into the fan casing and located partly over and upstream of the rotor blade tip. Inside the recess casing is usually equipped with guide vanes and a shroud ring. The purpose of the guide vanes is to remove as much as possible of the whirl components of the reversed flow from the rotor tips into the recess, and the shroud ring fitted to the inner edge of the vanes is to separate the recess flow and main flow passage and serve as a middle reservation part between entry and exit of the recess.

The casing treatment used by **Azimian** et al. (1989) was based on **Ivanov**'s design and is further modified here. Three configurations in all were designed and tested.

Configuration 1

This configuration (**Fig.3-3-a**) comprised 24 vanes, half of that used by **Azimian** et al. 1989), giving an overall pitch/chord ratio of approximately unity. Several spacer rings were designed and placed inside the casing treatment such that the width of the inlet part of the recess could be varied. A perspex window with 35 holes permitted wool tuft flow visualisation and flow traversing measurements over the vane passage.

Configuration 2

The casing treatment designed by **Azimian** et al. (1989) based on the design by **Ivanov** et al. (1984), seems to have too much diffusion within the

recess which brings about a serious flow separation from the suction surface of the recess vanes. **Azimian** et al. (1989) modified their design with an airfoil section inner ring and a further improvement was obtained, however, it was a very costly design. To keep the production cost as low as possible, a simplified inner ring was designed.

This involved two major modifications as shown in **Fig. 3-3-b**:

i) The "airfoil section" inner ring used by **Azimian** et al. (1989) was simplified to a 30° wedge crowned by a 10mm radius circular arc;

ii) New vanes covered the whole recess length. These vanes consisted of a radially placed uncambered (flat) part and a radially cambered part over the rotor (see **Fig.3-3-b)**. The axial length of the recess was 8mm (approximately 7%) shorter than that of configuration 1.

Configuration 3

As **Fig.3-3-c** shows, this treatment consists of an outer casing with 24 slightly curved vanes and an inner ring of substantial cross section. The inlet part of the vane (section A-A) is cambered by 55° with respect to the radial direction to reduce the incidence of flow into the vanes. The leading edge of the inlet portion was cut back by 10mm (18% of the recess height) to avoid additional noise. The outlet part of the vane has 90° outlet angle (section B-B), re-introducing the flow into the main annulus in a radial direction. The vane is positioned with an inclined angle of 25° (with respect to the radial direction). Note that the radius of curvature of both inlet and outlet regions of the vanes has been increased from those used in Configuration 2. So this configuration is characterised by less diffusion in the flow passage and lower camber vanes which cover the whole recess length.

3.3 TECHNIQUES OF MEASUREMENTS

The performance of an axial-flow fan is usually presented by pressure/flow characteristics and efficiency. Total and static pressure rises across the fan, mass flow, rotational speed and work input must therefore determined to carry out a performance test. This section will discuss the general techniques and instrumentation used in this study to measure the parameters mentioned above.

Shaft Speed Measurement

The speed of the rotor was measured by the means of 16 bit counters and digital input on the CIO16jr A/D conversion board which monitored the pulse train generated by a magnetic pick up and a disc with 360 slots on its periphery. The design speed of the test rig is 1500rpm at which all the tests were conducted. In this case, the frequency of the blade pulse was about 9kHz, therefore, a setting of the frequency of the out2 (gate0) at not higher than 900 Hz is required to make an accurate measurement. A short program to control the counter and calculate the shaft speed is necessary. The output of the counter was checked visually to see that the wave form and timing were correct. An alternative method was to use a digital speed pick up to monitor the frequency of the white stripe on the end of the shaft.

An accuracy of shaft speed reading higher than 1% was expected. The measured speed value was corrected as follows

$$N = N_m \sqrt{\frac{288.15}{T_{in}}}$$

where N_m is measured shaft speed (rpm) and T_{in} the inlet total temperature(K).

Torque Measurement

The test rig was equipped with a dynamometer type of torque meter which provided with facilities for torque measurements. The torque meter has a long graduated balance arm which is graduated from 0 to 30 lb-ft (see **Fig.3-4**). The torque meter required a zero setting and this performed by means of a counter-weight on the small balance arm. Due to the friction in the cradle bearing, static unbalance of cradle motor and windage torque it was necessary to calculate the torque loss. The torque loss calculation by **Schmidt** (1985) was given as

$$T_{loss} = \frac{1.35582 \times (0.163N - 10.1)}{1000} \qquad (Nm)$$

The accuracy of the torque measurement was 0.0136 Nm (0.01 lb-ft).

Pressure Measurement and Instruments

The test rig was equipped with conventional slow response wall **static** *tappings* at inlet, the inter-row gaps, and the outlet of the compressor. At each measuring station, four static tappings are equally spaced around the circumference and connected to a common bank of a manometer. To avoid averaging error, it is recommended that the static tappings should be connected in pairs by two equal length of tubes.

The bank of manometers consists of 36 channels filled with methylated spirits (specific density K=0.792) and its inclination setting angle α could be varied between 18° and 90° degree. Density calibration every three months is strongly recommended because methylated spirit density will increase due to evaporation of spirit and absorption of moisture if it is exposed to air for a long time. The pressure can be derived as follows.

$$H = H_m \times K \times Sin(\alpha) \quad (cm \quad H_2O)$$
$$P = 98.06H \quad (Pa)$$

The main difficulty in pressure measurements results from the fact that in most cases, swirling flow conditions are present downstream of the fan and upstream as well in stalled condition, with the result that uneven pressure distributions are present across the duct. Therefore, detailed traverse measurements are often indispensable for accurate results. A three hole 4mm diameter cylindrical pneumatic probe was used for this purpose so that reliable **total and static pressure** reading can be obtained. The probe calibration was performed by use of a small wind tunnel. The calibration is given in the form of coefficients C_a, C_t, C_s against the flow angle. The three governing equations are

$$C_\alpha = \frac{P_1 - P_2}{P_t - P_s}$$

$$C_t = \frac{P_1 - P_t}{P_t - P_s}$$

$$C_s = \frac{P_1 - P_m}{P_t - P_s} \times \frac{P_s}{P_m}$$

$$P_m = 0.5 \times (P_2 + P_3)$$

where C_a, C_t, C_s are the coefficients related to the yaw angle α , total and static pressure respectively; P_1, P_2, P_3 are the readings obtained from the centre and two sides tapping respectively; P_t and P_s are the derived total and static pressure respectively. C_s is commonly defined as

$$C_s = \frac{P_t - P_s}{P_1 - P_m} \times \frac{P_m}{P_s}$$

The reciprocal of C_s is used here to avoid the problem of discontinuity in $C_s(\alpha)$ when α is about 40 degree. One of the calibration results is shown in **Fig.3-5**. Calculation of P_t, and P_s based on P_1, P_2 and P_3 involves an

iterative procedure where P_t and P_s initially are assumed to be $P_t = P_1 - P_m$; $P_s = P_m$.

The local **atmospheric pressure** was measured by means of a digital pressure indicator. A barometer of the direct reading mercury column type situated in the compressor house was also alternatively used when the digital data was not available.

Mass Flow Measurement

The effect of compressibility can be neglected as the flow velocity is much lower than 60m/s(Mach Number<0.2). From Bernoulli's equation

$$\frac{1}{2}\rho V^2 = P_t - P_s$$

$$V_m = \sqrt{\frac{2(P_t - P_s)}{\rho}} = \sqrt{\frac{2\Delta P}{\rho}}$$

$$\rho = \frac{P_s}{R\,T_s}$$

Two different methods for measuring V_m before stall and post stall were applied. In steady flow conditions, there was no evidence of any flow disturbance at 150mm upstream of the rotor. In this case, a simple method based on the averaged static pressure in the bell mouth ahead of the rotor was adopted. The measurements agree well with the results obtained by 10 points traversing measurements.

In the stall condition, large regions of retarded and reversed flow upstream of the rotor affected the measurement of the static pressures and the calculated mass flow rate was no longer considered to be an indication of the real flow. Instead of upstream, the measurements were taken at the section 900mm from the end of the downstream duct where it was believed to be free from the effects of rotating stall. A higher accuracy, eight-point

log-linear traverse method was used. In this method. it is assumed that the velocity distribution along a diameter can be represented by the equation

$$V_y = A + B \log \frac{y}{d} + C \frac{y}{d}$$

where V_y is the point velocity at a distance y from the wall of the pipe of diameter d (here d=508mm) and A, B, C have the dimensions of velocity.

The location of measuring points were 0.021d, 0.117d, 0.184d, 0.345d, 0.655d, 0.816d, 0.883d, 0.979d as described in British standards 1042, part 2A, 1973[ ]. The pressure measurement can be done by both 3-hole pneumatic probe and hot-wire probe.

$$Vm = \frac{1}{8} \sum V_i \qquad (i = 1, 2, 3 \ldots\ldots 8)$$

3.4 THREE-DIMENSIONAL FLOW MEASUREMENTS WITH A SINGLE SLANTED HOT-WIRE

The flows involved in the casing treatment and the rotor region are very complex, and it was therefore necessary to carry out full 3-D velocity measurements. Because the manometers were insensitive to the periodic fluctuations, a pitot tube can not detect the unsteady flow characteristics. The high frequency data acquisition system (**Fig.3-6**) for 3-D flow measurements and data reduction program were developed for the purpose. The variations in time and space of three orthogonal velocity components in the casing treatment recess were found by three consecutive measurements of a hot wire probe orientated in three mutually perpendicular directions as proposed by **Whitfield** et al. (1972). Using this method, the prong support interference effects associated with three-wire probe was avoided. In **Whitfield**'s method, it is assumed that only first order cooling effect are important, i.e. the probe is sensitive only to the flow perpendicular to its

axis and insensitive to the flow parallel to the wire. For more accurate measurements, enhancements were necessary as described below.

The Principle

The easiest way to position the probe in three mutually perpendicular direction is to use a slanted probe of 54.7° angle and rotate it through successive 120° increments. As this kind of probe was not commercially available at this time, it was necessary to modify a probe with a slant angle of 45° (common type 55P12 probe) to one with 54.7°.

From the **cosine** law relationship (**Lomas** 1986), the relationship between the maximum flow cooling rate ($V_{\theta=0}$) and flow cooling rate at angle θ can be expressed as follows,

$$V_e^2 = V^2(\cos^2\theta + K^2\sin^2\theta)$$

where θ is the flow angle with respect to the normal to the axis of the wire and K is the yaw factor, including the addition cooling by the tangential

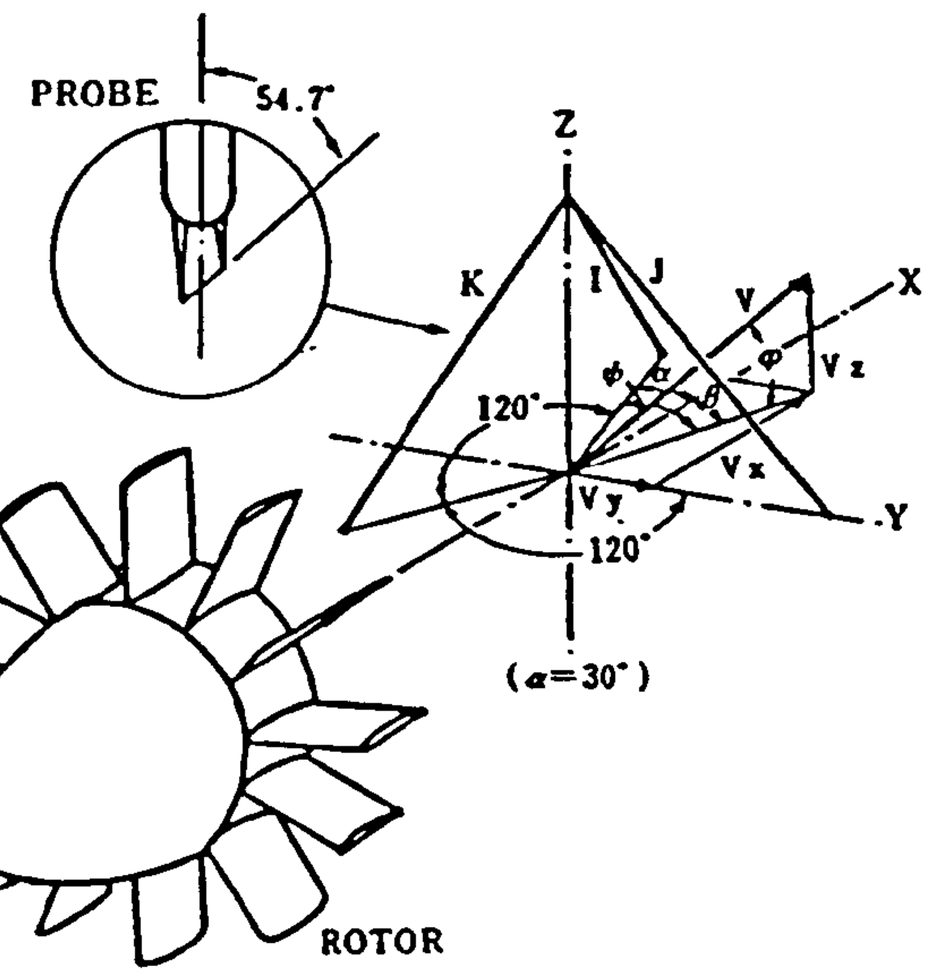

Fig.3-7 Hot-wire Position and the Co-ordinate System

component of velocity.

The test rig co-ordinate system x-y-z and probe co-ordinate system i-j-k are shown in **Fig.3-7** (page 37). The wire has a slant angle of 54.7° to its radially orientated stem and it was first put in i- direction. By rotating the stem through successive 120° increments, the probe was positioned in three mutually perpendicular direction j- and k-. In the i-j-k co-ordinate system, the angles between the velocity vector and i-,j-,k- axes are given as α(the limitation on α will be discussed later), β and γ respectively. Using the **Hinze** yaw-angle relationship above, the effective cooling velocity for each axes may be written as

$$V_{ei}^{\,2} = V^2\left(\cos^2\alpha + \mathrm{K}^2\sin^2\alpha\right)$$

$$V_{ej}^{\,2} = V^2\left(\cos^2\beta + \mathrm{K}^2\sin^2\beta\right)$$

$$V_{ek}^{\,2} = V^2\left(\cos^2\gamma + \mathrm{K}^2\sin^2\gamma\right)$$

These equations may be rearranged to give the direction cosines of the velocity vector:

$$\cos\alpha = \frac{1}{V}\sqrt{\frac{V_{ei}^{\,2} - K^2V^2}{1-K^2}} \qquad (1)$$

$$\cos\beta = \frac{1}{V}\sqrt{\frac{V_{ej}^{\,2} - K^2V^2}{1-K^2}} \qquad (2)$$

$$\cos\gamma = \frac{1}{V}\sqrt{\frac{V_{ek}^{\,2} - K^2V^2}{1-K^2}} \qquad (3)$$

Since $$\cos^2\alpha + \cos^2\beta + \cos^2\gamma = 1$$

These four equations are combined to give the magnitude of the velocity vector:

$$V = \sqrt{\frac{V_{ei}^{\,2} + V_{ej}^{\,2} + V_{ek}^{\,2}}{1+2K^2}} \qquad (4)$$

Considering the output of the anemometer in its three orientations at one particular measuring point, and assuming that **Cosine** law is valid here, the wire in orientation i responds to velocity in direction j and k.

Thus

$$v_i^2 = V_{ej}^2 + V_{ek}^2$$

Similarly

$$v_j^2 = V_{ei}^2 + V_{ek}^2$$

$$v_k^2 = V_{ei}^2 + V_{ej}^2$$

Hence

$$V_{ei}^2 = 0.5(-v_i^2 + v_j^2 + v_k^2) \quad (5)$$

$$V_{ej}^2 = 0.5(v_i^2 - v_j^2 + v_k^2) \quad (6)$$

$$V_{ek}^2 = 0.5(v_i^2 + v_j^2 - v_k^2) \quad (7)$$

Using equations (5) to (7), the equations (1) to (4) can be rewritten as follows:

$$\cos\alpha = \frac{1}{V}\sqrt{\frac{-v_i^2 + v_j^2 + v_k^2 - 2K^2V}{2(1-K^2)}} \quad (8)$$

$$\cos\beta = \frac{1}{V}\sqrt{\frac{v_i^2 - v_j^2 + v_k^2 - 2K^2V}{2(1-K^2)}} \quad (9)$$

$$\cos\gamma = \frac{1}{V}\sqrt{\frac{v_i^2 + v_j^2 - v_k^2 - 2K^2V}{2(1-K^2)}} \quad (10)$$

$$V = \sqrt{\frac{v_i^2 + v_j^2 + v_k^2}{2(1+2K^2)}} \quad (11)$$

If (β_{xi}, β_{xj}, β_{xk}), (β_{yi}, β_{yj}, β_{yk}) and (β_{zi}, β_{zj}, β_{zk}) are the direction cosines of i, j, and k to the direction of x, y, and z respectively, the velocity components in x-y-z co-ordinate system and direction angle ϕ, θ can be found.

$$V_x = V\,(\,\beta_{xi}\cos\alpha + \beta_{xj}\cos\beta + \beta_{xk}\cos\gamma) \tag{12}$$

$$V_y = V\,(\,\beta_{yi}\cos\alpha + \beta_{yj}\cos\beta + \beta_{yk}\cos\gamma) \tag{13}$$

$$V_z = V\,(\,\beta_{zi}\cos\alpha + \beta_{zj}\cos\beta + \beta_{zk}\cos\gamma) \tag{14}$$

$$\phi = \tan^{-1}\sqrt{\frac{V_z^{\,2}}{V_x^{\,2} + V_y^{\,2}}} \tag{15}$$

$$\theta = \tan^{-1}\left(\frac{V_y}{V_x}\right) \tag{16}$$

Hot-wire Calibration

Velocity-Voltage Calibration

A standard DISA 55M10 CTA constant temperature hot-wire anemometer and a DISA calibration air jet nozzle were used to perform the calibration. The anemometer was set up initially as described in the instruction manual. The wire was operated in the jet nozzle flow with an angle of 90°, ensuring the wire perpendicular to the flow direction. The voltage output with each variation of the velocity(from zero to 50m/s) was sampled and averaged then automatically recorded as a calibration data file. The data file was input to a polynomial curve fitting program and a velocity-voltage relationship was found.

$$V(E) = C_0 + C_1E + C_2E^2 + C_3E^3 + C_4E^4$$

where C_0, C_1, etc. are calibration constants. It is a common method to use King's law to fit the calibration curve but it was found that a polynomial method is more suitable for the case of very low velocity. **Fig.3-8** shows an example of the calibration results.

Calibration of Deviation From Cosine Law

In Hinze yaw angle relationship, the relationship between the maximum flow cooling rate ($V_{\theta=0}$) and flow cooling rate at angle θ can be expressed as follows,

$$V_e^2 = V^2(K^2 sin^2\theta + cos^2\theta)$$

where θ is flow angle with respect to the normal to the axis of the wire and K is an experimentally determined parameter reflecting deviations from the cosine law (given by K=0).

As **Fig3-9** shows, the expression above agrees well with the calibration result for a common type P11 hot wire (K=0.26), however, a slanted wire differs. **Fig.3-10** shows the yaw characteristics of a 54.7° slanted hot wire. Due to the shielding of the longer prong, the yaw characteristics from 0° to 180° are no longer symmetrical with those from 0° to -180°. This indicate that a different calibration curve is required for negative yaw angles, as ignoring this difference can cause significant errors.

3-D Velocity Direction Calibration

The velocity direction calibration discussed above reflects the deviation of the single slanted wire from the Cosine Law, but this by no means guarantees that the 3-D result derived from three separated results is accurate. Three-D direction calibration was carried out by using the 3-D flow measurement method to measure a known flow to get information about the error. A special instrument with which the flow direction against the probe can be varied to examine both yaw and pitch sensitivity of the probe were used.

From a great amount of calibration test with different ϕ and θ, the experimental relationship between ϕ_{err} and angle ϕ', $\phi_{err}=f_1(\phi')$, and $\theta_{err}=f_2(\theta', \phi')$ can be determined by the method of least squares .

Fig.3-11 and **Fig3-12** shows respectively the calibration result of flow angle ϕ and θ (refers to the drawing in **Fig3-11** for the definition). Put this result into computer for result correction and measure a known flow again and an accurate result was obtained. The error is not independent of the velocity, therefore, calibration for different flows is required.

Restrictions

- The method cannot be used in time-dependent flow measurement unless the flow is periodic, because the method needs three consecutive measurements which involves time change.
- From the calibration above we can see, the method can only be used in situations where the range of flow angle is known to fall within the calibration range of the probe. The calibrated range is restricted due to the prong shielding as the longer prong fall upstream of the sensor.
- The equations (1 to 4) in section 3.31 remain valid only if

$$v_j^2 < v_k^2 + v_i^2 - 2K^2V$$

$$v_i^2 < v_j^2 + v_k^2 - 2K^2V$$

$$v_k^2 < v_i^2 + v_j^2 - 2K^2V$$

In order not to exceed the above restrictions, it is necessary to position the probe in such a way that i- direction (first position of the probe) is within $\pm 20^\circ$ of the mean flow direction. Thus the method requires prior knowledge of the approximate mean velocity direction. This can be found by a trial-and-error method based on the fact that cooling is maximised with the sensor perpendicular to the mean velocity vector or by using flow visualisation techniques. In this study, both wool tufts for flow visualisation and trial-and-error methods were used.

Uncertainty of the measurements

Wall interference and probe stem affect need to be taken into account and related to how the flow around the probe head behaves during rapid changes of direction and velocity. Such effect may be complex, especially if vortices are shed from the wedge apex. It is not known what effect such phenomena may have nor how valid it is to use the steady-state aerodynamic calibration in a highly unsteady (stalled) flow field. More work is required to investigate these issues.

The method of 3-D measurements with a slanted hot-wire proposed by **Whitfield et al. (1972).** has been used by many others. In this method, it is assumed that only first order cooling effect are important, i.e. the probe is sensitive only to the flow perpendicular to its axis and insensitive to the flow parallel to the wire. In fact, there is an significant error if the deviation of the cooling effect from the **cosine** law is ignored. Considerable efforts have been made to increase the accuracy of the measurements and careful calibration of the deviation coefficients and 3-D calibrations of the probe were carried out beforehand as described previously. After correction, less than ±2% of the measurement uncertainty in time-averaged flow measurements would be expected in most of measurement range. Since the movement of the hot-wire probe was restricted to the radial direction only and the axis of the probe had to be in radial direction, the yaw angle and velocity measurements were affected by the stem of the probe if the mean velocity vector is in radial sense. In this case the uncertainty of the measurement would be a bit higher.

3.5 CLOSURE TO THE CHAPTER

The experimental fan rig and detailed casing treatment design have

been explained. Low speed responding instrumentation used in the performance tests and high speed data acquisition system used in flow measurements were detailed. The general measuring techniques used in both time-averaged and time-dependent measurements were presented, including the techniques of three-dimensional flow measurement with a slanted hot-wire. The results and discussion of the performance test and effectiveness of the vaned recess anti-stall devices will be provided in Chapter 4, and the flow measurement results and discussion will be given in Chapter 5. The further particulars and special problem encountered in the measurements will be detailed in the responsive Chapters where the techniques are discussed.

CHAPTER 4 EFFECTS OF THE CASING TREATMENT

In this chapter, detailed experimental procedure, test results and analysis of the overall performance are presented. The performance of the casing treatment is evaluated by stall margin improvement, pressure rise improvement and peak efficiency loss. The effect of the vane number, rotor axial chord exposed to the recess, inlet width, and outlet flow angle of the casing treatment are examined.

4.1 OVERALL PERFORMANCE

Definitions

The overall performance of the compressor with various casing treatments was examined. Total to static pressure rise coefficient ψ and total to total efficiency η are presented as a function of flow coefficient ϕ.

Total to static characteristics are widely used, since they are generally true when the total pressure at the compressor inlet and static pressure at the outlet are nearly uniform over the compressor annulus at a given operating point. Even at stall condition, averaged static pressure is almost uniform although the static pressure measured in stalled flow upstream of the rotor is usually higher than that in unstalled flow region due to the whirl flow (see **Fig.5-14** the results of the pressure measurements). The pressure rise coefficient ψ is defined by

$$\psi = \frac{P_{2s} - P_{1t}}{0.5\,\rho\,U_m^{\,2}} \qquad (4-1)$$

where

P_{2s} is static pressure downstream of the rotor, obtained by averaging the readings from the static tappings mounted at four circumferential positions at the tip and hub 58mm downstream the trailing edge of the

rotor.

P_{1t} is total pressure at the inlet. In the calculation, atmospheric pressure at the inlet was used as the intake pressure loss is negligible;

U_m is blade velocity at the mean blade height.

Total to total efficiency η is calculated by

$$\eta = \frac{60M\Delta P}{2\pi N\tau\rho C_p} \qquad (4-2)$$

This is extra

where

M is mass flow rate (kg /s);

ρ is air density (kg / m^3);

C_p is specific heat of air at constant pressure(J /kg. K);

τ is measured torque (Nm);

N is measured rotor speed (rpm);

ΔP is total pressure rise and $\Delta P = P_{2t} - P_{1t}$ (Pa).

P_{2t} denotes the average stagnation pressure measured at 56mm downstream of the trailing edge of the rotor. It was found that taking an accurate measurement of P_{2t} is not an easy job because the direction of the absolute velocity at the outlet varies with both mass flow rate and radial position of the measuring probe. So usually the mass-average value of P_{2t} is required. In the case of a compressor stage with a stator installed, the existing total pressure rakes can provide a facility for measuring P_{2t}, but in the case without stator, the rakes can not be used because it is impossible to orientate each tapping to the flow direction. A 3-hole pneumatic probe was used to make spanwise traversing measurement of P_{2t} at five stations: 10%, 30%, 50%, 70%, 90% span.

The overall performance characteristics were measured at a constant (corrected) rotational speed of 1500rpm. The performance of the casing treatment is evaluated by the parameters *stall margin improvement* $\Delta\phi$ (**Takata** et al. 1977), *pressure rise improvement* $\Delta\psi$ and *peak efficiency loss*

Table4-1 Overall Performance of the Isolated Rotor With Various Casing Treatments

Build No	Sketch	Description	Ce/Ca	$\Delta\phi$	$\Delta\psi$	$\Delta\eta_m$	Note
0	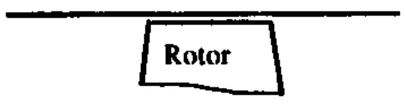	Solid Casing	/	ϕs= 0.61	ψ_m= 0.26	η_{sm}= 93.2%	Datum Fig4-1
1-1	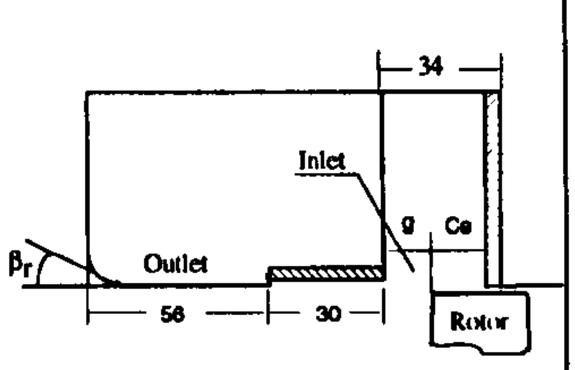	g=12,βr=90°	66%	51.0%	115%	0.5%	Fig4-2,
1-2		g=7, βr=90°	66%	51.2%	114%	0.45%	
1-3		g=5, βr=90°	66%	51.1%	115%	0.51%	Fig4-9
1-4		g=1, βr=90°	66%	29.2%	71.9%	1.2%	Fig4-8
1-5		g=5, βr=5°	66%	16.4%	58.0%	-1.1%	Fig4-9
2-1	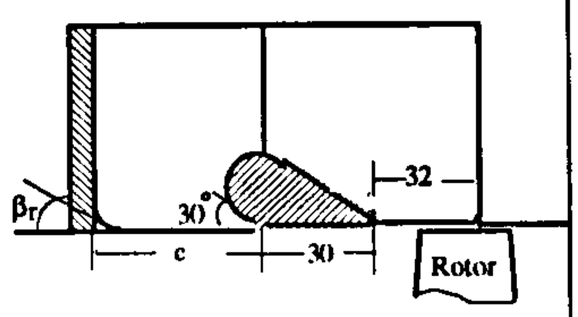	βr=30°, c=50	62.5%	36.7%	42.8%	0.4%	Fig4-9
2-2		βr=90°, c=50	62.5%	58.7%	114%	0.75%	Fig4-9
2-3		βr=30°, c=58	62.5%	46.4%	76.2%	0.67%	
2-4		Cut back vane L.E	62.5%	17.3%	92.3%	1.03%	
3-1	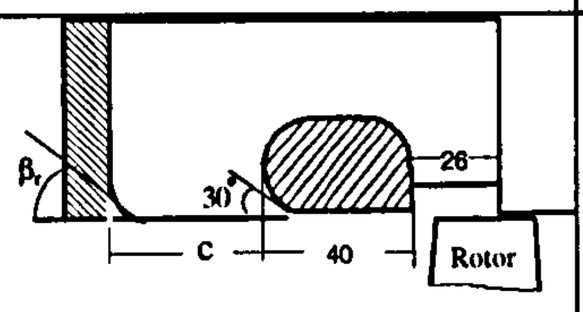	βr=90°, c=40	66%	62%	106%	0.01%	
3-2		βr=90°, c=54	66%	67%	120%	-0.5%	Fig4-2
3-3		βr=60°, c=40	66%	42%	62%	-0.8%	

$\Delta\eta_m$ on the base line of the solid casing build.

$$\Delta\phi = 1 - \frac{\phi_{ts}}{\phi_{ss}} \qquad (4-3)$$

$$\Delta\psi = \frac{\psi_{tm}}{\psi_{sm}} - 1 \qquad (4-4)$$

$$\Delta\eta_m = \eta_{sm} - \eta_{tm} \qquad (4-5)$$

where

ϕ_{ss} flow coefficient at stall point for solid casing;

ϕ_{ts} flow coefficient at stall point for treated casing;

ψ_{sm} peak pressure rise coefficient for solid casing;

ψ_{tm} peak pressure rise coefficient for treated casing;

η_{sm} peak efficiency for solid casing;

η_{tm} peak efficiency for treated casing.

The treatments were tested at various setting of the design parameters such as axial stations relative to the rotor leading edge, inlet width, out-flow angle (β_r see Table4-1) etc. The results were shown in Table4-1. The following discussion relates to the optimum position for each treatment.

Solid Casing

The performance of the solid casing build is shown in **Fig.4-1**. The pressure rise coefficient increases smoothly from 0.07 to 0.26 while the mass flow coefficient ϕ drops from 0.76 to 0.61. The former point corresponds to the throttle being fully open and the latter point corresponds to the peak pressure rise. This part of the pressure rise characteristic is referred to as the unstalled characteristic. When ϕ is between 0.61 and 0.41, the compressor suffers tip stall and the flow breaks down with an abrupt fall in pressure rise which is shown by a dotted line. The operation is unstable and no accurate measurement is available in this region. The compressor operation becomes more stable with pressure increasing as the flow rate is further reduced. As this occurs, the compressor enters a deep stall regime and nearly half the annulus height ahead of the rotor is occupied by axisymmetrical swirling flow with strong reverse flow in the tip region. On the other hand, the axial flow in the hub region is quite substantial and uniform as shown in Chapter 5, and the fan with the solid wall casing appeared to be tip critical. In the stalled region, the work input is considerably reduced.

Configuration 1

The optimum results for each configuration tested are shown in **Fig.4-2,** in which the result for solid casing is used as a base line.

It will be noted that Configuration 1 gave worthwhile stall margin improvement ($\Delta\phi$=51%) and pressure rise improvement ($\Delta\psi$=115%) with 0.5% efficiency penalty ($\Delta\eta$=0.5%). Between ϕ=0.61 and ϕ=0.3 which is referred to as extended unstalled region, there was no noticeable evidence of

rotating stall, however, the noise level does increase as the flow rate is reduced. There was also a sign of stall inception at flow coefficient around 0.4, indicated by a dip in the pressure rise curve. This result is very comparable to the results obtained by **Azimian** et al (1989) for the 48 vane build 14. This was not too surprising as this difference was the number of recess vanes and the result indicates the change to be insensitive to this over the range examined.

Configuration 2

Configuration 2 gave an improvement in stall margin over Configuration 1 ($\Delta\phi$=59% compared with 51%), but it had no advantage in pressure rise ($\Delta\psi$=114%) or efficiency ($\Delta\eta$=0.75%). Additionally, a whistling noise was heard during the experiment, which was apparently due to the vane/rotor blade interaction. Cutting back the vane leading edges in a modified build by 20mm eliminated the noise but reduced the performance ($\Delta\phi$=17.3%, $\Delta\psi$=92.3% and $\Delta\eta$=1.03%). However, the results were not conclusive as after trimming, the vanes were then not cambered sufficiently to ingest the reversed flow from the rotor tip as effectively, so the reason for the performance shortfall may not be attributed to the cut back.

Configuration 3

The best results were obtained with Configuration 3 (they are also shown in **Fig.4-1** for clarity of comparison). Up to 67% of stall margin improvement, more than twice of pressure rise ($\Delta\psi$=120%) and a slight increase in peak efficiency were obtained. The signs of stall inception at flow coefficient around 0.4 found in both configuration 1 and configuration 2 were removed and a smooth pressure rise characteristic in extended unstalled region was obtained. These advantages are attributed to the new vane passage. It is also noteworthy that the peak efficiency point was found to be moved to a higher flow rate, ϕ=0.75, compared to that for the other configurations at ϕ=0.72.

Generally, all the configurations have offered a potent improvement on stall margin and remarkably increased pressure rise with negligible change

in peak efficiency. It appeared that the vane shape tested had only marginal effects on the rotor performance. What is surprising is that the treatment converted the fan rig from a tip critical to a hub critical machine. It is discovered that tip stall found in the solid wall build at low flow rate is completely removed by the vaned recess and instead, flow separation in hub region (possibly stall) was found when the flow rate is below the extended stall point. Because this would sets a new limit to the stall margin, it is not too surprising to find similarity of results for the modified builds.

Effect on Work Input

The work input of the test fan can be derived by measured torque τ and rotor speed N and mass flow M, i.e.

$$\Delta H = \frac{2\pi N\tau}{60M}$$

Fig.4-3 shows the work input characteristics in term of the work coefficient $\Delta H/U_m^2$. It was found that in the stalled region, the work input is considerably reduced with solid casing and the casing treatment caused a large increase in work input with the pressure rise in the extended unstall range. The work input characteristics for three treated builds are very similar. Work input coefficient for configuration 3 achieved the highest value of all, and so does the pressure rise.

The case of the solid wall configuration at stalled condition can be approximated to cells of zero axial velocity (M=0) and to regions of high axial velocity (unstalled). This implies no work in the stall cell and a low work coefficient in the unstalled region. With casing treatment, However, rotating stall is not permitted and so the work coefficient goes on increasing as flow rate decreases. That more work input is required to maintain higher pressure rise with the treatment may be the most pertinent point for explaining why the treatment does not bring out a marked increase in efficiency in the extended unstall range even at the point, for example ϕ=0.4 (see **Fig.4-2**), where the difference between the two pressure rise curves is so large.

4.2 EFFECTS OF MAJOR DESIGN PARAMETERS

A vaned recess casing treatment is to replace the original solid wall casing with a recess casing which is incorporated into the fan casing and positioned partly over and upstream the rotor blade tips. Inside the recess casing is usually equipped with guide vanes and a shroud ring. As mentioned before, the purpose of the guide vanes is to remove as much as possible of the whirl components of the reversed flow from the rotor tips into the recess. Besides the function of separating the recess flow and main flow passage, the shroud ring fitted to the inner edge of the vanes also serves as a middle reservation part between entry and exit of the recess.

It is proved that the recess casing treatments described above have a significant beneficial effect on fan/compressor performance. However they are not functionally equal. Some are more effective than others. The effectiveness is strongly influenced by the treatment design, and differs with individual fan or compressor used. There has been no purely theoretical method can be followed to optimise the design and often comprehensive tests are indispensable. It is however almost impossible that costly experimental tests cover all possible fans. Identifying the critical factors and some guide lines for casing treatment design are therefore desirable, although in some circumstances, the findings in a particular machine cannot be straightforwardly transferred to others. This section will investigate the critical factors for the casing treatment design and elaborates only the main points here.

4.2.1 Shape of Recess Guide Vanes

The recess vanes are essential to remove the tangential component of the recess flow and reintroduce it into the main stream. The design of the vanes must enable the treatment to achieve these gaols and an effort must be made to avoid causing any separation. It was thought that there might be a potential improvement by a proper guide vane design.

The investigation was carried out with different vane shapes to obtain

additional information regarding the potential gain in stall margin available from optimum treatment configurations. Three configurations in all were designed and tested. As previously mentioned, it was found that the results of the modified builds are very similar, see **Fig.4-2**. It appeared that the vane shapes tested had only marginal effects on the rotor performance. Nevertheless, this is not conclusive as hub stall is discovered in the test fan when the flow rate is below the extended stall points as evidenced by the flow measurement and wool tufts discussed in the next chapter. It is the hub stall that sets a new limit to the stall margin and further optimising the casing treatment could not significantly change it. This serves to explain why the three different casing builds yielded very similar results.

Although results of the modified builds are some what disappointing, it is clearly an advantage for this kind of machine in view of the close association with the production cost. A complicated design should always be avoided when a simpler one will equally serve the ends. It is therefore

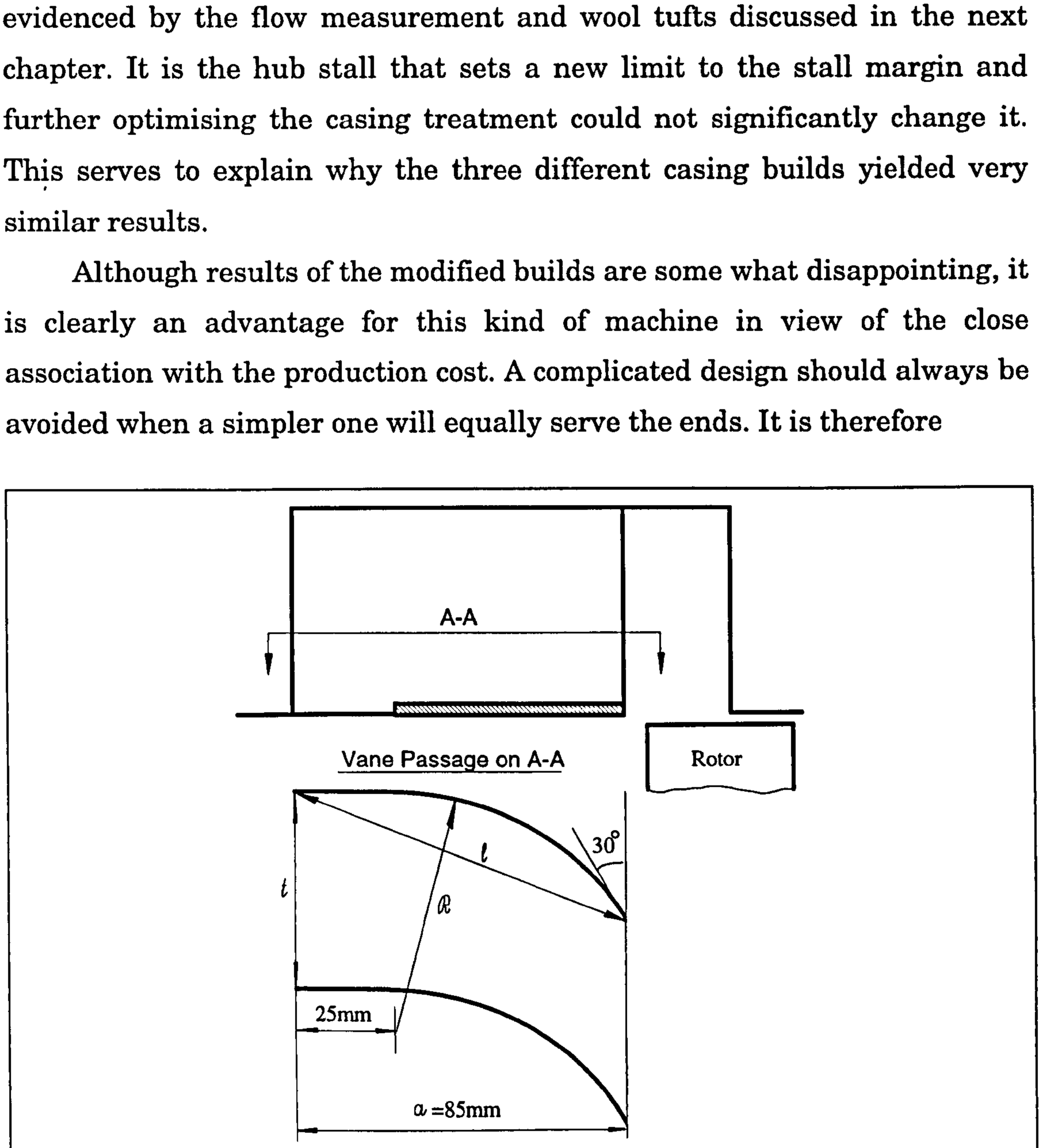

Fig.4-4 Sketch of Recess Vane and Arrangement---Example 1

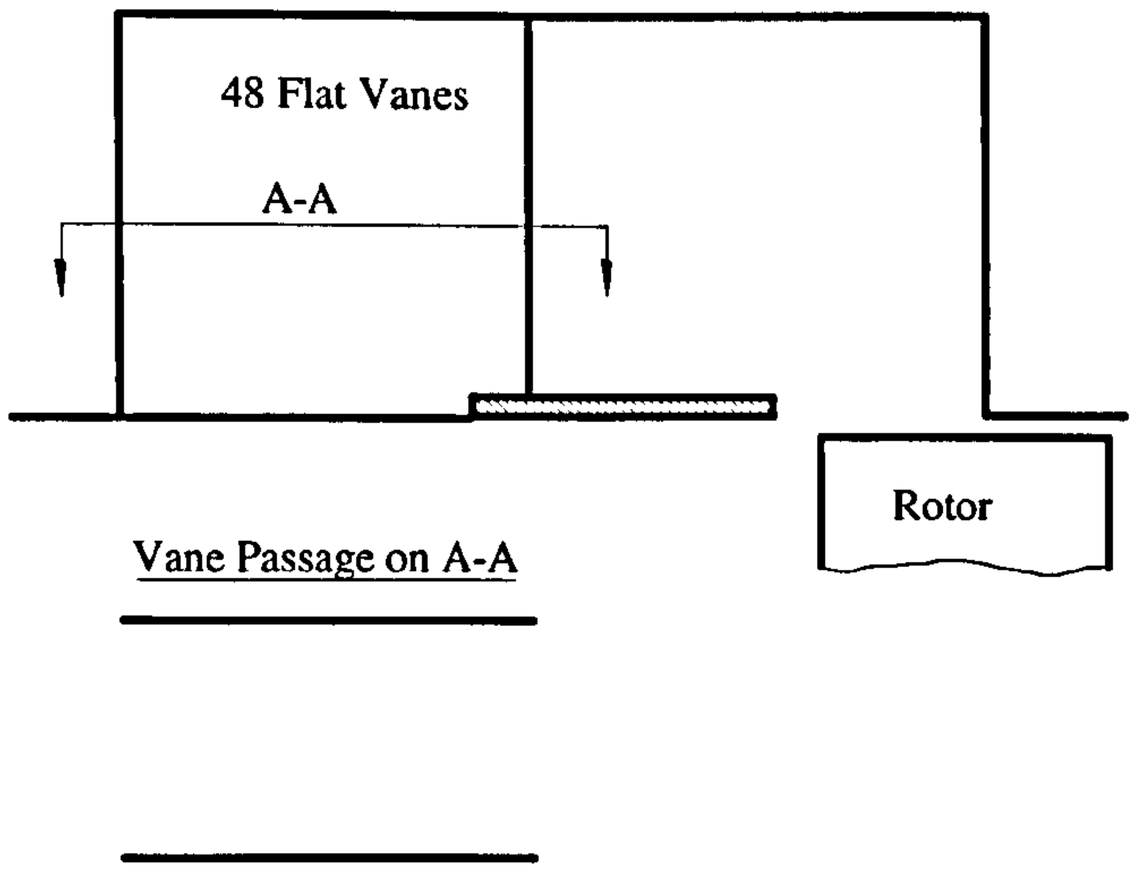

Fig.4-5 Sketch of Recess Vane and Arrangement---Example 2

advisable to select a simple vane structure if there is no significant performance loss caused. As an example, the modified configuration 1 shown in **Fig.4-4** (page 52) consists of a flat part and a untwisted arc part with a relatively larger arc radius to reduce the separation. In the untwisted arc profile vane design, the deviation of the out flow angle which is often encountered should be considered. The plane part of the vanes serves to reduce the deviation. A further simplified design, a design without the circular arc components but with more plane vanes as shown in **Fig.4-5**, is believed worth a try. High incidence and probable separation is expected in this case but it might not be important if you pursue a low production cost.

4.2.2 Optimum Pitch of Recess Guide Vanes

The number of the vanes is of great importance to the functional effectiveness, efficiency loss and production cost as well. It may be asked what is the most favourable blade pitch, which is a great concern to us. The question to be answered can be outlined in following way. Where the blade pitch is too narrow the surface friction will lower the efficiency. Where the pitch is too large separation occur with high losses, and swirl cannot be removed as effectively. According to the research by **Azimian** et al.(1989),

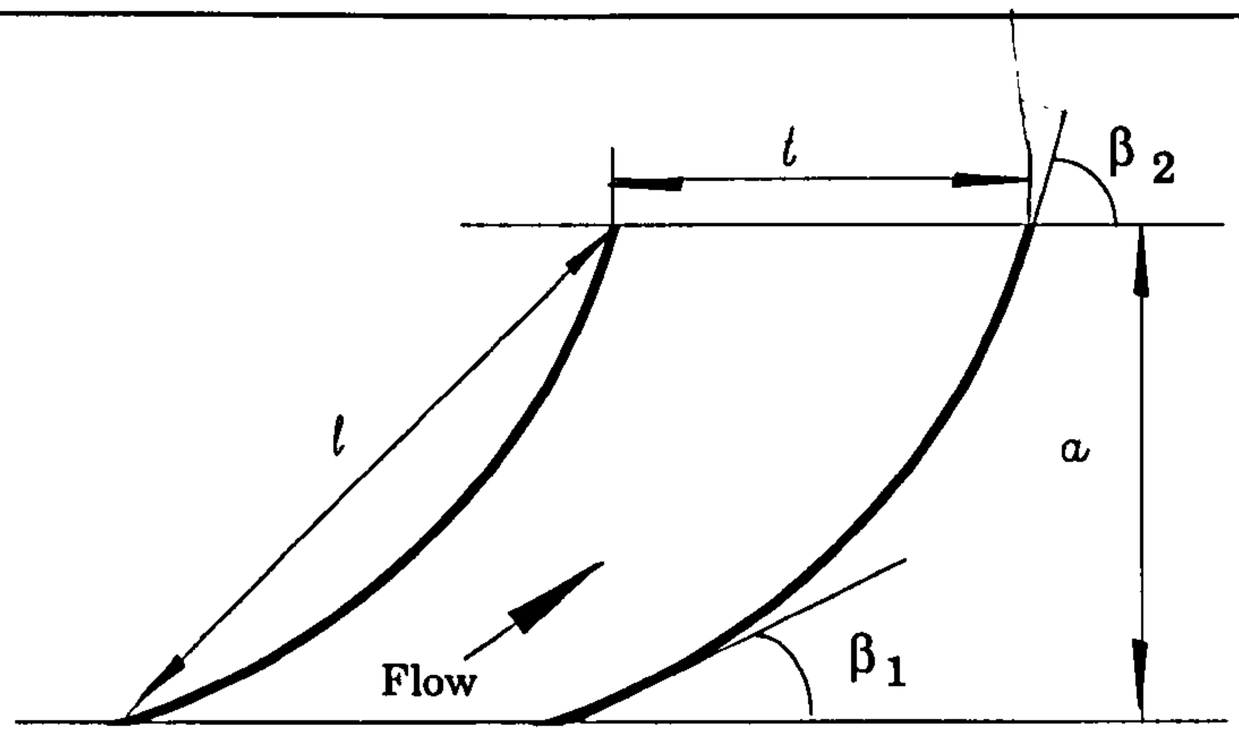

Fig.4-6 Optimum blade pitch according to **Zweifel**

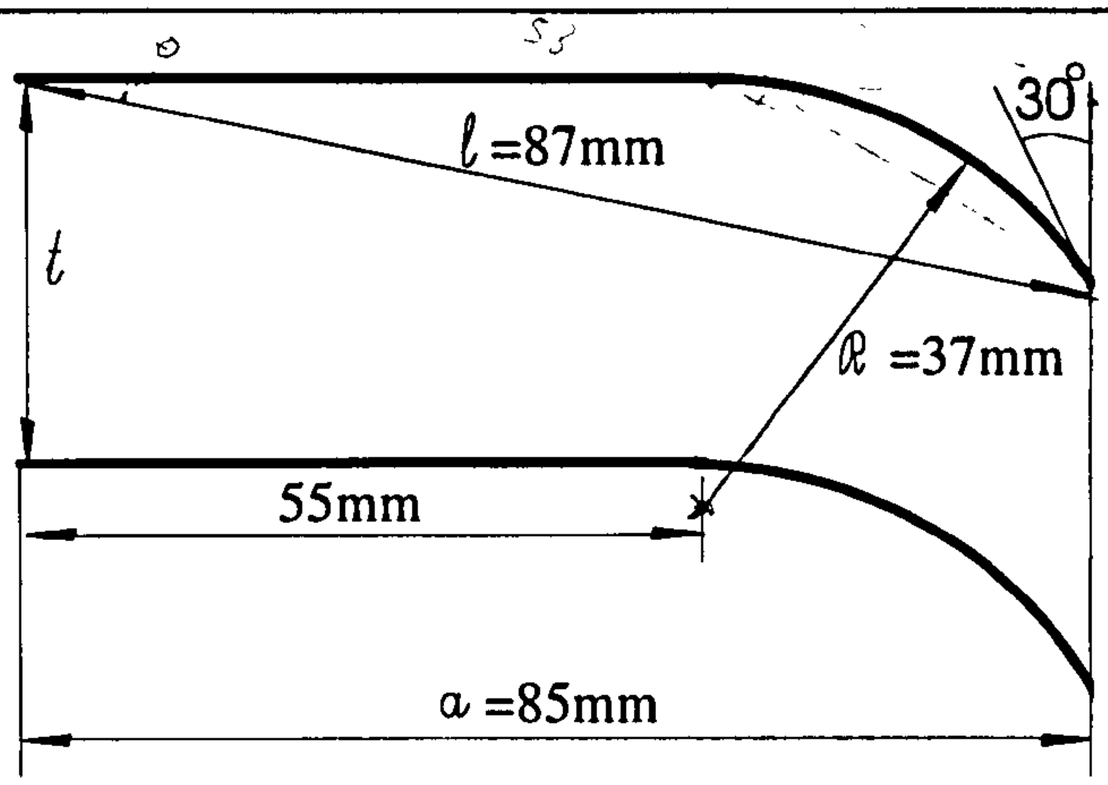

Fig.4-7 Sketch of the Recess Guide Vane of Configuration 1

the 48 vane builds showed a much better result than vaneless builds. The author thought that 24 vane builds gave a further improvement, but this was an ambiguous conclusion as in the test, not only the number of vanes was changed but also other geometrical parameters were significantly changed. This made it difficult to simply conclude which modification was the major contributor.

According to **Zweifel**, the most favourable blade pitch for a cascade (**Fig.4-6**) can be calculated by the formula:

$$\frac{a}{t} = 2.5\sin^2\beta_2\left[\cot\beta_1 - \cot\beta_2\right]$$

In the case of configuration 1 (see **Fig.4-7,** page 54),

$$\beta_1=30^\circ,\ \beta_2=90^\circ,$$

$$a/t = 2.5\cot\beta_1 = 4.33$$

$$l/t = 4.33/\cos 30^\circ = 5.0$$

$$t/l = 0.2$$

This implies that the optimum pitch should be 1/5 of the vane chord in order to deflect air from 30° to 90°. According to this analysis based on **Zweifel**'s formula, the pitch of the arc vane in configuration 1 was too large (or the radius was too small). This is probably the reason for the separation observed in the recess. The design with the same pitch but larger arc radius, as shown in **Fig.4-4**, could be better.

The latest experimental result shows that the pitch has only a marginal effect in the range tested. **Table4-2** shows the performance of the casing treatment with various number of recess blades. As already stated before, the result for the 24 vane build is very comparable to the results obtained by **Azimian** et al (1989) for the 48 vane build, indicating the change of overall pitch/chord ratio to be insensitive to the performance over the range tested. However the efficiency for 24 vane build was lower due to more severe separation suffered.

By means of **Zweifel**'s formula, the favourable pitch/chord ratio can be simply chosen. However, it was understood that vane profile of configuration 1 is not a common type and flow through the vane passage is also of some what peculiar, and therefore **Zweifel**'s formula does not accurately apply. One thing which should be borne in designer's mind is that the more blades the more production cost. The experimental results above indicates that much higher pitch/chord ratio does not make any significant difference. Additionally, the number of rotor blades should be considered since self-oscillation and resonant noise may occur when the same or an integer multiple of the number of rotor blades is chosen.

Table4-2 Effects of Number of Recess Blades

Number of Vanes	Pitch/Chord♣	Δφ(%)	Δψ(%)	Δη(%)♠
0		-2	-11.2	2.1
24	0.85	51.5%	115	0.5
48	0.42	50*	125**	-1.5

♣ at diameter d=508+56 mm

* taken from Azimian (1987)'s result for build 14

** derived from Azimian (1987)'s result for build 14

♠ positive value is a loss in efficiency

4.2.3 Rotor Axial Chord Exposure

The amount of the rotor axial chord exposed to the recess has a crucial influence on the behaviour of the fan. Azimian(1989)'s result showed that builds with more than 50% of rotor axial chord exposure were favourable and 67% were the best. However, no detailed information how the axial position effects the performance is given. Being aware that this might be related to the mechanism of the casing treatment, it is worth elaborating here.

Fig.4-8 provides the results of Configuration 3 in various axial position related to the rotor, which shows clearly how *Ce/Ca,* the amount of the rotor axial chord exposed to the treatment, affects the stall margin, pressure rise improvement and fan efficiency. This result indicates two distinct regions where performance is relatively insensitive to position (below *Ce/Ca*=40% and above *Ce/Ca*=67%) but that the transition between them is critically influenced by position and that the best result are achieved at *Ce/Ca*=67% where there is no apparent loss of efficiency. It appeared that the stall margin is significantly improved only when the middle part of the chord is exposed. More than 50% of blade chord exposure results in a very good improvement, whereas a poor improvement obtained when *Ce/Ca*<40% and almost none or a negative stall margin improvement

when *Ce/Ca* very low. On the other hand, the question arises: is it necessary to expose the front part of the rotor chord? The question will be answered in the next section on width of the Inlet.

It is well known that fan efficiency falls catastrophically as the blade tip clearance increases in size. In general, a fall of 1-2% can be stated to be the rule for a tip clearance increase 1% of rotor blade height. From this point of view, a exacerbated performance in unstalled flow region by the recess casing treatment may be expected as more than 50% of the rotor chord is exposed and gives a massive tip clearance to the front of the blade. In fact, this is not the case, even higher performance was obtained in some optimum builds. **Fig.4-8** shows an intriguing feature of the peak efficiency loss against the rotor chord exposure. When *Ce/Ca*<30%, the loss is about 2%, and when 40%<*Ce/Ca*<70%, there is no significant efficiency change, and when *Ce/Ca* big than 70%, the loss increases with exposure increase. Note that only about 2% loss in efficiency found as 90% of the rotor chord is exposed. Although there is some uncertainty in the efficiency measurements, they are quite repeatable.

It appeared that more than 50% of rotor axial chord exposure was favourable choice for a medium loaded fan or compressor. Bard (1993) obtained his best result by placing the casing treatment just upstream (i.e. *Ce* was approximately zero) of the industrial fan rotor which has a relatively low load. This suggests that optimum rotor exposure may have something to do with blade loading of a fan/compressor. It may be that the higher the blade loading, the more the instability, and more rotor chord exposure is required to improve the characteristics in the low flow rate range.

4.2.4 Width of the Inlet

The width of inlet port of the recess (see **Fig.3-3**) is an important parameter in the design, which is determined by the axial rotor chord exposed to the recess (C_e) and optimum gap (*g*) between the leading edge of the rotor blade and inner ring of the casing treatment. The effect of the gap g has not been investigated. The examination may lead to an answer to the

question: is it necessary to expose the front part of the rotor chord?

A series of experiments with various gaps and fixed Ce/Ca=2/3 were conducted. The results are shown in **Fig.4-9**. When 12mm> g > 5mm, the performance curves are almost identical. When g was reduced to 3mm and 1mm, however, early stall at middle flow rate range was observed and a dip in the performance curves can be seen. It appeared that the gap between the leading edge of the rotor and inner ring of the casing treatment is not critical until it is reduced to 5mm (15% of the rotor axial chord). In other words, a useful reduction of overall treatment axial length can be expected (in this case, the width of the inlet port can be reduced by 21% of original length of 34mm without losing any performance). Therefore the favourable width of the inlet is to be 80%--85% of the rotor axial chord.

4.2.5 Outlet Flow Angle β_r

It is worth pointing out that the flow leaving the recess and injecting into the main flow plays an important role in stall margin improvement. The greatest concern to us here is what is the optimum direction for the flow to leave the recess, since the outlet angle β_r (with respect to axial direction, see **Fig.4-11,** page 59) of the casing treatment recess has a crucial influence of the interaction, and therefore is an important design parameter, but poorly understood. If the injection serves to remove blockage and energising the low momentum flow found in the tip region of the solid build, turned the reversed flow through 180 degree, one would believe that the flow should leaves the vaned recess in axial sense. In fact, the following test results clearly reveal that the out flow with zero axial velocity (leaves recess radially) is the most favourable choice.

A β_r=0° flow deflector was used in the outlet port of the casing treatment recess by **Azimian** et al. (1989) to turn the flow towards the direction of the mainstream and reduce the interruption to the main flow. The negative effect was considered to be due to the fact that it restricted the outflow area for the reverse flow to re-enter the mainstream and outlet angle β_r was too small.

The further experiments to re-examine the effect of the outflow angle

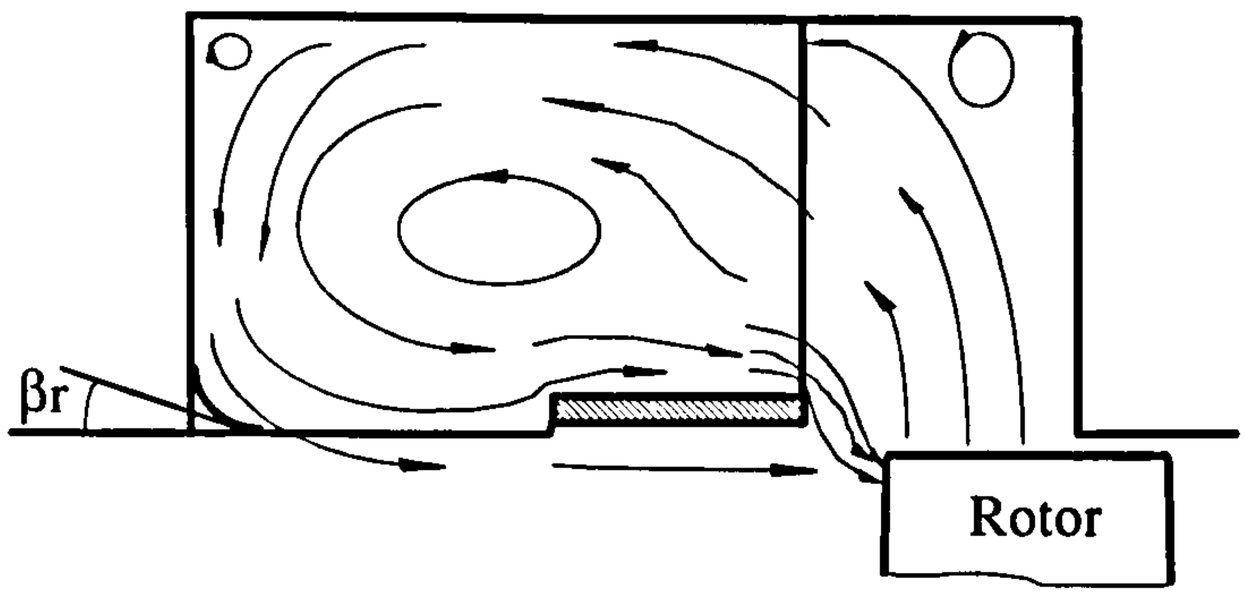

Fig.4-11 Sketch of the Recess Flow With a Small Outflow Angle β_r

was carried out with newly designed deflectors. The results shown in **Fig.4-10** clearly shows that the outlet angle β_r has a substantial influence of the performance and the most favourable angle is 90° (i.e. flow leaving recess in radial direction). All the builds with small outlet angle damaged performance. The experiments with the front wall of the recess and deflector moved further forward and backward made little difference although slightly better stall margin improvement but poorer pressure rise was observed when moved forward.

The mechanism involved has not been fully understood yet. The following discussion is thought to be pertinent to the explanation. The flow from the recess may need to cover about 50% of the span not only the tip region in order to bring the stall line to a very small flow rate. If β_r is too small, a great deal of reversed flow from the recess returns to the region immediately upstream of the rotor through the inside of the recess, instead of re-entering the mainstream as evidenced by wool tufts (**Fig.4-11**). Because of the turning angle of the vane, this flow increases the incidence and fan blade loading in the tip region, and consequently causes early stall. On the other hand, the other part of the recess flow is ejected into the very tip region of the rotor, as a result of excessive flow there, but under replenished in the region of 50--85% span where the flow is still severely stalled as flow rate is very low (say $\phi<0.4$). The radial flow from the recess may have a beneficial function of reducing the radial component of the main

flow within the rotor.

4.3 CLOSURE TO THE CHAPTER

This Chapter was focused on the effects of the vaned recess casing treatment on fan performance in both design and off-design conditions, and crucial points associated with the design of the devices. Detailed experimental data to examine the influence of the treatments on stall margin, pressure rise and operating efficiency of the test fan has been given, and more than 65% of stall margin improvements and over twice the pressure rise with insignificant peak efficiency penalties were obtained. The influence of the vaned recess was so crucial that it turns the fan into a hub critical machine. Because of the hub stall, it is not too surprising to find that the three recess builds with significantly different geometrical designs yielded very similar results.

The test fan has been proved to be tip critical with a natural solid wall casing, while it is the hub stall or separation that sets the limit to the stall margin of the treated fan. This is evidenced by detailed flow measurement results discussed in Chapter 5. The results described in this Chapter include some important features associated with the mechanism of the vaned recess but have not yet been elaborated. This will be left until Chapter 7 where all the relevant information, including that from the flow measurements (Chapter 5) and CFD results (Chapter 6), will be put together and analysed.

CHAPTER 5 DETAILED FLOW MEASUREMENT RESULTS AND DISCUSSION

The effect of casing treatment on flow field and flow in the casing treatment recess are of great importance to understanding the mechanism involved. There have been no quantitative measurements reported for steady and unsteady flow fields associated with the vaned recess casing treatment. Hence, fundamental understanding of the complex flow phenomena is poor and there is little with which to assess the integrity of prediction made by the growing number of CFD codes. The flows involved are complex and cannot be treated as a two-dimensional flow, since the radial velocity can be very large in the treatment recess and even in the rotor region. Therefore, a slanted hot-wire technique, as discussed in Chapter 3, was used to measure the velocity components in the rotor region and vaned recess, where the three-dimensional character of the flow was of interest. The supporting data were taken by means of a calibrated three-hole cylindrical pneumatic probe. Some important flow features which are related to the casing treatment are studied, while further detailed discussion of the mechanism involved is left to Chapter 7.

The method of 3-D measurements with a slanted hot-wire proposed by **Whitfield** et al. (1972). has been used by many others. In that method, it is assumed that only the first order cooling effect is important, i.e. the probe is sensitive only to the flow perpendicular to its axis and insensitive to the flow parallel to the wire. Present work found that there is a significant error if the deviation of the cooling effect from the **cosine** law is ignored. Considerable efforts have been made to increase the accuracy of the measurements and careful calibration of the deviation coefficients and 3-D calibrations of the probe were carried out beforehand as described in Chapter 3. After correction, less than ±2% of the measurement uncertainty

in time-averaged flow measurements would be expected in most of measurement range. Since the movement of the hot-wire probe was restricted to the radial direction only and the axis of the probe had to be in radial direction, the yaw angle and velocity measurements were affected by the stem of the probe if the mean velocity vector had a substantial radial component. In this case the uncertainty of the measurement would be higher than ±2% but less than ±4%.

5.1 ABSOLUTE VELOCITY PROFILE

As shown in **Fig.5-1**, the measurements were taken at the stations 6mm (17% of the rotor axial chord) upstream of the blade leading edge and 56mm (165% of the rotor axial chord) downstream the blade trailing edge. Because a casing flange made it difficult to arrange down stream measurements close to the rotor. Station 1 located 48mm (141% of the rotor axial chord) upstream of the rotor was to detect the influence of the recess

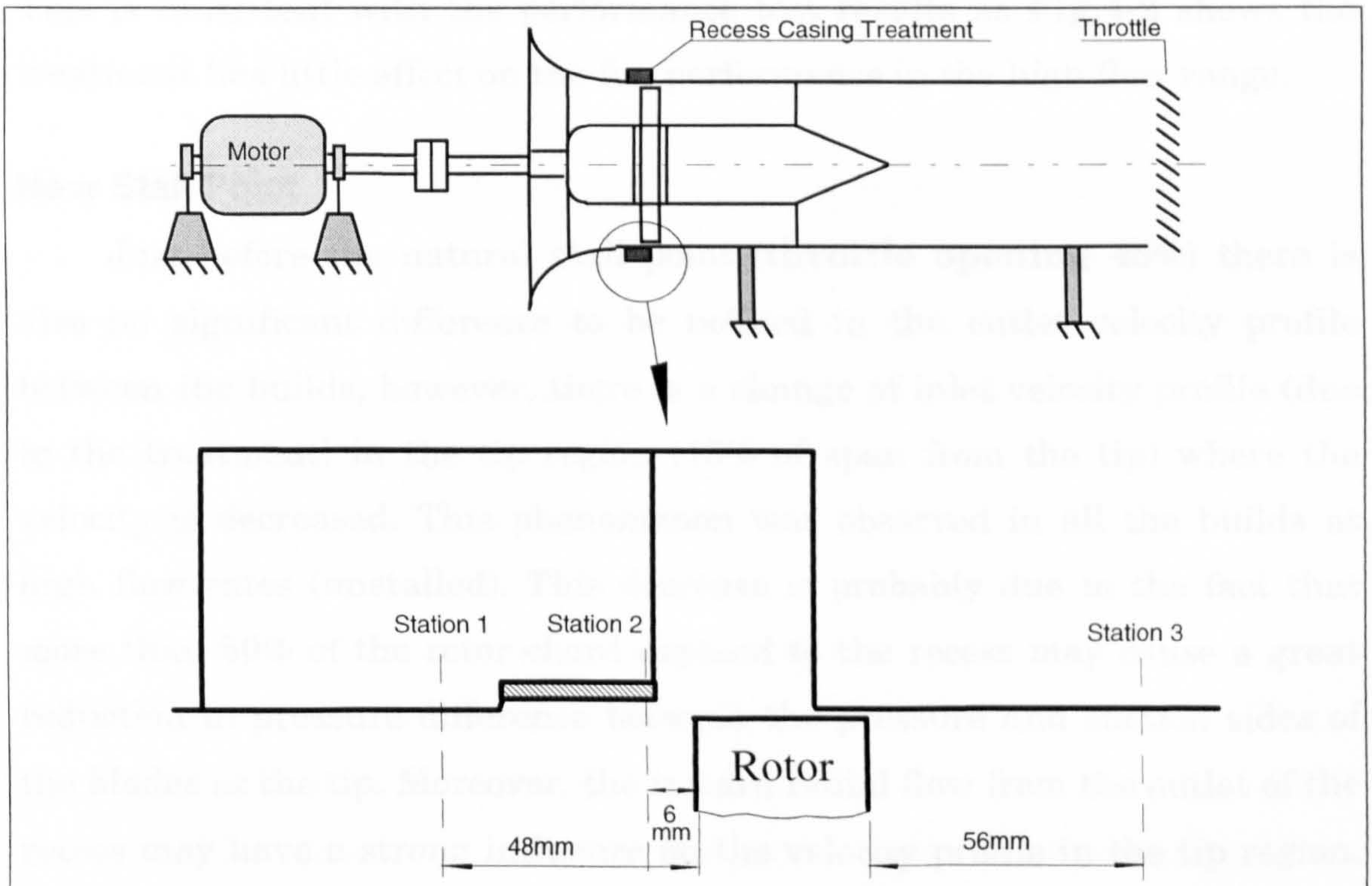

Fig.5-1 Flow Measuring Stations

flow by comparing with the flow at station 2.

The time-averaged radial profiles of the absolute velocity for the solid wall casing and treated casing (configuration 1) were measured at three flow rates (design flow rate, near natural stall point and near extended stall point) at stations described above. Data were averaged from fifty sample data taken at each probe location, which agree well with the pretest results averaged from 100 sample data.

At Design Flow Rate

At design flow rate (**throttle opening 60%,** throttle opening 85% corresponds to fully open), there is no significant difference between the upstream velocity profile of solid and treated builds as shown in **Fig.5-2, Fig.5-3, Fig.5-4** and **Fig.5-5**. Downstream of the rotor, both the solid and treated builds have also very similar profiles (**Fig.5-6** and **Fig.5-7**). These indicate that the vaned recess hardly affects the fan flow field before it is throttled to a high pressure-rise condition (near the previous stall point). This is consistent with the performance test results as **Fig.4-2** shows the treatment has little effect on the fan performance in the high flow range.

Near Stall Point

Just before the natural stall point (**throttle opening 45%**) there is also no significant difference to be noticed in the outlet velocity profile between the builds, however, there is a change of inlet velocity profile (due to the treatment) in the tip region (15% of span from the tip) where the velocity is decreased. This phenomenon was observed in all the builds at high flow rates (unstalled). This decrease is probably due to the fact that more than 50% of the rotor chord exposed to the recess may cause a great reduction in pressure difference between the pressure and suction sides of the blades at the tip. Moreover, the inward radial flow from the outlet of the recess may have a strong influence on the velocity profile in the tip region. This would cause a reduction of blade tip loading. On the other hand, the vaned recess removed the tangential components which were found in the

solid build (see **Fig.5-3**), and consequently increase the blade loading. These may serve to explain the gain of the performance found just prior to the natural stall flow rate.

Near Extended Stall Point

Upstream

At low flow rate, **throttle opening 10%** (near the stall point for the treated build), the flow behaviour in the solid wall build differed markedly from that found in treated build. **Fig.5-2** and **Fig.5-3** demonstrate a serious deformation of flow pattern with a high tangential velocity in the tip region approaching the rotor blade speed, and a high axial velocity (because of continuity) in the hub region which decreases to a substantially negative value at the tip. The profile has demonstrated that the fan suffers severe tip stall at this flow rate. Ahead of the rotor, the stalled flow occupied approximately 40% of the radial span. With the treatment (**Fig.5-4** and **Fig.5-5**), the reverse flow (occupied approximately 25% span) in the tip region found in the solid build at the same throttle opening was completely removed and the axial velocity is much more uniform and the strong tangential component is eliminated. Previously stalled flow which rotated in the rotor direction in the solid build now is confined to the vaned recess. The inward radial flow out of the vaned recess causes a decrease in axial flow around the outlet of the recess, consequently causing an outward radial component at station 2.

The velocity profiles of the solid build (**Fig.5-2** and **Fig.5-3**) are very similar at measuring station 1 and station 2. The differences between the velocity profiles for the treated build (**Fig.5-4** and **Fig.5-5**) at the two stations reflects the influence of the recess flow, which is dominant at the tip region. It is worth to note that the substantial negative radial velocity profile can be seen in the upper 40% of span. This inward radial flow from the recess injecting to the main stream plays a very active role as pointed out in Chapter 4, which had been received little attention before.

Downstream

At low flow rate, throttle opening 10%, differences can be noticed between the two builds. The high whirl component found in the solid build tip region was greatly reduced and flow blockage removed; nevertheless, the profiles for the two builds are surprisingly similar, considering the stalled regime of the solid build compared with unstalled condition with the treated build. It appeared that rotating stall has a stronger influence on the flow upstream of the rotor than downstream.

Velocity Triangles

The velocity triangles, **Fig.5-8,** based on the flow measurements described above provide a clearer picture of the blade loading for the two builds. At near stall flow rate (45% throttle opening), the velocity triangles for the treated and solid builds at the inner half of the span are identical and not shown here. The velocity triangles (**Fig.5-8a**) in tip region show the differences between the two builds, which reflect the effect of the recess flow. The velocity triangle for solid build at 80% span (see **Fig.5-8b** thinner line) is somewhat unusual but not too surprising because it was heavily stalled in the tip region at this flow rate (10% throttle opening). Because of the radial flow, the axial velocity components measured upstream and downstream the rotor are different. The difference is quite substantial in some cases.

The triangles, **Fig.5-8,** reveal that the treatment does not have the function of reducing the inlet flow incidence onto the blade. On the contrary the reduced whirl in the tip region tends to increase the incidence in most cases. These observations suggest that the stall margin improvement due to the casing treatment was not achieved by reducing the incidence in the tip region.

Absolute Flow Angle

In order to check the hot-wire results shown above, the absolute inlet flow angles and outlet flow angles were measured by a three-hole pneumatic

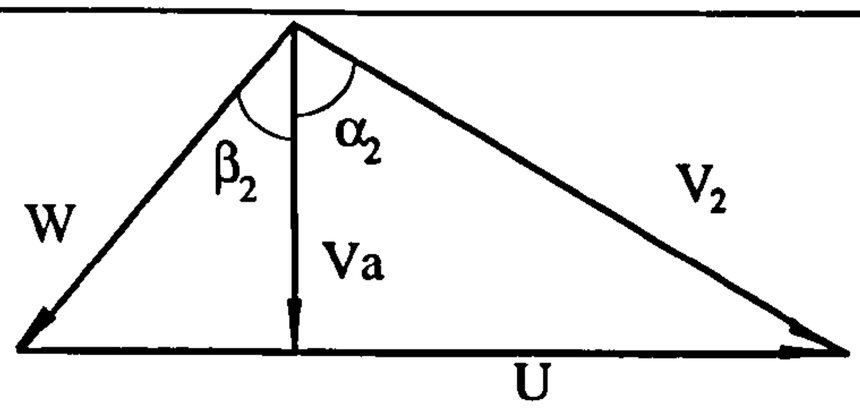

$$\delta 1 = (1.1 + 0.31\theta)\left(\frac{s}{c}\right)^{1/3}$$

$$\delta 2 = m\,\theta\left(\frac{s}{c}\right)^{1/2}$$

θ = camber angle; s = pitch; c = chord; m = a function of stagger angle

Fig.5-11 Designed Flow Angle α_2

probe at station 2 and 3 respectively.

The inlet flow angles and outlet flow angles for both solid and treated builds at high flow rates (unstalled) are shown in **Fig.5-9**. The flow angles of the two builds are very similar.

At low flow rate, near extended stall point, the flow angles for the solid build and treated build are very different, see **Fig.5-10.** The inlet flow angles of the solid wall build were above 90 degree in the tip region, indicating flow reversal, while the outlet angles was less than 90° implies no reversal of flow at the measuring station 3, however it does not mean that there was no reversal of flow in the tip region nearer to the rotor. For the treated build, the negative inlet flow angle in the first 20% span from the tip indicates a negative tangential component which also can be seen in **Fig.5-5.** This remains to be explained by further understanding the phenomena involved. Treatment reduced whirl velocity in the tip region, and result in much smaller flow angles. The high flow angles in the hub region indicates the flow blockage, probably corner stall there.

The flow angles of the two builds are very similar at high flow rate and quite different at low flow rate, which are consistent with the velocity measurements discussed above.

The design flow angles derived from blade angles β_2 (see **Fig.5-11**) are shown in **Fig.5-12** with a solid line without symbol. Compared with the

calculated flow angles, the measured flow angles are much smaller between 30% to 90% span. Moreover, over-turning is observed near the end-wall regions due to the effect of various flow mechanism such as annulus wall boundary layers, secondary flow and tip clearance flow. In order to gain further confidence in the measurement results, the flow deviation from blade angle is examined in **Fig.5-13**. The deviation is calculated based on two commonly used empirical models and the results show that they do not agree with each other very well. The measured flow angles show that there was a larger deviation. It is clear that if the above aspects are not taken into consideration and the measured Va and theoretical α_2 are used to derive V_2 and the dynamic pressure, an erroneous assessment of the fan performance will be obtained.

5.2 RADIAL PRESSURE PROFILE

In many cases the flow is rotational in an axial-flow fan, which causes a non-uniform static pressure change. It is useful to determine the spanwise variations of the pressure by radial traversing with a three-hole pneumatic probe. The total pressure and static pressure ratio (normalised by $0.5\rho U_m^2$) measured at station 1 and stations 3 for both solid build and build2-2 are shown in **Fig.5-14** and **Fig.5-15.** Because of the slow response of the probe, the data obtained at each radial location were of circumferentially time-averaged features.

In general, the casing treatment did not significantly alter the radial pressure profile before the stall point (i.e. throttle opening 45%) but did change it very much in the extended unstalled flow range of the treated build (i.e. to throttle opening 10%). In this low flow rate, with solid wall casing, an excessively high total and static pressure (produced by the high circumferential velocities) occurred in the tip region upstream of the rotor. The pressure profiles under these conditions differ markedly. Perhaps the solid casing is of little interest (because the rotor is heavily stalled), but the regularity of the treated casing results are notable at this low flow rate. At

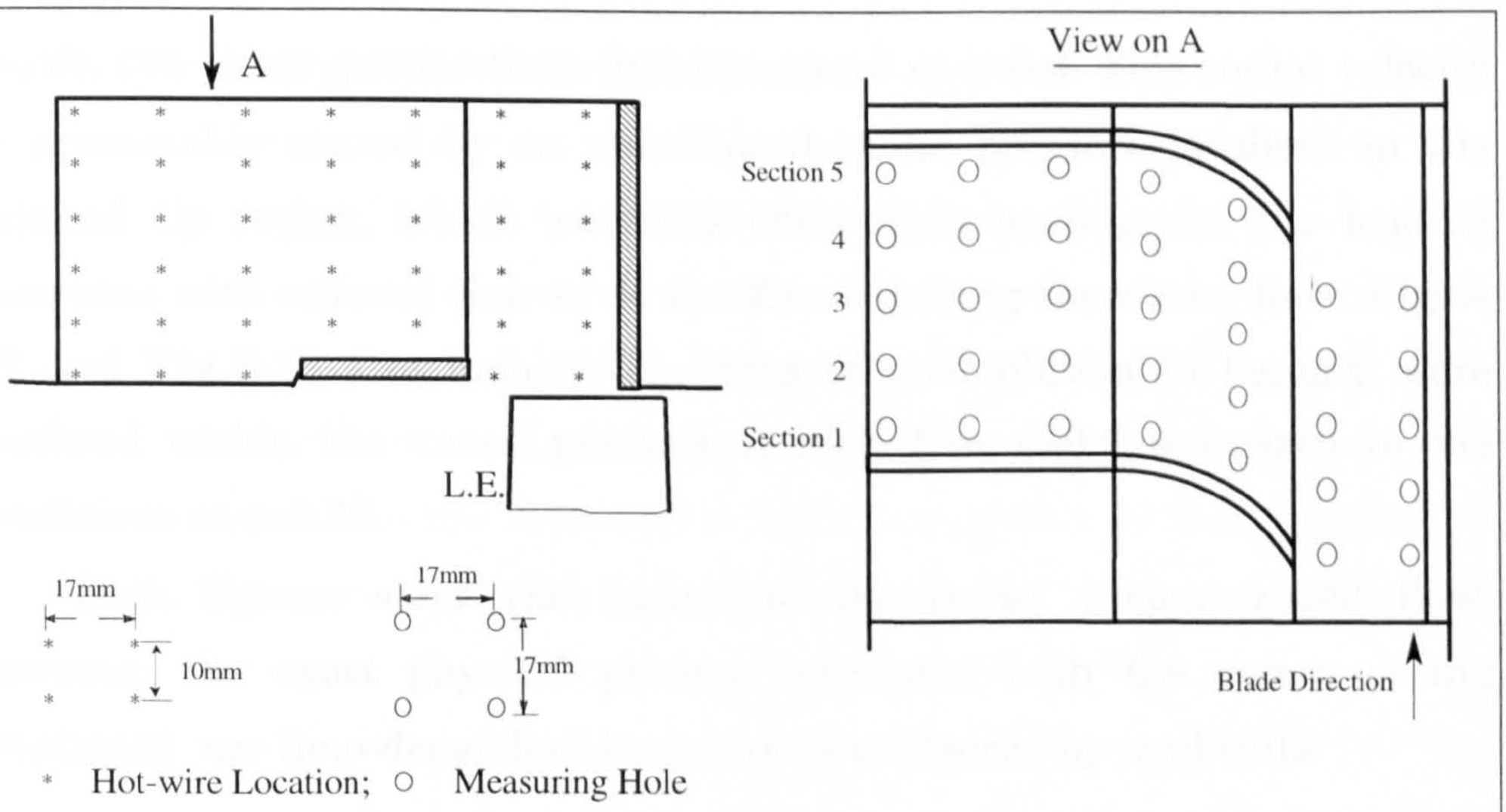

Fig.5-16 Sketch of the Hot-wire Locations

both flow rates, for the treated build, the upstream tip region were found to have decreased total pressure. This indicates that the treatment does not have the function of increasing the total pressure in the upstream tip region.

5.3 FLOW IN CASING TREATMENT RECESS

Flow measurements were taken in the casing treatment recess of configuration 1 by means of a slanted hot-wire in conjunction with the wool tuft. Because of the intense fluctuation of the flow, it was almost impossible to obtain a repeatable result of instantaneous flow measurement and only time-averaged results are presented. **Fig.5-17** and **Fig.5-18** present the time-averaged radial traverse results at ϕ=0.36 and ϕ=0.6 respectively. In these figures, the 3-D velocity components are shown by two sets of 2-D vector plots for various sections (as defined in **Fig.5-16)** and cylindrical surfaces.

Comparing **Fig.5-17** with **Fig.5-18**, it is found that the magnitude of the vectors in the recess is increased with decreasing flow rate. This increase is most noticeable in the inlet of the recess over the rotor where the velocity measured at ϕ=0.36 is approximately equal to the blade tip speed of

39m/s, two times greater than that measured at ϕ=0.6. This radial velocity is presumably caused by an unbalanced radial pressure gradient in the exposed tip region, which increases with blade loading. As the loading increases with reduced flow so do the forces driving the recess flow. **Fig.5-17** and **Fig.5-18** also indicate the area of recirculation to become more confined within the vaned passage at high flow ϕ=0.6 compared to the conditions at ϕ=0.36.

Both figures show the nature of the recess time-averaged flow, however, the exact physical process associated with the recess casing treatment are time-dependent in nature as evidenced by wool tufts.

5.4 INSTANTANEOUS (REAL TIME) VELOCITY PROFILE

Hot-wire Signal and Flow Uniformity

The uniformity of the flow can be qualitatively analysed by simply comparing the hot-wire signals between solid and treated builds. For this purpose, a hot-wire aligned normal to the axial flow direction was placed at station 2 (6mm upstream of the rotor) and traversed radially.

Fig5-19 shows the real-time history of the hot-wire, which represents the instantaneous inlet velocity distribution for the solid and treated casing measured at two radial positions, 50% and 75% span from the hub. The regular fluctuations (pulses) represents the blade to blade fluctuations with the clear blade passing frequency (27 pulses per revolution). The results taken at the different spanwise positions substantially agree except for the solid casing result for the stalled flow case (throttle opening 10%) which differs due to the significant tangential profile present (see also **Fig.5-3**). The interesting point to note in this set of results is the regular periodic nature of the treated cases and the comparative irregularity of the solid wall cases, indicating that the fluctuations other than blade to blade fluctuations which have been reduced (or removed) by the treatment. The implication here is that an unstable element in the flow (possibly the tip clearance vortex) has been significantly modified.

Instantaneous Velocity Components

Instantaneous values of velocity components of a flow field can be defined by means of hot-wire anemometry technique. A single modified P12 type slant wire was used for 3-D measurements as detailed in Chapter 3. The instantaneous or real time instrumentation for high speed data acquisition is shown in **Fig.3-6**. An ensemble-averaging technique was employed to overcome the randomness in the signal and for this purpose the measurements were phase-locked with respect to a fixed circumferential position.

$$V(t) = \frac{1}{N}\sum_{n=1}^{N} V(n,t)$$

where V(n, t) is an instantaneous velocity component; N is the number of consecutive rotor revolutions during which phase-locked data capture was carried out in response to a once-per-revolution trigger signal; and t is the temporal duration of each of the segmented data records.

The trigger pulse was generated by a trigger box which monitored the pulse of a white stripe on the compressor shaft. As the data are captured in response to a once-per-revolution signal, the rotor is in the same position each time the recording cycle is initiated and periodic changes in the flow field associated with unsteadiness is retained. The software specially for this data acquisition and data processing was developed.

The measurements were taken at 25%, 50%, 75% and 97% span from hub in two different operating condition: design point and near stall point. As an illustration of the unsteady flow nature of the test fan, **Fig.5-20** and **Fig.5-21** show the ensemble averaged inlet velocity component variations for solid and treated builds, and **Fig.5-22** and **Fig.5-23** show the outlet measurement results at the two flow rates.

At design flow rate which corresponds to the throttle opening of 60%, the velocity components show regular repetition of low turbulence. On the other hand, if the flow rate is reduced to near stall point (throttle opening of 45%), the velocity components show a relatively high turbulence containing

some low-frequency components. Because near stall point, fan operating is very vulnerable to stall and it was difficult to complete a data capture cycle. For this reason, the measuring flow rate was a bit higher than the flow rate at which high turbulence occurs. In other words, the turbulence was under assessed in this case. The ensemble-averaged velocities measured near extended stall point are very complex and the plots are not very meanful, and therefore not shown here.

The turbulence mentioned above especially the turbulence near the rotor tip, is not only caused by the stalling blades but also connected to the effects of the wall boundary layer, the tip leakage flow, secondary flow and so forth in a very delicate way. By all means, it is certain that the casing treatment exerts a great influence on these possible factors and strongly improve the flow. It is interesting to note that the flow improvement is evident even at the design operation condition. It is believed that this flow improvement contribute positively to stall delay and may compensate for the loss in treatment recess.

5.5 CLOSURE TO THE CHAPTER

Experiments to examine the effect of casing treatment on the flow field were carried out using a low-speed axial-flow fan with a tip clearance of 1.2% of the blade height. The first detailed results of flow measurements associated with the vaned recess casing treatment are presented. Using a modified method of 3-D flow measurements with a slanted hot-wire with careful and frequent calibration, time-averaged and ensemble-averaged flow measurements were carried out. A high frequency data acquisition system including both hardware and software was developed and the technique of the 3-D flow measurement has been enhanced. The flow features in both solid casing and treated casing builds are captured and comparison between the builds has been presented. The major observations of flow measurements are as follows:

- The vaned recess effectively reduced whirl component and removed flow

blockage found in the solid build in tip region.

- The first measurement results for the flow inside vaned recess treatment were reported. It is found that the magnitude of the flow vectors in the recess is increased with decreasing flow rate. The area of flow recirculation appeared to be more confined within the vaned recess passage with increasing flow rate.
- The inward radial flow from the recess injecting to the main stream as evidenced in Fig.5-4, plays a very active role on stall delay as pointed out in Chapter 4.
- The treatment does not have the function of reducing the inlet flow incidence onto the blade. On the contrary the reduced whirl in the tip region tends to increase the incidence in most cases. These observations suggest that the stall margin improvement due to the casing treatment was not achieved by reducing the incidence in the tip region.
- At both flow rates, for the treated build, the upstream tip region were found to have decreased total pressure. This indicates that the treatment does not have the function of increasing the total pressure in the upstream tip region.

The data presented in this chapter provide a fundamental understanding of the flow behaviour of a fan with a vaned recess casing treatment. However, it is unlikely that a full explanation of the operation can be gleaned from the results obtained. The analysis on the tip clearance flow with CFD method, which will be discussed in next Chapter, will hopefully shed more light on the mechanism involved.

CHAPTER 6. CFD MODELLING OF THE FLOW IN THE COMPRESSOR

Although the original interest of this chapter was in the flow field in casing treatment recess, it seems that better understanding of the flow field, especially the tip leakage flow and the interaction between 3D-blades and flow, was a prerequisite for dealing with the recess flow. The steady flow field of the test fan with varying tip clearances is simulated in the rotating frame with computational fluid dynamics (CFD) method to investigate the clearance effect on the end-wall flow development and to elucidate the behaviour of the tip leakage flow. Results and discussion are presented in this Chapter.

6.1 INTRODUCTION

It is highly desirable to enhance an aerodynamic understanding of the operation of the treatments by further study and possibly the application of CFD, so that optimum configuration can be more readily defined. Because of the complexities, it is not surprising to find that CFD on this aspect has been neglected by casing treatment researchers. The only two references available are published by **Crook** et al. (1993) for the slotted type hub treatment and **Hall** et al. (1994) for both slotted type and vaned recess casing treatments.

The flow in the endwall region of a compressor blade is complex and simplifying approaches that have worked well in other realms of fluid dynamics (e.g. secondary flow, boundary layer analysis) have not been helpful in providing the required insight here. For a full prediction of the flow in the vaned recess casing treatment, a CFD code should permit to handle both steady and time-dependent, three-dimensional viscous flow, and to use a multiple-blocked mesh discretization which provide flexibility

for analysing complex geometries as vaned recess casing treatment. A separate numerical grid system may be used for both the compressor rotor blade passages and recess vane passages to couple the flow field in the casing treatment recess. The CFD code available in this study, called TURBO3D, developed by **Tourlidakis** (1992), is a three-dimensional Navier-Stokes code for general analysis of steady viscous flow in turbomachinery. Strictly speaking, it is unable to handle unsteady flow and the boundary condition with sharp corners as is the case with the recess treatment. The code is developing extensively towards solving time-dependant problems. Unfortunately, due to time scale constraints on the project, it is unlikely to make a full prediction of the recess flow, but a steady analysis of the flow of the test fan with various tip clearances are presented. This flow field information is thought to be instrumental to a better understanding of the mechanism of the casing treatment.

6.2 BRIEF DESCRIPTION OF THE SOLVER AND CFD CODE

The CFD code used in this study is a 3-dimensional elliptic code for flow analysis of turbomachinery, developed by **Tourlidakis** (1992). A fully elliptic computational method for the analysis of steady viscous flow in high-speed centrifugal compressors with tip leakage is presented by **Tourlidakis**. A general system of Boundary Fitted Co-ordinates (non-orthogonal grid) was utilised and time-averaged Navier-Stokes equations were expressed in finite volume fully conservative form, and solved iteratively in a relative frame of reference using a a three-step pressure-correction technique. The computational procedure employed a non-staggered variable arrangement and a simple based method for coupling the velocity and pressure fields to remove the related pressure oscillations. For the simulation of the turbulence effects the two-equation k-ε turbulence model was used and modified to incorporate the curvature and rotational effects on the structure of turbulence. Near-wall viscous phenomena were modelled through the wall function method, thereby reducing the

computational effort required to incorporate wall effects on the turbulent flow. The program includes a variation of boundary conditions to simulate walls, periodic boundaries, rotating or stationary boundaries etc.

The code is capable of predicting turbomachinery 3-dimensional flows, incompressible or compressible, laminar or turbulent, with stationary or rotating parts, and with or without tip leakage. The input requires to specify a particular flow phenomena to be predicted and boundary conditions. The first part of the input is the geometrical information specified by the grid which covers the flow domain in terms of Cartesian x, y, z co-ordinate values. The other part of the input is mainly inlet conditions, program control parameters, physical property data and dependent variables etc.. More detailed information on the computational procedure and techniques can be found from **Tourlidakis** (1992).

6.3 GRID GENERATION AND BOUNDARY CONDITIONS

Grid Generation

A three-dimensional grid generation program for the numerical construction of meshes of the flow passage of axial-flow turbomachinery is developed based on a two-dimensional generation method developed by **Tourlidakis** (1992). The program can be used to generate meshes in an irregular flow passage as encountered in most turbomachinery. This method is based on the solution of a system of coupled elliptic Poisson type equations. The main features of the computational methodology are the control of the grid spacing of the first grid line from the blade wall surfaces and enforcement of the angle at which grid lines intersect the blade walls and periodic boundaries to be orthogonal.

The grid generation plays an important role in CFD, since this will affect not only the efficiency but also the accuracy of the computation. A grid system has to fulfil some conditions so far as the following features are desired:

- A mapping which guarantees a unique correspondence ensuring that

grid lines of the same family do not cross each other;

- The distribution of the grid should be smooth, with first derivatives everywhere continuous. No sudden change in shape in the same grid line nor from one grid line to the adjacent one;
- Orthogonality or near orthogonality between the lines forming the grid is a desirable feature although difficult and sometimes impossible to achieve especially in the highly irregular shaped 3-D space;
- A proper grid clustering method may be needed to enable the grids to have lines concentrated in regions of steep gradients (where significant change in flow variables are expected) in order to have higher numerical resolutions in these areas.

Boundary Conditions

The geometry of the rotor blade has previously been shown in Table3-1. The rotor has 27 C4 profile blades with a fixed tip clearance of 1.2% of the blade height. The chord of the blades is 48.5mm, In the configuration simulated, an isolated rotor section (without stator and IGV) was assumed. The regions upstream and downstream of the rotor blade passage are extended to one chord length in the axial direction. The angle of the direction of the upstream and downstream regions with respect to the axial direction are always taken equal to the blade angle at the leading and trailing edges respectively. As will be discussed later, probably the angle of the direction of the upstream region should have set to zero (in axial direction).

The grid used in this computation consists 22x26x60 mesh points, 60 points in streamwise direction, 26 points in radial direction and 22 points in blade-to-blade direction. The number of the mesh points is not very large but appears to be sufficient for the modelling of large scale effects. An exponential clustering of the mesh points was implemented in the near wall regions of the blade to blade and hub to tip directions and axial direction as well, in order to facilitate the proper resolution of the viscous effects and the high gradients of the flow parameters occurring in these regions. An

example of the three-dimensional computational grid is shown in **Fig.6-1**. For a clearer illustration, 2D plots of the grid at three different radial positions are shown in **Fig.6-2.**

6.4 FLOW PREDICTION AT DESIGN & OFF DESIGN POINTS

The geometry of the rotor blades is provided in **Table3-1** and thickness distribution of the C4 airfoil were calculated from analytical relation provided in Appendix A. **Fig.6-1** shows the geometrical domain and outline of the grid. The flow at two operating points (one at the maximum efficiency condition (measured) and the other at the point between stall point and peak efficiency point) was modelled in the rotating frame of reference where it is assumed to be steady. A circumferentially repeating condition was imposed for all flow variables along the periodic boundaries upstream and downstream of the impeller passage, and for the grid points which are located in the tip clearance gap.

The initial settings of the code was as follows. The isolated rotor was operated at design speed of 1500rpm, a mass-flow rate of 4.0kg/s (ϕ=0.72) and 3.63kg/s (ϕ=0.66) respectively. The tip clearance was set to 1.2% of the blade height, which is the true value of the test rig. At the inlet of the flow domain, a uniform total pressure equal to 101325 Pa and an uniform total temperature equal to 288.15K were assumed. The absolute velocity on the stationary shroud and the diffuser walls was set to zero. The relative velocity is set to zero on the surface of the rotor blades and on the hub. The flow was assumed to be axial and with an inlet boundary layer thickness of 15% of the span, as observed by traverses. Turbulence parameters were assumed uniform at the inlet, and inlet turbulence intensity has a value of 5% (**Tourlidakis** 1992). The computer code was run on a digital Alpha 200 $^{4/100}$ work station. As an example, a convergent computing procedure with 22x26x60 mesh point grid takes about one hour. The plots to be shown were basically created by a non-commercial flow visualisation software called VIGIE (VIsualisation Generale Interactive d'Ecoulements). VIGIE is at the

stage of trial and inconveniences in applications are often encountered. Therefore considerable work in modification of the postscript file may be needed to adjust the scale, position, write the chart titles in etc. for the best presentation.

Before going over the graphs, consider some ideas about the co-ordinate system used in these presentations. The Cartesian co-ordinate system x-y-z is illustrated in **Fig.6-1**, in which z is in axial flow direction and x is in blade-to-blade (suction to pressure) direction. In this system, z=0 refers to the plane going through the radial stagger axis (near to the middle of the chord) of the blade, and z is negative on the upstream side and positive on the downstream side. The flow is visualised comprehensively on the cut-planes which are shaped by z=constants or y=constant planes cutting the computational volume formed by the computational grid. It is realised that y=c plane may cross several layers of the grid. The positions of z=constant cut planes are shown in **Fig.6-2**.

The predicted pressure distribution on x-y planes (z=constants) at five different axial positions are shown in **Fig.6-3**, and **Fig.6-4** shows the pressure on x-z planes (y=constants) at five radial positions. The both charts present typical pressure contours with a high radial gradient. The flow redistribution very rapid and dramatic after rotor and the flow becomes nearly axisymmetric at the plane z=62.9 (about one and a half of the axial chord). Compared to the measurement results shown at the upper left corner in **Fig.5-15**, the predicted pressure rise generally agrees with the pressure measurement. **Fig.6-5**, to **Fig.6-7** provide more information about pressure distribution on the blade surface through the plots of the pressure along the boundary on the cut-planes. Compared with the mid-span chart **Fig.6-5**, the blade loading in the tip is much higher, and this also can be seen from the pressure contours in **Fig.6-3**. Perhaps the pressure scale is a bit large, which makes the pressure on the suction side looks too low, particularly at the leading edge.

Fig.6-8 and **Fig.6-9** present the predicted total relative velocity

contours. An unreasonably high velocity area upstream the blade leading edge is seen. In this calculation, the hub upstream of the rotor rotats with the blades. The induced velocity by the rotating hub is the most likely cause. The centre of the low momentum fluid is located about two-third of the axial chord from leading edge clearly shown by the contours at plane z=0 and plane y=247 as well and **Fig.6-14** makes it clearer.

From the contour plots of the axial velocity shown in **Fig.6-10**, and **Fig.6-11**, a reversal flow area can be clearly seen even at design operating point, and the reversed flow rate up to 19m/s has been predicted at the blade tip, around the two-third of the axial chord again. Consistently, the significant radial component associated with this reversal flow around the trailing edge on the near tip plane (**Fig.6-12**) can be also seen. In this figure, the velocity vectors in the upstream region is supposed to be in axial direction. The angled upstream computational volume is the most likely cause for this under prediction. Perhaps the upstream region of the grid should have a zero angle with respect to the axial direction rather than the angle equal to the blade angle at the leading edge. **Fig.6-13** provides a clearer picture about the reversal flow. This may serve to explain why the region from the mid-chord to the two-third rotor axial chord is critical to stall inception and more than 50% of the chord exposure is necessary in casing treatment design for the best results discussed in Chapter 4.

Fig.6-13 and **Fig6-14** provide a comparison between design point (ϕ =0.72) and off design point (ϕ=0.66). It is clear that reversal flow and low energy flow and turbulence increase with the mass flow decrease. Because the difference of the mass flow rate is small, there is no other significant fluid phenomena found.

6.5 INFLUENCE OF TIP CLEARANCE ON END WALL FLOW FIELD

In a normal axial flow fan or compressor, a clearance between rotor blades and casing is essential, unless the blades are shrouded. This clearance flow is an important source of unsteadiness and three

dimensionality of the flow in turbomachinery, while contributing significantly to loss of efficiency, producing disturbances in the flow around blade end regions and a great effect on delivery mass flow, and pressure rise ability. The casing treatment as discussed in previous chapters modifies this clearance in both size and shape, and eventually the clearance flow. In this connection, the tip clearance flow is associated with the mechanism of the casing treatment which is of interest here.

The flow at the same running conditions (ϕ=0.72, N=1500rpm) was simulated for five different tip clearances, 0, 2%, 3% 4%, and 1.2% of the blade height which is the true value of the test fan. It seems that the mid-span working conditions are not sensitive to small variations (about 1%) of the tip clearance, therefore only the flow parameters on the near tip planes were presented here.

Pressure contours for various tip clearances are shown in **Fig.6-15** under the same colour legend, in which "gap" refers to the tip clearance and the local extreme values are shown at the bottom of each frame. The minimum suction pressure shown in the legend frame is produced when the gap=2% and the maximum pressure rise occurs when gap=1.2%. It is interesting to notice that the pressure rise ability at the tip without tip clearance is rather low compared to the results with tip clearance. **Fig.6-16** shows the pressure distribution along the boundary of the cut plane considered. The effect of variation of the tip clearance may be clearly seen by observing that, the higher values of tip clearance have lower values of the blade loading at the tip while low tip gap corresponds to a higher blade loading. Nevertheless, the highest blade loading values correspond to a tip clearance of 1.2% rather than without tip gap as could have been expected. The pressure difference between the pressure and suction side of the blade produces a leakage flow through the blade tip. This flow causes the formation of vortices, increases disturbances in these regions and in turn decreases the pressure difference. It is supposed that these vortices and turbulences are the main mechanism for the energy dissipation in the tip

region. This effect depends on the boundary layer shape and thickness and, eventually the gap size.

Fig.6-17 provides a view of the pressure difference and extreme pressures versus tip clearance, indicating that the maximum pressure produced is not so sensitive to the tip clearance while the suction pressure differs with the tip clearance values. On the other hand, the pressure difference curve shows a some what complex behaviour of the blade loading at the blade tip when the tip clearance is varied. It seems strange to observe that the suction pressure for gap=4% is slightly lower than that for gap=3%, but it is possible. The measurements taken from the same rig by **Schmidt** (1985) showed a similar trend see **Fig.6-18** which is derived from Fig.V-2 when ϕ=0.72 (Appendix B). The measurements were taken at the mid span and the effect of the tip clearance must be different. Fig.V-1 (Appendix B) was based on the measurement at the tip and showed that when the clearance is small (0.34% and 1.24%), the curves are steeper and when the clearance is large (1.8% and 2.6%) the curves become less steep or horizontal. Considering the case of high flow rate, a large clearance would corresponds to a high stage loading.

More information about the tip clearance influence is given in **Fig.6-19** to **Fig.6-21** for the total relative velocities on the tip planes. There is no significant difference between the contours for different tip gaps except for the result without tip clearance (gap=0). As stated in last section, the low momentum flow centred at the position two-third of axial chord from the leading edge can be seen in all plots apart from the first one without clearance. The relative velocity distributions along the boundaries of the cut-planes shown in **Fig.6-20** is interesting. Note that the relative velocity on the blade surface is almost zero as expected when gap$\leq$ 2% and there is significant change in the case of gap$\geq$ 3%, indicating the occurrence of flow separation in both leading edge and trailing edge areas.

It is realised that the effect of the tip clearance size differs with the running condition of the compressor. The flow modelling was carried out at

lower flow rate (M=3.63kg, ϕ=0.66). Unfortunately, only the results with gap=2% and gap=0 are available (the reason for this will be discussed below). **Fig.6-22** to **Fig.6-24** display the modelling results. By comparision of the results between ϕ=0.72 and ϕ=0.66 for 2% tip clerance, It is found that the highly loaded blades (low flow coefficient) are more sensitive to the tip clearance change, enhancing therefore the importance of this anti-stall orientated investigation.

Although considerable effort has been made in modifying the grid and changing the parameter settings, It is hard to get a convergent solution at further reduced flow rate conditions with this code. The resolution of tip clearance flows requires specialised grids. The abrupt transition from the blade passage to the tip gap, with the sharp corners at the blade tip and the large gradients in flow properties, make the use of H grid impractical. A commonly used approach of "thin blade approximation" was adopted. This simplifies the computer coding because no special treatment is needed in the tip region apart from the implementation of the periodicity boundary condition in this region. For a machine with considerable blade thickness at the tip like an axial flow compressor, the assumption of a sharp edge, however, causes a highly non-orthogonal grid in the clearance region and poor grid resolution for the flow phenomena occurring in the clearance gap, and sometimes causes non-converged computational procedure. In this case, a multi-block structured grid or embedded O-grid within the main grid in the tip gap and additional coding are needed.

6.6 CLOSURE TO THE CHAPTER

The steady flow field of the test fan at design and off design with a tip clearance of 1.2% of the blade height is simulated in the rotating frame with computational fluid dynamics (CFD) method. The investigation of the effect of the tip clearance size on the end-wall flow development and pressure rise ability of the fan has been made. From the flow visualisation on various cut-planes, the following conclusions may be drawn:

- Generally, the higher values of tip clearance have lower values of the blade loading and more severe leakage flow at the tip. However, the best results correspond to a tip clearance of 1.2% rather than without tip gap, indicating that the optimum tip clearance value is between zero and 2% of the blade height but not including zero.
- In addition to indicating total pressure distributions and the regions containing low-energy fluid and secondary flow, the position of this low momentum flow and reversal tip clearance flow is identified. That low momentum flow and reversal tip clearance flow centered around 2/3 axial chord position is thought to be associated with the mechanism of the casing treatment, and may help to explain why more than 50% of the axial chord exposure is neccessary in the casing treatment design and the best result achieved when 2/3 of the chord is exposed.
- It appears that the effect of the tip clearance size differs with the operating conditions and that more loaded blades (low flow coefficient) are more sensitive to the tip clearance change.
- Because of the limitation of the information on the complex end wall flow, it is difficult to reach a thorough understanding of the phenomena involved and provide further conclusions. Clearly, more detailed research is needed. The primary objective of the CFD work is to seek the solution of the mechanism of the casing treatment and optimise the casing treatment design through flow simulation with both solid wall casing and treated casing. A great deal of work remains to be done on this subject. As a first step, it is hoped that the information expressed in this chapter can serve as an aid for later investigations and so contribute towards the further development of the casing treatment application.

CHAPTER 7 GENERAL DISCUSSION AND CONCLUSIONS

The main objectives of this thesis have been to study the potential effects of the vaned recess type anti-stall devices, to study the flow phenomena involved for a better understanding of the mechanism of the device and to provide more information about the casing treatment design. In response to these objectives, a discussion of the mechanism and applications of the anti-stall are firstly addressed in this Chapter. Some overall conclusions from the present work are drawn, and subsequently a few key areas for possible future research are suggested.

7.1 DISCUSSION OF THE MECHANISM OF THE CASING TREATMENT

While these experiments and flow simulations have given some clues to the mechanism by which the treatment operates, a general discussion based on all the information obtained is still needed. The mechanism has not been fully elaborated, but it is hoped that the following conjecture may provide a better understanding of the phenomena involved and provoke some further thought from readers.

Elimination of The Inlet Whirl Velocity

It seems conclusive that eliminating inlet tangential velocity is an essential part of the casing treatment mechanism. The present measurements revealed that whereas without the treatment, there is a high whirl velocity ahead of the rotor in the stalled regime. The treatment separates the recirculating flow, removes the tangential velocity and re-introduces it into the rotor with a high relative velocity. This increases the work input and makes possible the higher pressure rises observed without development of rotating stall cells until a much lower flow rate. The action

of the vanes in eliminating tangential velocity from flow leaving the rotor tip is seen as essential to the stall delay mechanism. This is supported by the fact that almost no stall margin improvement was obtained with a vaneless configuration (not presented but tested). The importance of the removal of high whirl velocity has been consistently pointed out by a number of investigators, in both slot type treatments (**Smith** et al. 1984) and vaned recess treatments (**Ziabasharhagh** et al. 1992). The research showed that the axial skewed slot is most effective among small scale treatments, radial hole has almost no effect and reversed skewed slot (the flow emerged from the slots in the direction of the rotor blade rotation) has an adverse effect (**Takata** et al. 1977). This also implies that reducing the whirl velocity is essential to the stall delay mechanism.

Stabilising Effect on the Inlet Main Flow

If a stall cell forms in the tip region of the rotor, a circumferential variation in static pressure must exist around the rotor. For reasons of manufacture the tip clearance is never exactly evenly distributed around the circumference, and this gives rise to another unfavourable source of the pressure maldistribution. In this case, the treatment recess serves as a pressure stabiliser which permits the unbalanced pressure to be equalised by interaction between mainstream and recess flow and therefore increases the tolerance to the inlet flow turbulence of a compressor and delays the formation of stall cells. This conjecture is supported by the instantaneous velocity measurements (**Fig.5-19**) and **Fig.5-20** to **Fig.5-23**. In these results, there is a significant contrast between the regular periodic nature of the flow for treated casing and the irregularity of the flow for solid wall case. In Chapter 4, it was found that the flow leaving the recess and injecting into the main flow plays an important role in stall margin improvement and reveal that this out flow with zero axial velocity (leaves recess radially rather than axially) is the most favourable direction (**Fig.4-10**). This implies that the interaction of the flow is more important than the function of increasing the axial flow velocity and energising the low momentum flow in the tip region.

Modifying the Tip Clearance Flow

The complicated flow near the end-wall is recognised to be detrimental to the stability of axial compressors. The transportation of boundary layer on the blade surface towards the end-wall, the tip leakage flow, the presence of a vortex caused by the roll-up of the leakage flow and the entrained flow etc. make the end-wall flow very complicated and would result in blockage. The overall magnitude of the tip leakage flow is related to the aerodynamic loading of the blades and the static pressure in the tip region is the control factor governing the chordwise distribution of the flow across the tip (**Storer**, et al. 1991). After casing treatment, the pressure field in the end-wall region is significantly modified due to more than 50% of the blade chord exposed to the recess, and eventually the tip clearance flow is definitely modified. It appeared that this modification is another key factor to the stall margin improvement mechanism.

As already stated, exposing the rotor mid-chord to the recess was found to be extremely critical, which is believed to have a close link with the mechanism being sought. In **Fig.6-9**, **Fig.6-13** and **Fig.6-14** Chapter 6, it is clearly visualised that the low momentum flow and reversal flow are centred around the two-third axial chord position. **Lakshminarayana** et al. (1982) studied the three-dimensional flow field in the tip region of a low speed, moderately loaded axial compressor and also found that the tip leakage flow originates near the quarter-chord and peaks around the mid-chord with intensive turbulence. It is interesting to relate these observations to the functional sensitivity of the treatment (**Fig.4-8**) where both the stall margin and pressure rise were dramatically changed when the rotor mid-chord is exposed to the treatment. Furthermore, the measurements indicate a strong radial flow from the rotor tip into the treatment recess. Under these conditions, it is highly probable that the treatment significantly modifies the leakage flow, possibly eliminating the normal tip vortex flow with a radial flow into the recess instead. Such proposals are supported by the hot-wire measurements taken upstream of

the rotor (**Fig.5-19**) which were more repetitive with the treatment suggesting the removal of some non-periodic perturbation (possibly the tip vortex).

Moreover, it must be pointed out that the combined function of the treatment is stressed here, although each of the function of the treatment is individually discussed. Unlike what has been found in slot type treatment, the vaned recess treatment neither has the function of increasing the total pressure in the upstream tip region nor the function of reducing the inlet flow incidence onto the blade. These observations suggest that the stall margin improvement due to the casing treatment was not achieved by reducing the incidence nor by increasing the total pressure in the upstream tip region.

Why Little Effect on Efficiency ?

Increasing the blade tip clearance of a compressor causes a deterioration of its performance. From this point of view, an exacerbated performance may be expected in the unstalled flow region with the recess casing treatment due to enlarged tip clearance as more than 50% of the rotor chord is exposed to the recess. In fact, this is not the case, even higher performance was obtained in some optimum builds. As **Fig.4-2** shows, an intriguing feature of the overall performance obtained is that the efficiency curves for both solid and treated casing configurations are very close to each other. Why does the treatment not yield significant loss of peak efficiency? Why does the treatment not bring out a marked increase in efficiency in the extended unstalled range even at the point, for example ϕ=0.4, where the difference between the two pressure rise curves is so large?

Although it is realized that efficiency is a very complicated topic and it is difficult to give a clear answer to the above questions, it is possible to conjecture that in the unstalled region that the losses associated with the tip clearance vortex (solid casing) and casing treatment are approximately equal but whereas the tip flow breaks down with the solid casing the recess vane permits a more progressive operation whereby the recess flow and it

losses increase with blade loading (and reduced flow rate). Additionally, the efficiency in the extended unstalled flow range for the treated builds was not significantly different and pressure rise for the treated build was significantly higher indicating more work input. The measurement results, **Fig.4-3,** show that the casing treatment caused a large increase in work input with the pressure rise in the extended stall range. In the solid wall case, rotating stall can be approximated to cells of zero axial velocity (i.e. zero mass flow) and regions of high axial velocity (unstalled). This implies zero work in the stall cell and a low work coefficient in the unstalled zones consistent with the high flow coefficient. With casing treatments, however, this rotating stall is not permitted and so the work coefficient goes on increasing as the flow rate reduces. More work input is required to maintain higher pressure rise with the treatment, and hence the efficiency did not increase with the pressure rise.

On the other hand, peak efficiency penalty depends, to some extent, on the proportion of the rotor chord exposed to the casing recess. Generally, the greater the exposure, the greater the efficiency penalty, but the result for build3-2 shows that minimum efficiency loss was in the range of Ce/Ca=50%-70%, as illustrated in **Fig.4-8**. Hitherto, no mention has been made about the presence of the efficiency improvement on the optimum builds tested. Although the amount is within the error band of the efficiency measurements, it is possible that a small efficiency improvement can be achieved with a well-designed anti-stall device.

7.2 POTENTIAL APPLICATIONS

The anti-stall devices developed would provide an extended continuously increasing pressure characteristic which peaks at a much lower flow rate without significant peak efficiency change. Such an anti-stall device would also reduce the operational and maintenance costs, reduce or remove cumulative fatigue damage that fan blades often suffer, increase the level of safety of operation and enable the fan and compressor

industries to be more competitive in the world wide market. Although an additional production cost may be involved, it could often be recovered by the potential gains in performance and reduced need for variable anti-surge devices such as bleed valves and variable stagger stators. The application of this technique may be of a significance.

Aero-engine Applications

The extent of the stable operation of a gas turbine is greatly influenced by the stalling characteristics of the compressor. Stall delay techniques are particularly significant for aircraft applications, because, in general, improving the stall margin of the compressor and fan means improving the useful operation range of the engine. It is also possible to reduce the total number of compressor stages by increasing pressure ratio per stage through the use of the stall delay techniques. It has been proved experimentally that recessed casing treatment is capable not only of increasing stall margin but also increasing the tolerance to inlet flow distortion (**Ziabasharhagh** et al. 1992). This might lead to solving the problem of the in-flight shutdown encountered by some engines during lighting of an afterburner at high altitude and low indicated airspeed (**Gao** et al.1982).

Industry Fan Applications

For the general fan industry, improving the stall margin, reliability, tolerance to flow distortion, life span and operating cost are all interesting. There are a number of applications where industrial fans would benefit from the recessed casing treatment:

Room ventilation fans where a continuously rising pressure flow characteristic and a very low noise level over the performance range are usually specified. This kind of anti-stall device may enable a higher blade angle to be used with consequent advantages to fan size, efficiency and sound level.

For road and rail tunnels, their designers must provide ventilation systems that are economical in routine operation and effective in non-

routine operation. Jet fans in restricted rail tunnels can experience considerable pressure pulses due to the passage of trains. The breakdowns may occur due to the influence of abrupt changes in cross-sectional area of a railway tunnel on the propagation of pressure waves caused by passing trains. In tunnels with uni-directional traffic flow, the pressure difference may be increased or decreased by the piston effect of moving vehicles. This necessitates the fan being operated, in such a bad condition, free from the risk of stalling. An anti-stall device would reduce or remove cumulative fatigue damage that fan blades often suffer, and increase the safety of operation.

Fans applied to systems which may be considered unusual to some degree, such as ventilation fans for coal mines, for long tunnels during the pre-breakthrough stage of the construction, are required to be equally effective in variable flow conditions. Following an explosion at Houghton Main Colliery in 1975 the National Coal Board introduced a 'Fan Acceptance Scheme' which established standards for the design of fans for underground use. The development of a range of relatively inefficient fans was approved by this scheme which nevertheless fulfilled the requirements for ventilating underground tunnels. A new variable flow fan has to be developed (**Burrell** 1994) and the anti-stall device may offer some help to achieve the design goals.

The maximum efficiency of a conventional axial fans often occurs just before the stall line. In order to avoid stall for safety operation reasons, the operation range of the fan is usually selected in such a way that a maximum of 90% of the stall line pressure is used, consequently often missing maximum efficiency. For a large capacity fan used in industrial process such as boiler fans in power plant, the fan efficiency is crucial for the cost of operation. An anti-stall device would make it possible to optimise the fan selection for efficiency in the normal duty range without the risk of stalling.

Industrial Pump Applications

The technique of casing treatment described in this thesis can be easily transferred to pump applications and a similar favourable effect would be

expected. This is not discussed further as it is outside the scope of this thesis.

Summary of the Applications

As may be apparent from the preceding discussion, the casing treatment would offer significant benefits in a variety of applications. However, it has found fairly limited use and the casing treatment has not been adopted as a standard item by designers. The most likely reason is that in most cases, the stall margin improvement was at the cost of efficiency, and that there could be mechanical and manufacturing difficulties associated with casing treatment. There may also be some commercial reasons. Because the best machine cannot always be immediately rewarded by the market. The biggest attractions of the vaned recess casing treatment are more effective stall control and almost no efficiency penalty. This would encourage the applications.

7.3 CONCLUSIONS

An experimental investigation to examine the influence of the vaned recess casing treatment on stall margin, operating efficiency and flow field of a low speed axial flow fan with aerospace type blade loading is presented. Detailed 3-D flow measurements in the end-wall region and in the casing recess were carried out with a slanted hot-wire, providing some insight to the operation of the device. Based on this investigation, the following conclusions are drawn.

On Performance

- Different geometrical designs of the vaned passages were examined and more than 65% of stall margin improvements and over twice the maximum pressure rise were obtained. The research suggests that it is difficult to gain any further improvement of this rig by casing treatment. It seems that the hub stall or separation sets a new limit to the operating range.

- The treatment did not significantly alter the efficiency curve. Neither the peak efficiency nor the efficiency in the extended unstalled range was significantly changed. This is clearly a great advantage over the slot type casing treatment.
- The different vanes tested had only a marginal effect on the overall performance of the compressor. It is always advisable to select a simple vane structure if there is no significant performance loss caused. A simplified vaned recess passage has been suggested (Chapter 4).
- It appeared that with solid casing the work input was considerably reduced as flow reduced into stall region. In contrast, the casing treatment caused a progressive increase in work input as well as the pressure rise in the extended unstalled range.

On The Flow Field

- The treatment has a strong influence on the end-wall flow field, and the influence on rotor inlet flow is much stronger than on the rotor outlet flow. It has also been found that the vaned recess hardly affects the fan flow field until the fan is throttled to a high pressure-rise condition (near the normal stall point).
- The first quantitative measurement results for the flow inside the vaned recess treatment are reported. It is found that the magnitude of the flow vectors in the recess is increased with decreasing flow rate. The area of flow recirculation appeared to be more confined within the vaned recess passage with increasing flow rate.
- The vaned recess effectively reduced the whirl component and removed flow blockage found in the solid build in the tip region.
- The treatment does not have the function of reducing the inlet flow incidence onto the blade. On the contrary the reduced whirl in the tip

region tends to increase the incidence in most cases, and also the relative inlet velocity to the rotor.

- At both low and high flow rates for the treated build, the upstream tip region was found to have decreased total pressure due to decreased whirl velocity.

On the Mechanism

- It is concluded that eliminating the whirl component of the inlet flow is an essential part of the stall delay mechanism.
- It appeared that the casing treatment significantly modified the clearance flow and removed the flow reversal into the recess. These are also important features associated with the mechanism of the treatment.
- CFD modelling found that the low energy (low momentum) flow and reversal flow in untreated builds are centred around 2/3 axial chord position. Exposing at least the leading 50% of rotor chord to the recess is found essential for casing treatment to produce the maximum effect on these unfavourable flows.
- The inward radial flow from the recess injecting to the main stream with a varying velocity, plays a very active role on stall delay as pointed out in Chapter 4. This flow is thought to be a contribution to stabilising effect on the inlet flow.
- Unlike that found in slot type treatment, the stall margin improvement due to the casing treatment was found not to be achieved by reducing the incidence nor by increasing the total pressure in the upstream tip region.

7.4 SUGGESTIONS FOR FUTURE WORK

While great achievements of research on anti-stall devices have been made, it should be realised that the research is far from complete. There is much work remaining to be done before it is accepted as a standard item by

designers. It is hoped that the following suggestions may provoke new ideas for further investigations.

- In this study, extensive flow measurements were made in the casing treatment recess, upstream and downstream of the rotor and the data presented provide a fundamental understanding of the flow behaviour of a fan with a vaned recess casing treatment. However, no measurement was taken on the blade surface nor in the blade passage close to the tip and consequently it is unlikely that a full explanation of the operation can be gained from the results obtained. It is thought that detailed measurements in the rotor blade passage with and without casing treatments could provide much more information about end wall flow pattern and how casing treatments modify tip clearance flow. These would probably provide a better understanding of the mechanism of the casing treatment operation.
- As stated before, more than 50% of rotor axial chord exposure to the recess is necessary for optimum stall margin improvement. However, an exception was noticed in Bard's design, which obtained successful results when the recess treatment was placed upstream of the rotor without rotor exposure. This apparent contradiction here suggests that the blade loading of the machine may have a significant effect. Blade pitch (or stagger) angle changes cause a marked change of operating load in terms of the work coefficient $\Delta H/U^2$ and it is desirable to find out how the blade angle affects the casing treatment design. To accomplish this, a fan with a variable blade setting angle would be needed.
- To a great extent, the geometrical parameters of casing treatment design were chosen by trial and error and empirical methods. Theoretical research is needed to understand the fluid mechanics involved in casing treatment to enable us to optimise the treatment configuration more expeditiously than in present by empirical experiments. The use of CFD methods can provide much more detailed

information at much reduced cost and time scales than the current experimental techniques. The effect of different upstream or downstream conditions, the impact of alternative geometrical configurations are the examples of areas where the CFD can provide enhanced aerodynamic understanding of the mechanism involved and large scale reductions in cost and time for a new design. Therefore it is desirable to continue seeking CFD solutions of casing treatment design.

- That no significant peak efficiency penalty was involved in the vaned recess casing treatment applications is clearly an advantage. However, mechanical and manufacturing difficulties and cost involved can be a limitation to wide applications. Therefore, research to seek a simpler structural design is demanding, particularly for the commercial fan industry. For the aircraft engine industry, the treatment configuration also should be as small as possible, particularly in its radial direction. This calls for efforts to miniaturise the current design.
- The anti-stall device developed could improve stall margin of this kind of machine by some 60%, but research suggests that it is difficult to gain a further improvement of this rig by casing treatment. It seems that the hub stall or separation sets a new limit to the operating range. Hence, a further improvement may be expected by means of hub treatment. **Azimian** found that the casing treatment gave a much smaller stall margin improvement for rotor with stator builds than for rotor only. For low hub/tip radio stages, the stator hub is most often the first section to stall, and the rotor tip at a lower flow. Perhaps both rotor casing and stator hub treatment should be combined for the maximum effect, which are worth investigation.
- The technique of casing treatment described in this thesis can be easily transferred to the pump applications. It is worth considering research in this field.

REFERENCES

Amann, C. A., Nordensen, G. E., and Skellenger, G. D. "Casing Modification for increasing the Surge Margin of a Centrifugal Compressor in an Automotive Turbine Engine", Trans. ASME, J. Eng. Power, Vol. 97, p329-336, July 1975

Azimian, A. R., "Application of Recess Vaned Casing Treatment to Axial Flow Compressors", PhD Thesis, Cranfield Institute of Technology, 1987

Azimian, A. R., Elder, R. L. and McKenzie, A. B. "Application of Recess Vaned Casing Treatment to Axial Flow Fans", ASME 89-GT-68

Bard, H. "Unstable Characteristics for Fans", AMCA Engineering Conference, Atlanta, Georgia, April 2-4, 1984

Bard, H. "Fan Stability by Anti-stall in Tunnels and Industrial Process Ventilation", Turbo Compressor and Fan Stability, I Mech E Seminar, April 8, 1993

Bailey, E. E. and Voit, Charles H. "Some Observation of Effect of Porous Casing on Operating Range of a Single Axial-flow Compressors", NASA TM X-2120, Oct. 1970

Bailey, E. E. "Effect of Grooved Casing Treatment on the Flow Range Capability of a Single Stage Axial Flow Compressor", NASA TM X-2459, Jan. 1972

Burrell, "Fan For Hazardous Applications", I Mech E seminar, 4 October 1994

Camarata, F. J., Greitzer, E. M., Joslyn, H. D., and Nikkanen, E. P., "Effect of Casing Treatment on the Near Tip Flow Field of a Large-scale Rotor", United Technologies Research Publication R7512136683-1, Dec. 1975

Cheng, P., Greitzer, E. M. and Tan, C. S. "Effects of Compressor Hub Treatment on Stator Stall and Pressure Rise", J. Aircraft Vol.21, No.7,

P469-475, July 1984

Cheshire, L. J. "The Design and Development of Centrifugal Compressors for Aircraft Gas Turbines", Proc. I. Mech. E. (London) Vol. 153, p426-440, 1945

Corbert, A. G. and Elder, R. L. "Stability of an Axial Flow Compressor With Steady Inlet Condition", J. Mech. Eng. Sci. Vol.16, No. 6, 1974

Crook, A. J., Greitzer, E. M., Tan, C. S., and Adamczyk, J. J. (1993) "Numerical Simulation of Compressor Endwall and Casing Treatment Flow Phenomena", Trans. ASME, Journal of Turbomachinery, Vol. 115/501

Emmons, H. W., Pearson, C. E. and Grant, H. P. "Compressor Surge and Stall Propagation", Trans. ASME, Vol. 77, P455-469, April 1955

Fabri, J. and Siestrunck, R. "Rotating stall in axial flow compressors", J. Aero. Sci., 24, 1957

Fabri, E. E. and Reboux, J. "Effect of Outer Casing Treatment and Tip Clearance on Stall Margin of a Supersonic Rotating Cascade", ASME 75-GT-95, 1975

Fujita, H. and Takata, H. "A Study on Configurations of Casing Treatment for Axial Flow Compressor", Bulletin of JSME, 1984

Gao, Yao-Lin and Li, Ke-Ming "Effect of Rear Stage Casing Treatment on the Overall Performance of a Multistage Axial Flow Compressor", ASME 82-GT-110, 1982

Grant, H. P. "Hot Wire Measurements of Stall Propagation and Pulsating Flow in an Axial Flow Induced Centrifugal Impeller System", Pratt and Whitney Res., Rep. No. 133, June 1951

Greitzer, E. M., Nikkanen, J. P., Haddad, D. E., Mazzawy R. S. and Joslyn, H. D. "A Fundamental Criterion of The Application of Rotor Casing Treatment", Trans. ASME. J. Fluid Eng. Vol. 101, p237-242, June 1979

Greitzer, E. M. "Review--axial Compressor Stall Phenomena", Trans. ASME, J. Fluid Eng. 102, p134-151, June 1980

Hall, Edward J, Crook, Andrew J., and Delaney, Robert A., "Aerodynamic analysis of compressor casing Treatment With a 3-D Navier-Stokes Solver", AIAA-94/2796, Paper presented at: AIAA/ASME /SAE/ASEE

30th Joint Propulsion Conference, June 27-29, 1994, Indiana

Huppert, M. C. and Benser, W. A. "Some Stall and Surge Phenomena in Axial Flow Compressor", The paper presented at Institute of Aeronautical Sciences' 21st Annual Meeting, N. Y. Jan. 1953

Iura, T. and Rannie, W. D. "Experimental Investigations of Propagation Stall in Axial Flow Compressors", Trans. ASME, Vol. 76, P463-471, 1954

Ivonov, S. K. "Axial Flow Ventilation Fan", U. K. Patent Application (19) GB(11) 2 124, 303A. 1984

Janson, W., Carter, A. F. and Sworden, M. C. "Improvement in Surge Margin for Centrifugal Compressors", Presented at AGARD 55th Specialists' Meeting Centrifugal Compressor, Flow Phenomena and Performance, Brussels, 1980

Johnson, M. C. and Greitzer, E. M. "Effects of Slotted Hub and Casing Treatment on Compressor End Wall Flow Fields", Trans. ASME, J. Turbomachinery, Vol. 109, P380-387, July 1987

Koch, C. C., and Smith, L. H., Jr., "Experimental Evaluation of Outer Case Blowing or Bleeding of Singal Stage Axial Flow Compressor, Part I---IV", NASA CR-54587--54590, 1966, 1968

Koch, C. C., "Experimental Evaluation of Outer Casing Blowing or Bleeding of Single Stage Axial Flow Compressor", NASA CR-54591-54592, 1969, 1970.

Lakshminarayana, B., Davino, R. and Pouagare, M. (1982) "Three-dimensional Flow Field in the Tip Region of a Compressor Rotor Passage-part I: Mean Velocity Profiles and Annulus Wall Boundary Layer; Part II: Turbulence Properties", Trans. ASME, Journal of Engineering for Power, Vol. 104, Oct.

Li, K. M., "Effect of Casing Treatment on Axial Flow Compressor Performance", Aircraft Engine, 1st Issue, 1980

Lomas, Charles G. "Fundamentals of Hot Wire Anemometry", Cambridge University Press 1986.

Marble, F. E. "Propagation of Stall in a Compressor Blade Row", J.

Aero. Sci. 22, 1955. also Inst. 21st Meeting, N. Y., Jan. 1953

Macdougal, I. and Elder, R. L. "The Improvement of Operating Range in a Small, High Speed, Centrifugal Compressor Using Casing Treatments", I. Mech. E. C32/82, 1982

McDougall, N. M. "A Comparison Between the Design Point and Near-stall Performance of an Axial Compressor." Trans. ASME, J. Turbomachinery, Vol. 112, P109-115, Jan. 1990

McKenzie, A. B. "Passive Stall Control for Fans and Compressors", Turbo Compressor and Fan Stability, I Mech E Seminar, April 8, 1993

Miyake, Y., Inaba, T. and Kato, T. "Improvement of Unstable Characteristics of an Axial Flow Fan by Air-separator Equipment", Trans. ASME, J. Fluid Eng., Vol. 109, P36-40, March 1987

Moor, R. D., Kovich, G., and Blade, R. J., "Effect of Casing Treatment on Overall and Blade-element Performance of a Compressor Rotor", NASA TN D-6338, Nov. 1971

Moss, John E. Jr. "Effect of Slotted Casing Treatment on Performance of a Multistage Compressor", NASA TM X-3350, 1976

Osborn, W. M., Lewis, G. W., and Heidelberg, L. J., "Effect of Several Porous Casing Preatment on Stall Limit and on Overall Performance of an Axial Flow Compressor Rotor", NASA TN D-6537, Nov. 1971

Osborn, W. M. and Moore, R. D. "Effect of Casing Treatment on Overall Performance of Axial Flow Transonic Fan Stage With Pressure Ratio of 1.7 and Tip Solidity of 1.5", NASA TM X-3477, Feb. 1977

Paulon, J. and Dehondt "Influence of Casing Treatment on the Operating Range of Axial Compressors". ASME 82-GT-103, 1982

Prince, D. C. Jr., Wisler, D. C. and Hilvers, D. E. "A Study of Casing Treatment Stall Margin Improvement Phenomena", ASME 75-GT-60, 1971

Russell, B. A. and Mahmoud, A. A. "Stall-fee xial Flow Fan", U.K. Patent Application (19) GB(11) 2 101685 B, London, The Patent Office, Aug. 1984

Schmidt, M. J. P. "Blade Tip Clearance Effects of an Axial Flow Compressor Rotor", PhD Thesis, Cranfield Institute of Technology, 1985

Shulze, W. M., Erwin, J. R. and Westphal, W. R. "Investigation of an Impulse Axial Flow Compressor Rotor Over a Range of Blade Angles", NACA RML50F27A, 1950

Smith, G. D. J. and Cumpsty, N. A. "Flow Phenomena in Compressor Casing Treatment." Trans. ASME, J. Eng. Gas Turbine Power, Vol. 106, p532-541, July 1984

Smith, L. H., Jr. "NASA/GE Fan and Compressor Research Accomplishments", ASME, Journal of Turbomachinery, Vol. 116, p555-569, Oct. 1994

Snyder, R. W., and Blade, R. J., "Analytical Study of Effect of Casing Treatment on Performance of a Multistage Compressor", NASA TN D-6917, 1972

Storer, J. H. and Cumpsty, N. A. "Tip Leakage Flow in Axial Compressors", Trans. ASME, J. Turbomachinery, Vol. 113, P252-259, April 1991

Takata, H. and Tsukuda, Y. "Stall Margin Improvement by Casing Treatment--its Mechanism and effectiveness", Trans. ASME, J. Eng. Power, Vol. 99, Jan. 1977

Tesch, W. A. "Evaluation of Range and Distortion Tolerance for High Mach Number Transonic Fan Stage, Task IV Stage Data and Performance Report for Casing Treatment Investigation, Volume I", NACA CR-72862, May 1971

Tourlidakis, A. "Numerical Modelling of Viscous Turbomachinery Flows With a Pressure Correction Method", PhD Thesis, Cranfield Institute of Technology, March 1992

Urasek, D. C. "Effect of Casing Treatment On Performance of a Two-Stage High-Pressure-Ratio Fan", NASA TP-1409, 1979

Urasek, D. C., Lewis, G. W. Jr. "Effect of Casing Treatment On Performance of an Inlet Stage for a Transonic Multistage Compressor", NASA TM X-3347, 1976

Whitfield, C. E., Kelly, J. C. and Barry, B. (1972) "A Three-Dimensional Analysis of Rotor Wakes", Aeronautical Quarterly, Nov. 1972

Wisler, D. C., and Hilvers, D. E., "Stator Hub Treatment Study", NASA cr-134729, Dec. 1974

Ziabasharhagh, M., McKenzie, A. B. and Elder, R. L. "Recess Vane Passive Stall Control", ASME 92-GT-36

Ziabasharhagh, M., "Recess Vane Passive Stall Control for Axial Flow Fans", PhD Thesis, Cranfield Institute of Technology, 1992

APPENDIX A DESCRIPTION OF BLADE GEOMETRY OF C4 & NACA 65-(12A10)10 AEROFOILS

The thickness distribution of the C4 aerofoil is calculated from analytical relations as a function of the fraction distance p from the leading edge along the camber line of the blade and the designated maximum thickness of the blade t_{max}, Tourlidakis (1992):

if p<0.3,

$$t = 2(28.110p^3 - 25.281p^2 - 6.563p + 15.492p^{0.5})\frac{t_{max}}{10}$$

if p≥0.3,

$$t = 2(3.448p^3 - 14.632p^2 + 7.848p + 3.869)\frac{t_{max}}{10}$$

APPENDIX B FIG.V-1 & FIG.V-2

Fig.V-1 and Fig.V-2 from **Schmidt** (1985) are shown here for a quick reference. Note that $\phi = V_a/U$, compared to $\phi=V_a/U_m$ used by present author.

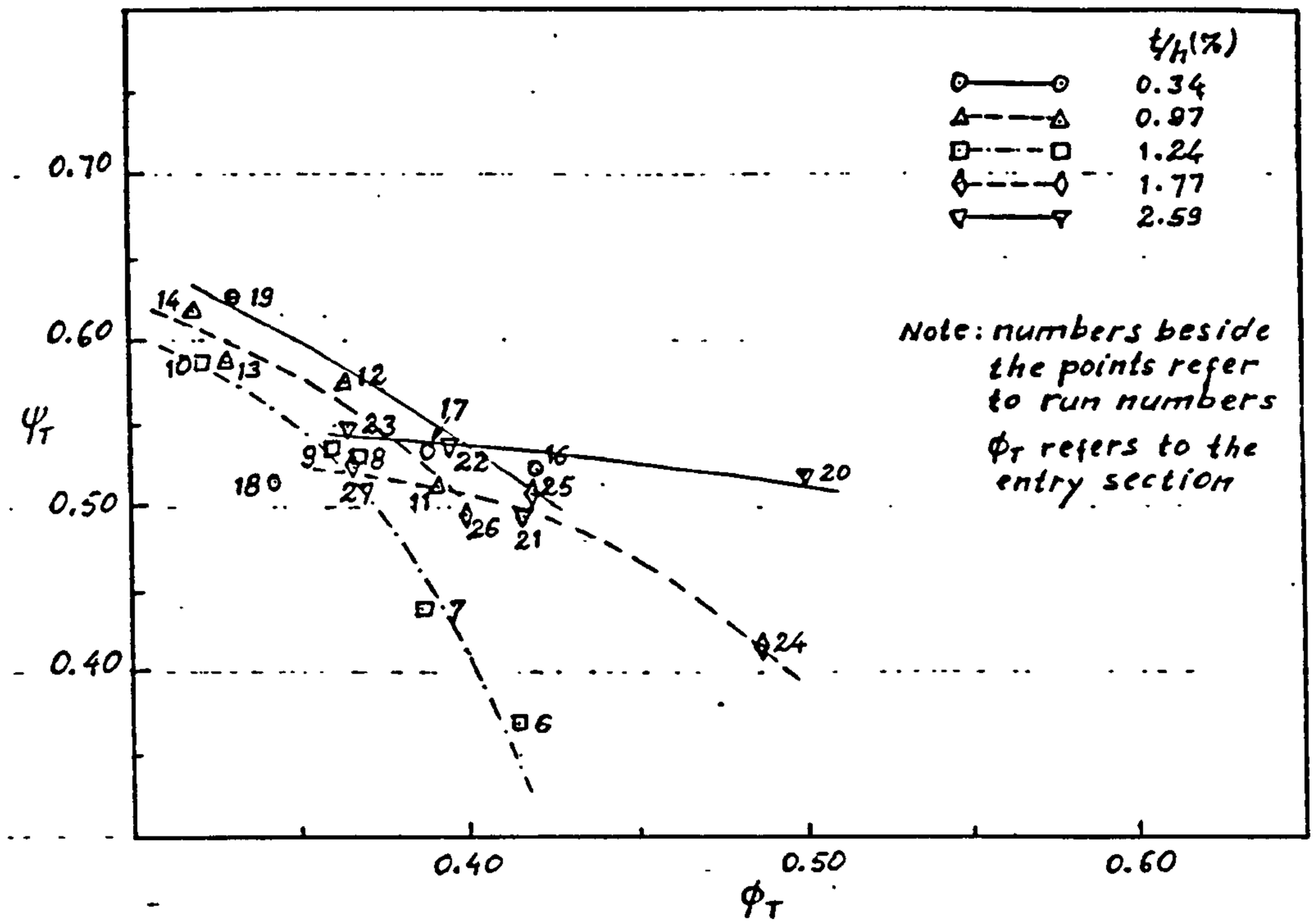

Fig.V-1 -Stage Loading and Flow Coefficient at the Tip

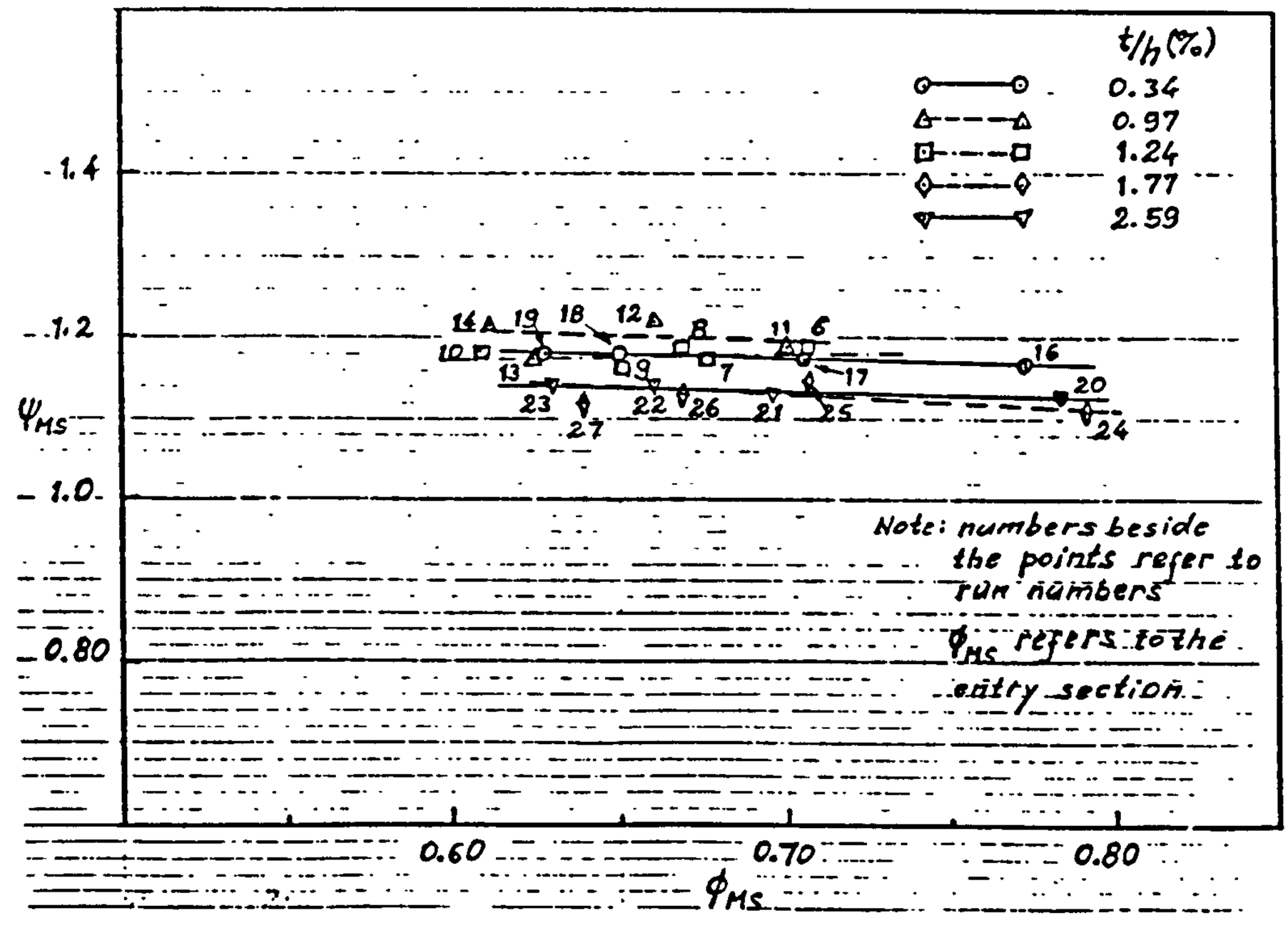

Fig.V-2 -Stage Loading and Flow Coefficient at the Mid-Span

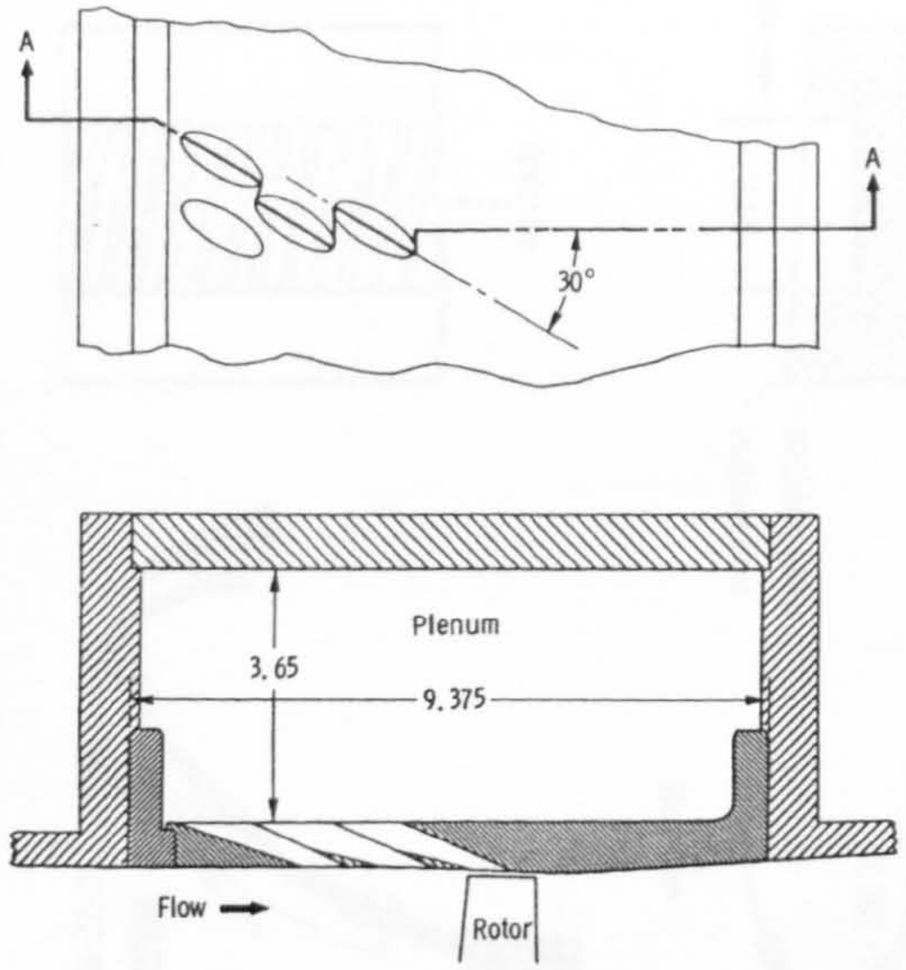

(a) Sketch showing hole orientation and location.

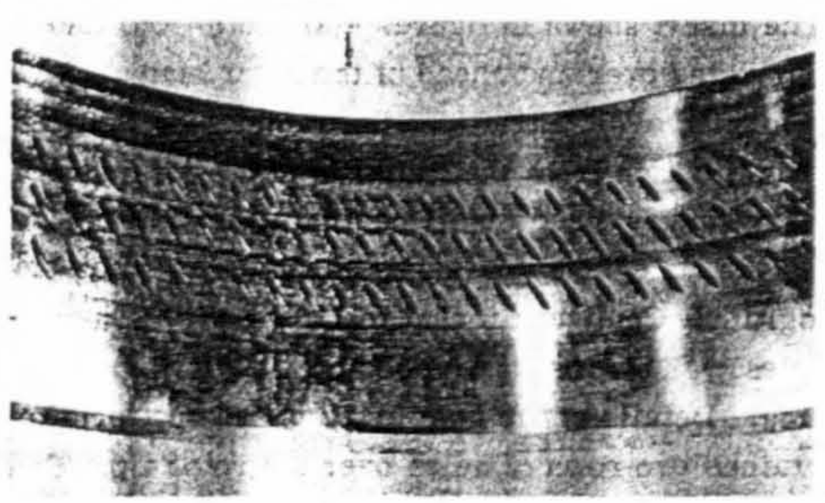

(b) Inside of tapered-hole casing.

Figure 3. - Tapered-hole porous casing. (Dimensions are in inches.)

Fig.2-2 Tapered-hole Porous Casing(Bailey and Voit, 1970)

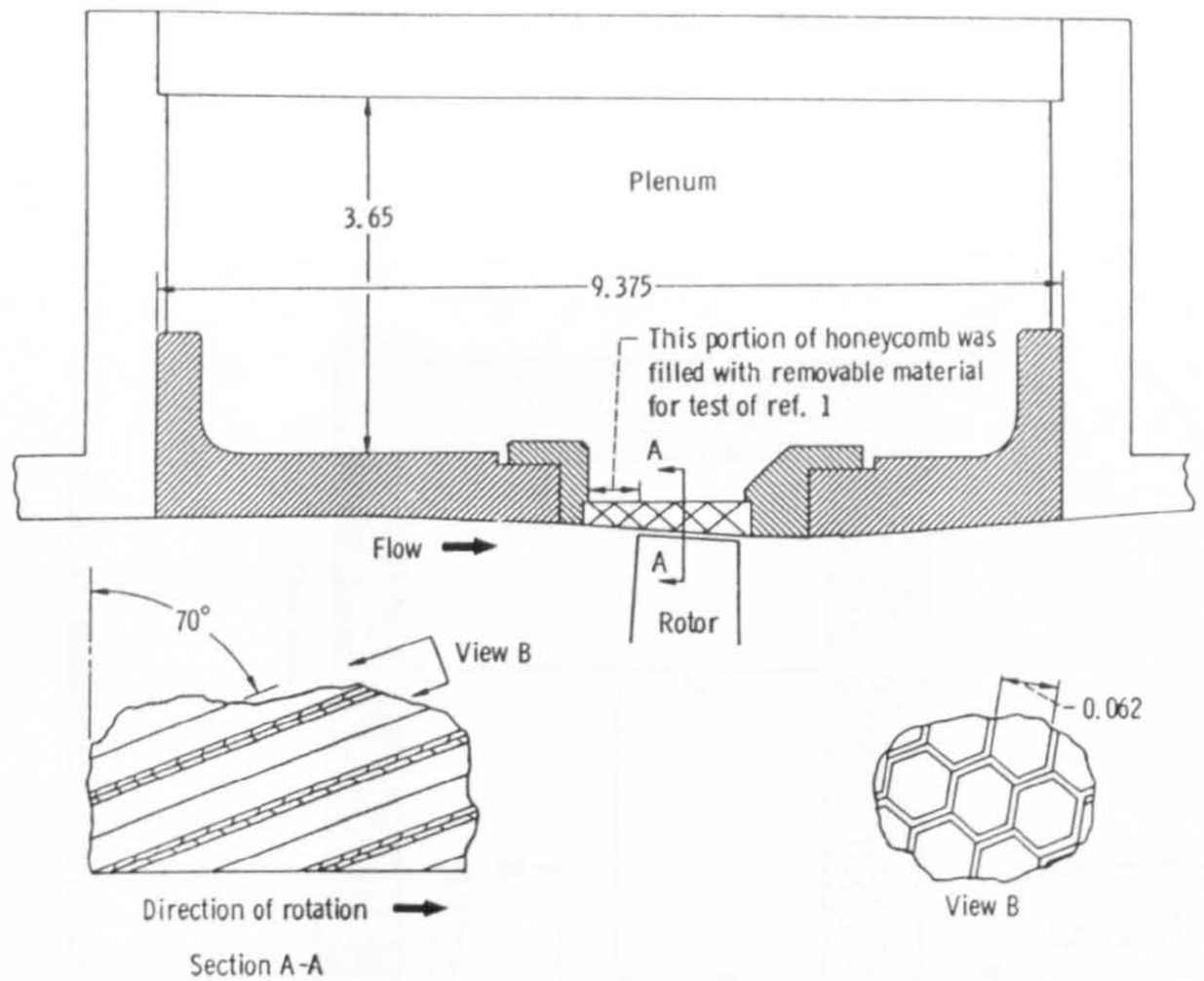

(a) Sketch showing honeycomb orientation and location.

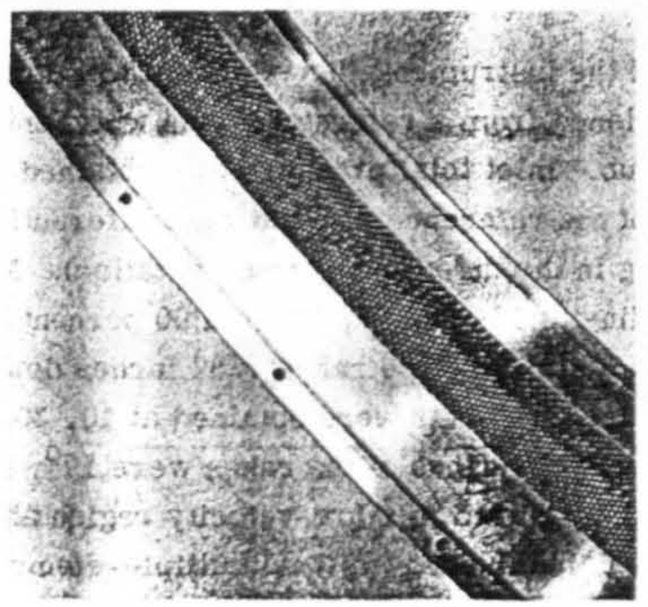

(b) Inside of honeycomb casing.

Figure 4. - Honeycomb porous casing. (Dimensions are in inches.)

Fig.2-3 Honeycomb Porous Casing(Bailey and Voit, 1970)

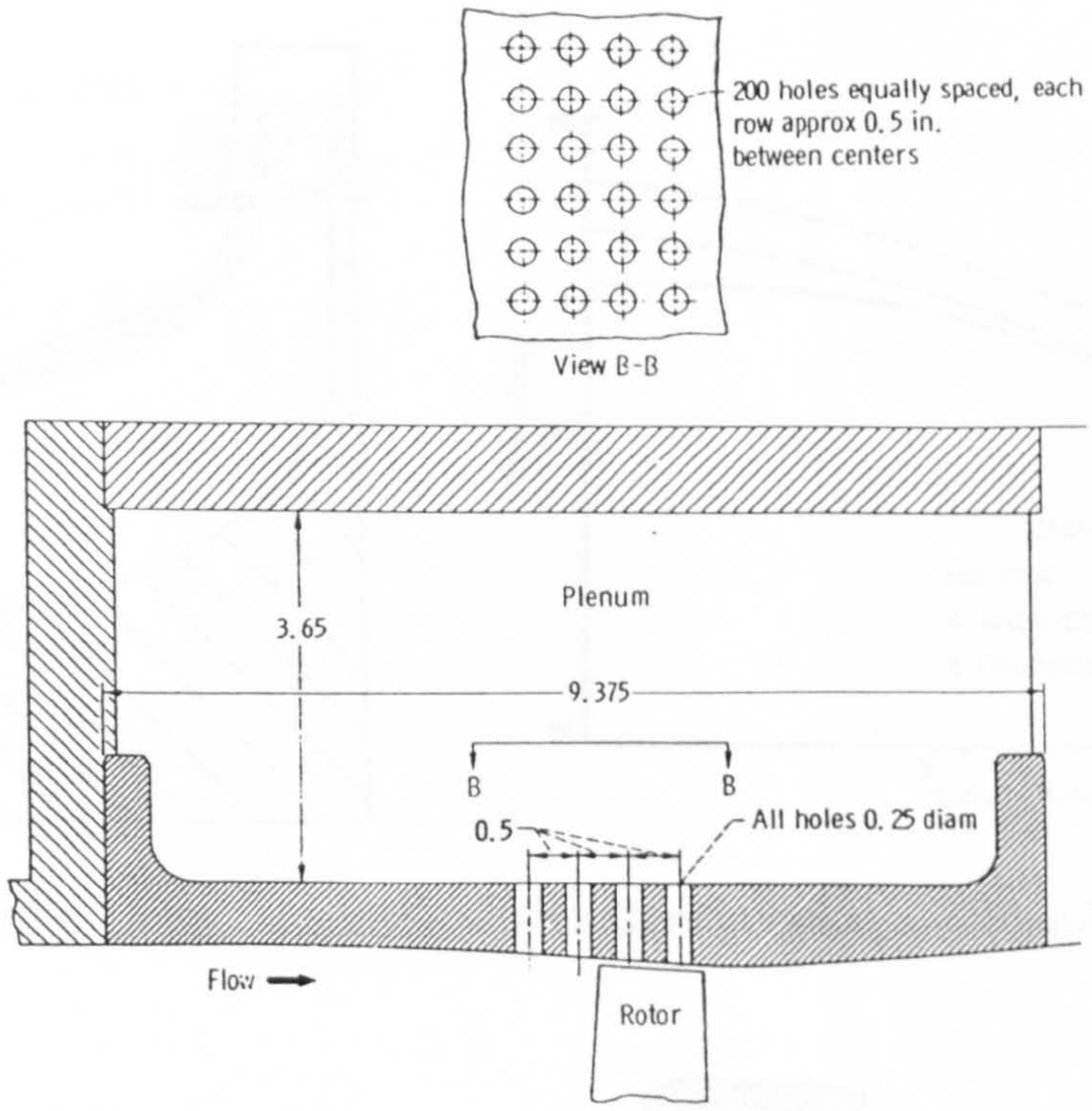

Figure 5. - Radial-drilled-hole porous casing. (Dimensions are in inches.)

Fig. 2-4 Radial Tapered-hole Casing (**Bailey** and **Voit**, 1970)

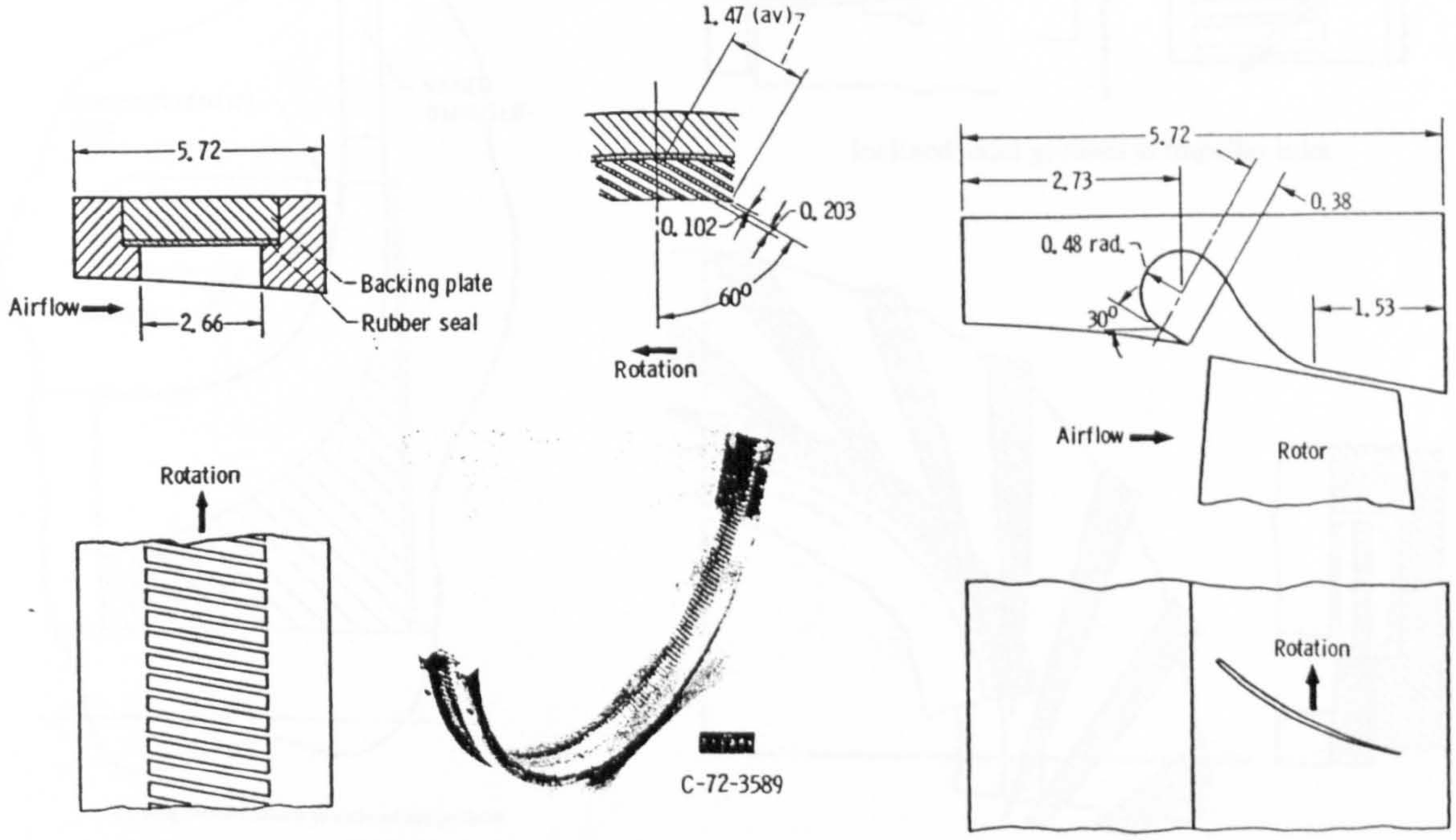

Figure 5. - Skewed slot insert. (Dimensions in cm.)

Figure 7. Teardrop Insert

Fig. 2-5 Slot type Casing and Teardrop Casing(**Osborn** and **Moore**,1977)

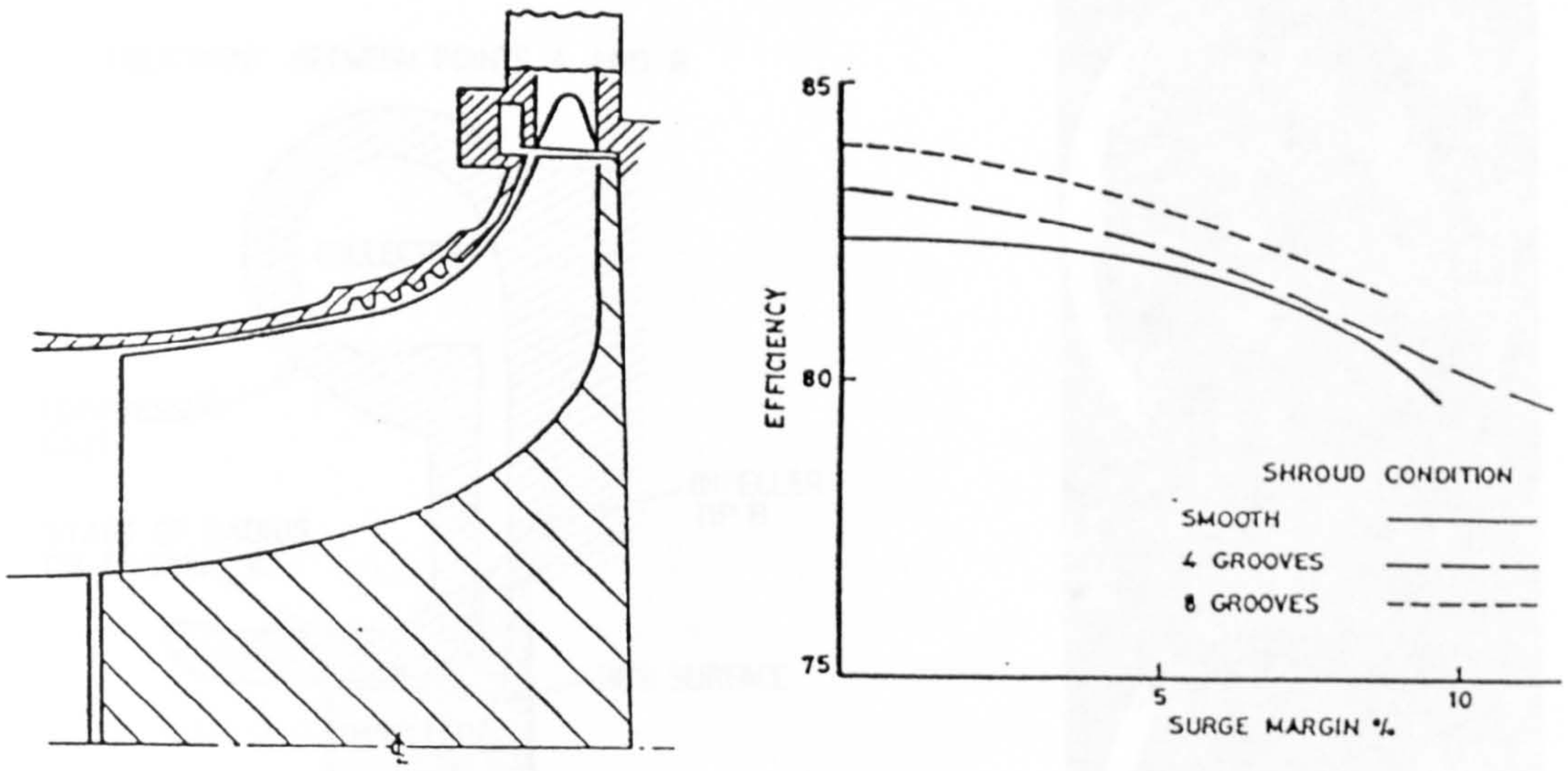

Fig.2-6 United Aircraft Research Configuration and Results

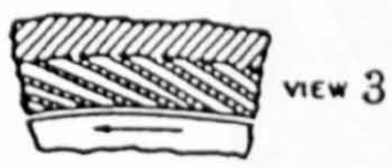

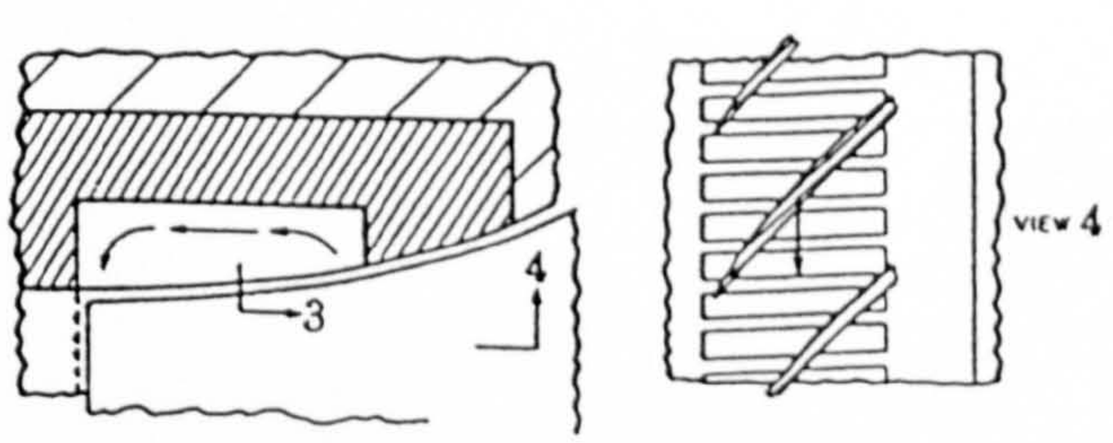

Inclined axial grooves at impeller inlet

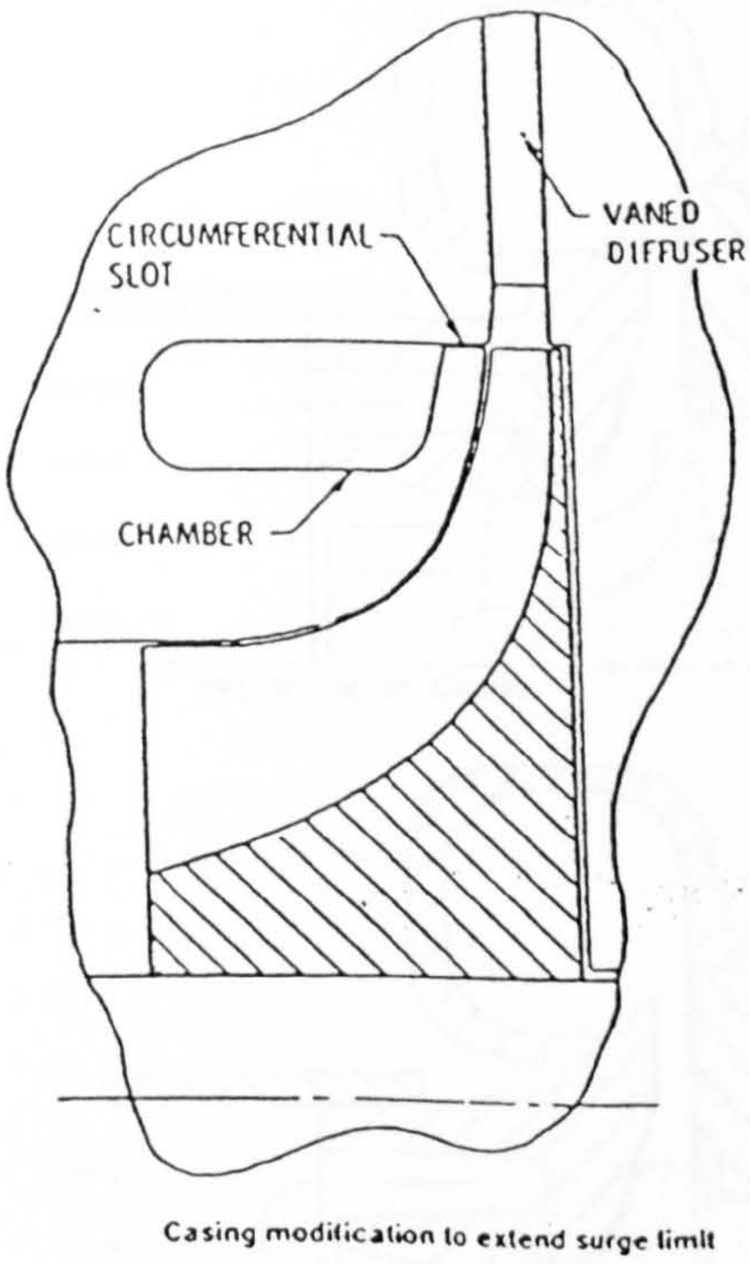

Casing modification to extend surge limit

Fig. 2-7 Circumferential slot with Chamber at impeller exit (Amann et al. 1975)

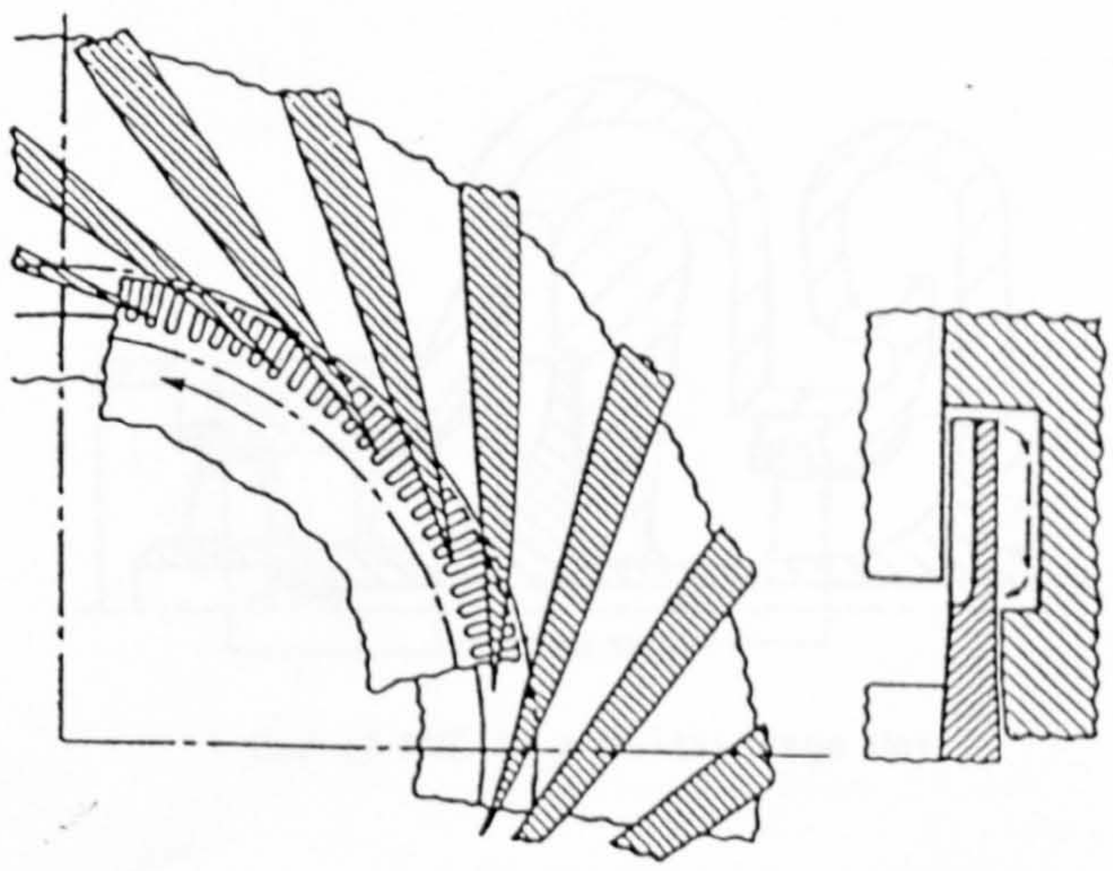

Casing Treatment at impeller exit

Fig. 2-8 Casing Treatment Proposed by Jansen et al.(1980)

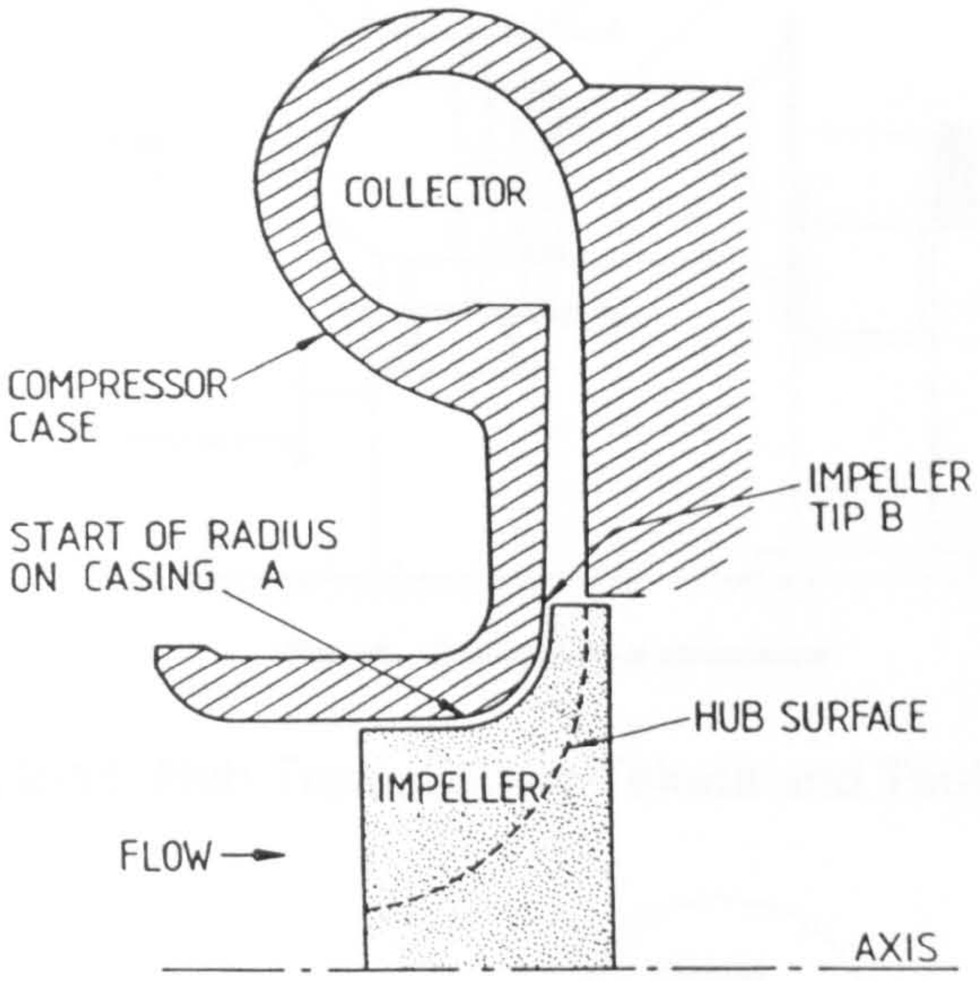

Fig.2-9 Slot and Circumferential groove Treatment(MacDougal and Elder, 1982)

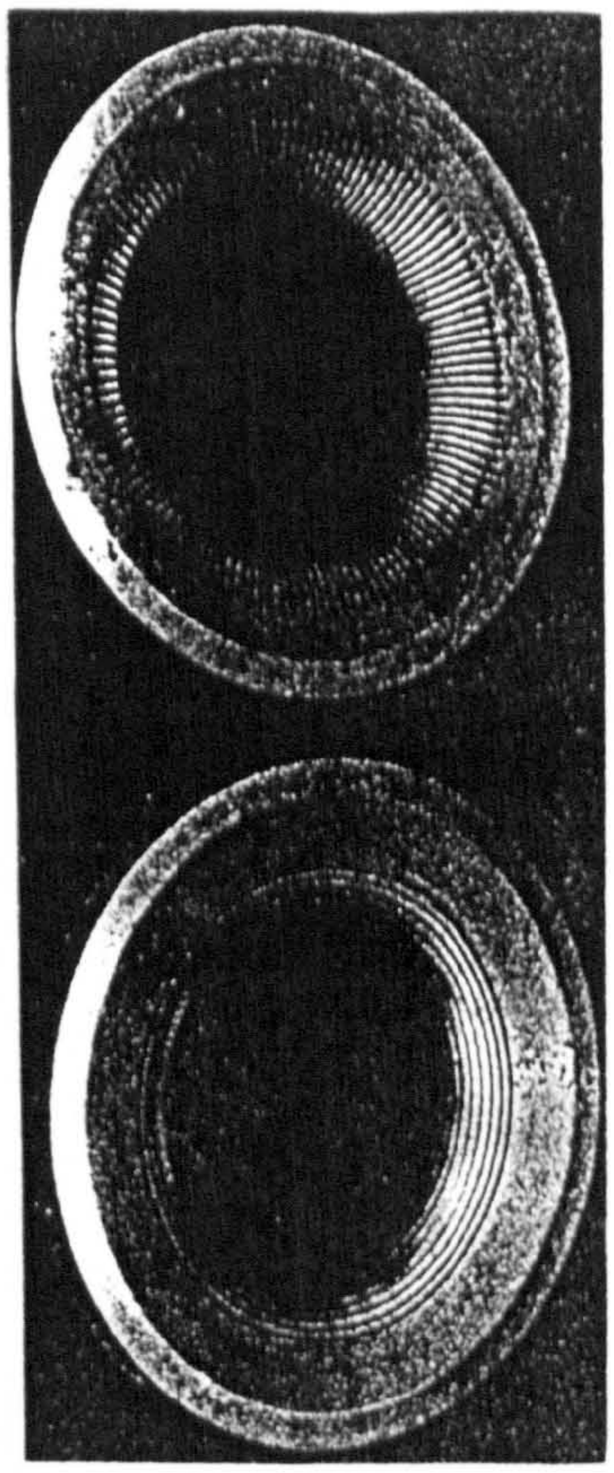

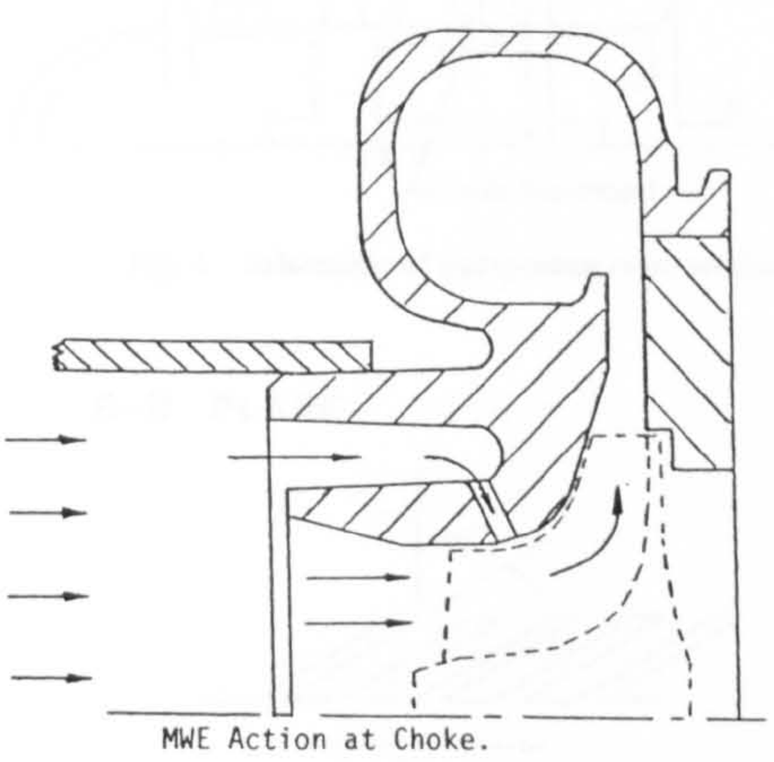

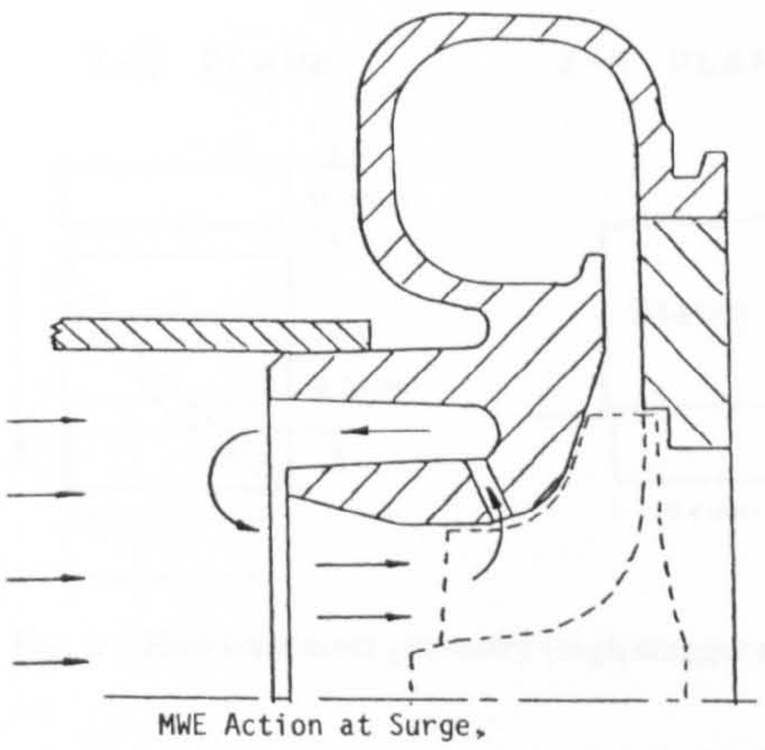

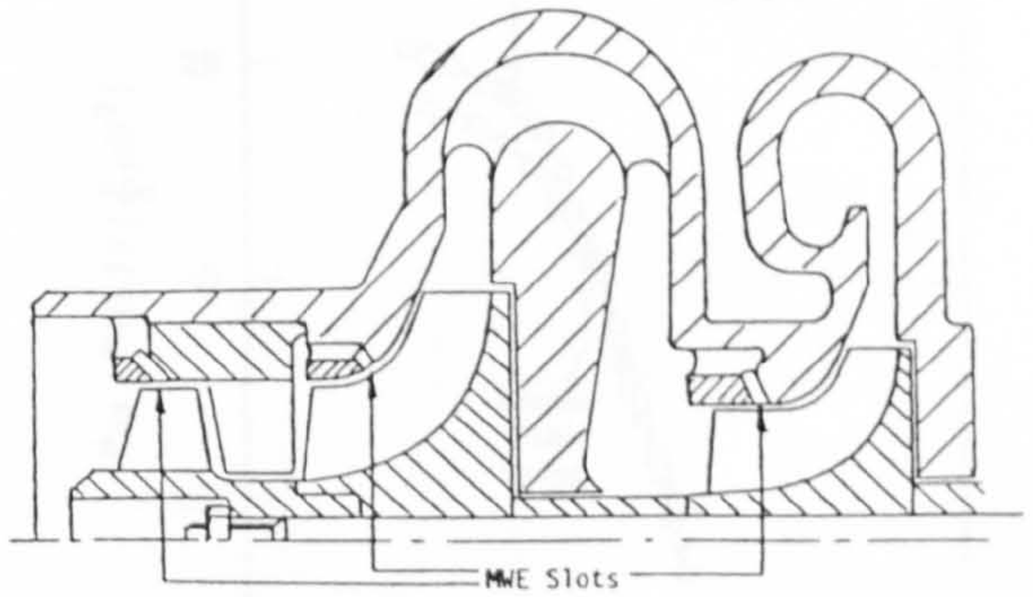

Use of MWE in a Multi-Stage Unit.

Fig. 2-10 Inducer Shroud Bypass as Bleed(Fisher,1988)

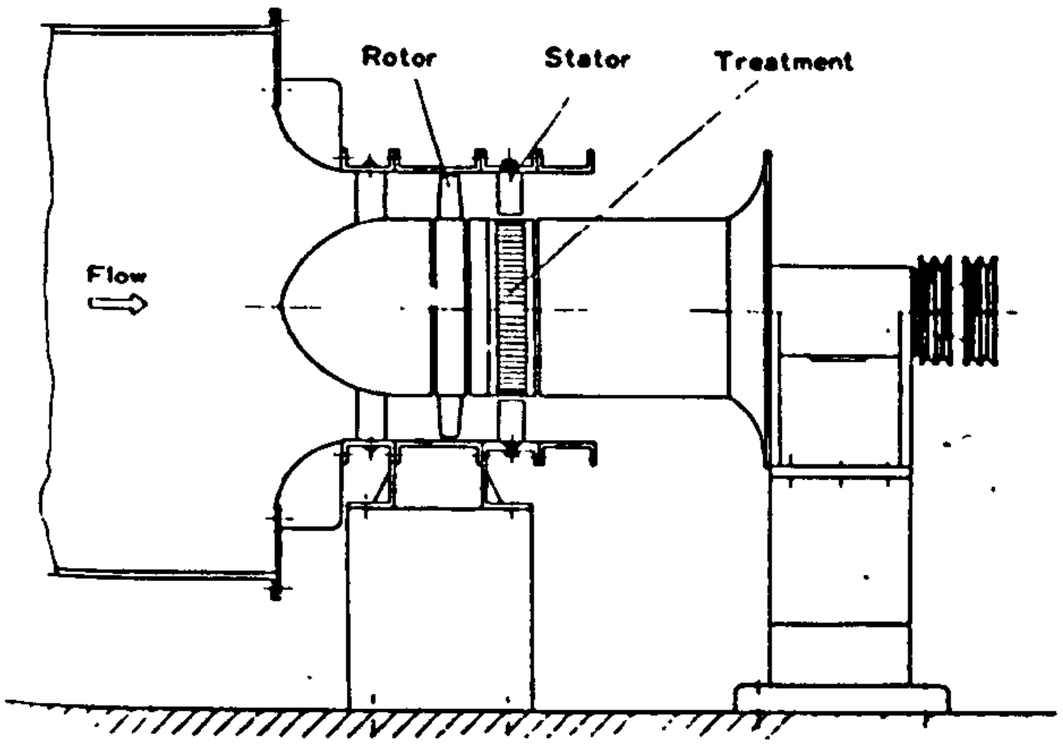

Fig. 18 One-stage test compressor

Fig.2-11 Hub Treatment by **Takata** and **Tsukuda**(1977)

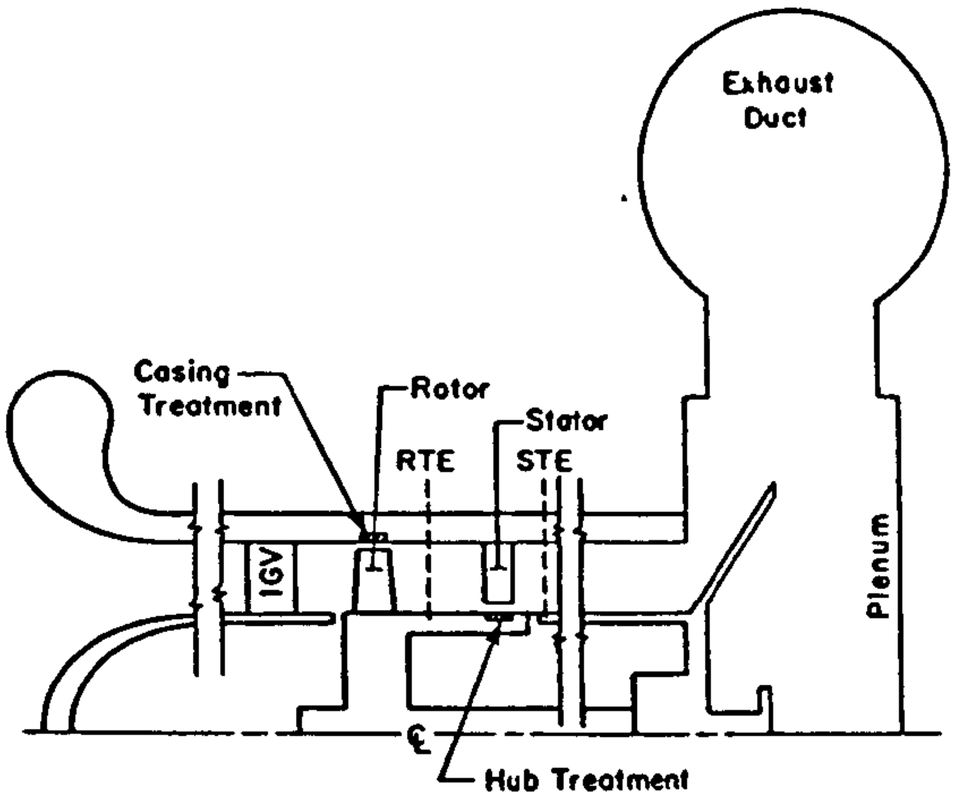

Fig. 1 Schematic of compressor cross section.

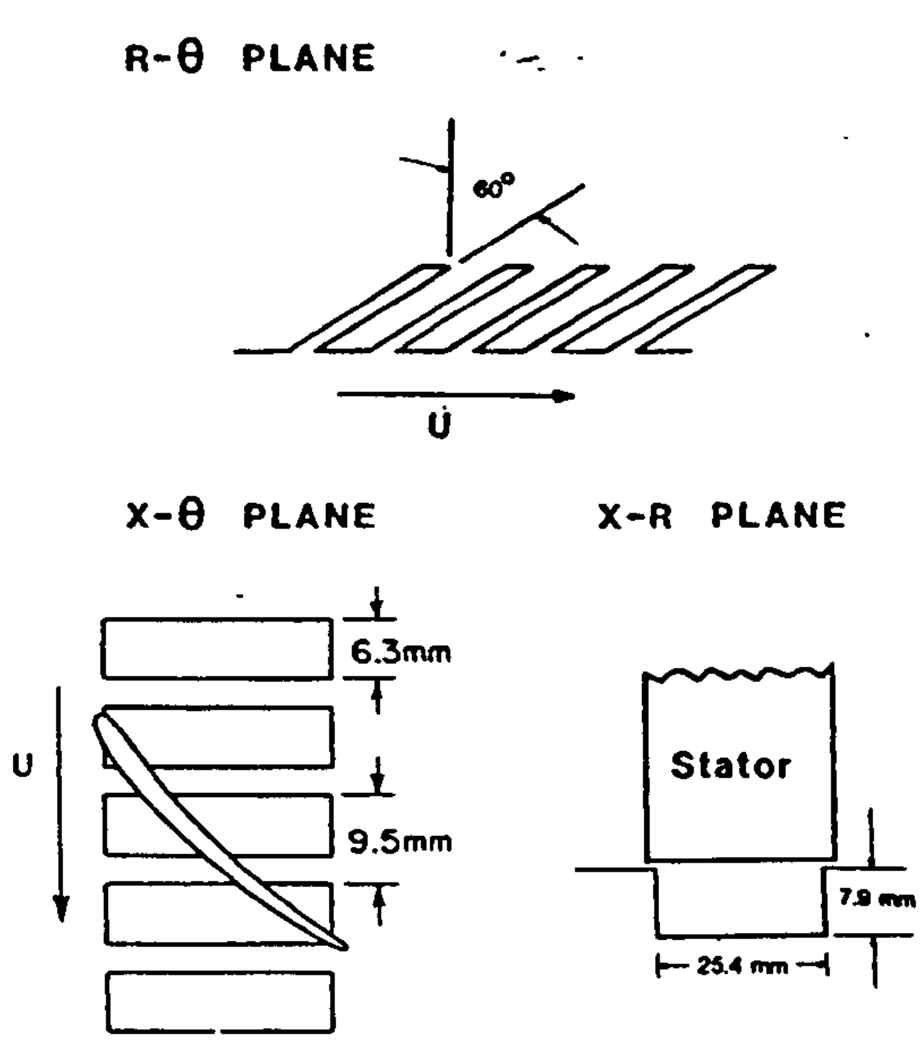

Fig. 2 Hub treatment geometry (high stagger stator).

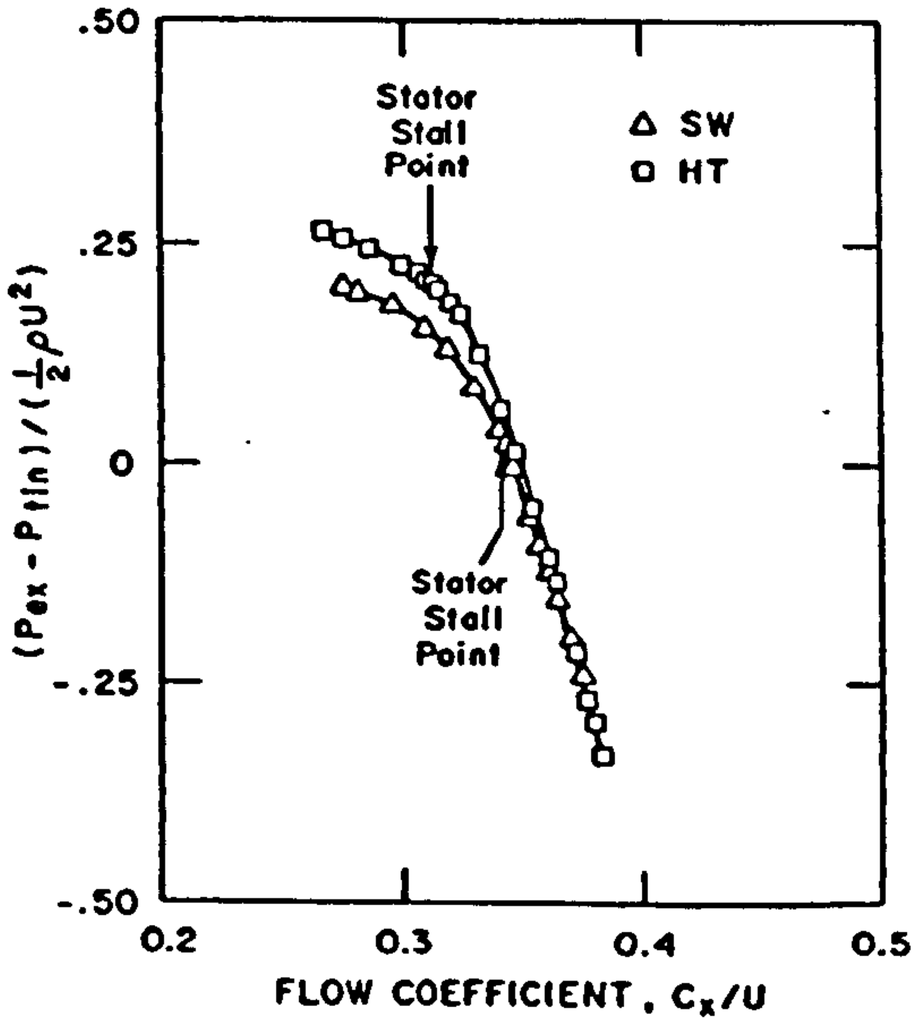

Fig. 4 Exit static minus inlet total pressure rise stage characteristic (high stagger stators) with solid wall (SW) and hub treatment (HT).

Fig.2-12 Hub Treatment by **Cheng** et al. (1984)

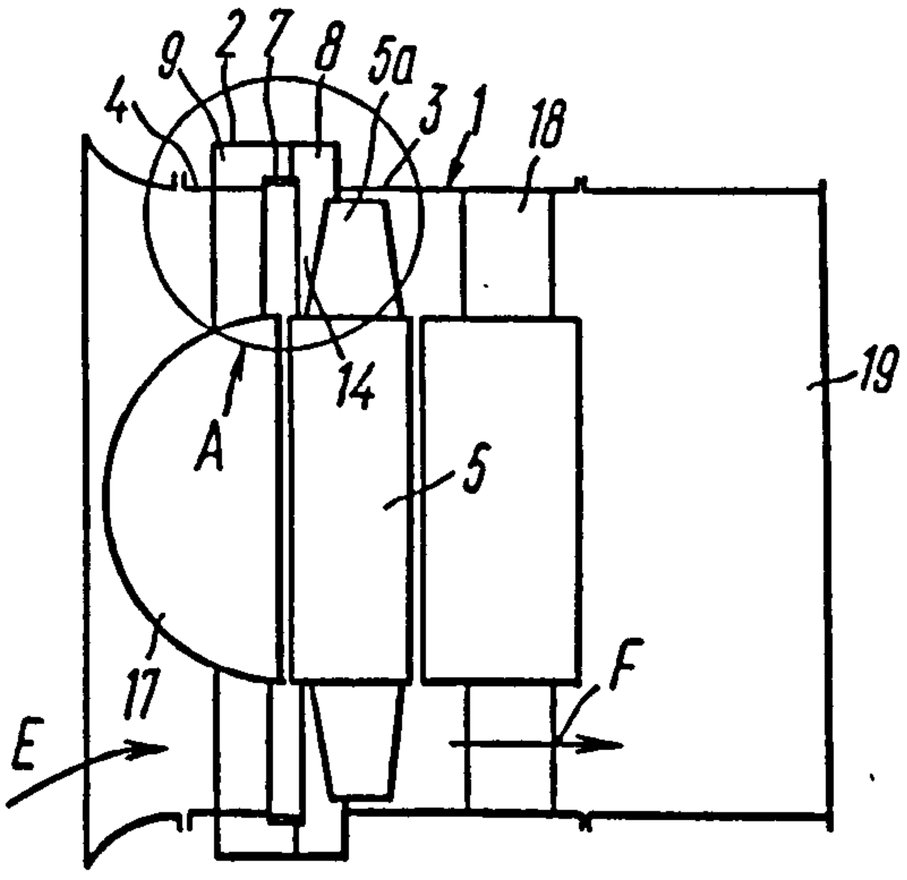

FIG. 1

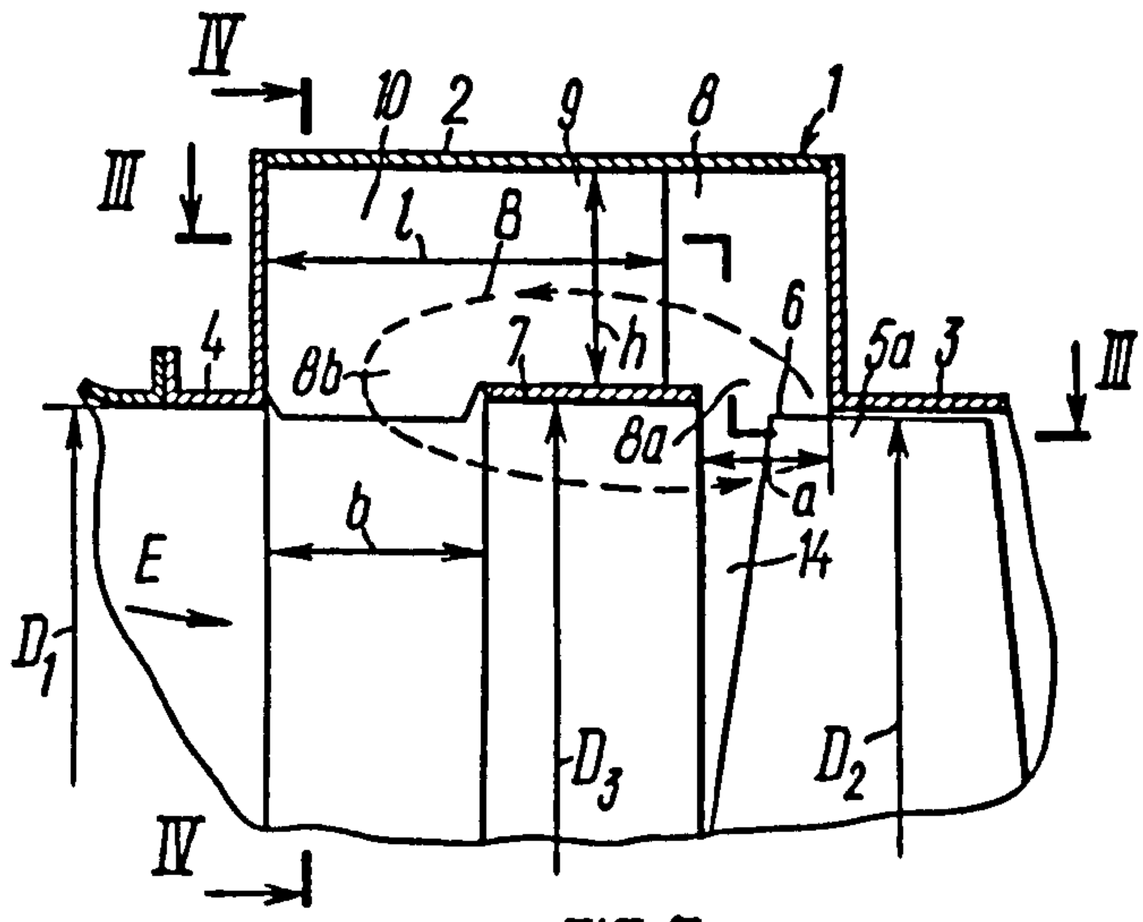

FIG. 2

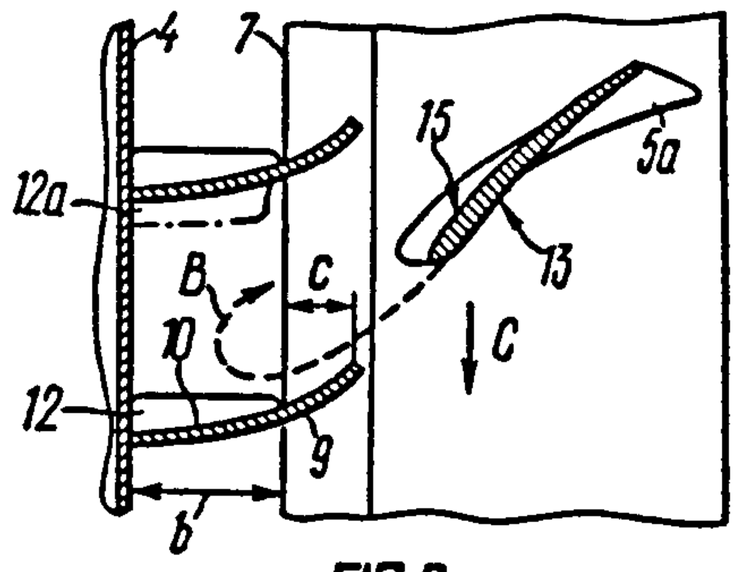

FIG. 3

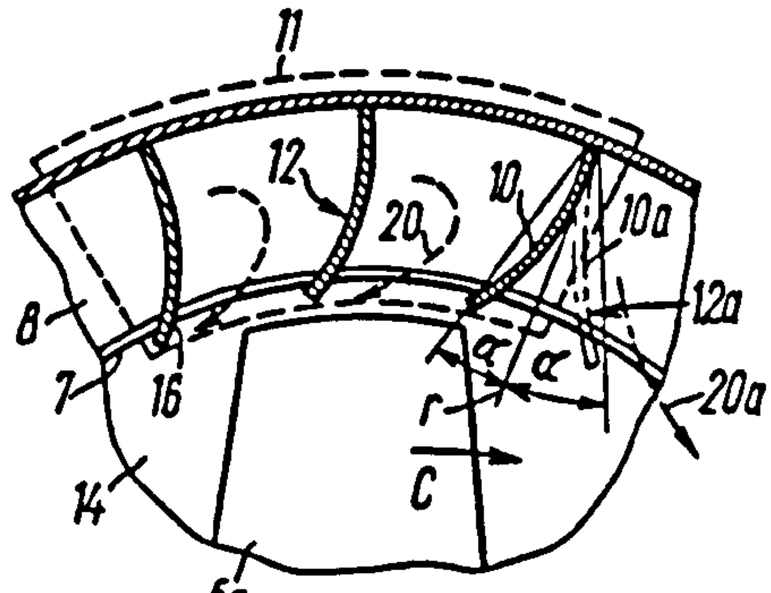

FIG. 4

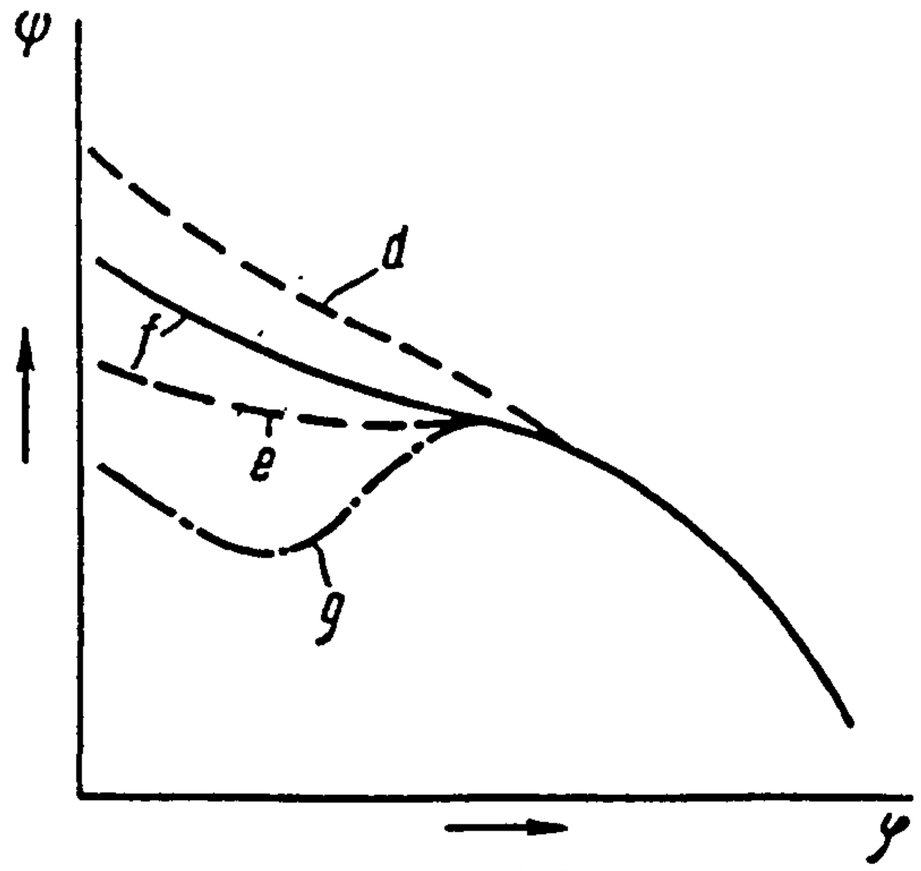

FIG. 5

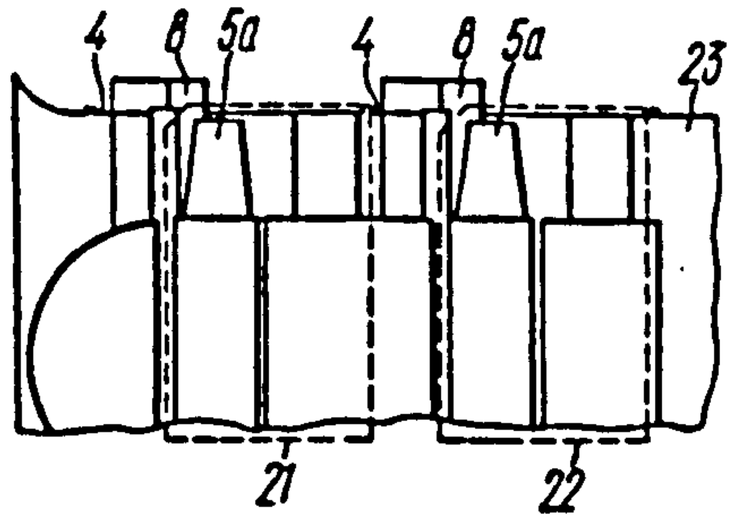

FIG. 6

Fig.2-13 Casing Treatment and Performance Proposed by **Ivanov** et al. (1984)

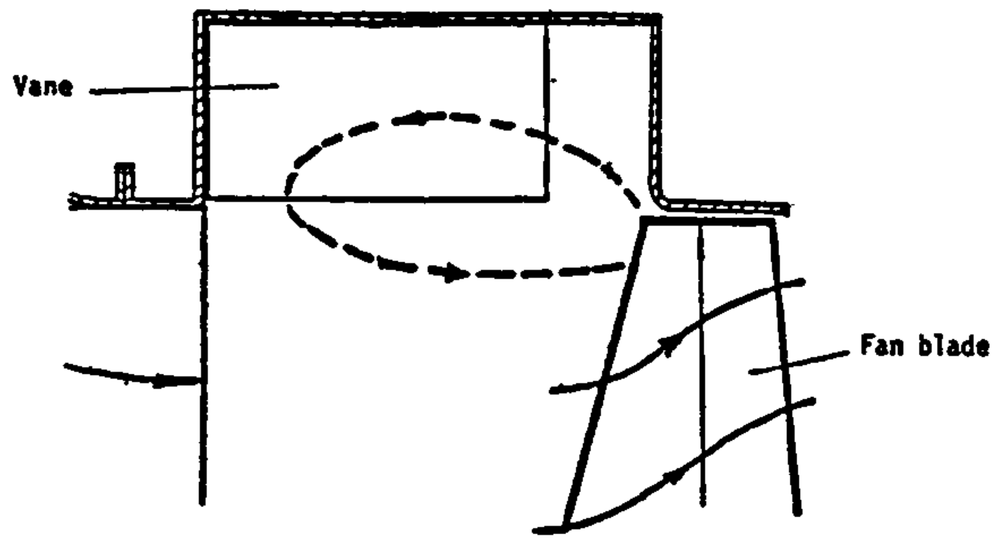

Fig 6 Annular chamber of anti-stall design

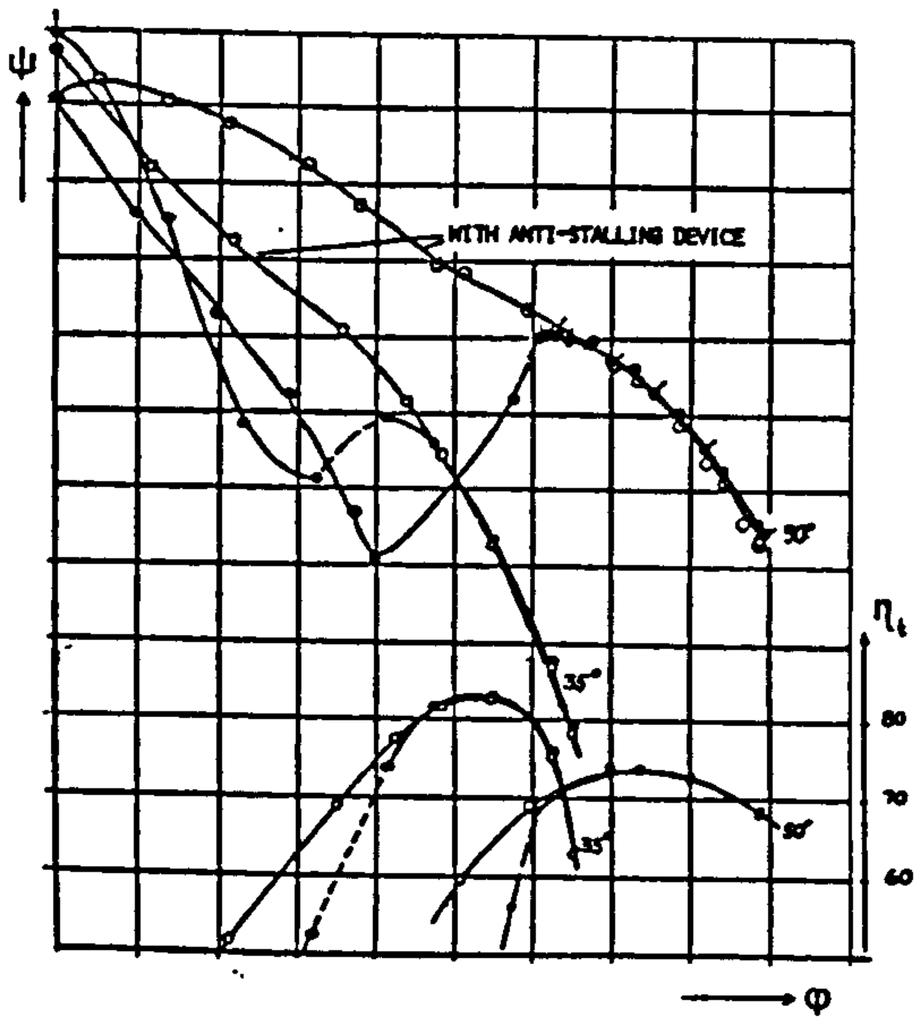

Fig 7 Fan performance characteristic with and without anti-stalling device

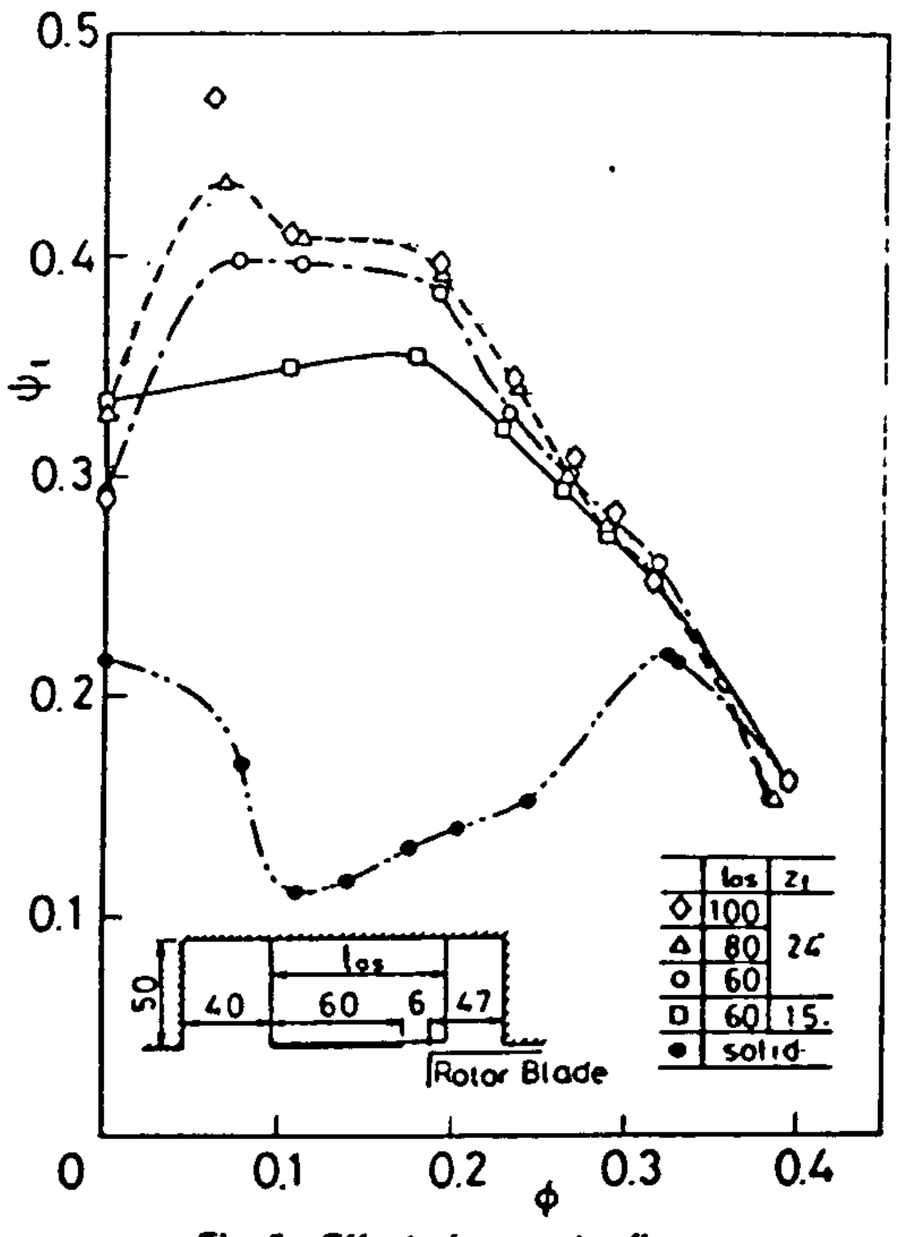

Fig. 5 Effect of separator fins

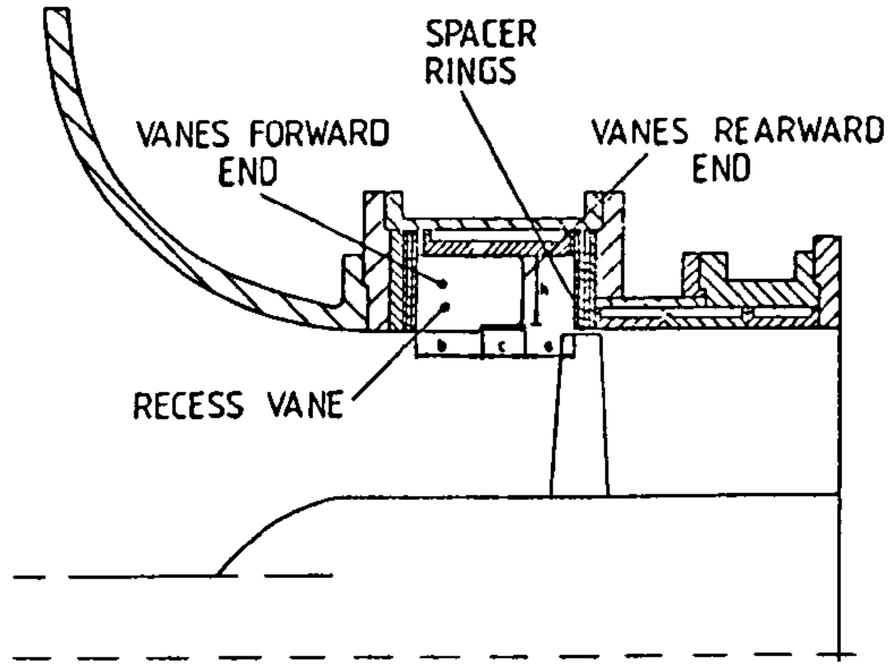

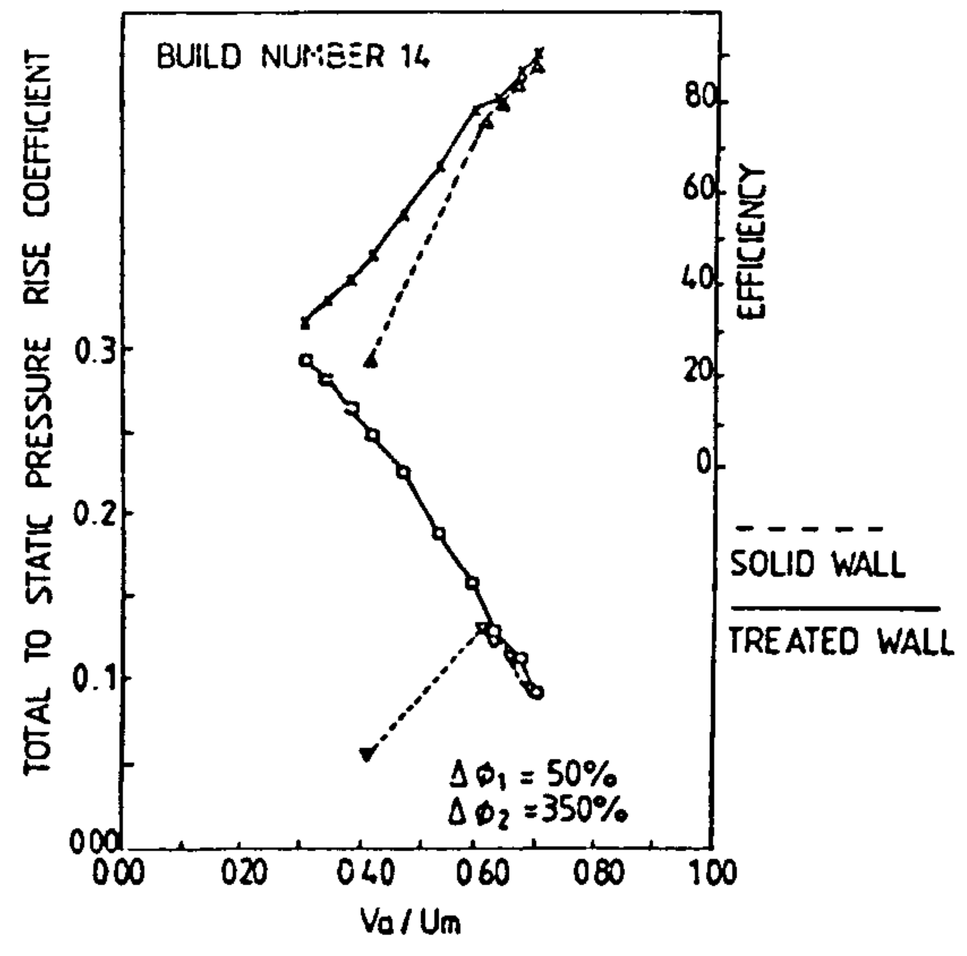

FIG 7 PRESSURE RISE CHARACTERISTICS WITH 67% OF AXIAL CHORD OF ROTOR EXPOSED TO THE TREATMENT

Fig.2-14 Anti-Stall Design and Performance (**Bard**, 1984)

Fig.2-15 " Separator" and Effect (**Miyake** et al.,1987)

Fig.2-16 Casing Treatment Design and Performance (**Azimian** et al.,1989)

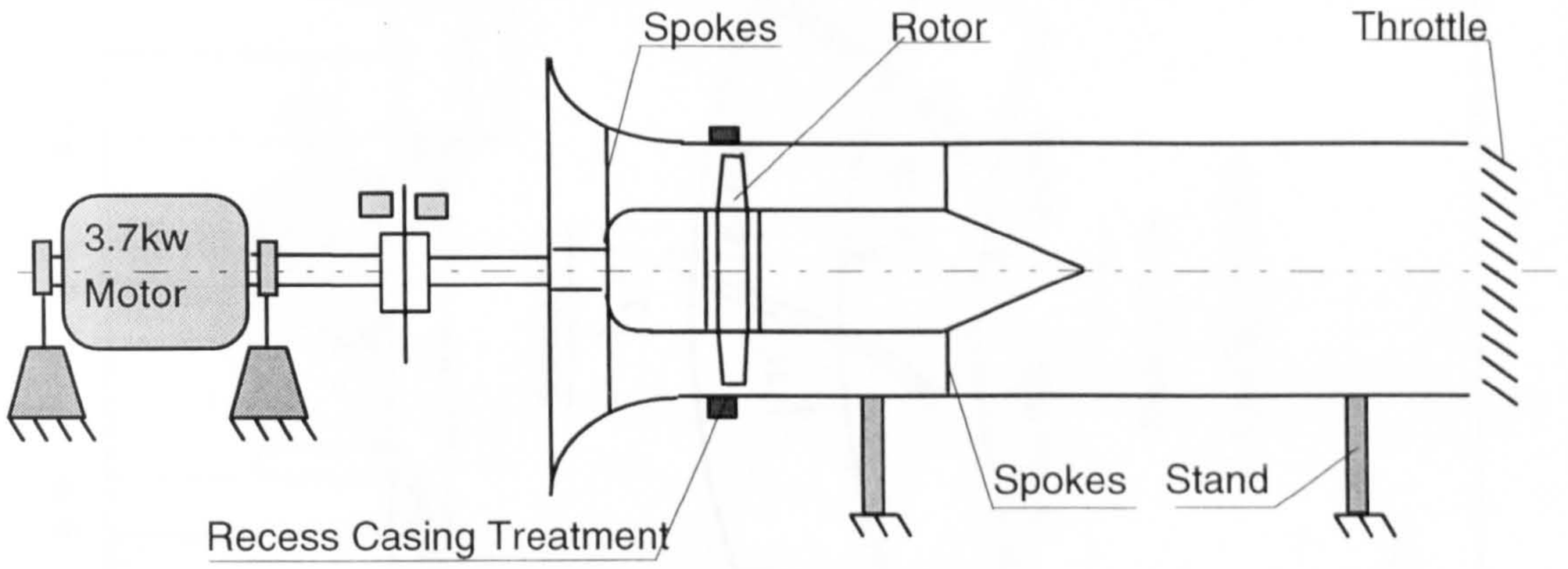

Outer Diameter	508mm
Hub-Tip Ratio	0.5
Rotor Speed	1500rpm
Rotor tip Speed	39m/s
Number of Blades	27
Blade Profile	C4
Rotor Chord	48mm

Fig.3-1 Sketch of the Low Speed Single Stage Fan Rig

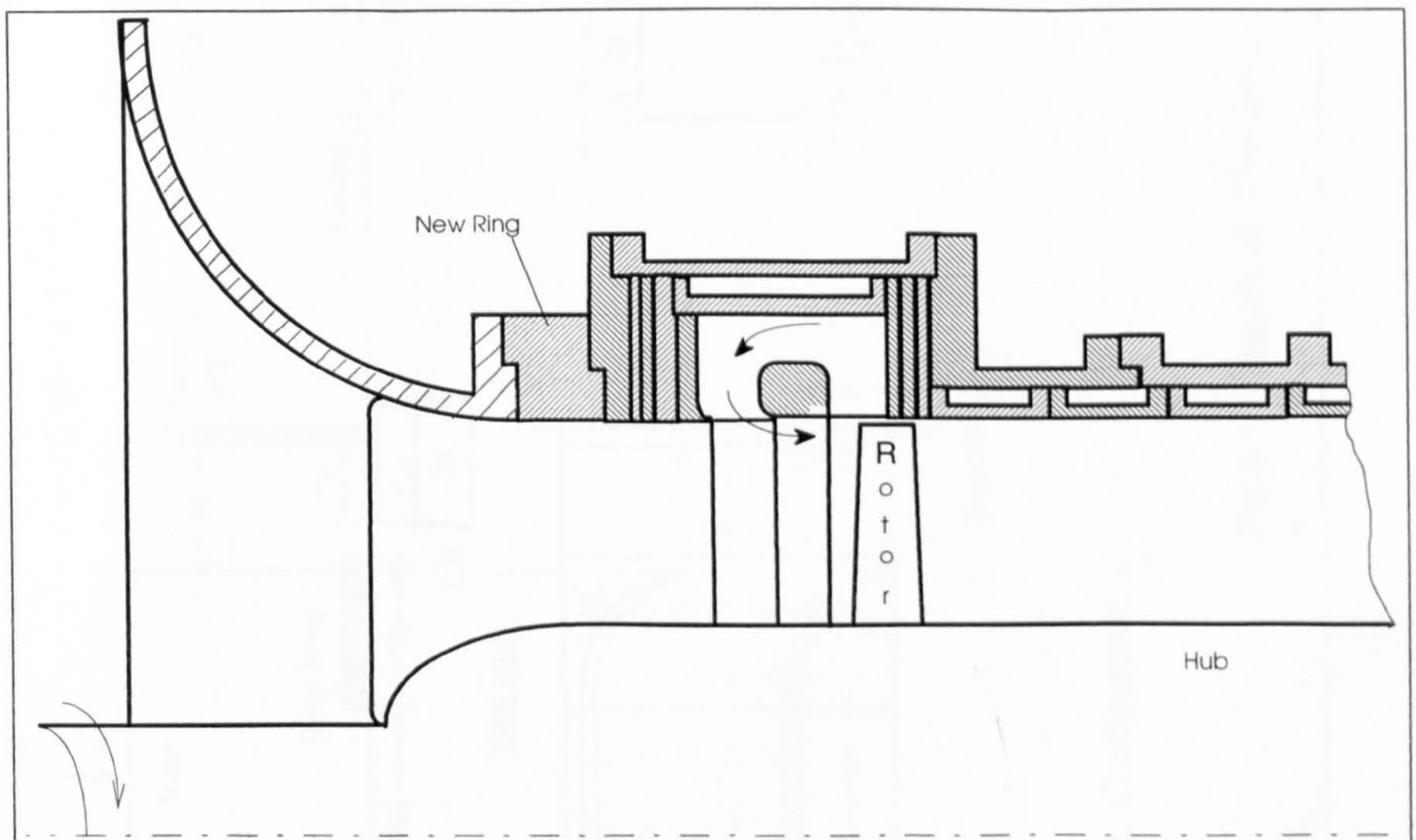

Fig.3-2 Treated Casing Section

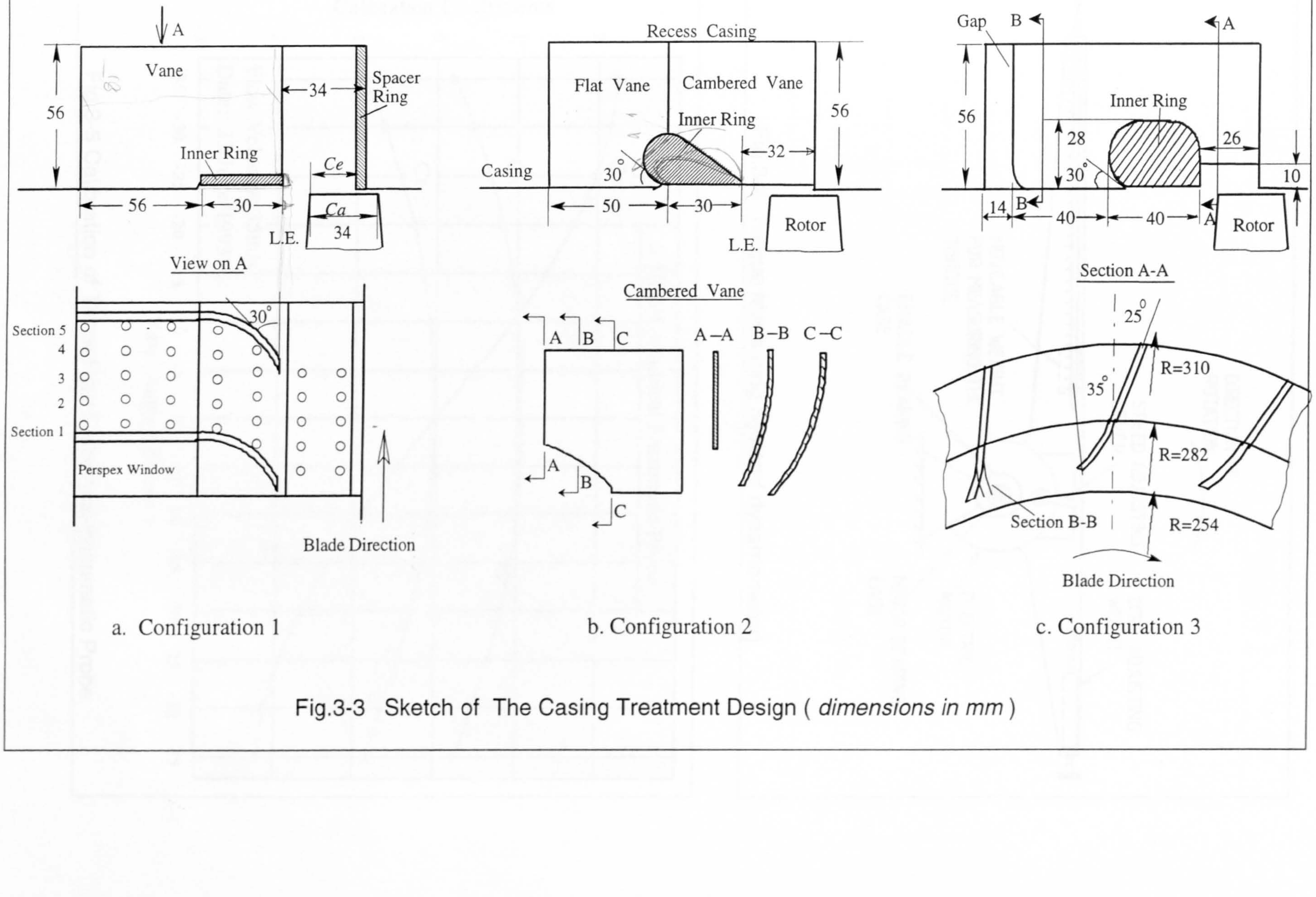

Fig.3-3 Sketch of The Casing Treatment Design (*dimensions in mm*)

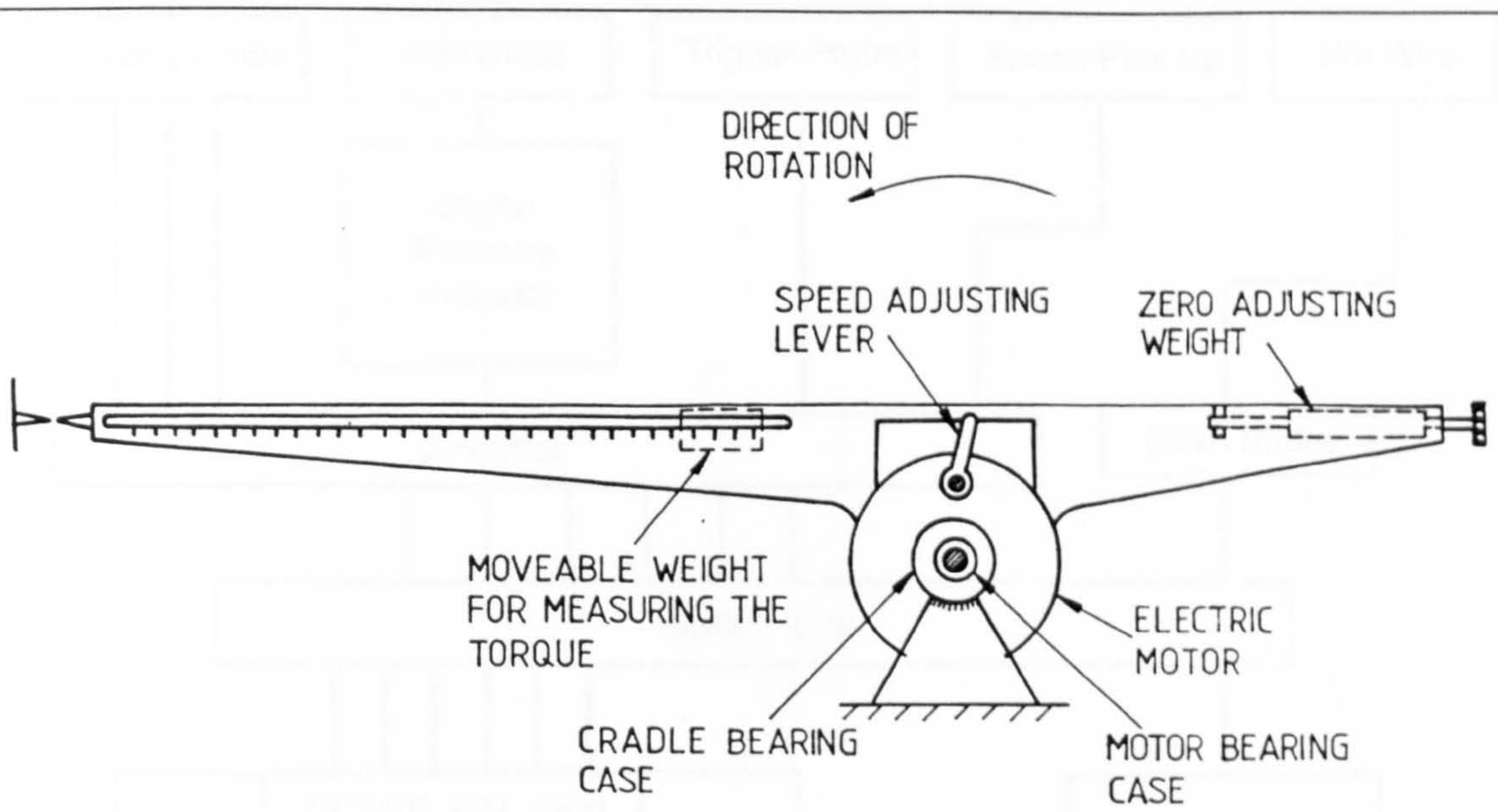

Fig.3-4 Torque Measuring System(dynamometer)

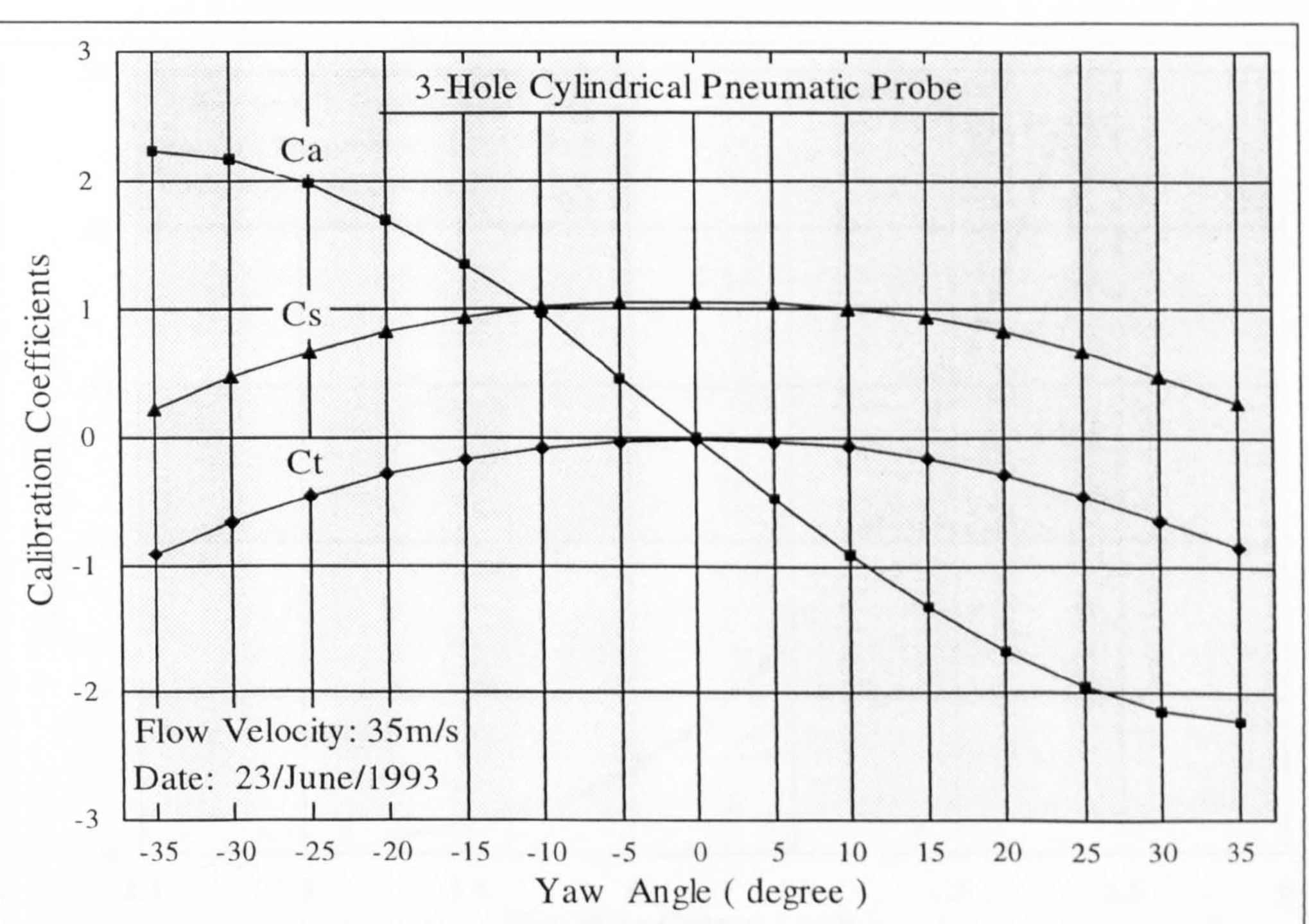

Fig.3-5 Calibration of Three-Hole Cylindrical Pneumatic Probe

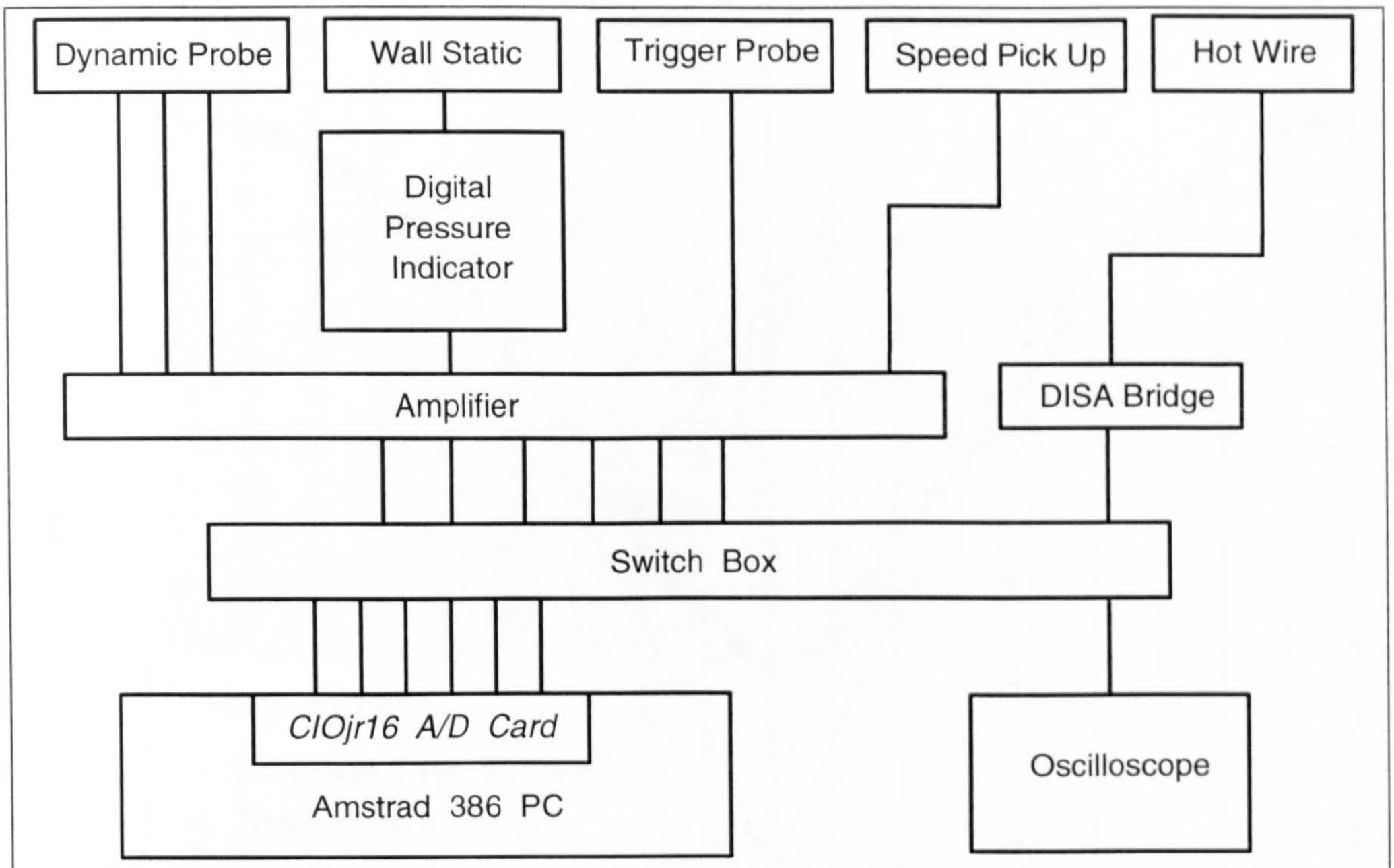

Fig.3-6 Data Acquisition System

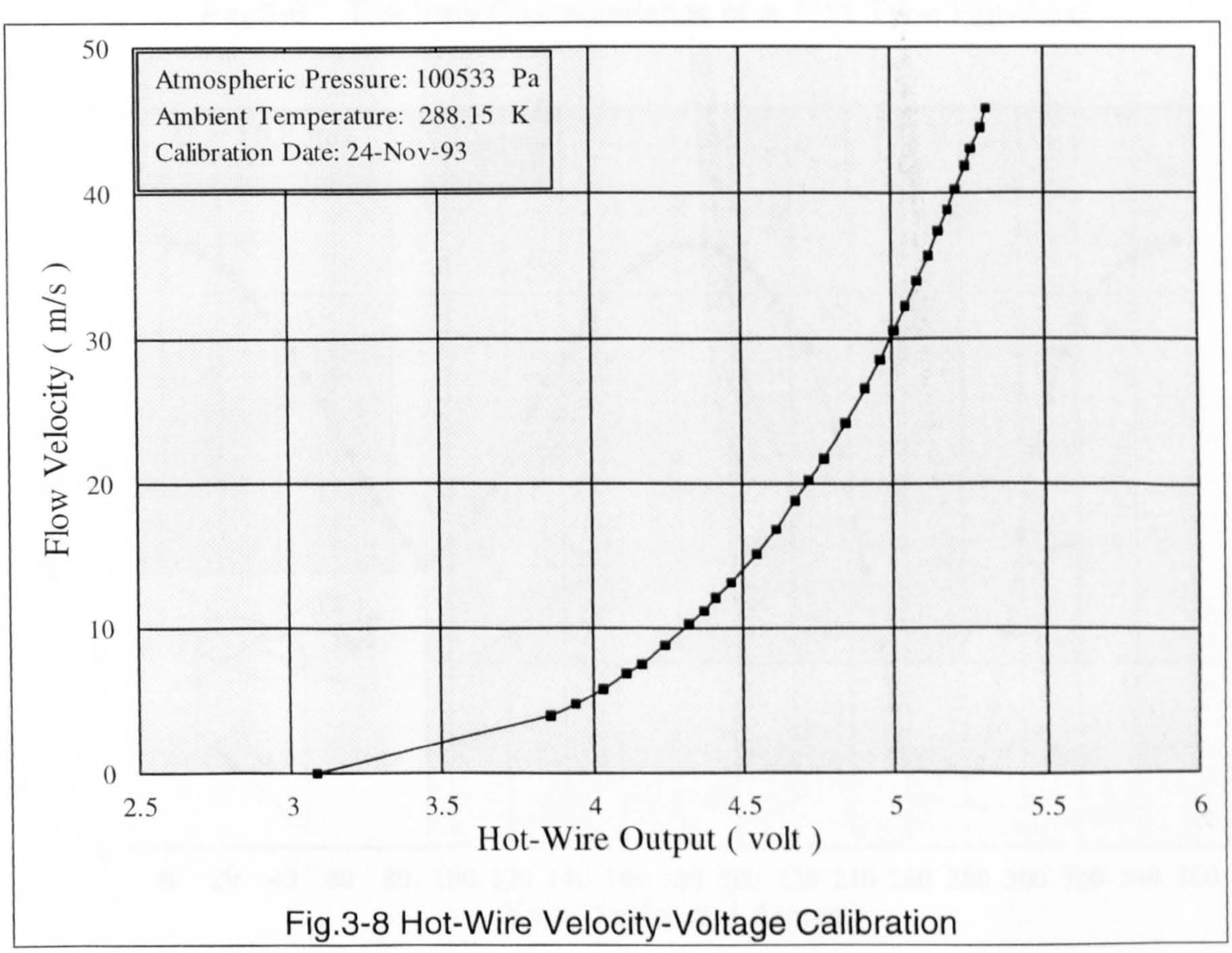

Fig.3-8 Hot-Wire Velocity-Voltage Calibration

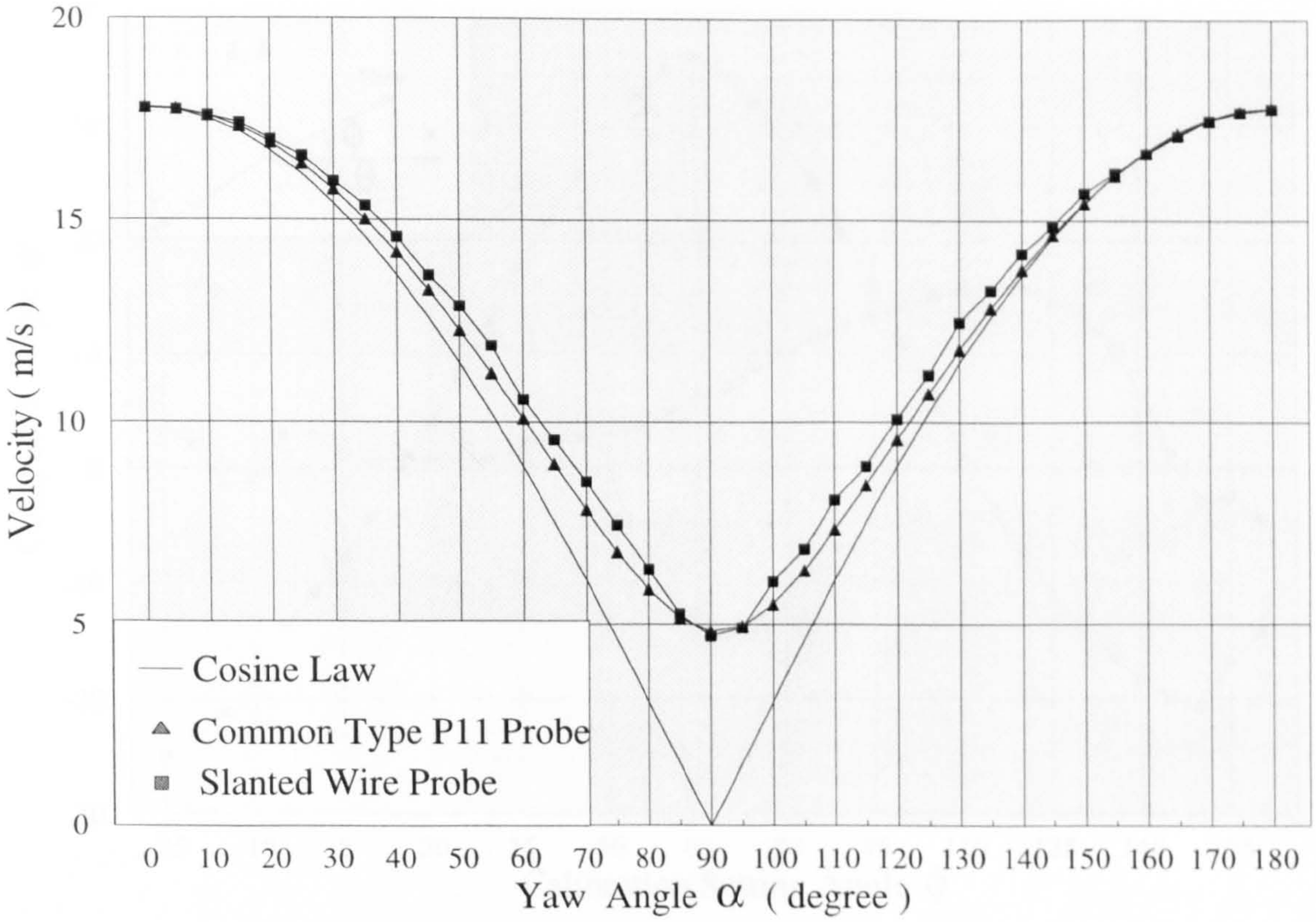

Fig.3-9 The Yaw Characteristics of a P11 Type Hot-Wire

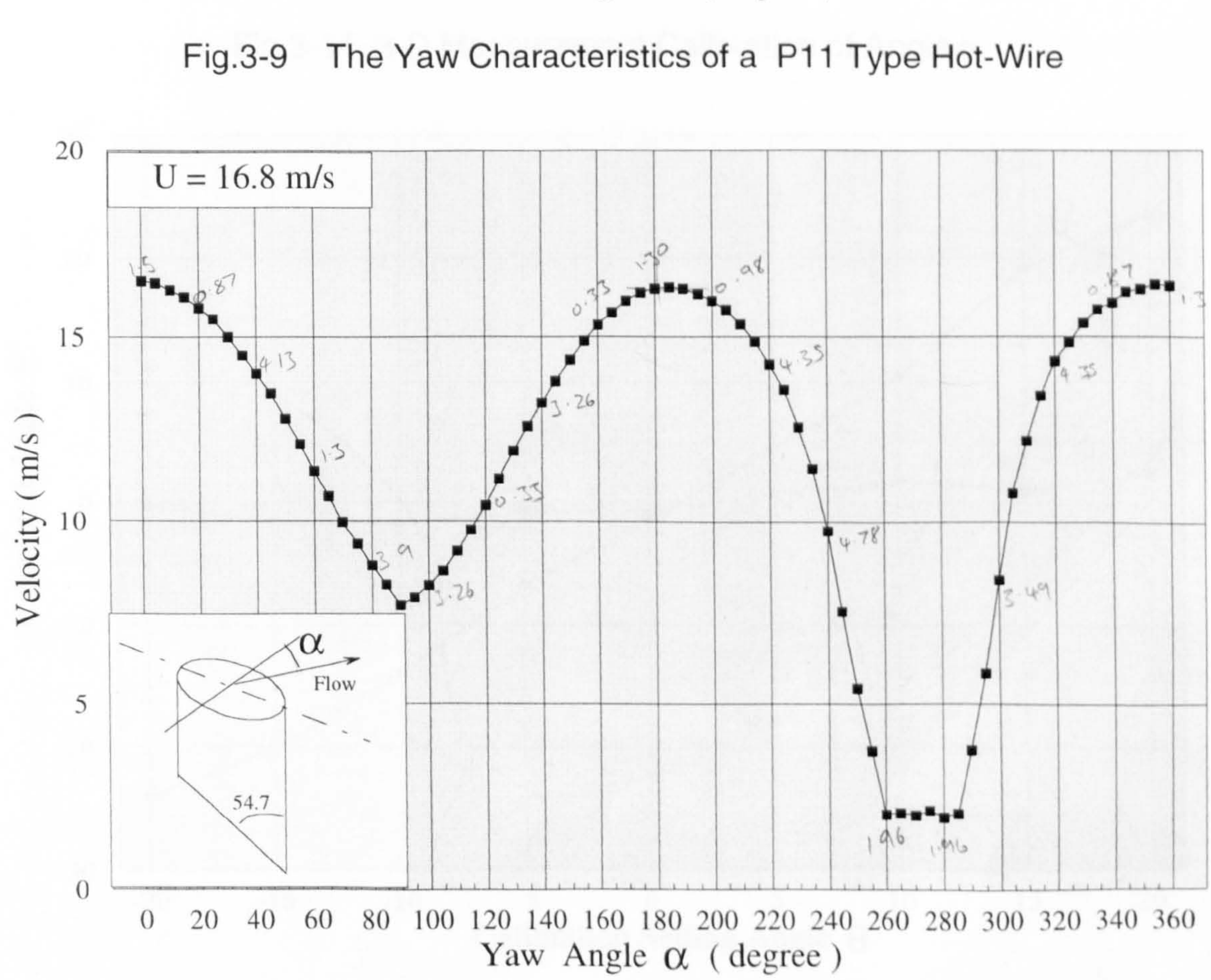

FIG.3-10 The Yaw Characteristics of a 54.7 Degree Slanted Hot-Wire

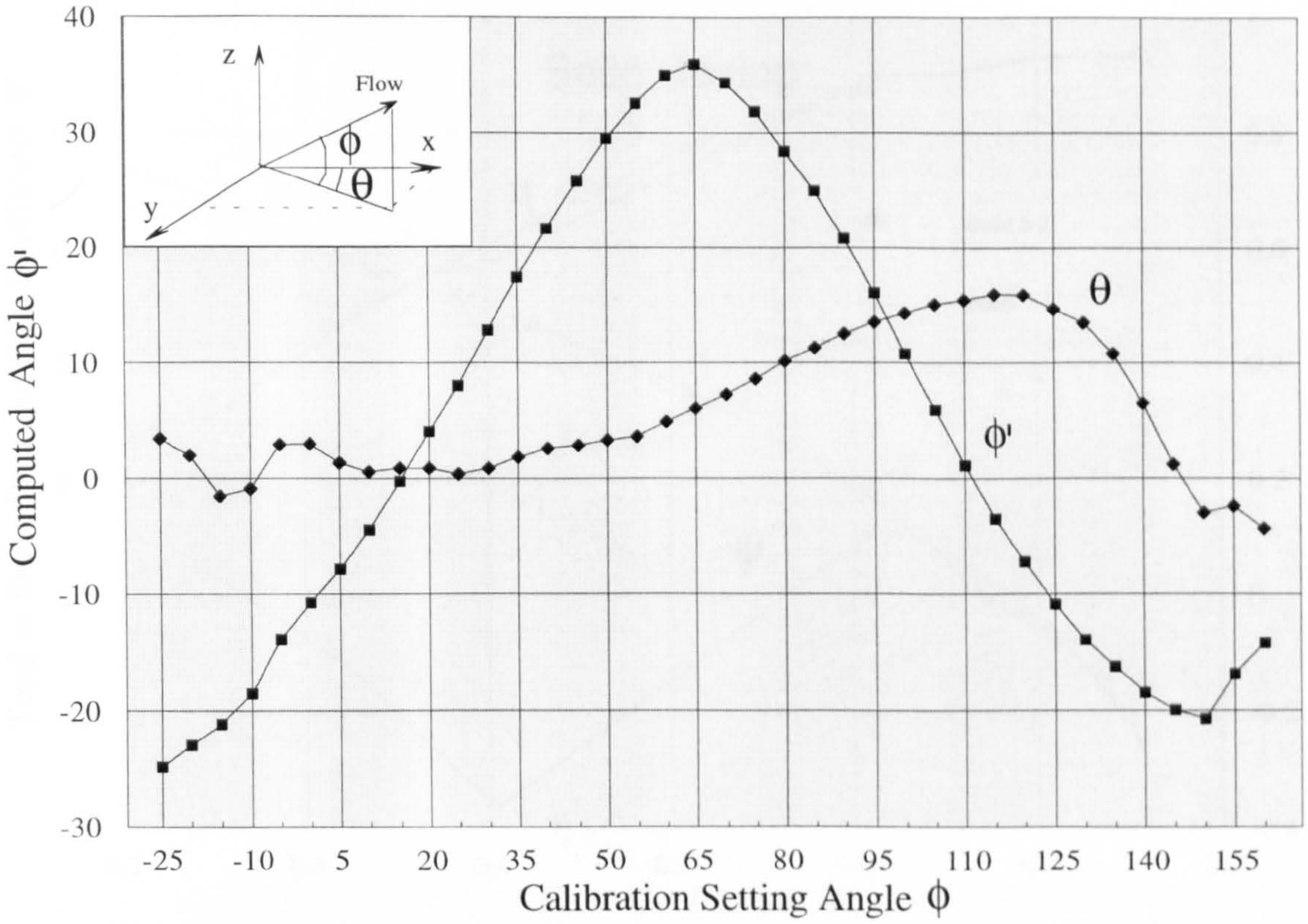

Fig.3-11 3-D Measurement Calibration of Angle ϕ

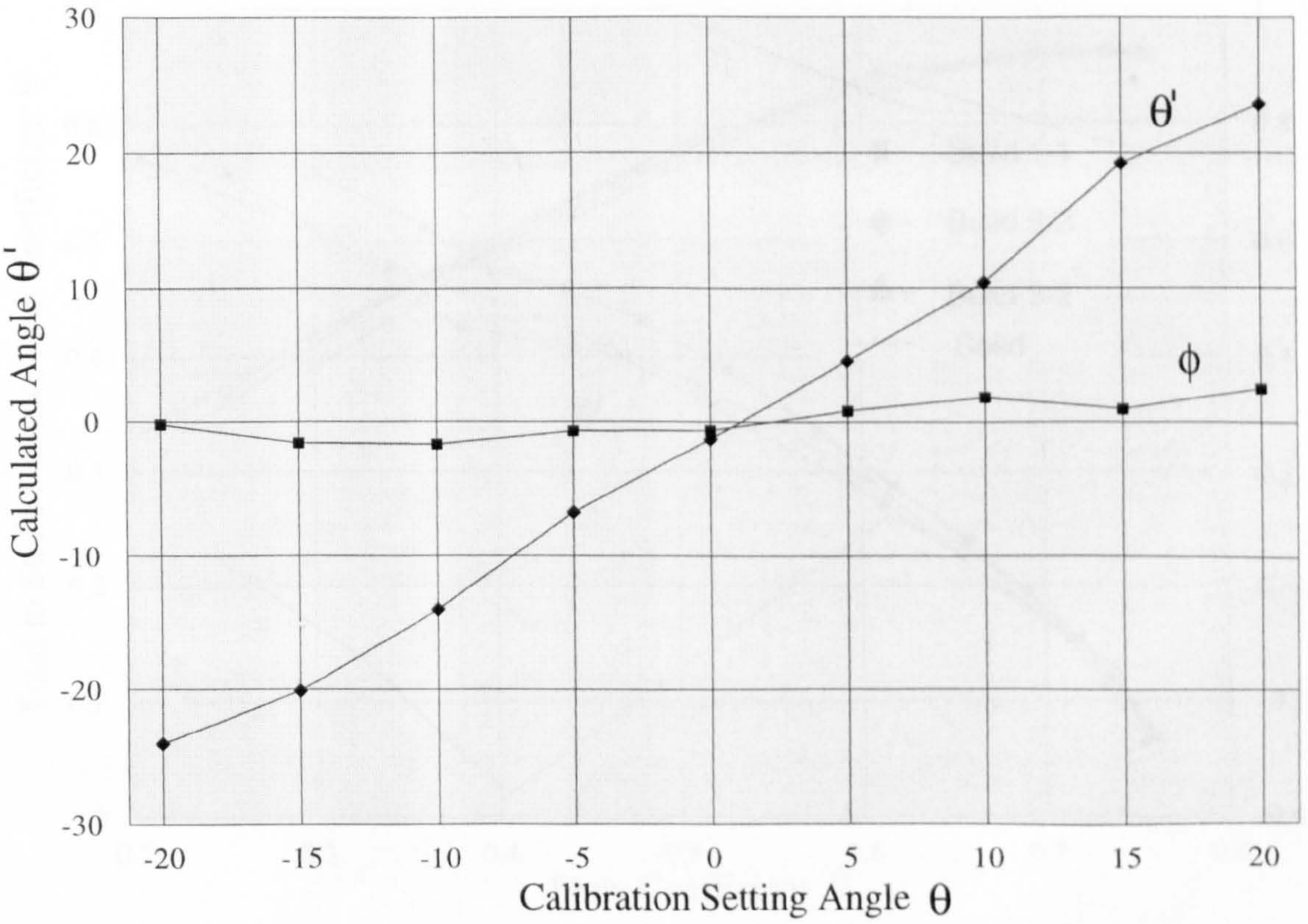

Fig.3-12 3-D Measurement Calibration of Angle θ

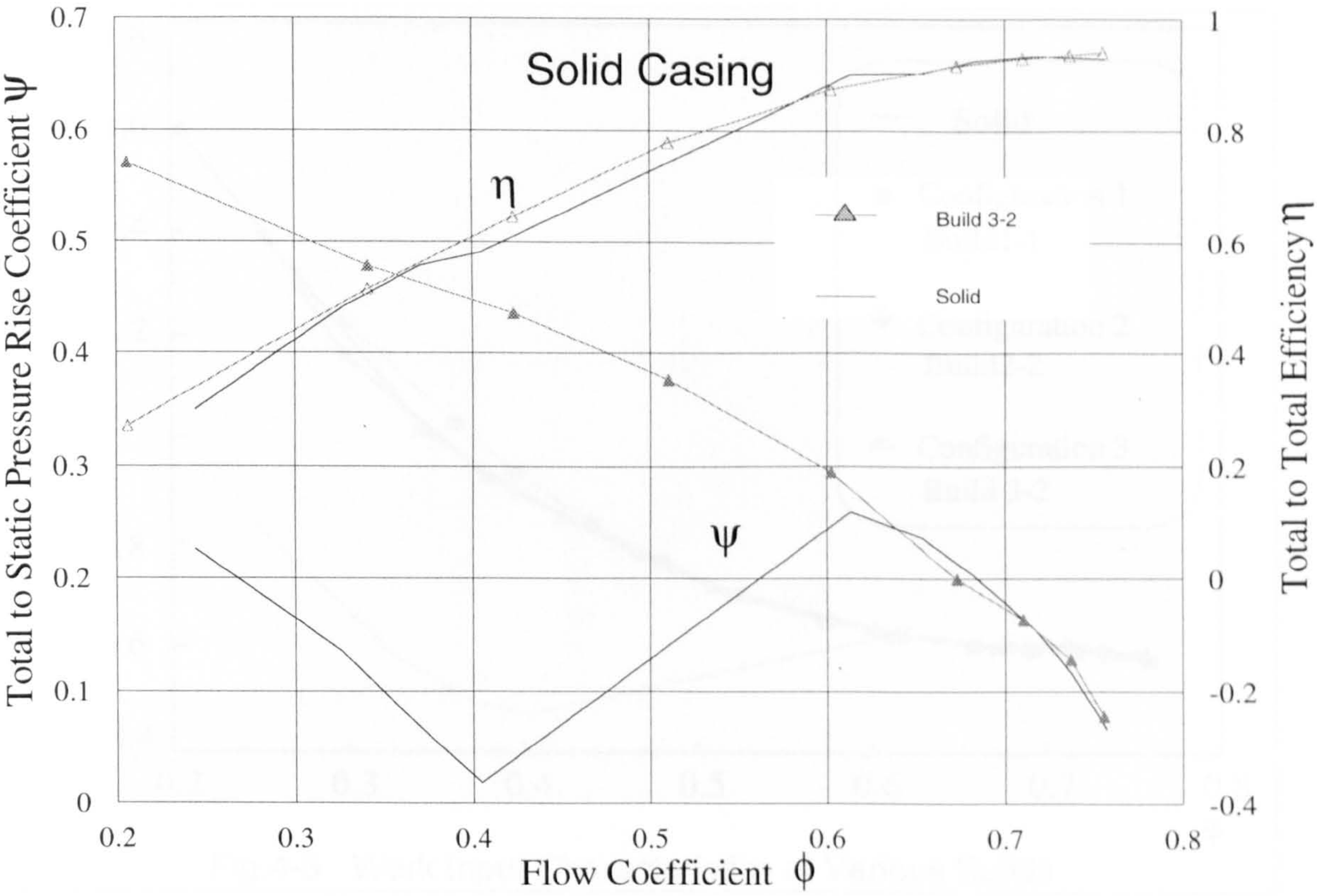

Fig. 4-1 Overall Performance of the Rotor with Solid Casing and Configuration 3

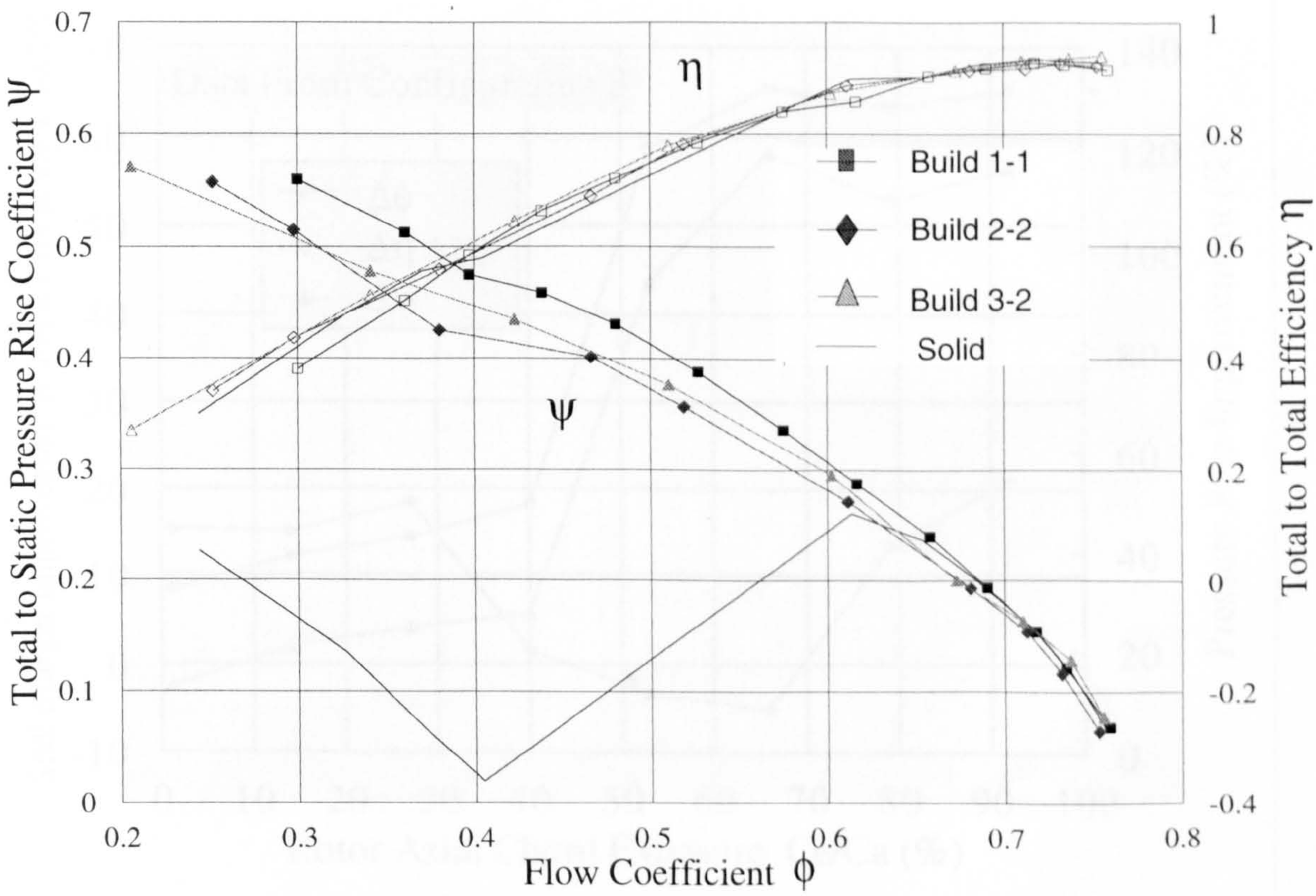

Fig.4-2 Overall Performance of the Isolated Rotor with Various Casings

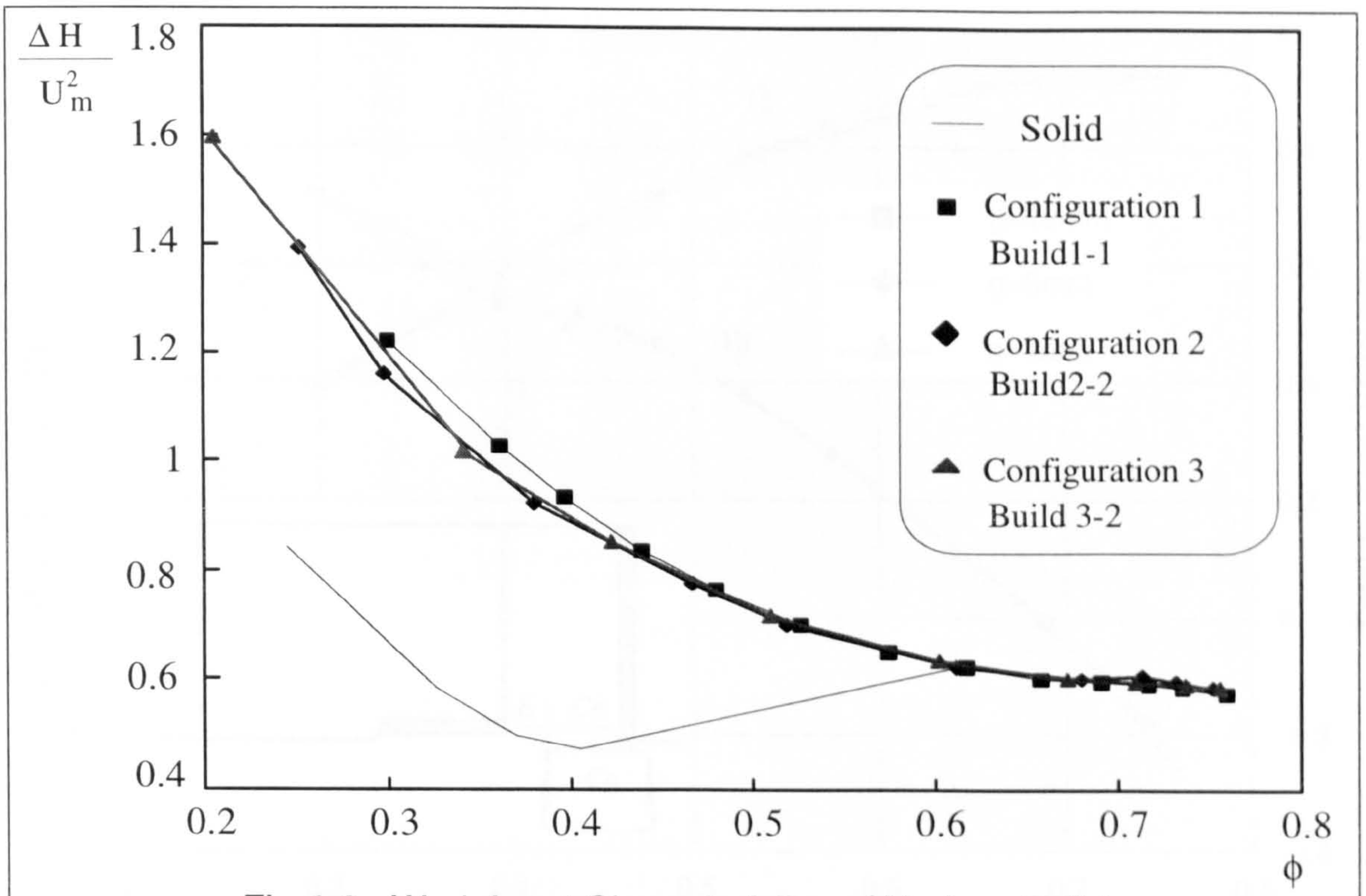

Fig.4-3 Work Input Characteristics of Various Builds

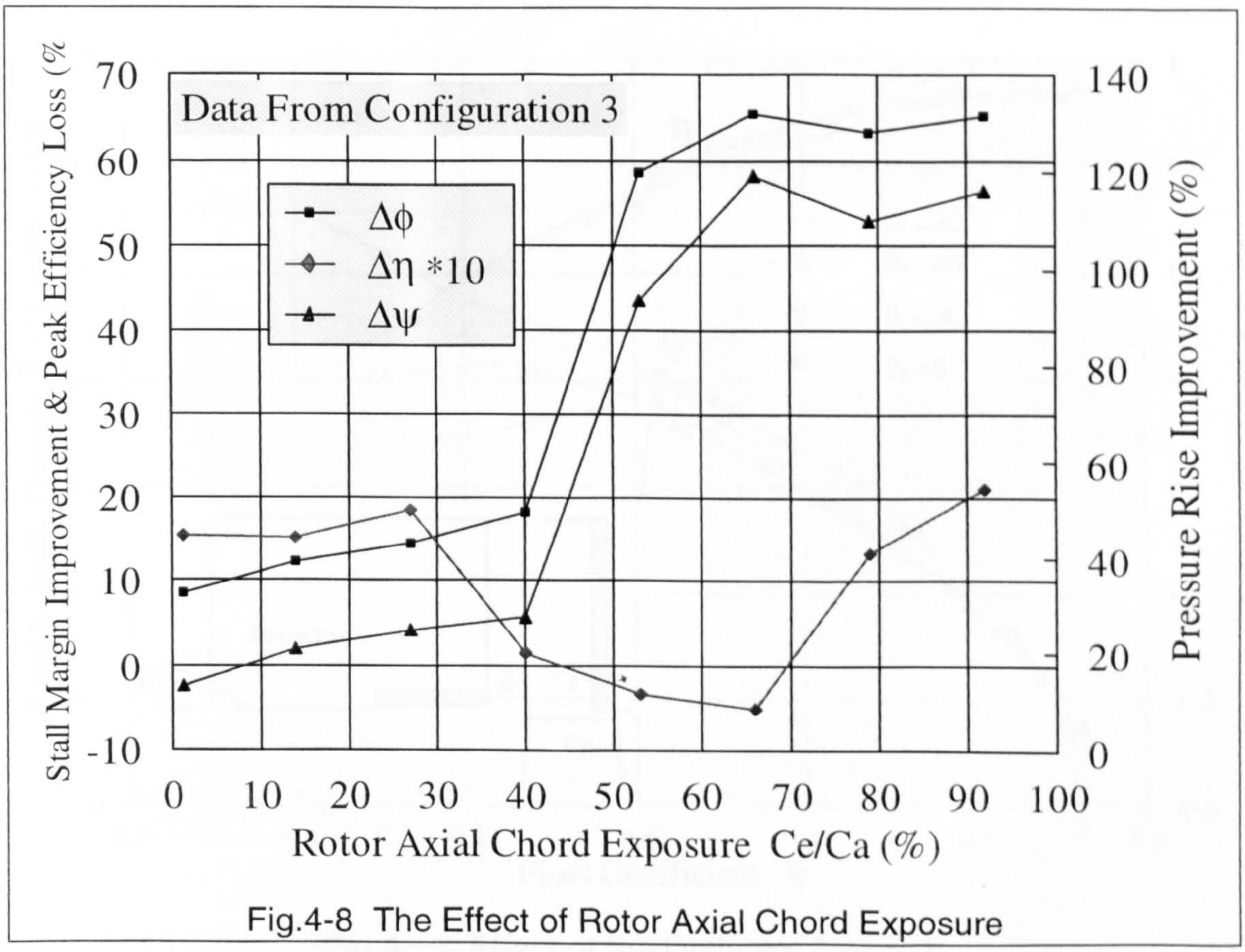

Fig.4-8 The Effect of Rotor Axial Chord Exposure

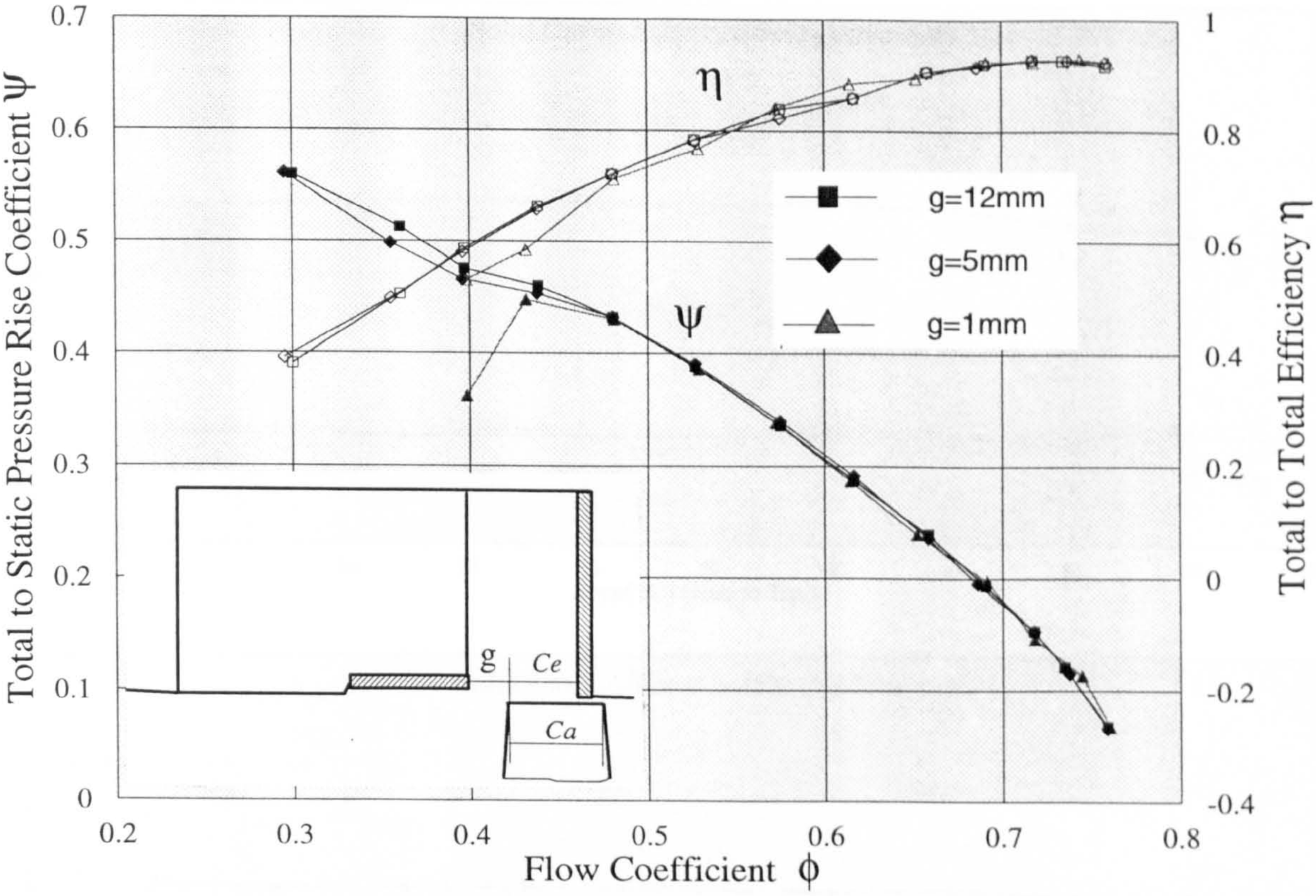

Fig.4-9 the Effect of Inlet Width of the Casing Treatment

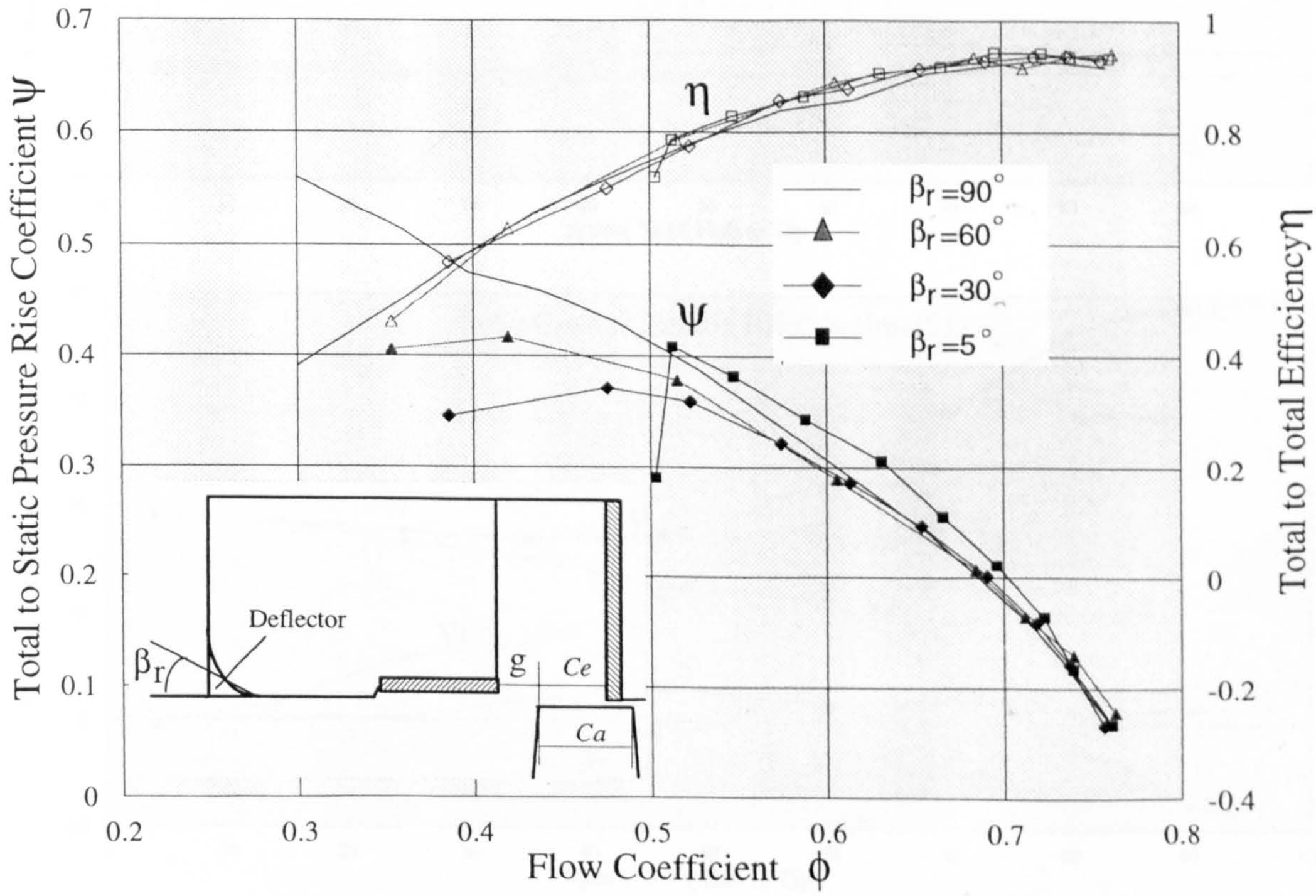

Fig.4-10 Effect of the Deflector Angle β

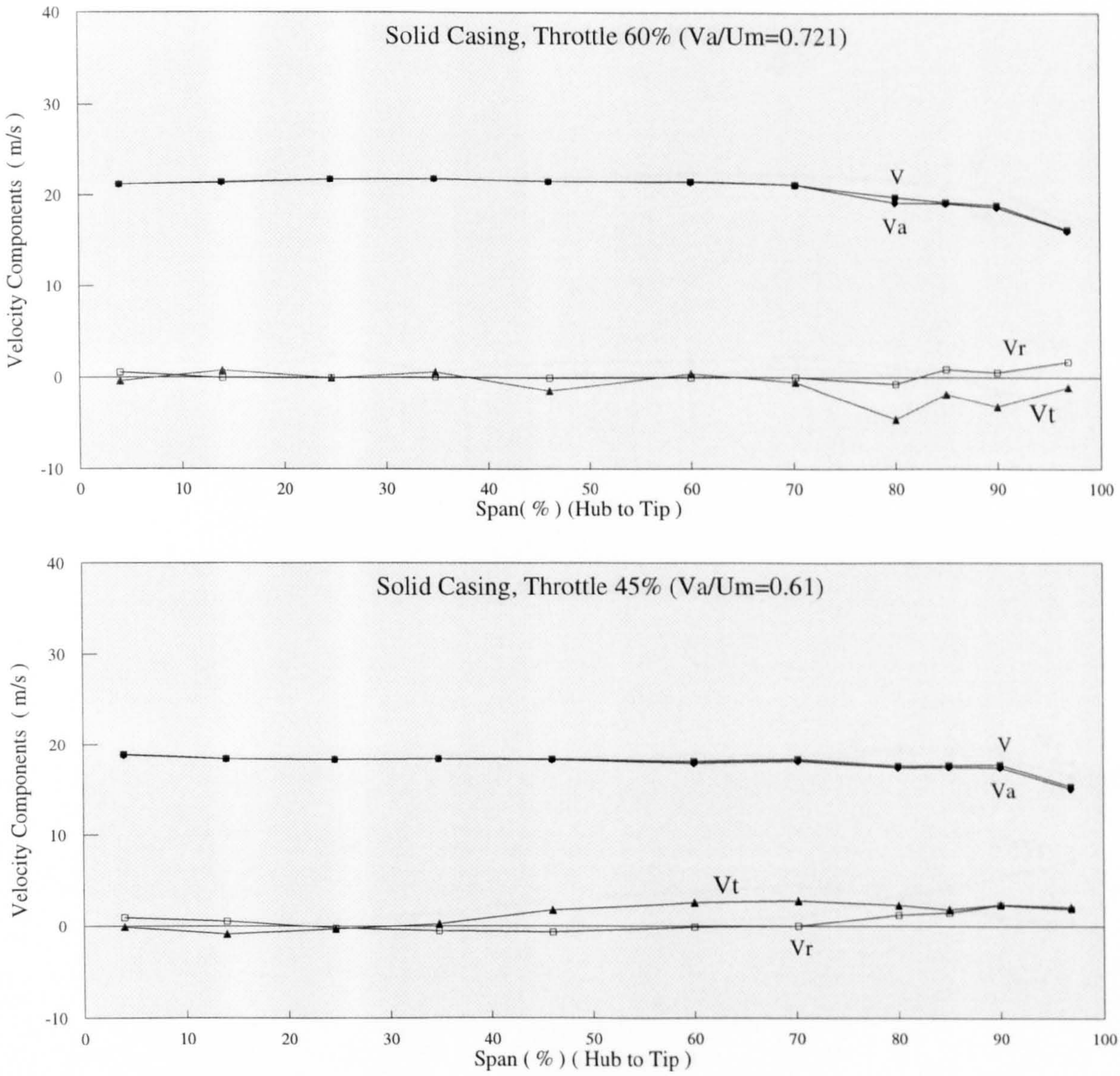

Fig.5-2 Radial Distribution of Inlet Velocity for Solid Casing (Station 1)

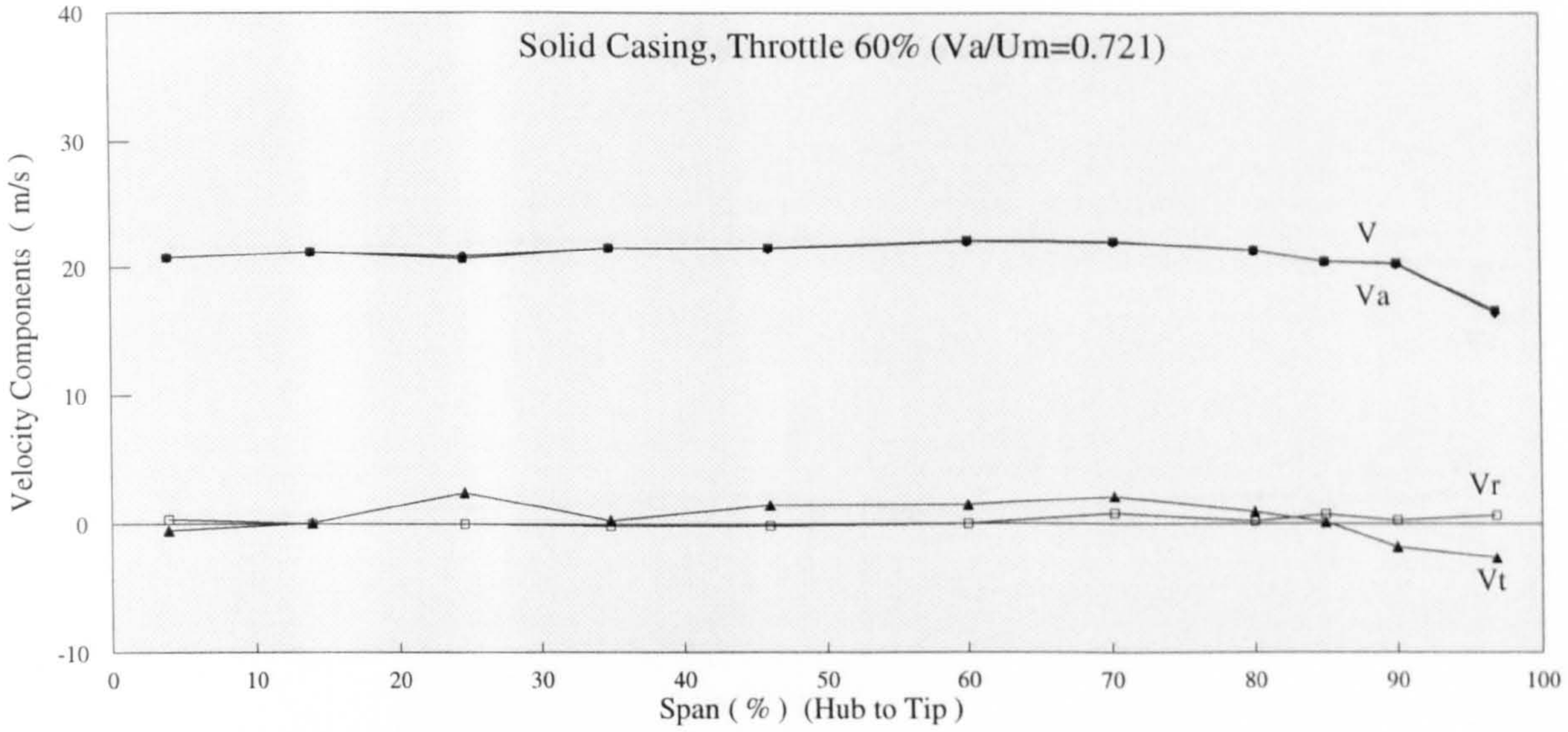

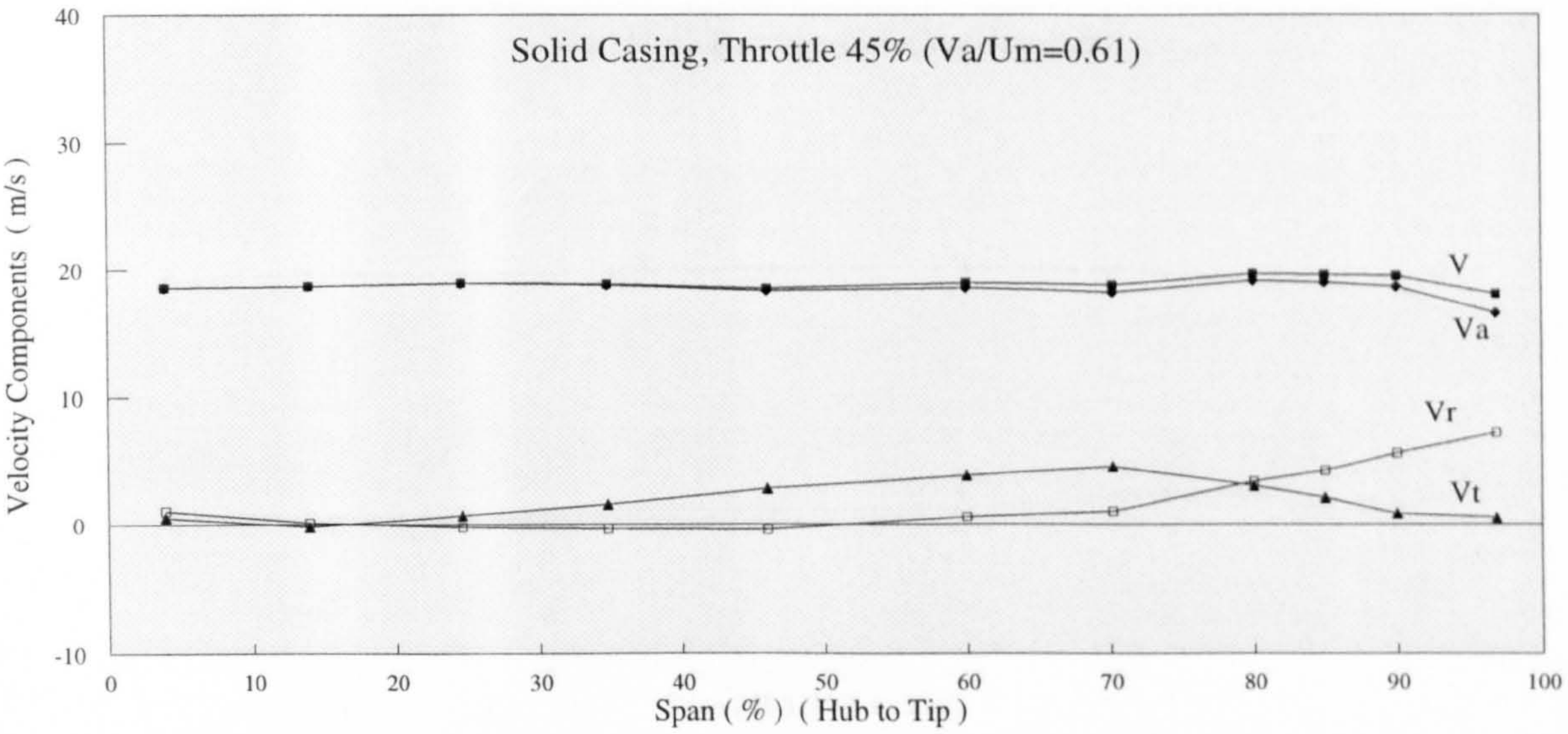

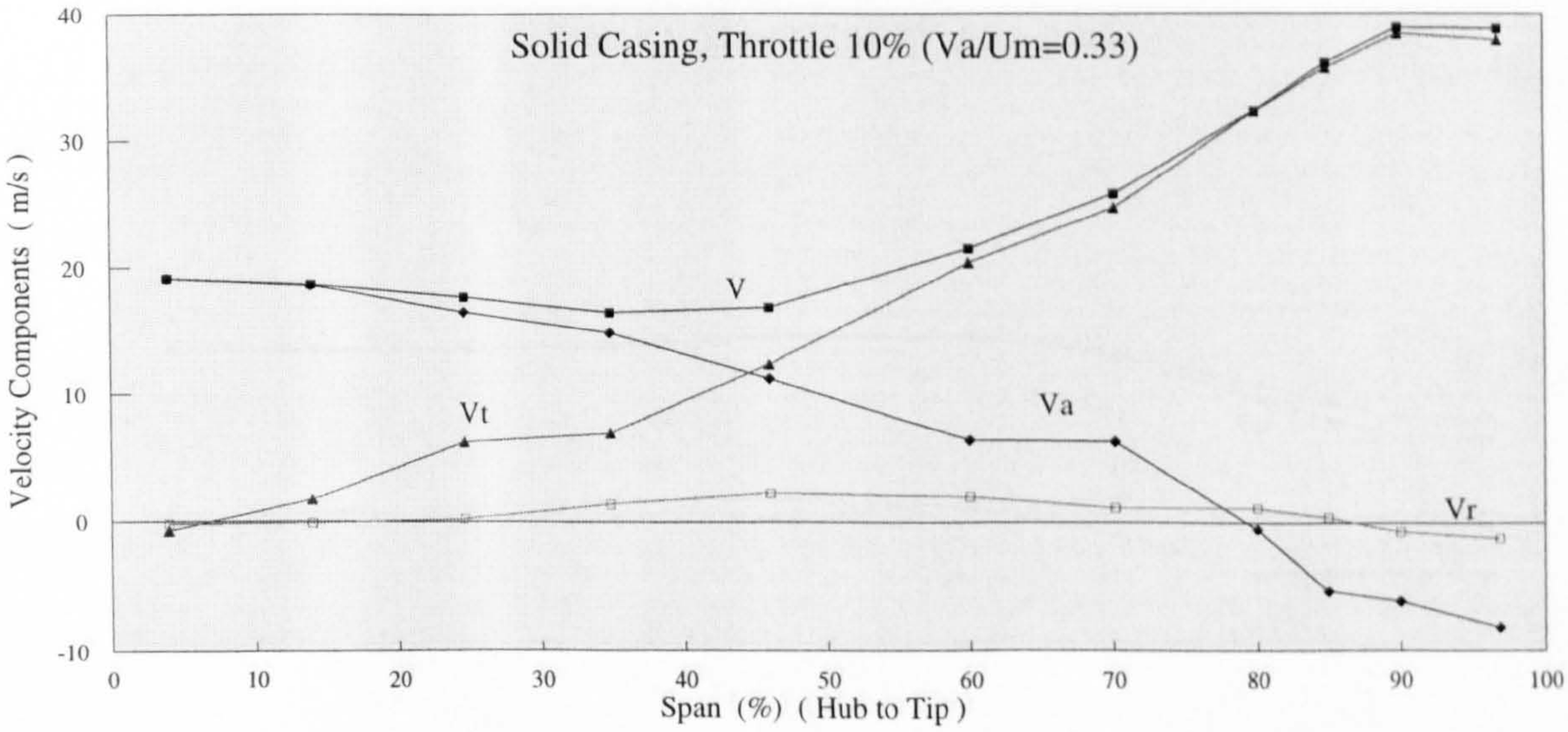

Fig.5-3 Radial Distribution of Inlet Velocity for Solid Casing (Station 2)

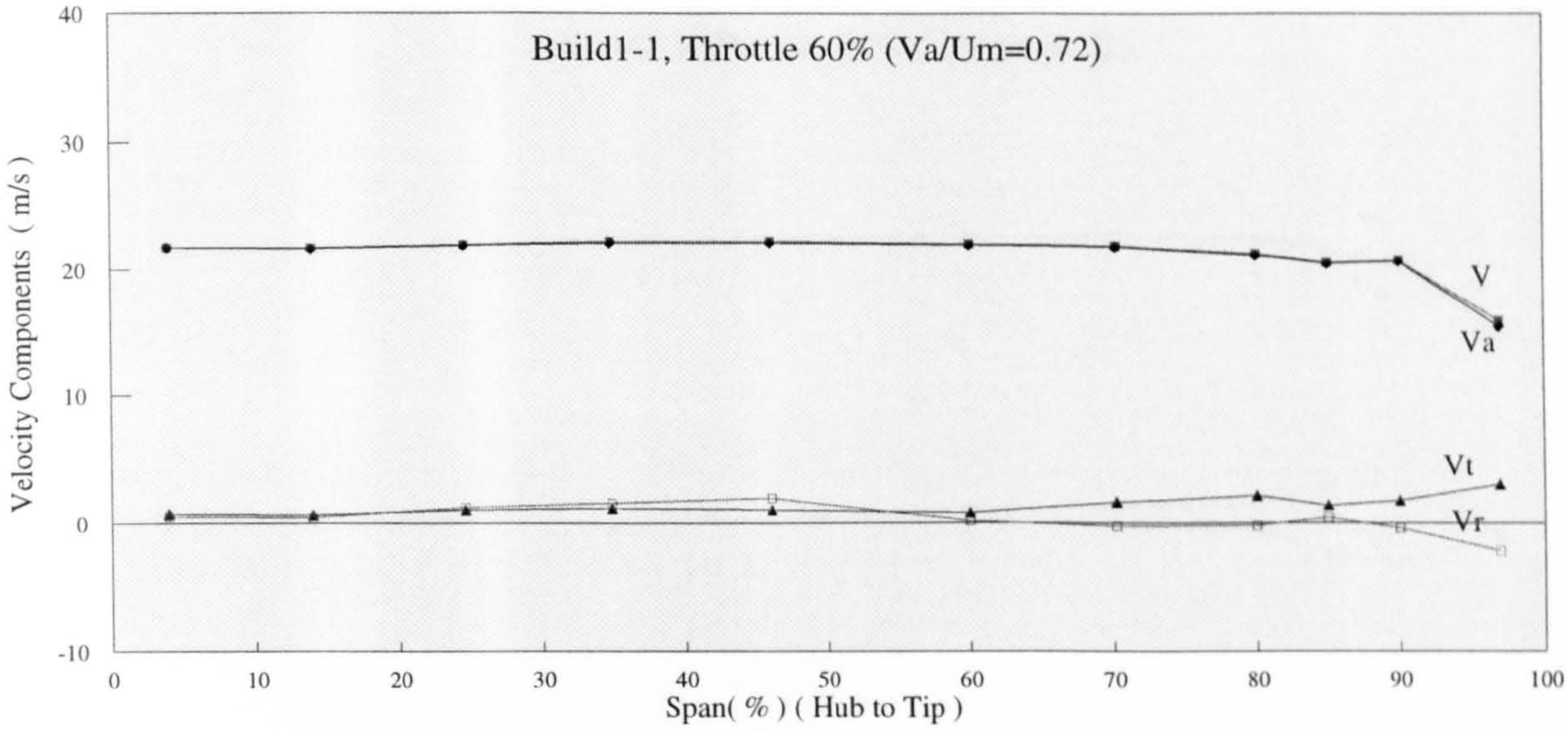

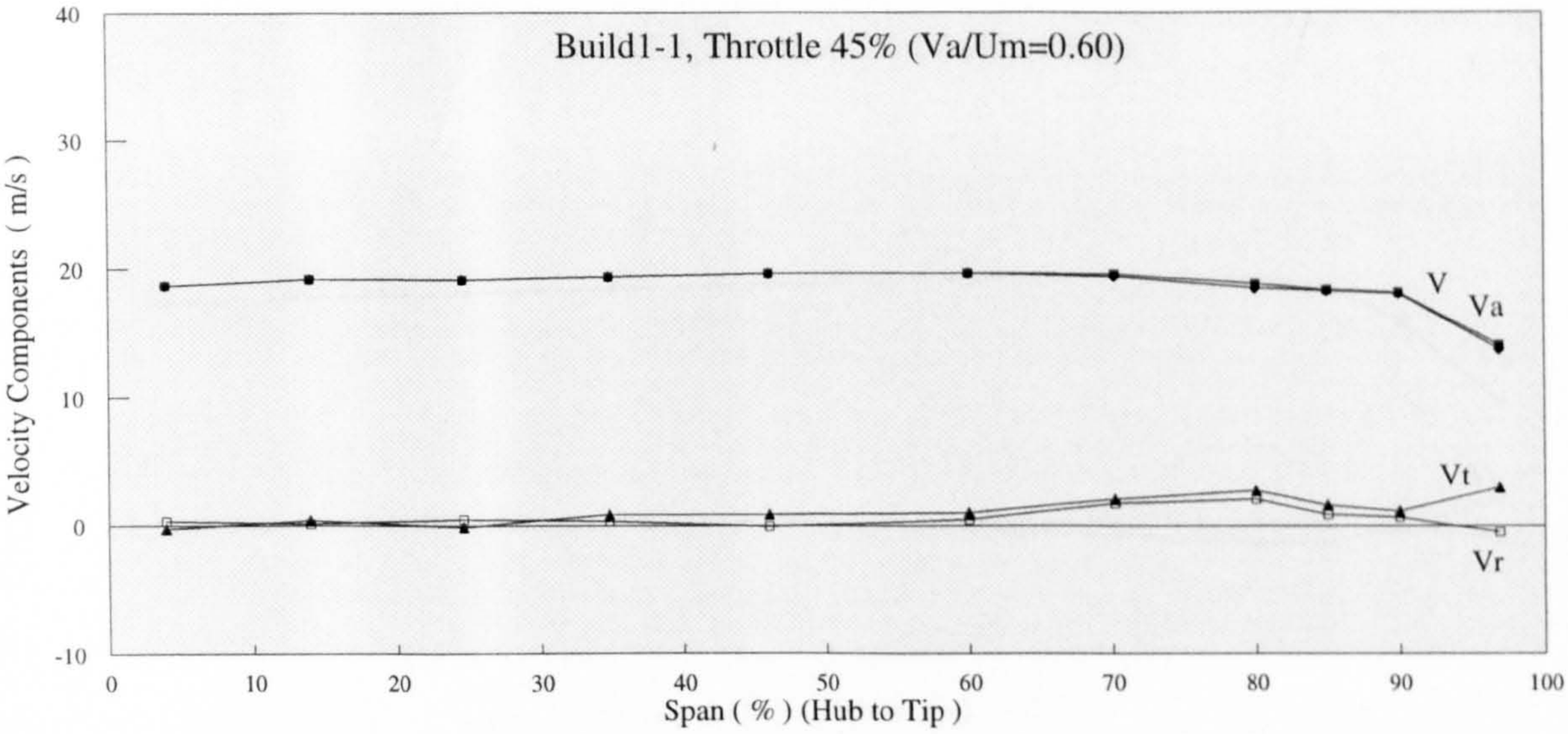

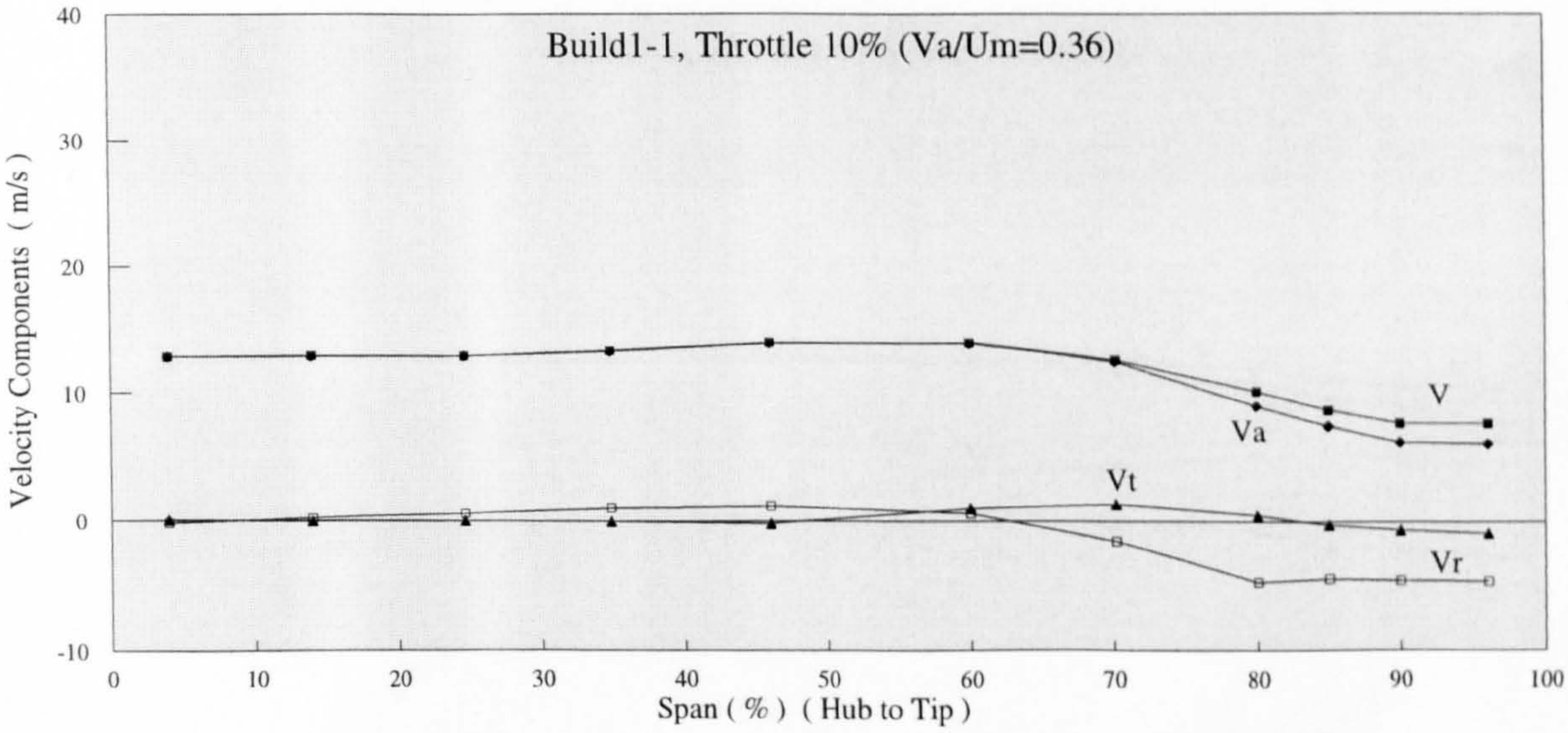

Fig.5-4 Radial Distribution of Inlet Velocity for Treated Casing(Station 1)

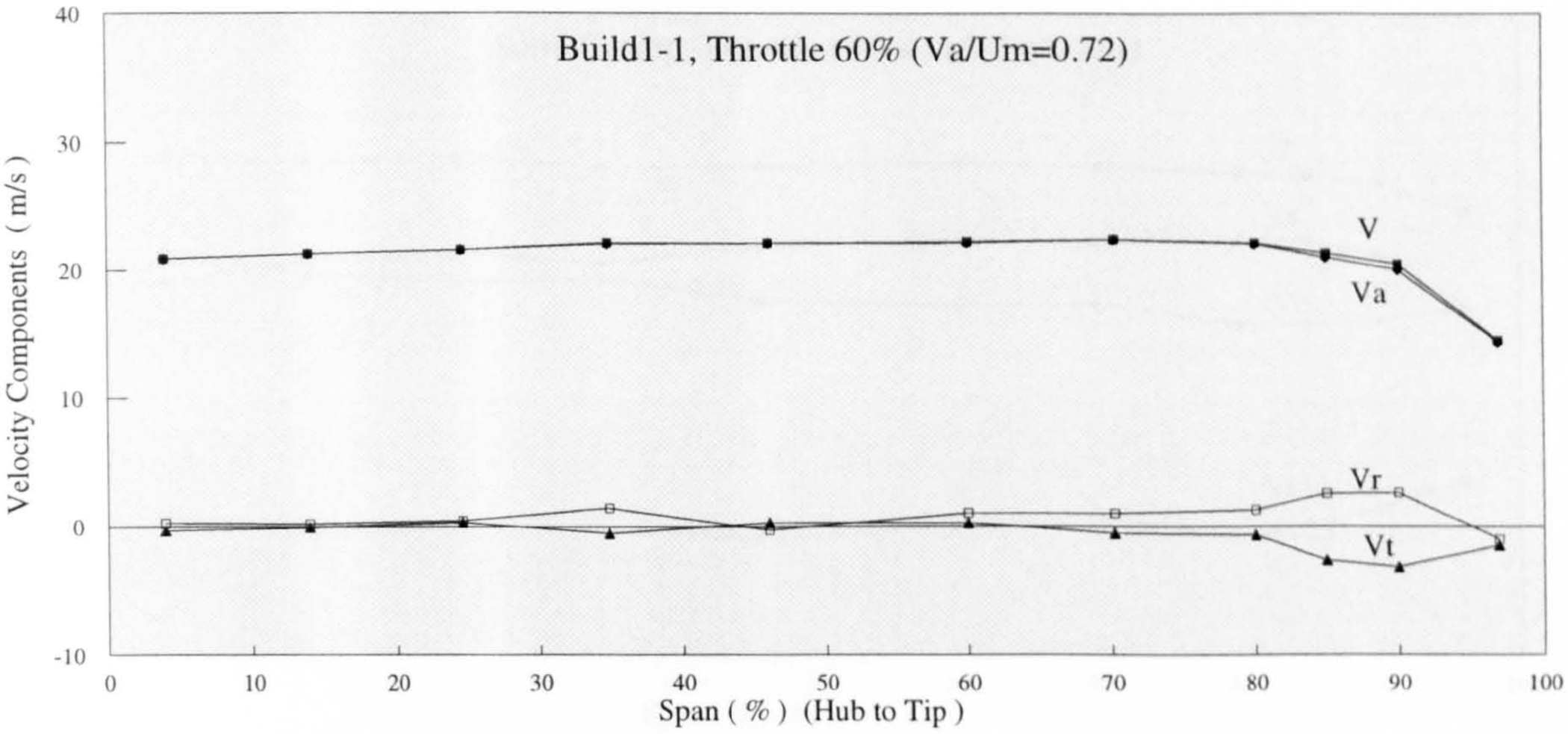

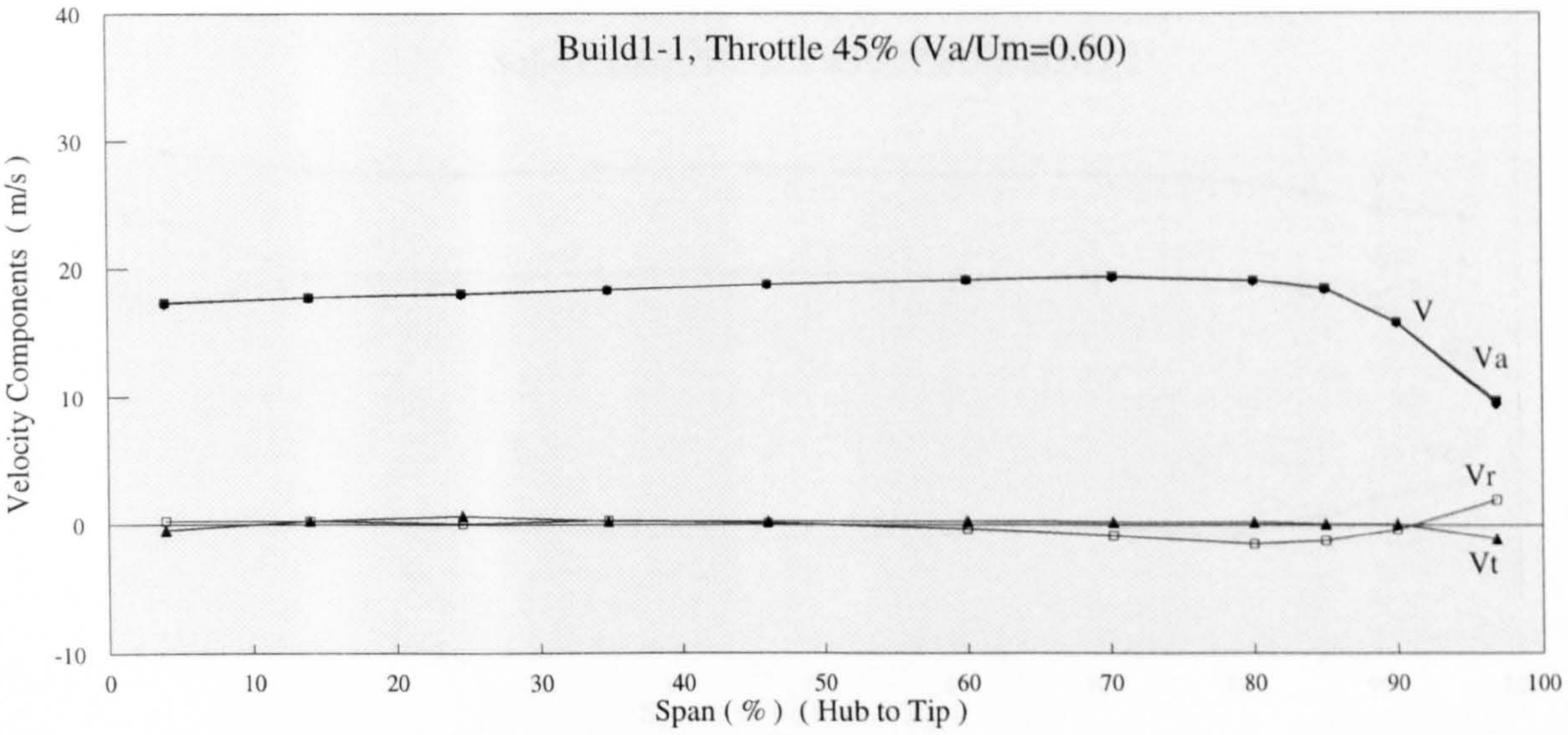

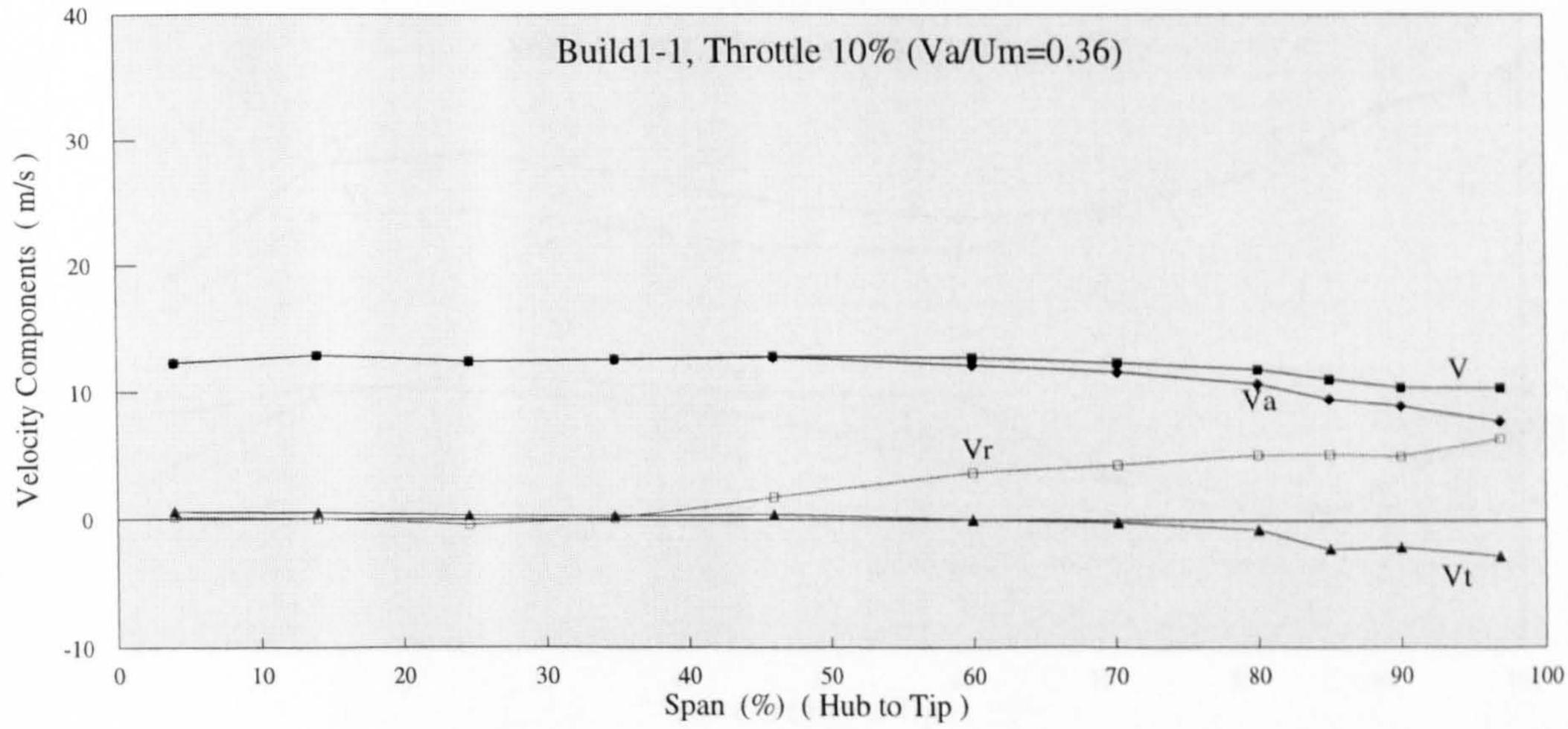

Fig.5-5 Radial Distribution of Inlet Velocity for Treated Casing (Station 2)

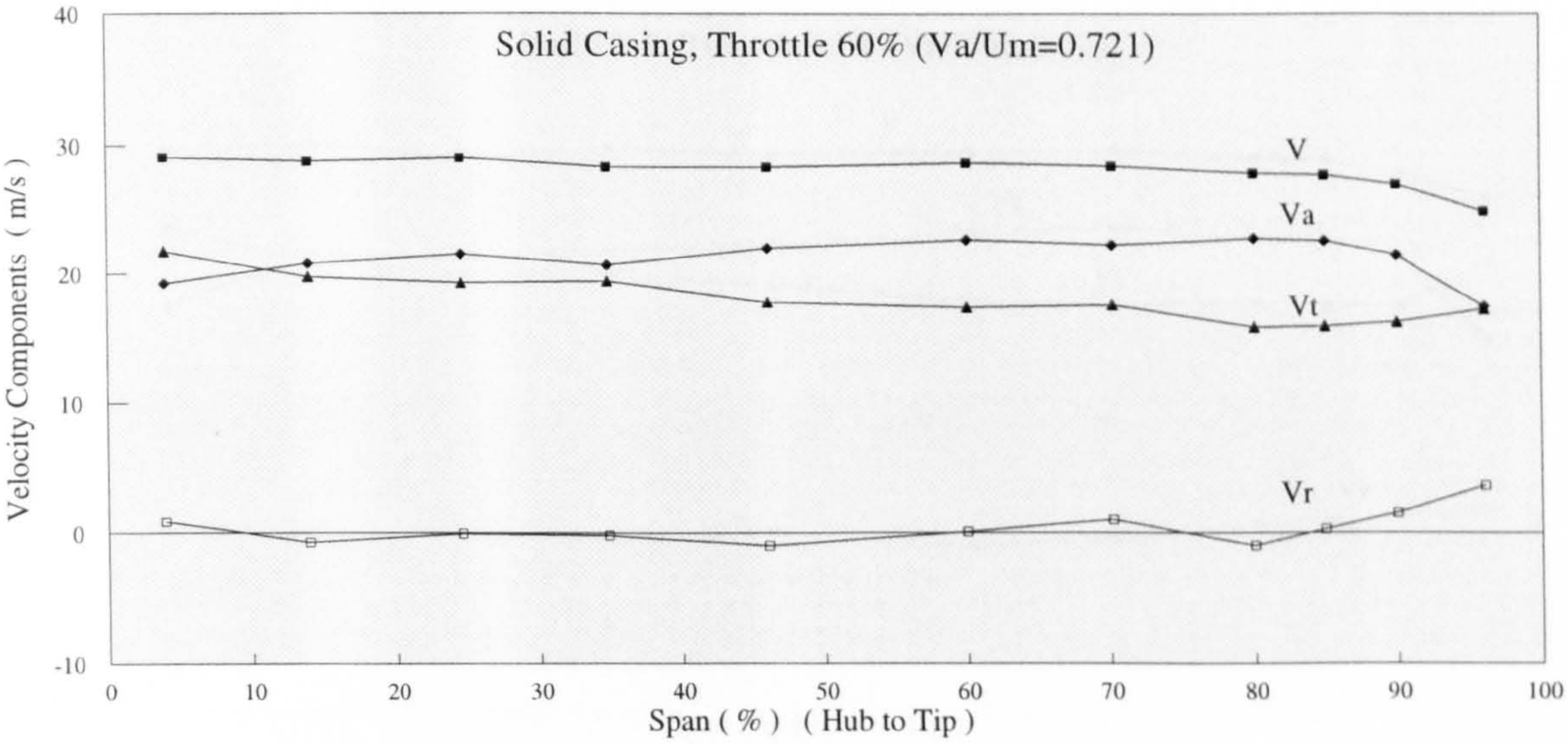

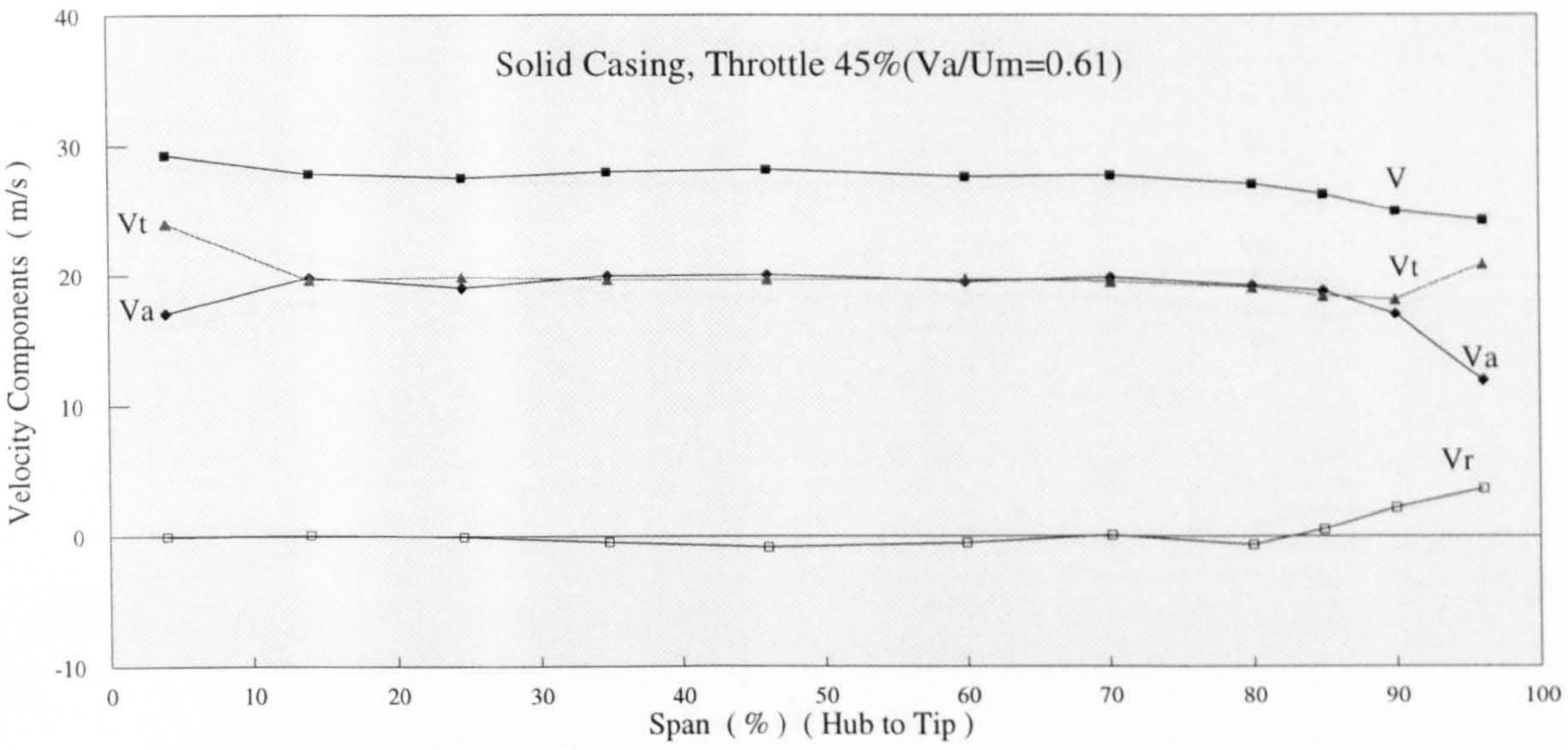

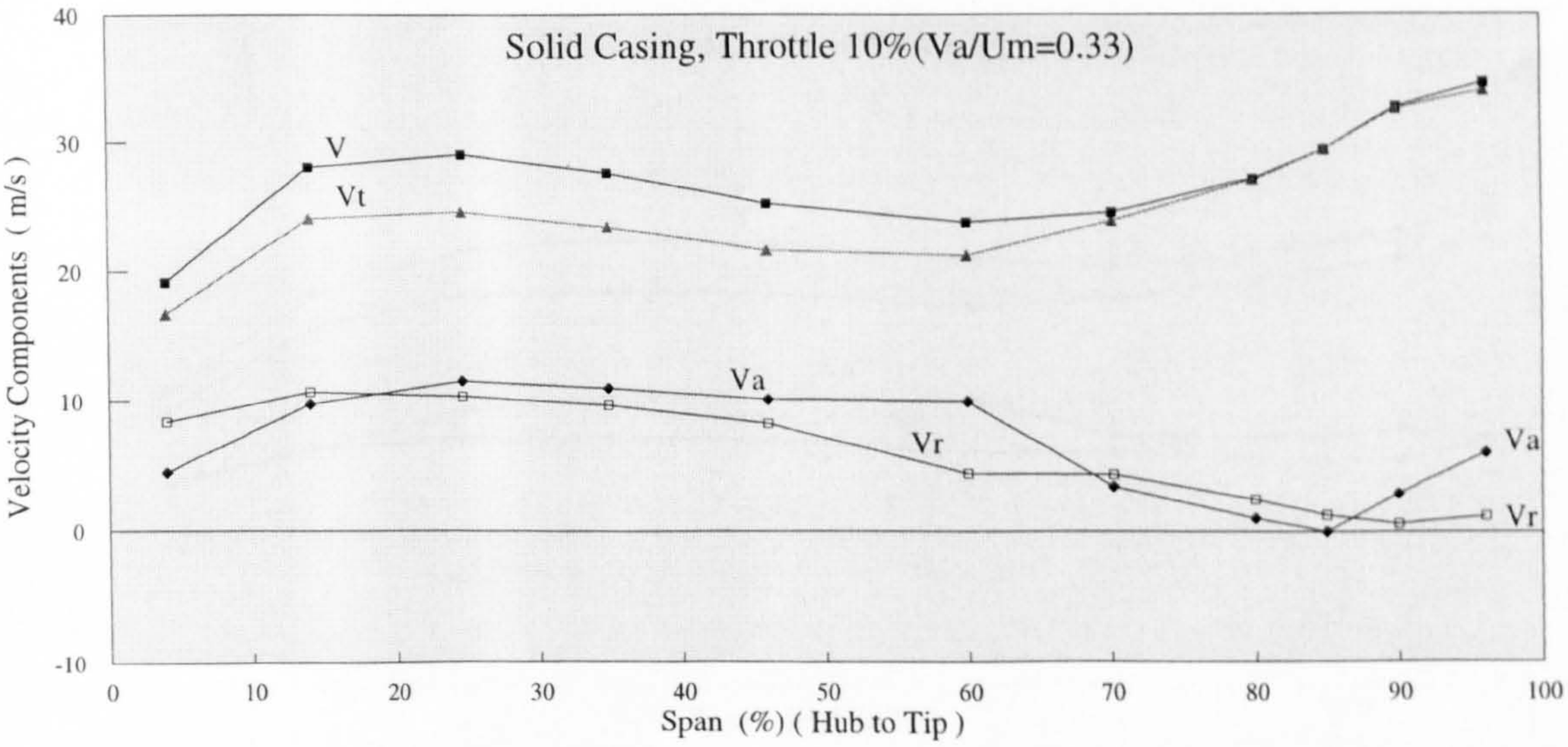

Fig.5-6 Radial Profile of Outlet Velocity for Solid Casing (Station 3)

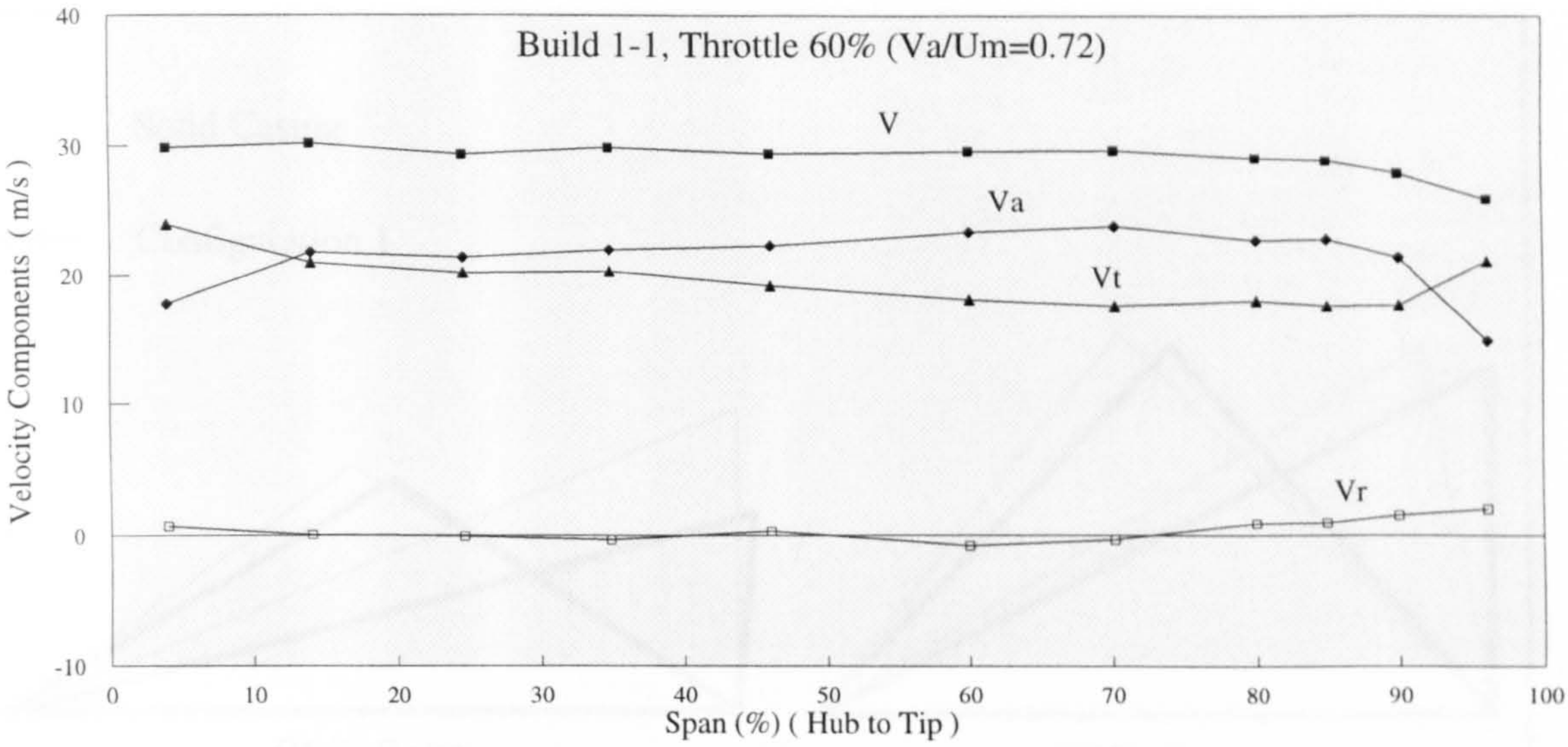

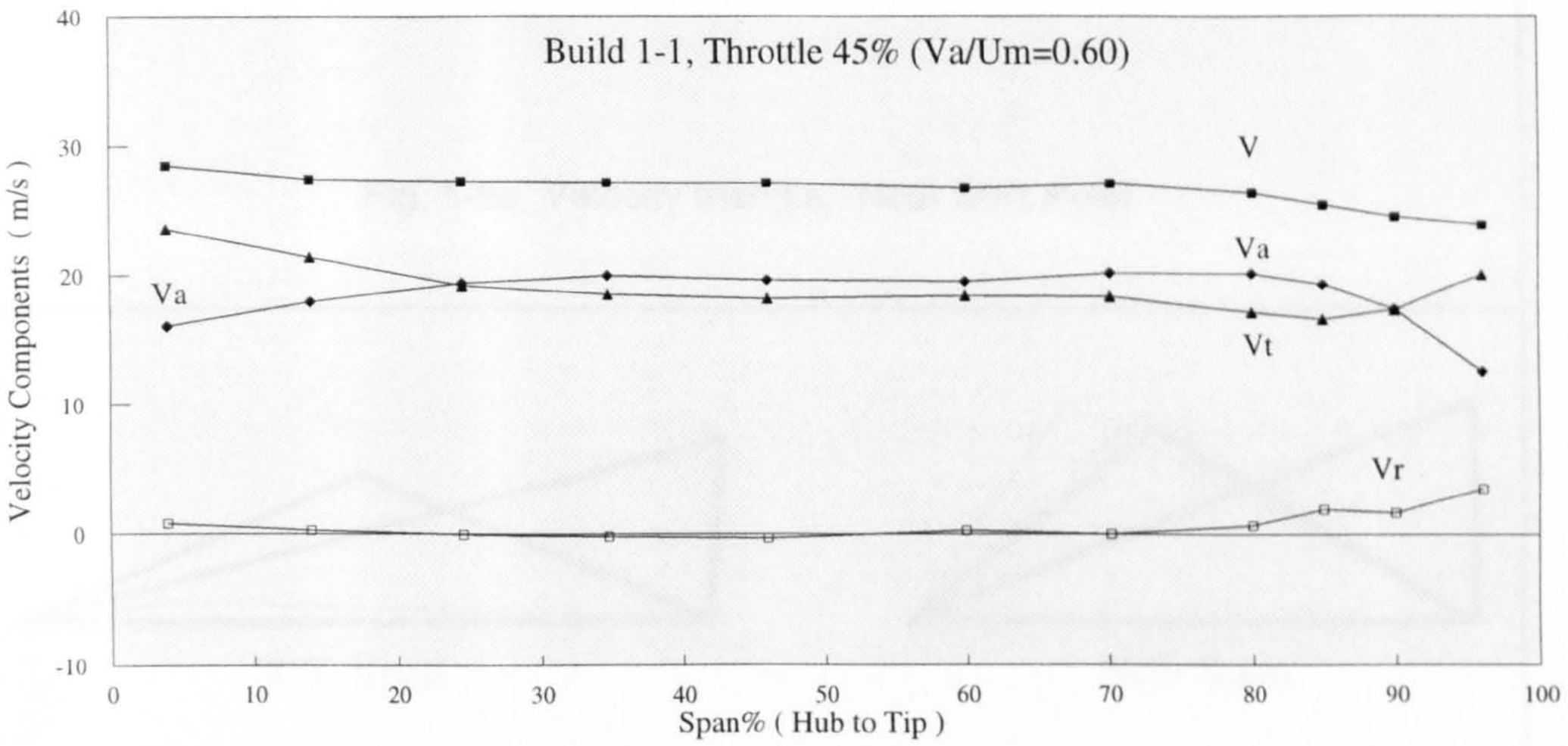

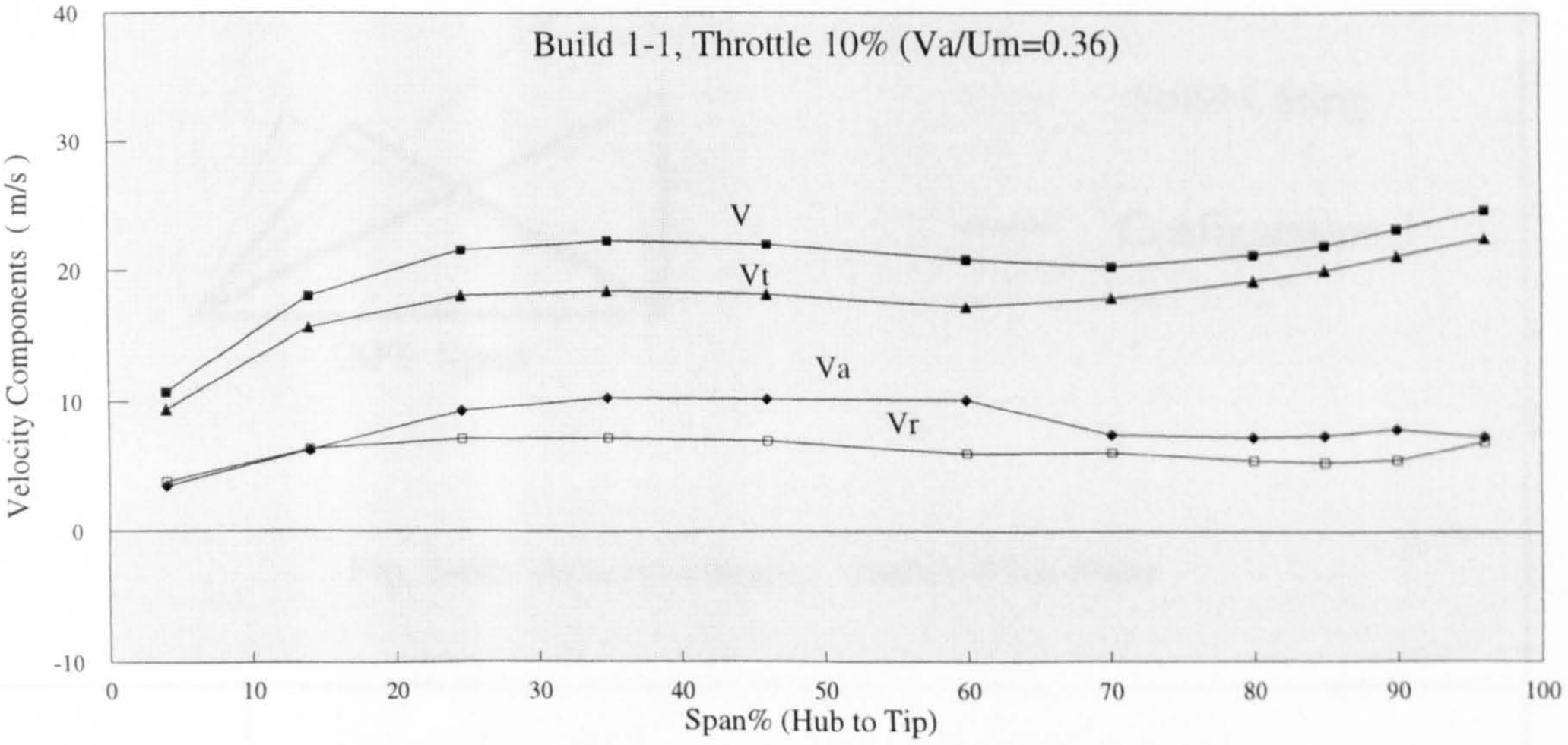

Fig.5-7 Ridial Profile of Outlet Velocity for Treated Casing (Station 3)

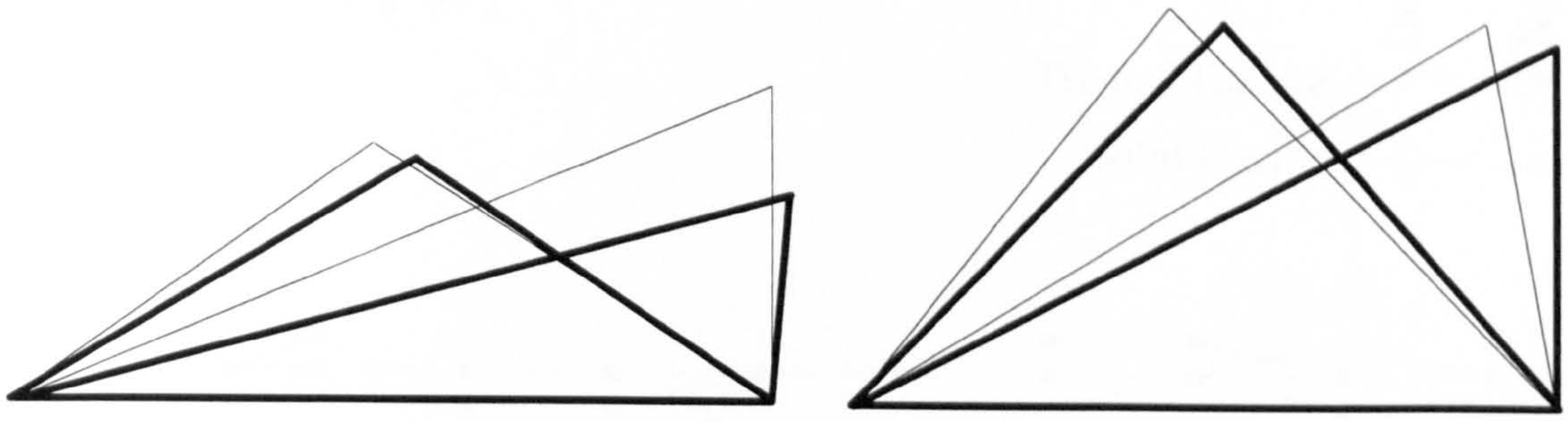

Fig. 5-8a Velocity triangle, Near Stall Point

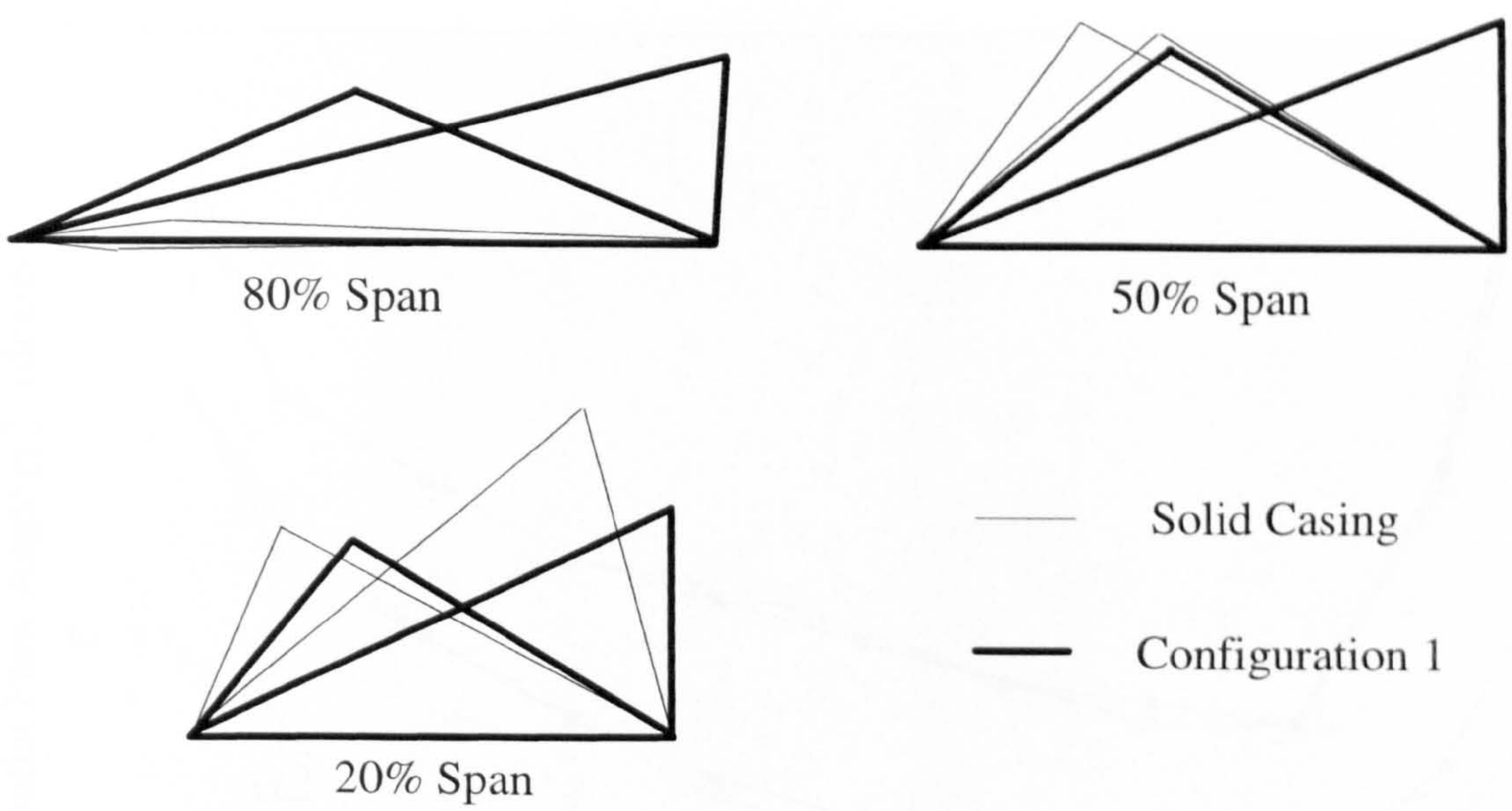

Fig. 5-8b Velocity triangle, Stalled Flow Rate

Fig.5-8	Comparison of Velocity Triangles

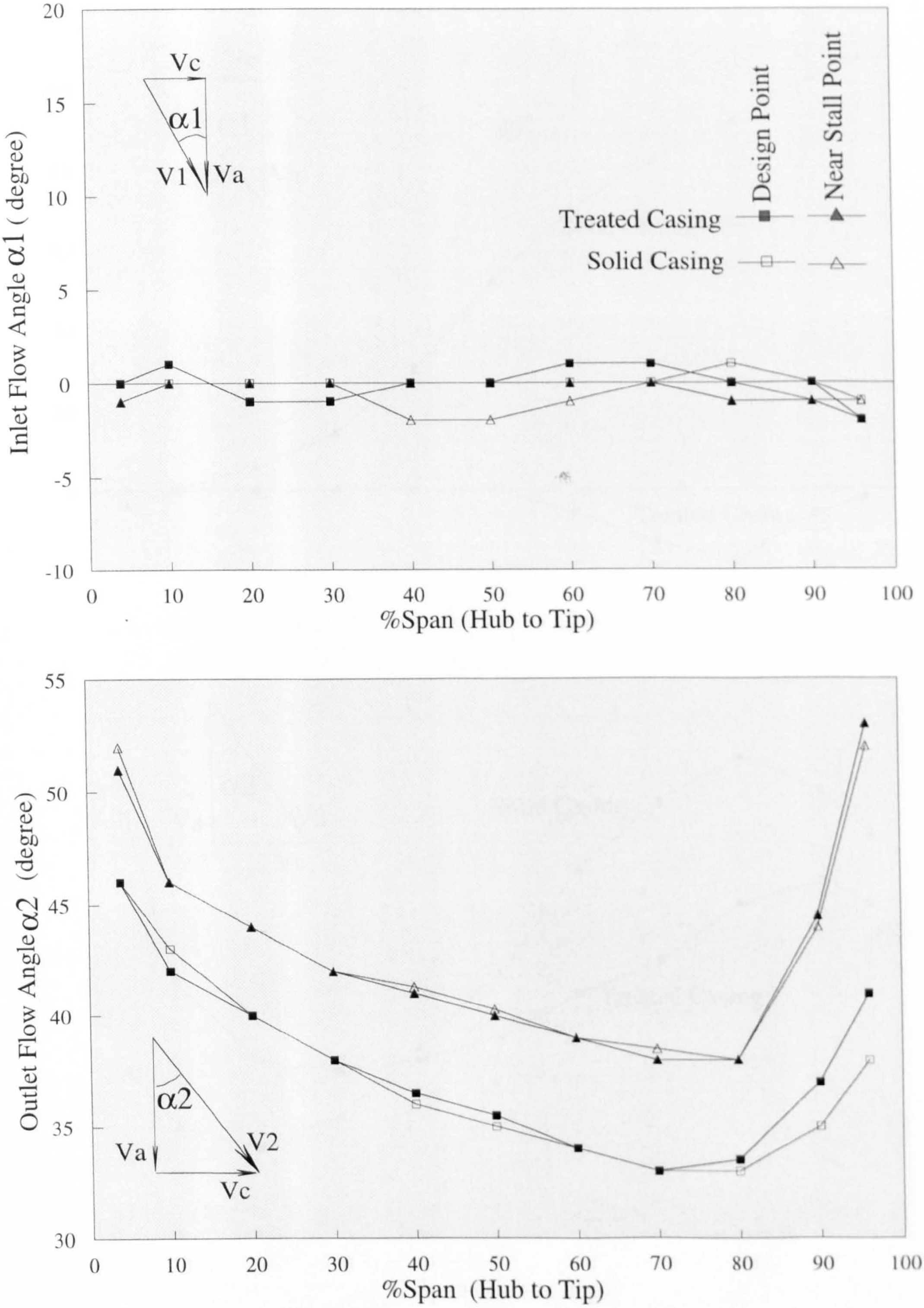

Fig. 5-9 Absolute Flow Angle, at Design & Near Stall Flow Rate

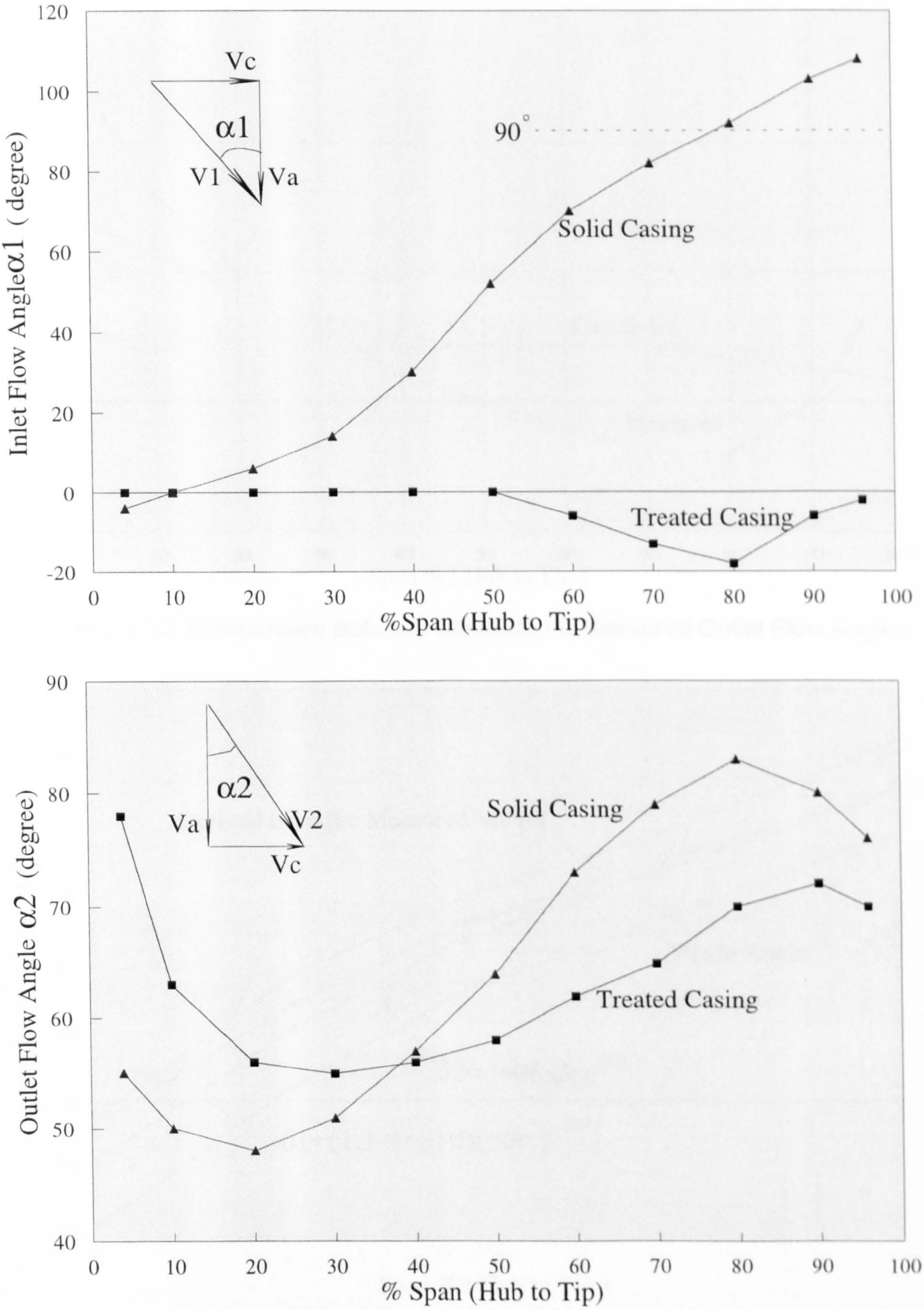

Fig. 5-10 Absolute Flow Angle, Near Extended Stall Point

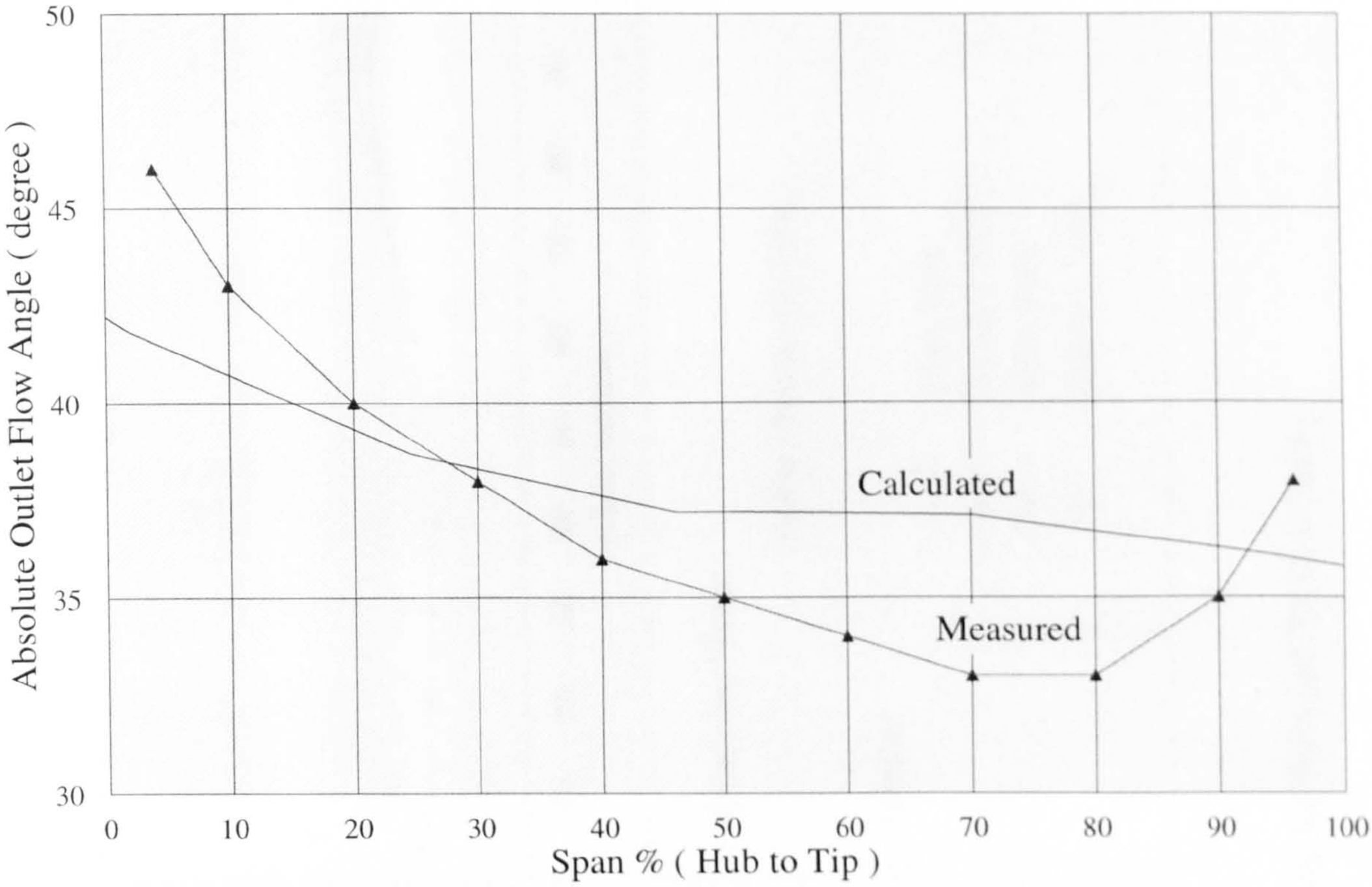

Fig. 5-12 Comparision Between Calculated & Measured Outlet Flow Angles

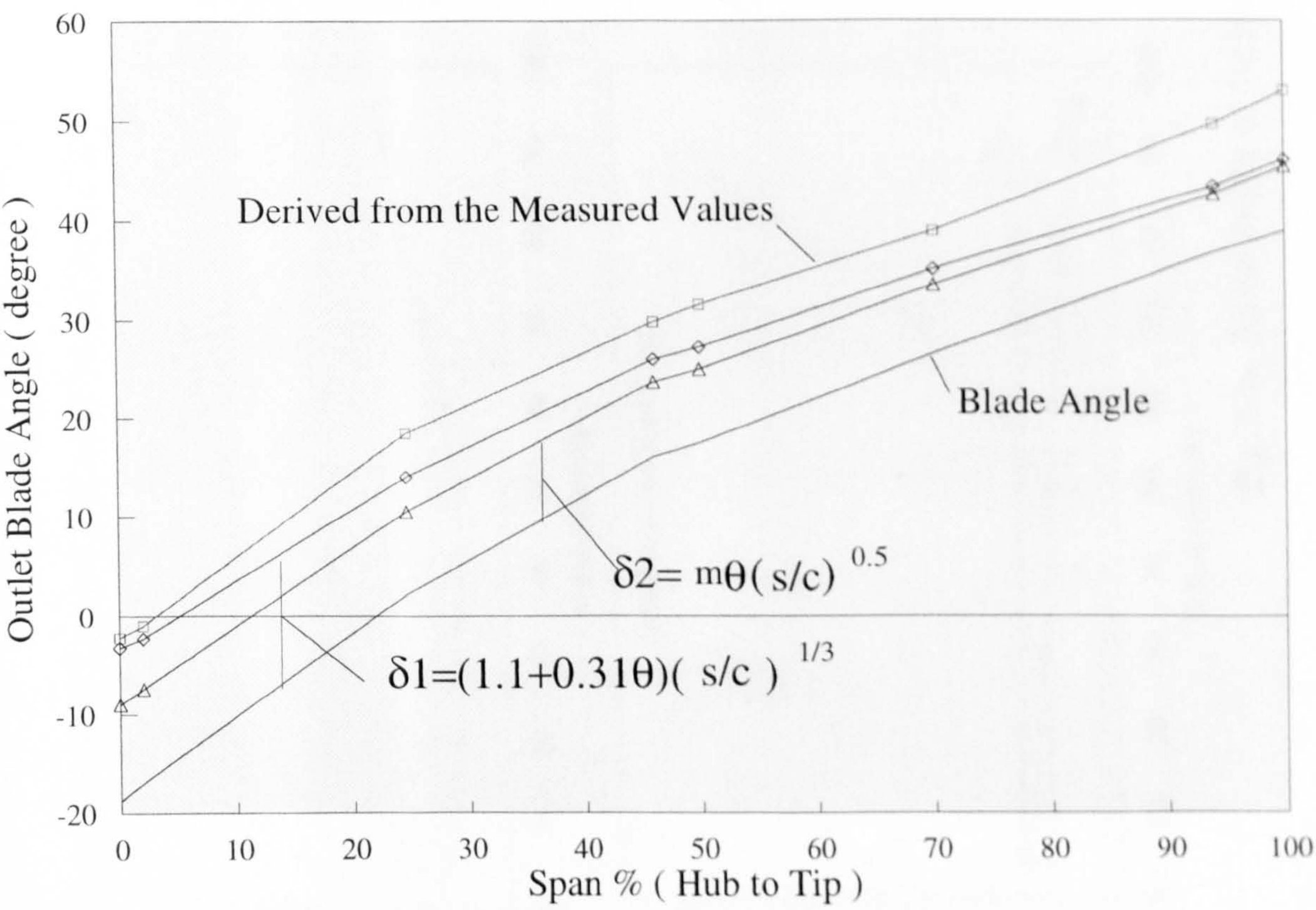

Fig. 5-13 Flow Angle Deviation from Blade Outlet Angle

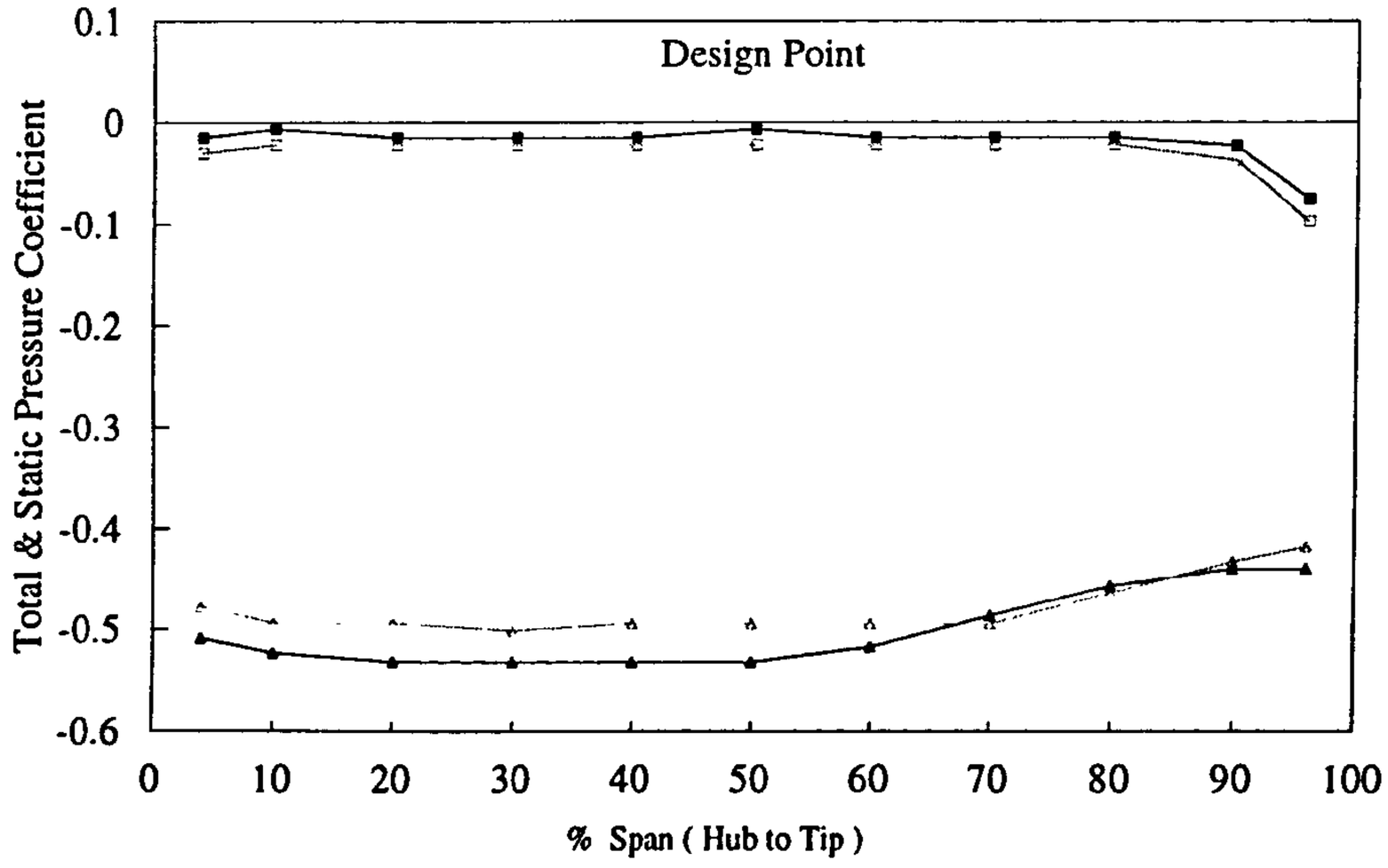

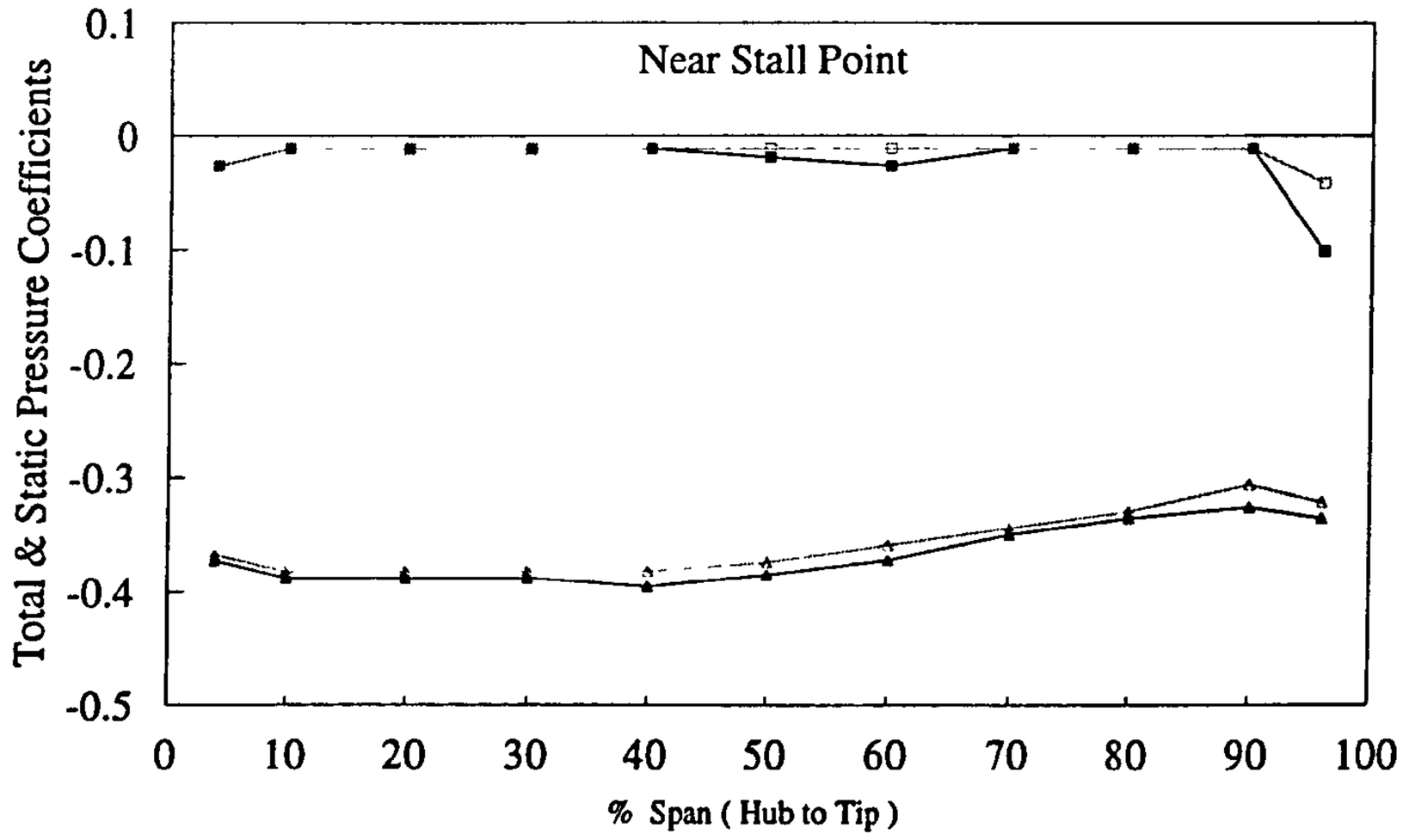

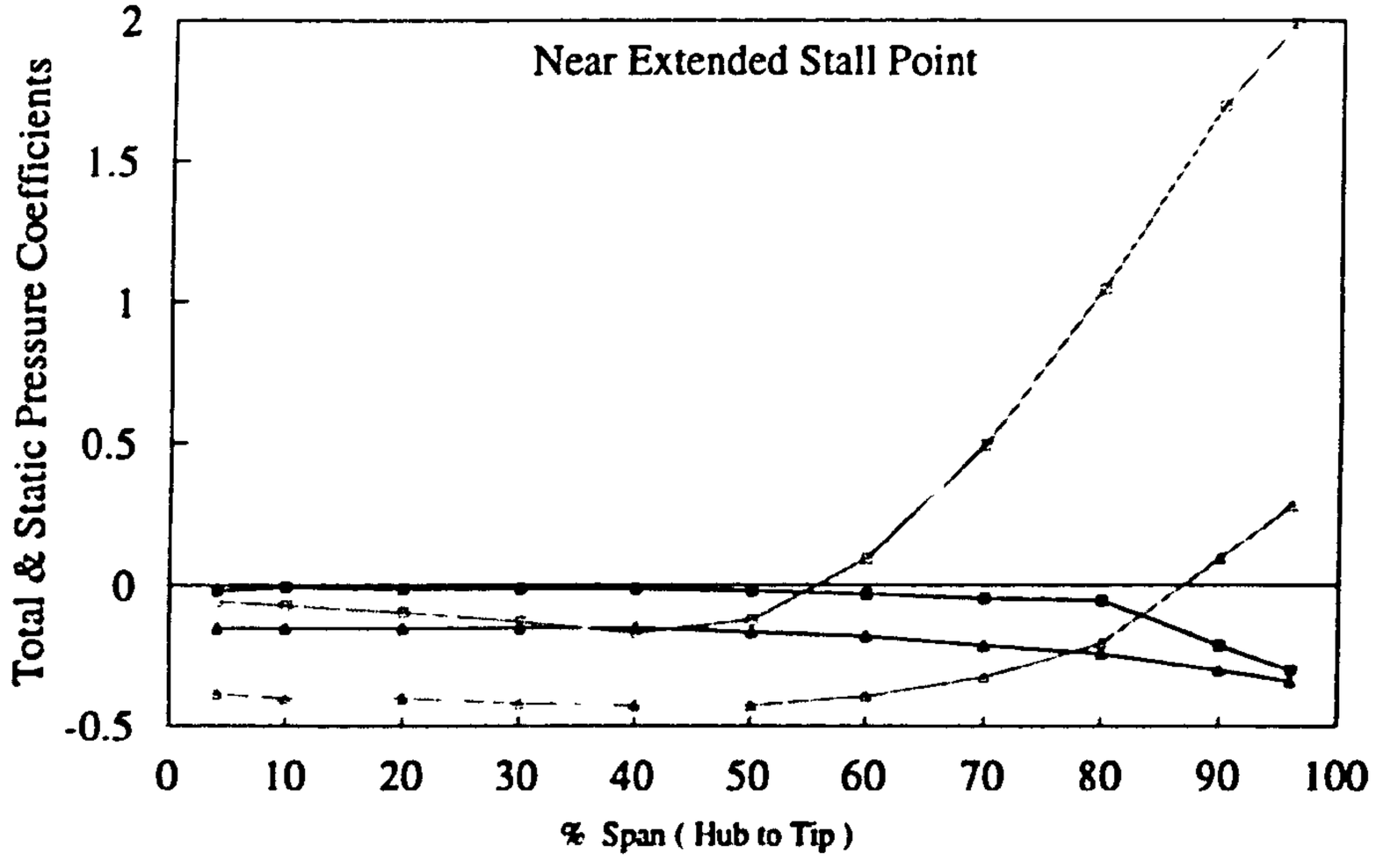

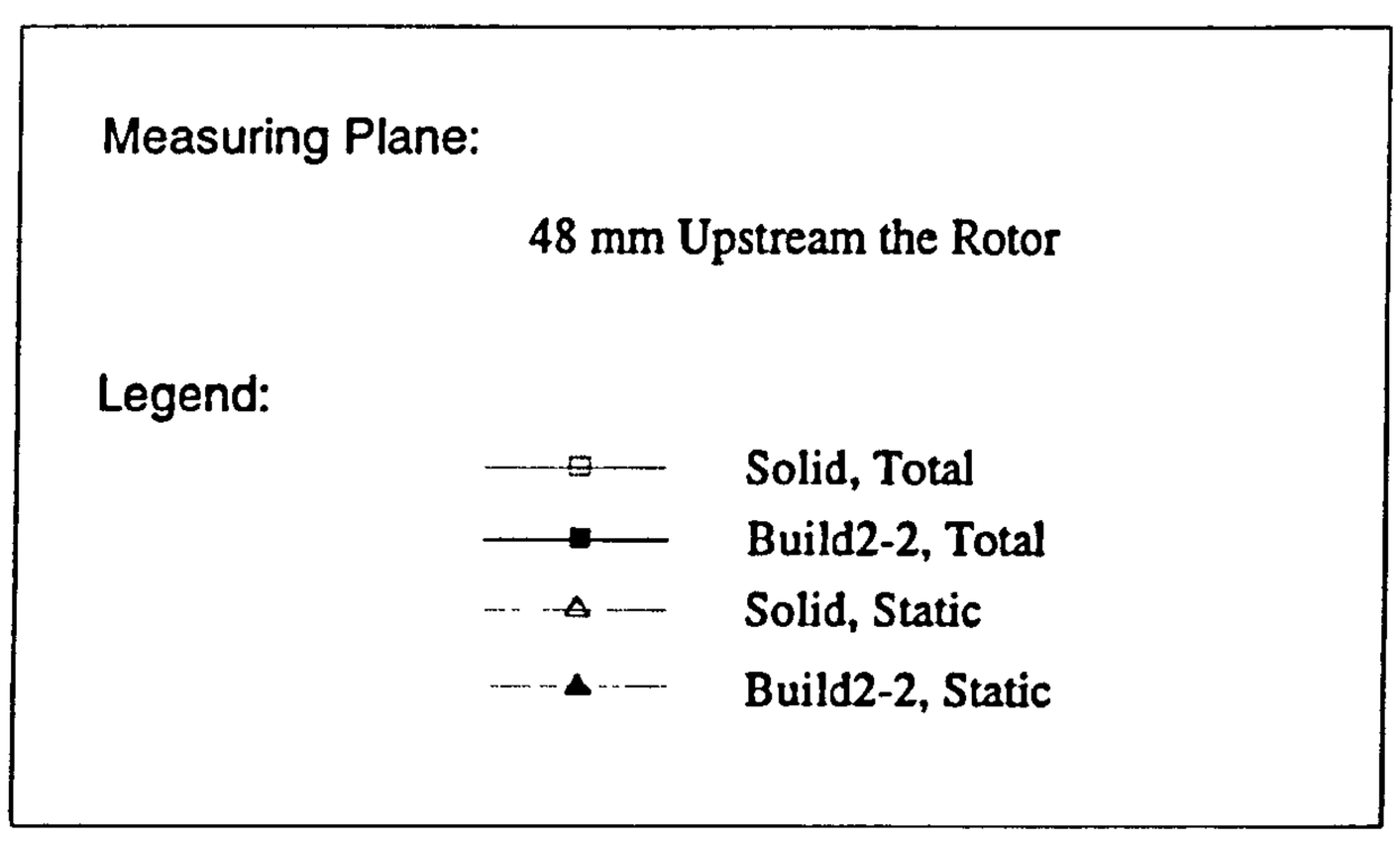

Fig. 5-14 Radial Profile of the Inlet Pressure for Solid and Treated Casing

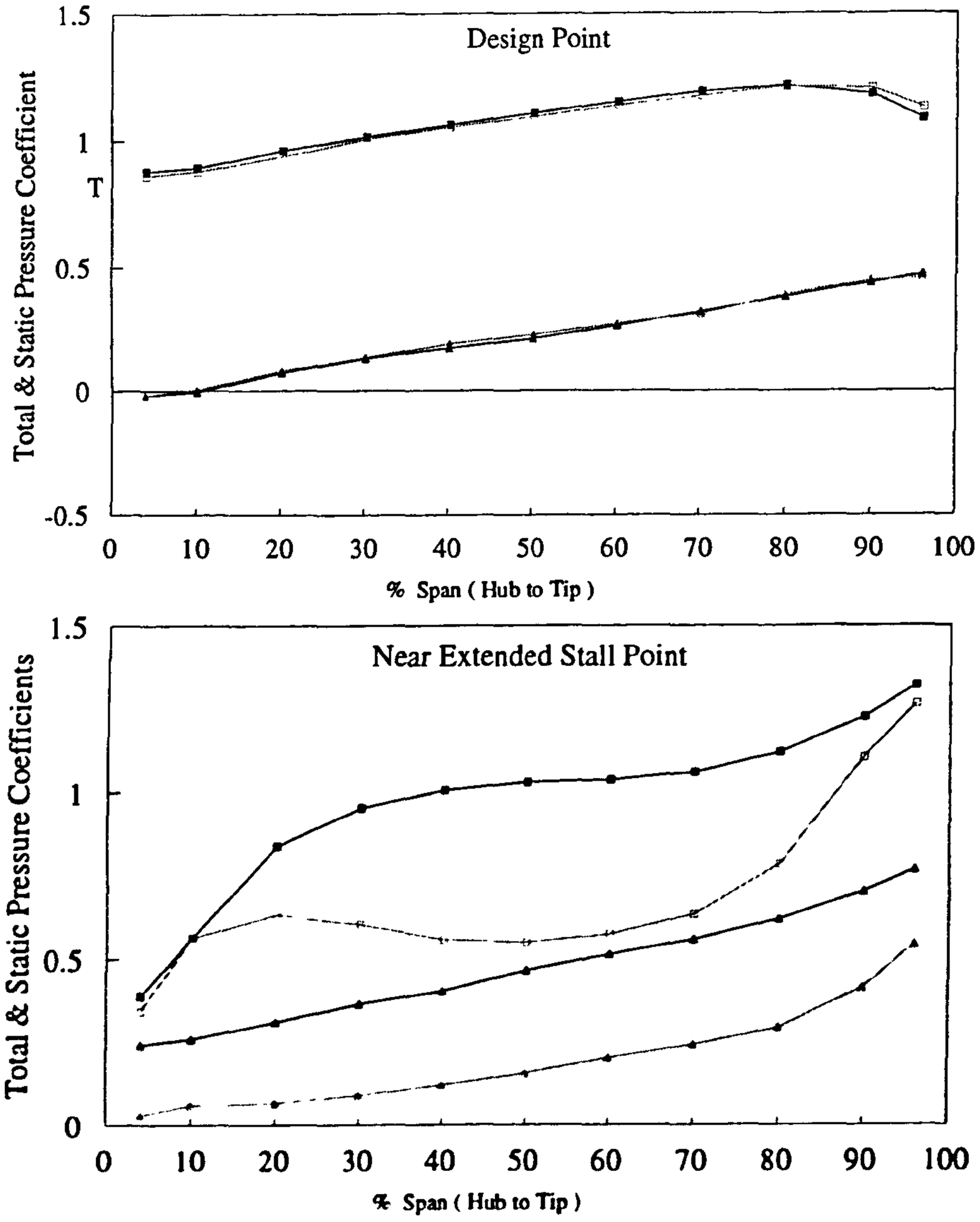

Fig.5-15 Radial Profile of the Outlet Pressure for Solid and Treated Casing

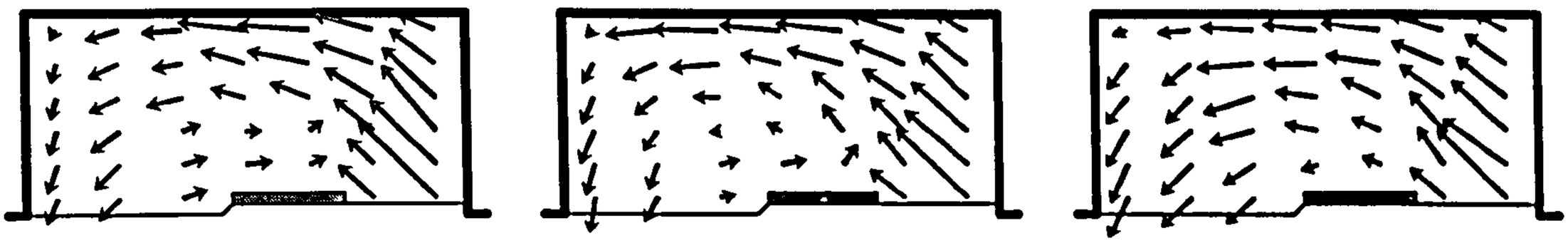

a) Vector Plot in Axial–Radial Plane

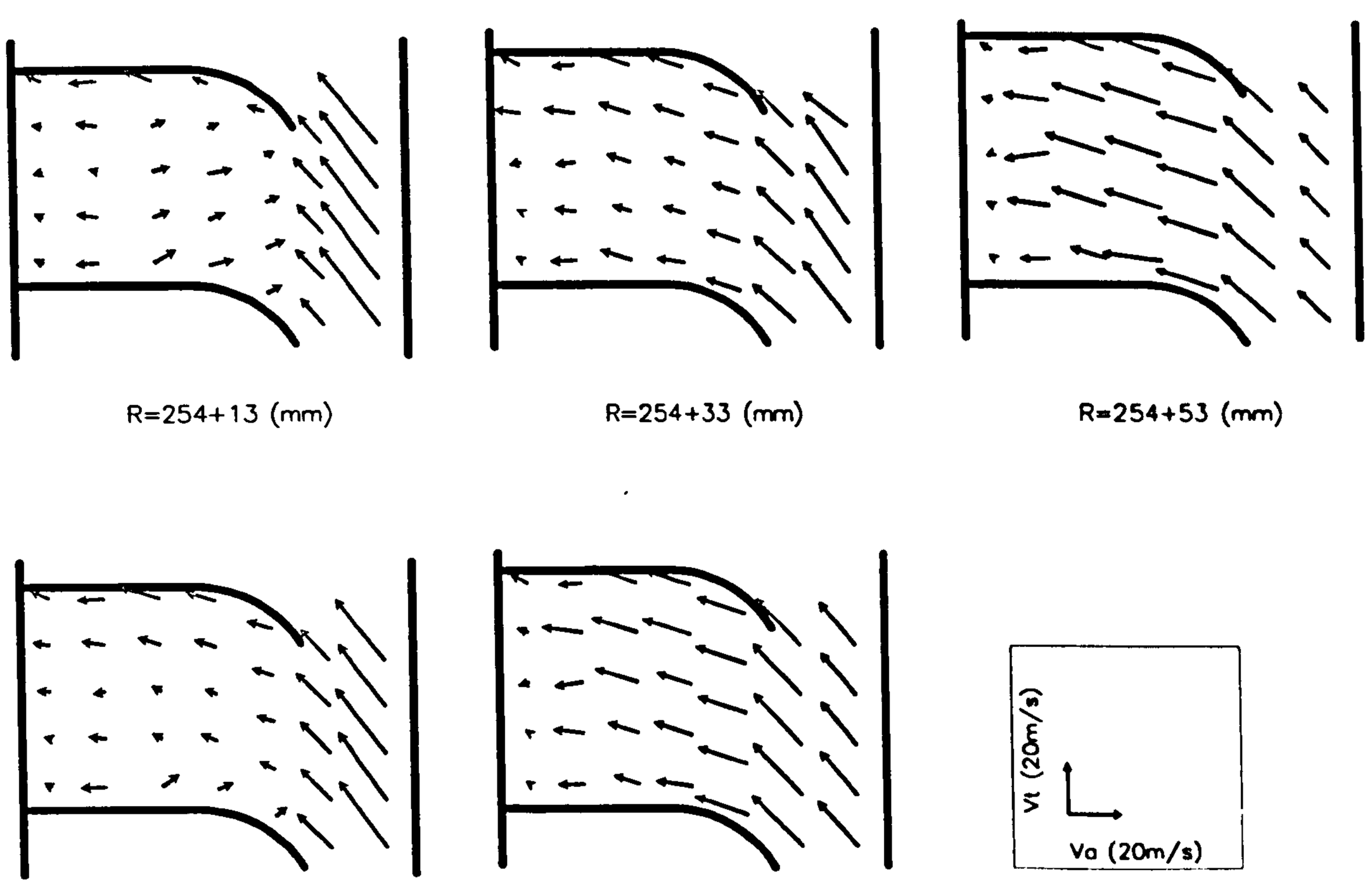

b) Vector Plot in Axial–Tangential Plane

Fig.5–17 Flow in Vane Passage of the Casing Treatment (Va/Um=0.36)

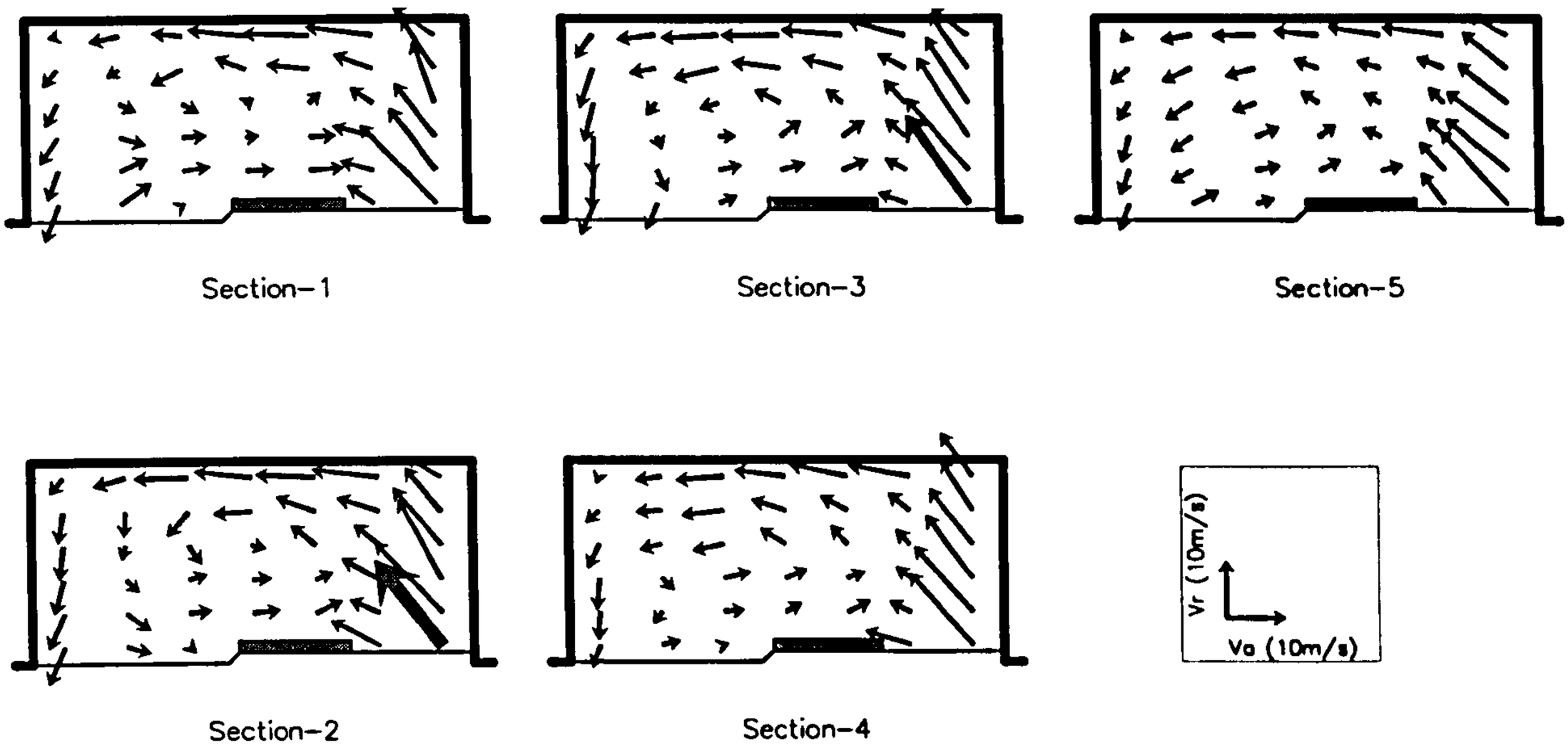

a) Vector Plot in Axial–Radial Plane

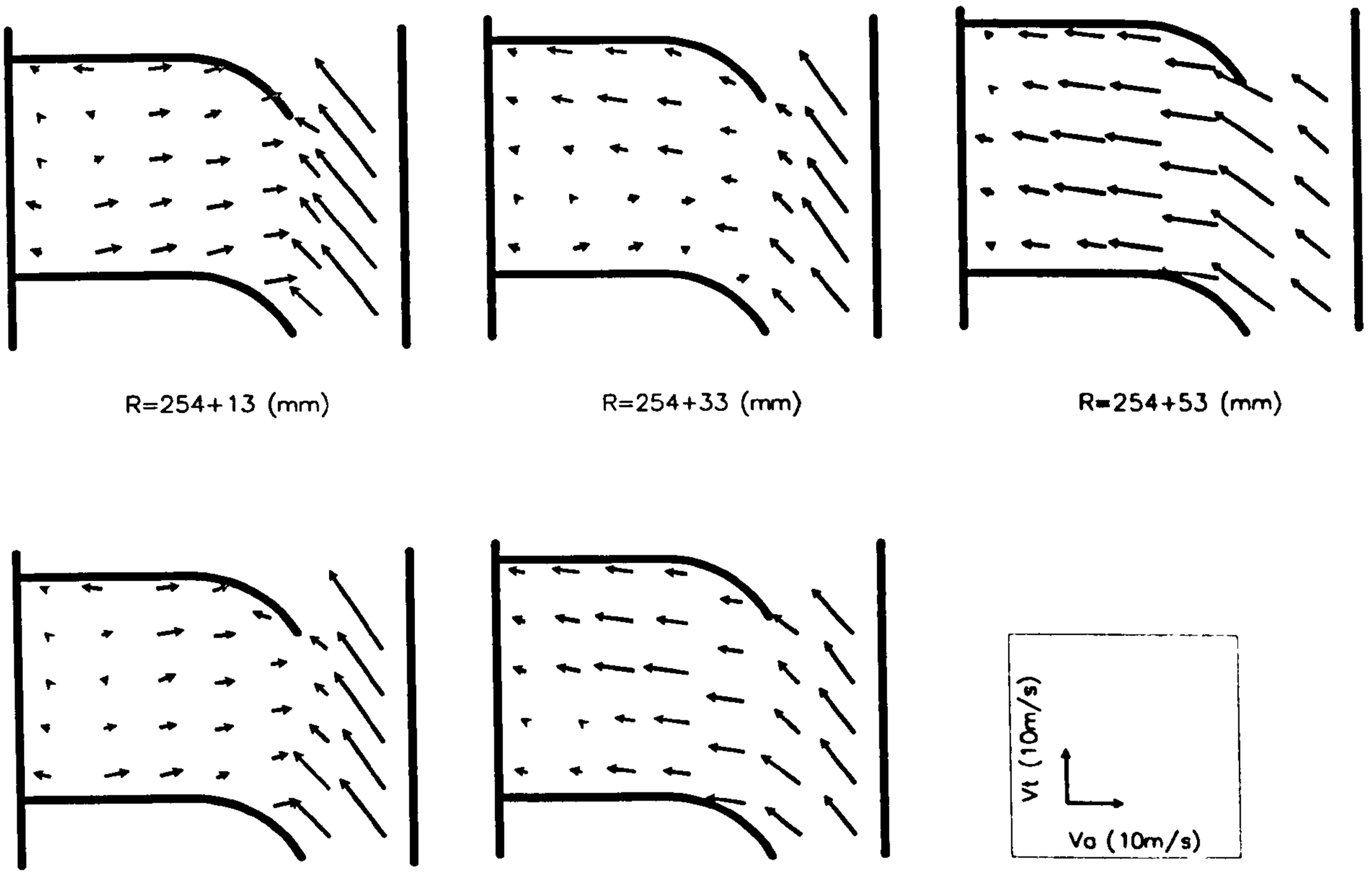

b) Vector Plot in Axial–Tangential Plane

Fig.5–18 Flow in Vane Passage of the Casing Treatment (Va/Um=0.6)

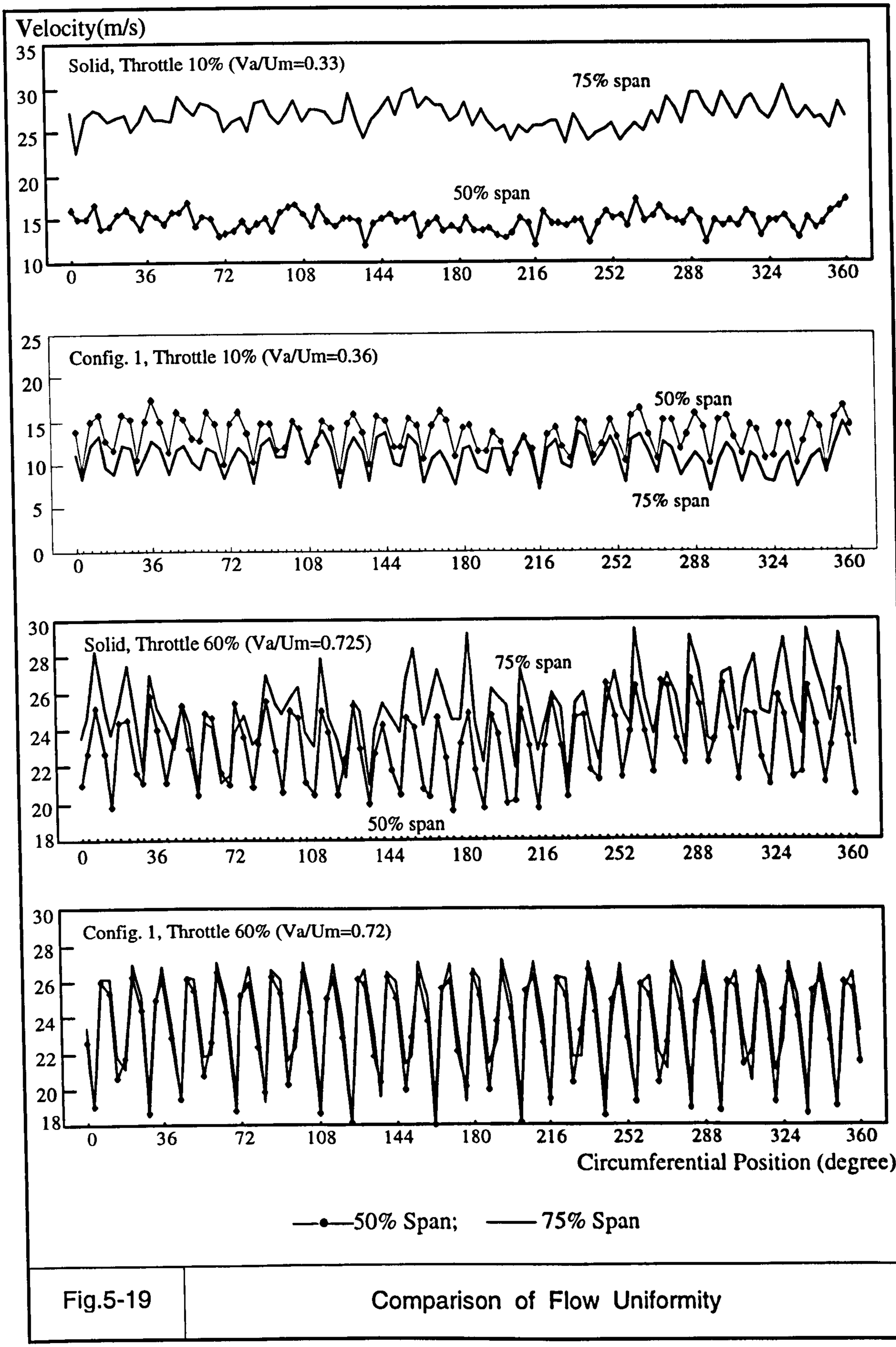

Fig.5-19	Comparison of Flow Uniformity

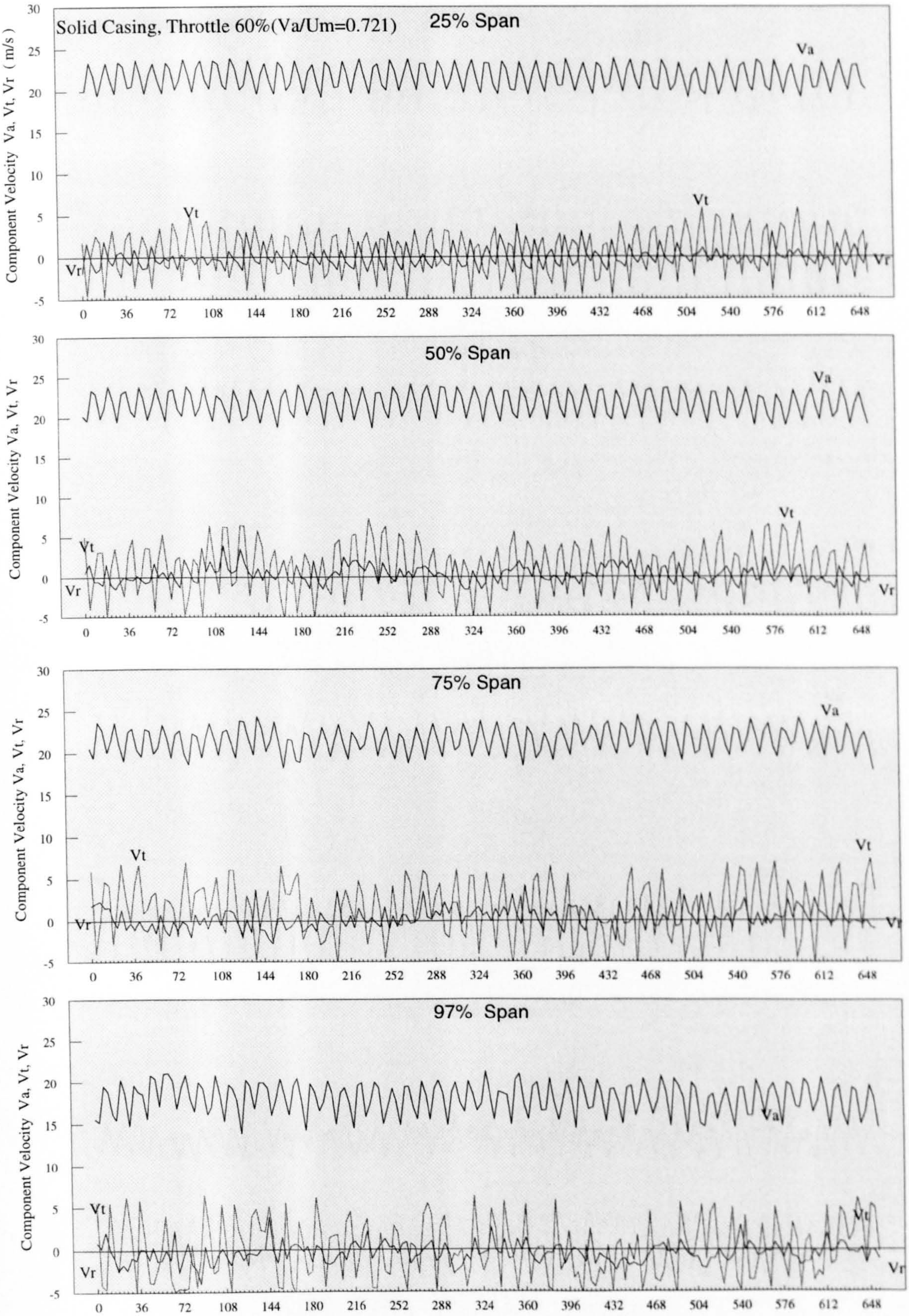

Fig.5-20a Instantaneous Inlet Velocity for Solid Casing (Design Point, ϕ =0.72)

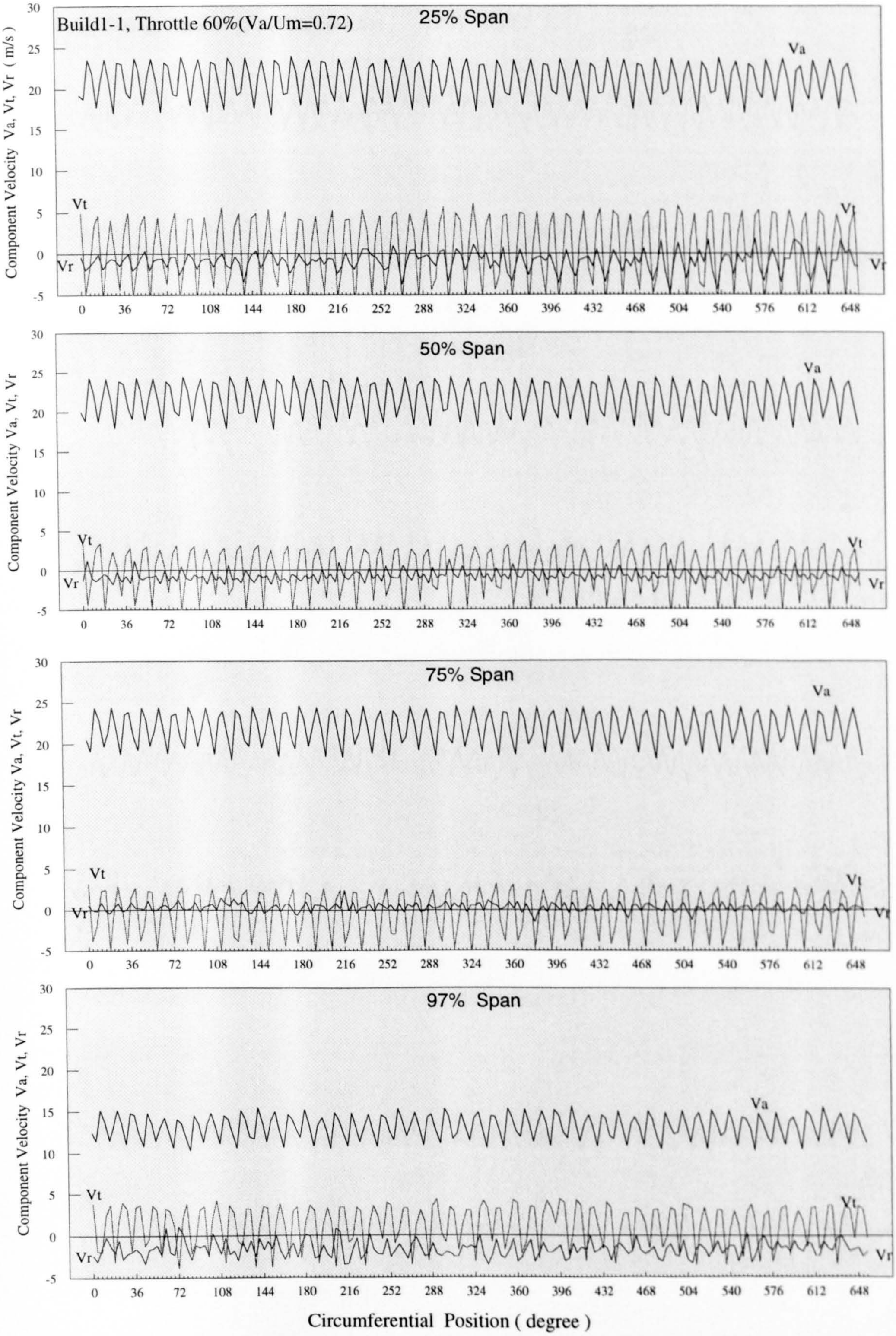

Fig.5-20b Instantaneous Inlet Velocity for Treated Casing (Design Point, ϕ=0.72)

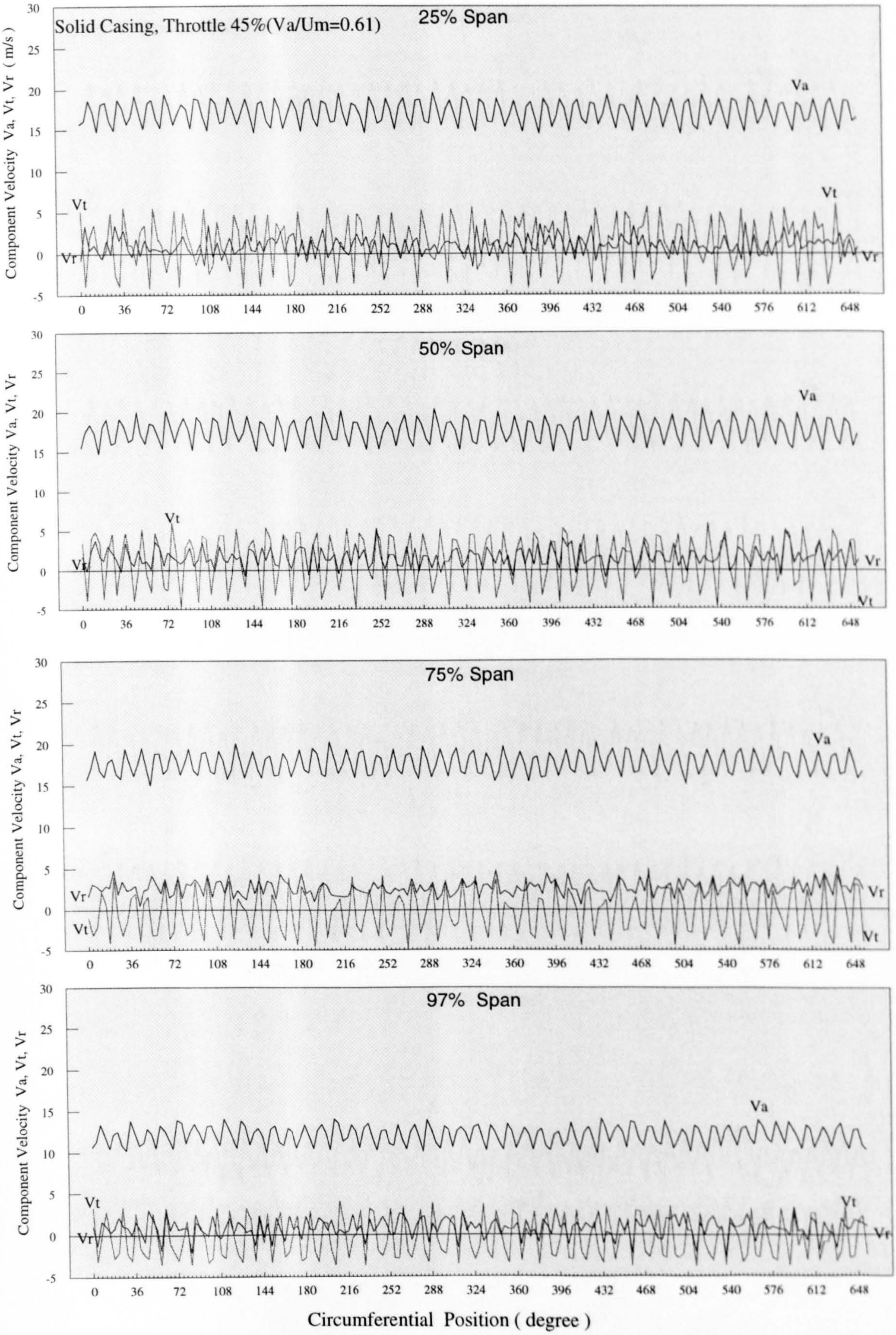

Fig.5-21a Instantaneous Inlet Velocity for Solid Casing (Near Stall Point, ϕ=0.61)

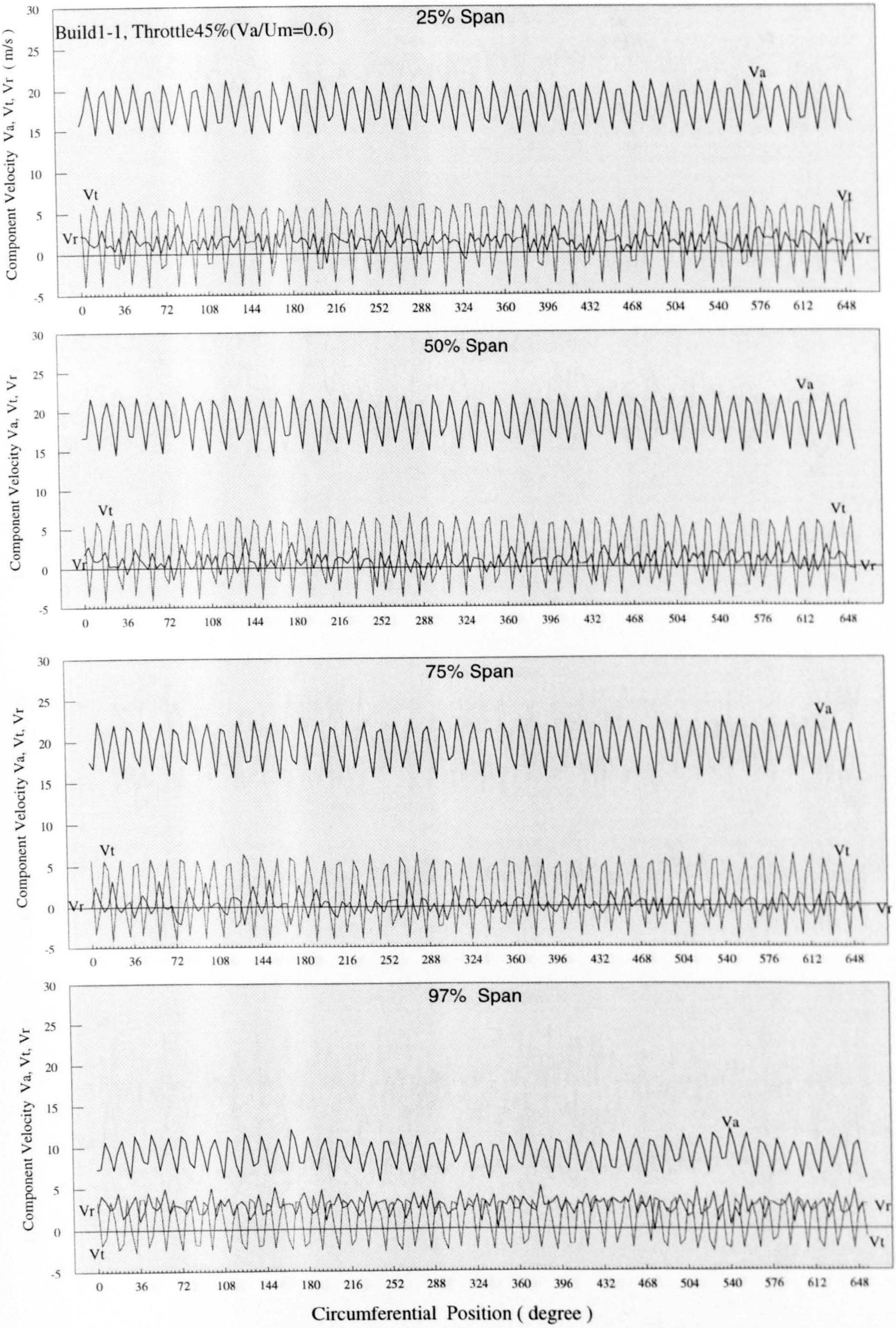

Fig.5-21b Instantaneous Inlet Velocity for Treated Casing (Near Stall Point, ϕ=0.6)

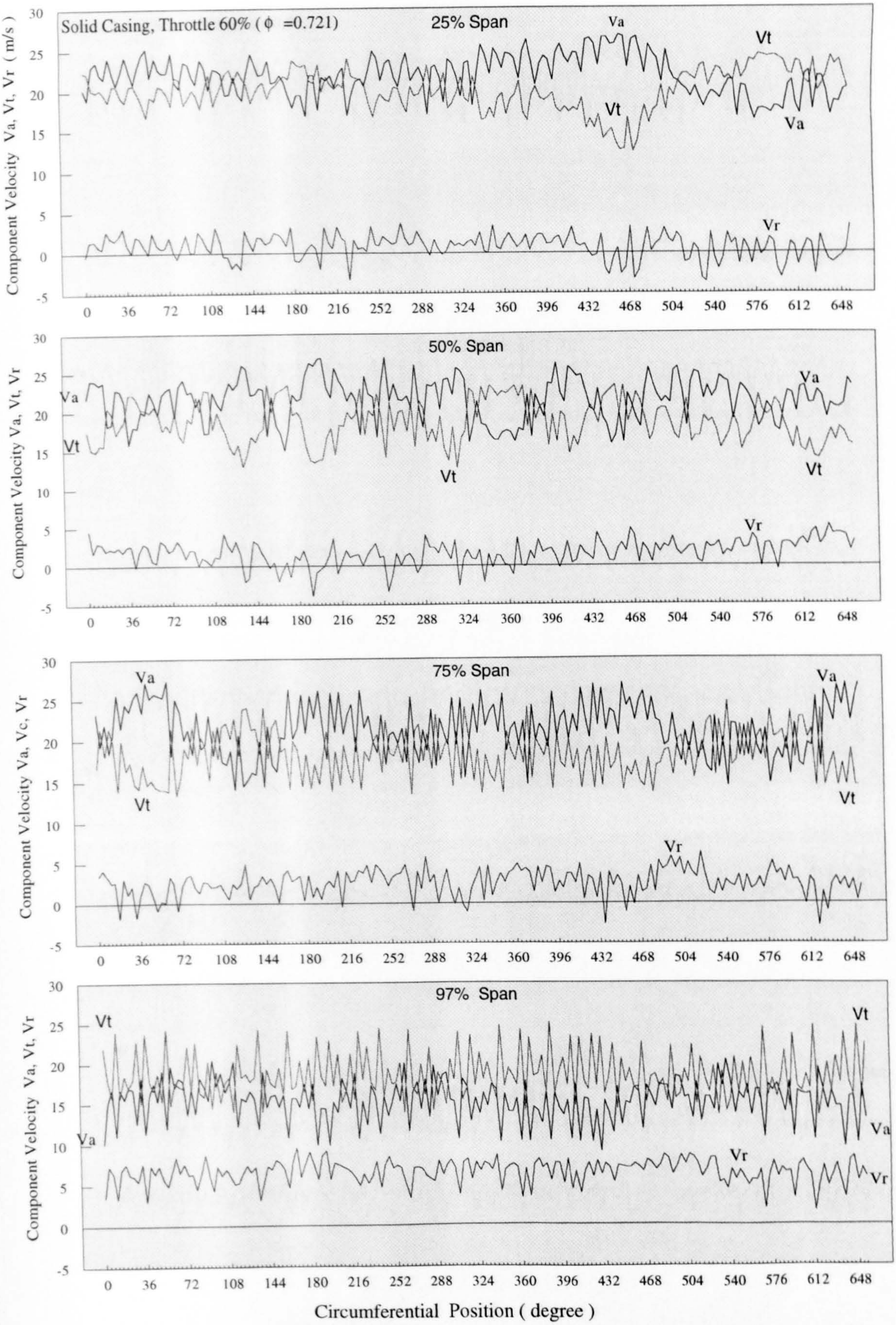

Fig.5-22a Instantaneous Outlet Velocity for Solid Casing (Design Point, ϕ=0.72)

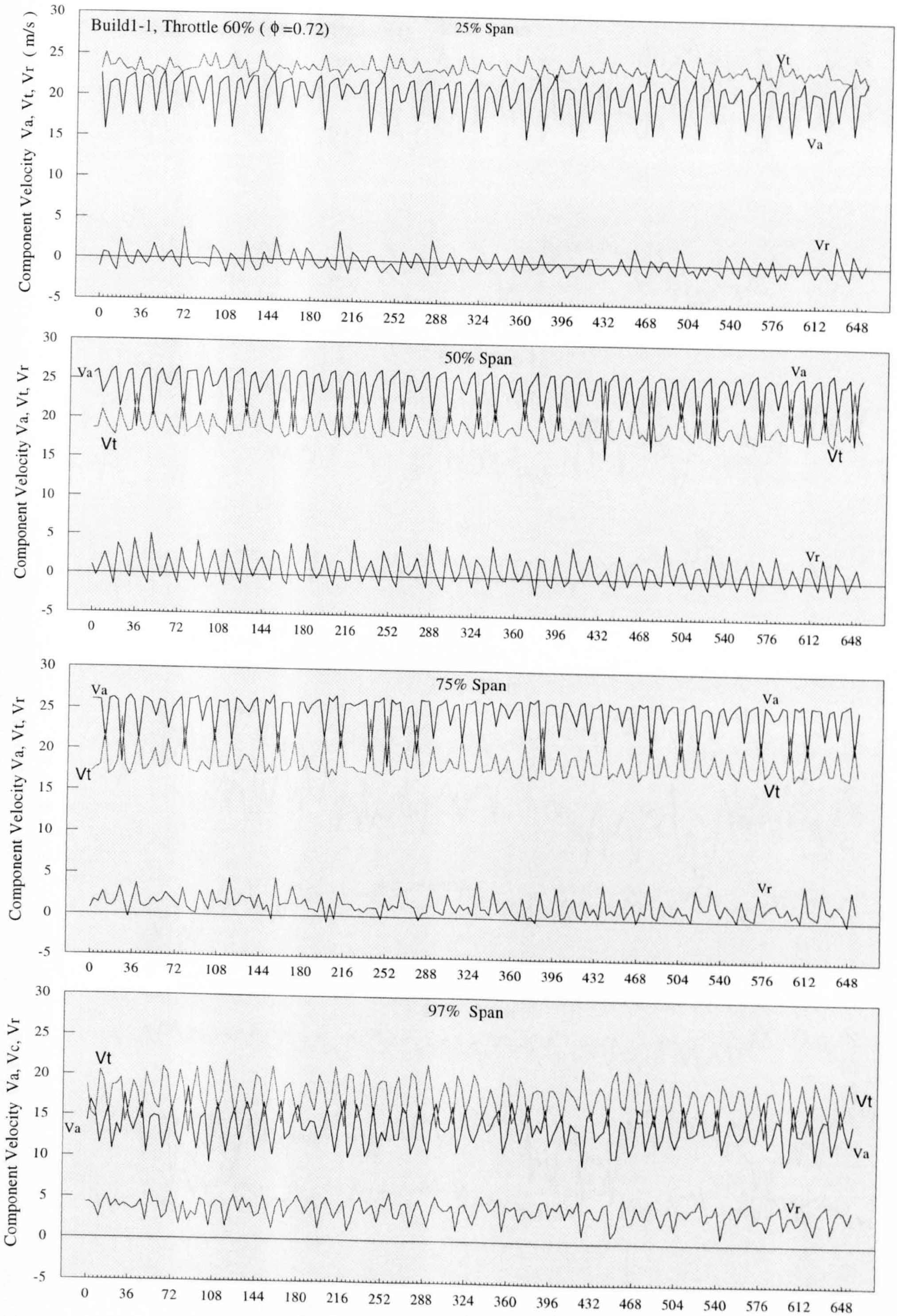

Fig.5-22b Instantaneous Outlet Velocity for Treated Casing (Design Point, ϕ=0.72)

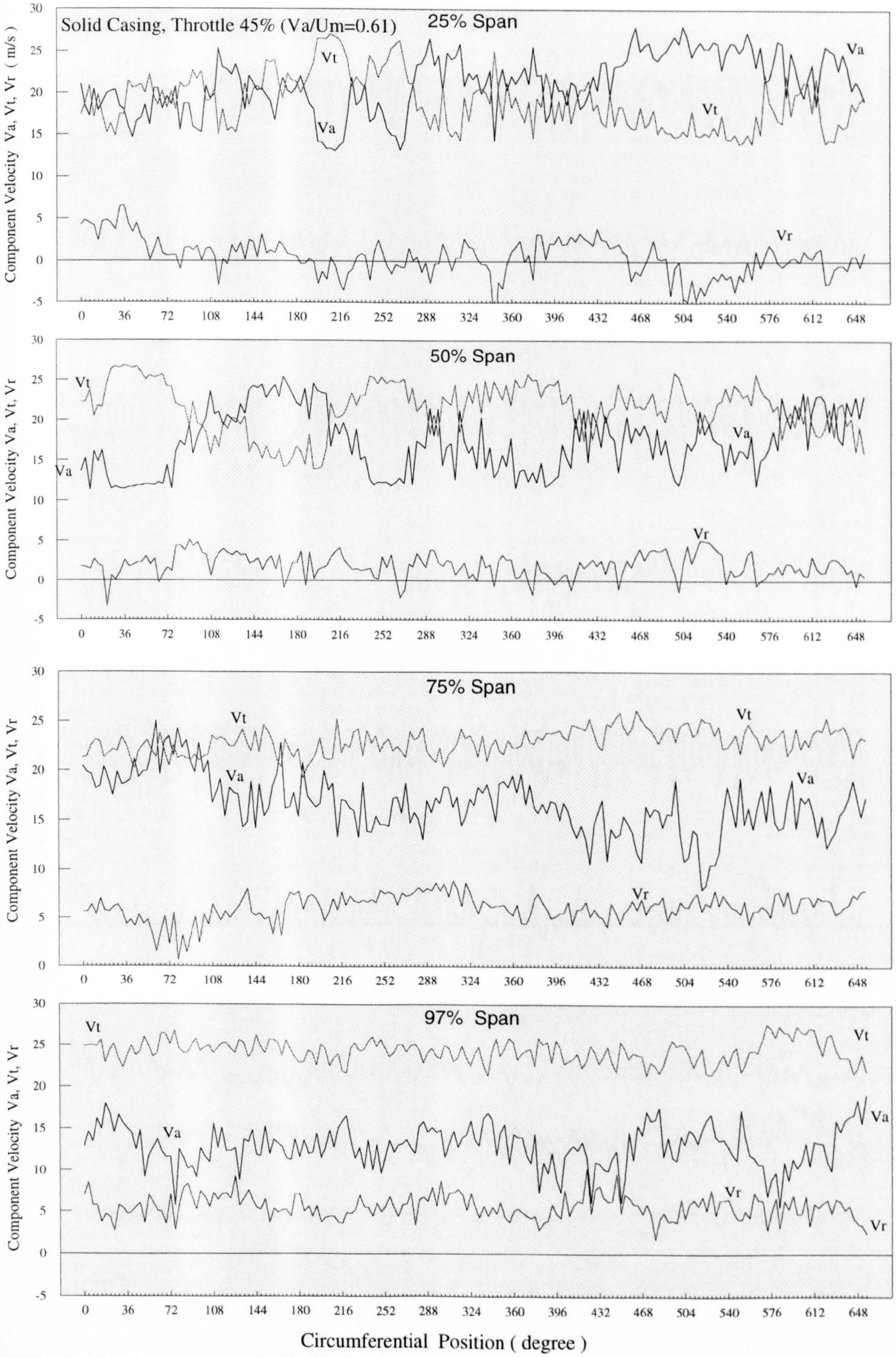

Fig.5-23a Instantaneous Outlet Velocity for Solid Casing (Near Stall Point, ϕ=0.61)

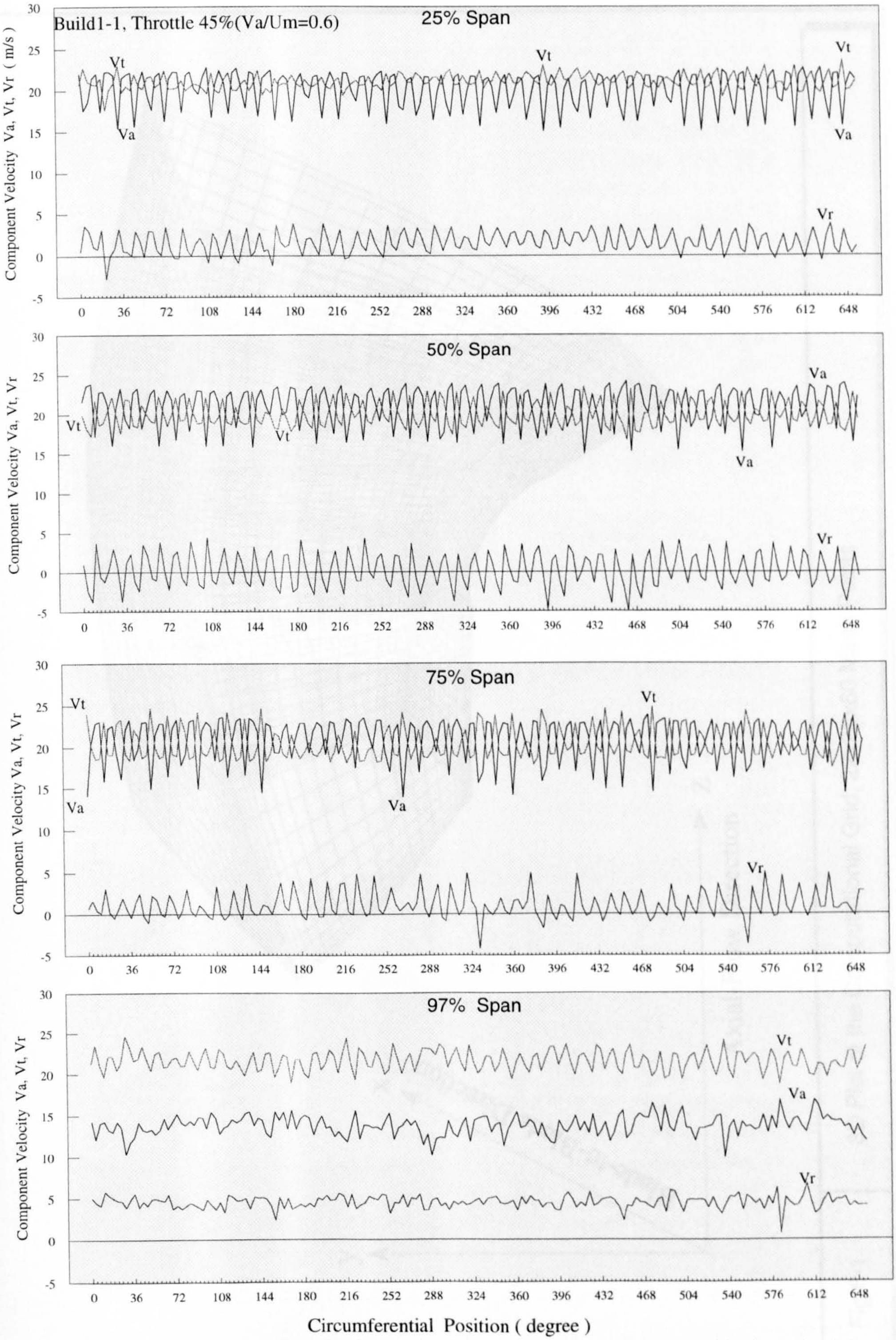

Fig.5-23b Instantaneous Outlet Velocity for Treated Casing (Near Stall Point, ϕ=0.6)

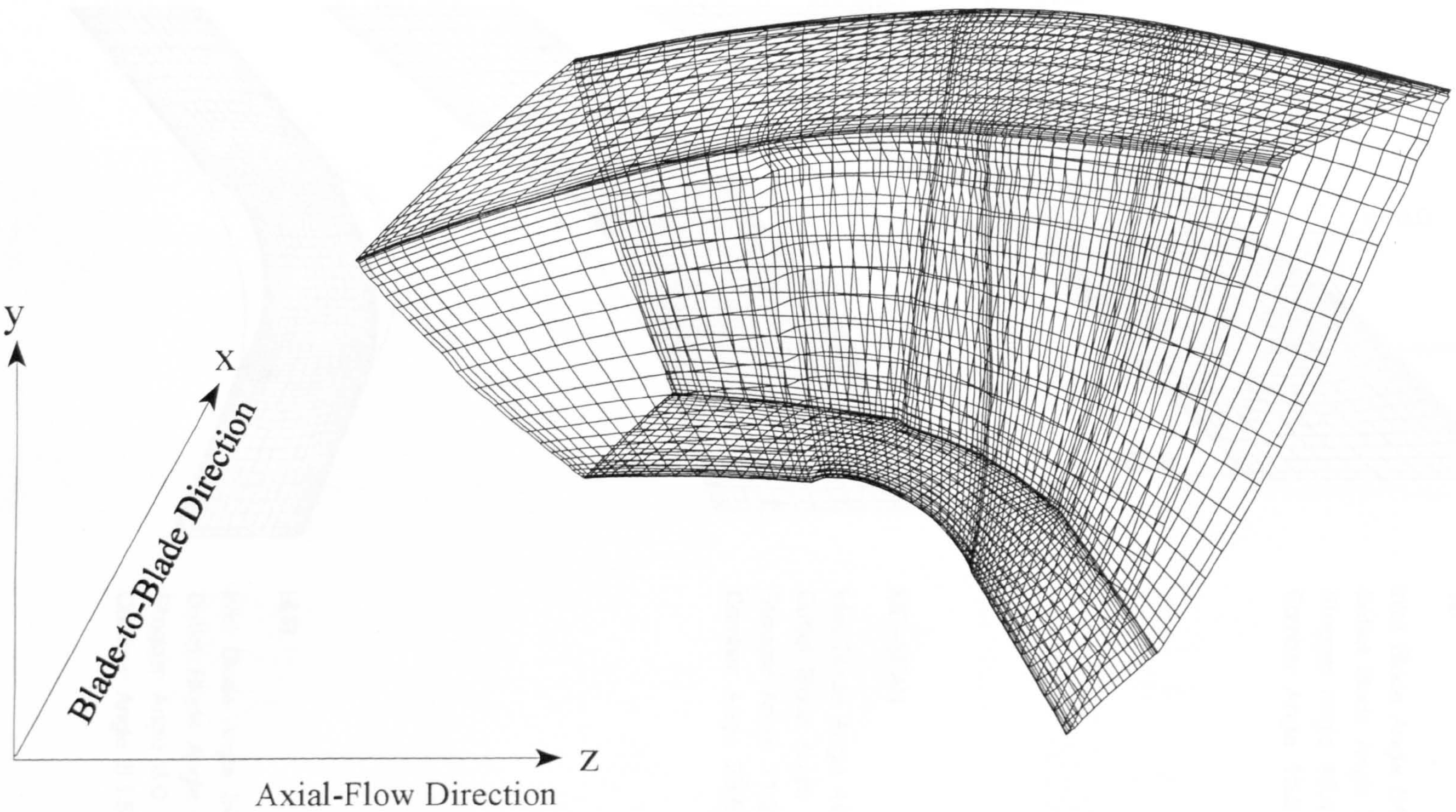

Fig.6-1	3D Plot of the Computational Grid, 22x26x60 Mesh Points

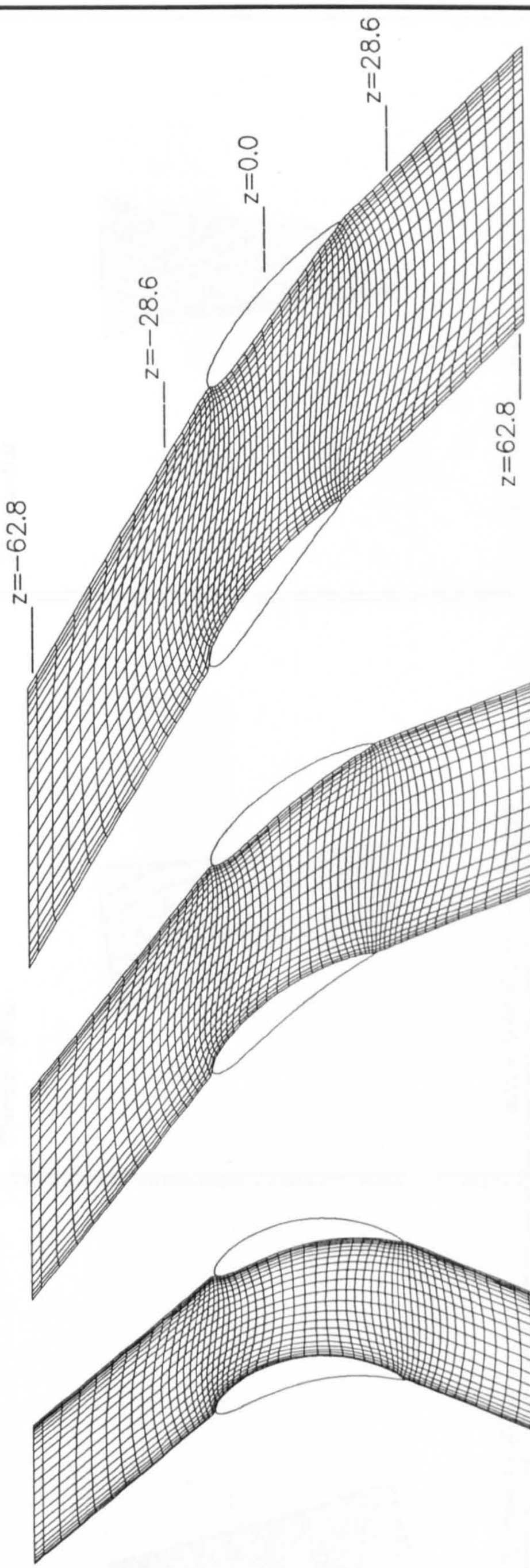

TIP

Inlet Blade Angle 54.2
Outlet Blade Angle 38.8
Stagger Angle 46.4
Camber Angle 15.5

MID-SPAN

Inlet Blade Angle 46.1
Outlet Blade Angle 17.5
Stagger Angle 31.8
Camber Angle 28.6

HUB

Inlet Blade Angle 34.9
Outlet Blade Angle −18.8
Stagger Angle 8.0
Camber Angle 53.5

Fig.6−2	2D Plot of Computational Grid at Tip, Mid−span and Hub

Fig.6-3 Contour Plot of the Pressure Distribution on X-Y Planes

(Va/U=0.72, Tip Clearance=1.2%)

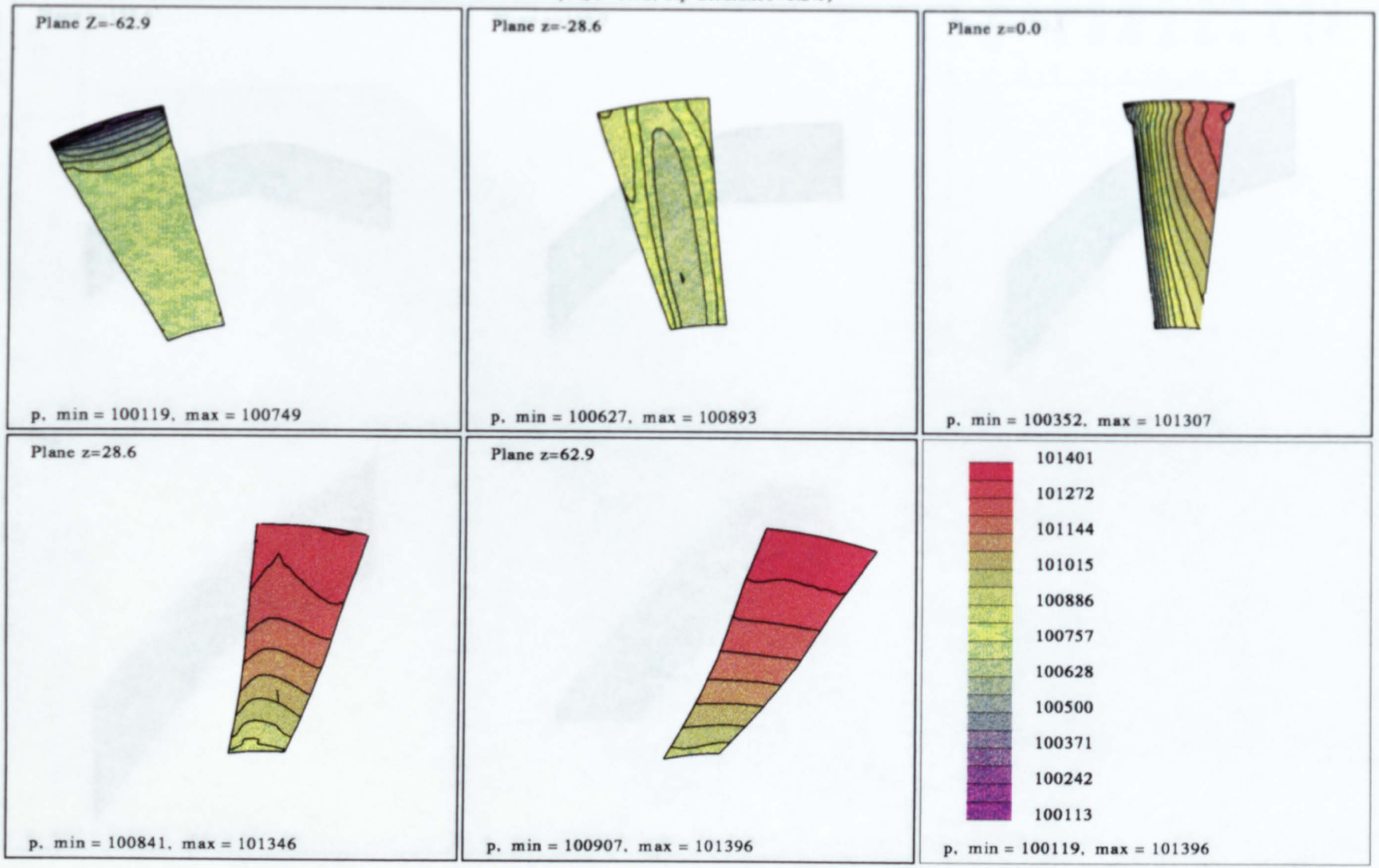

Fig.6-4 Contour Plot of the Pressure Distribution on X-Z Planes

(Va/U=0.72, Tip Clearance=1.2%)

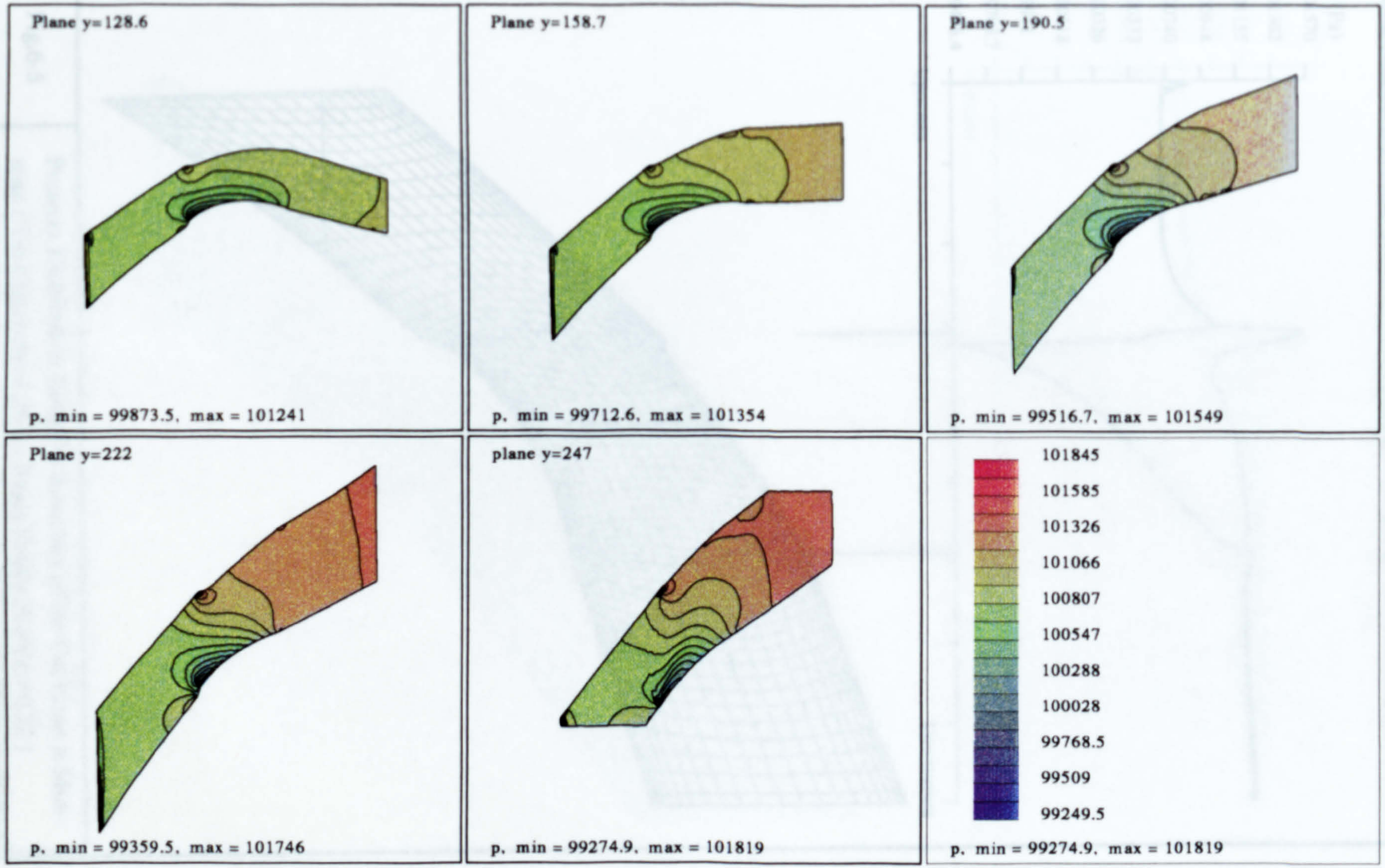

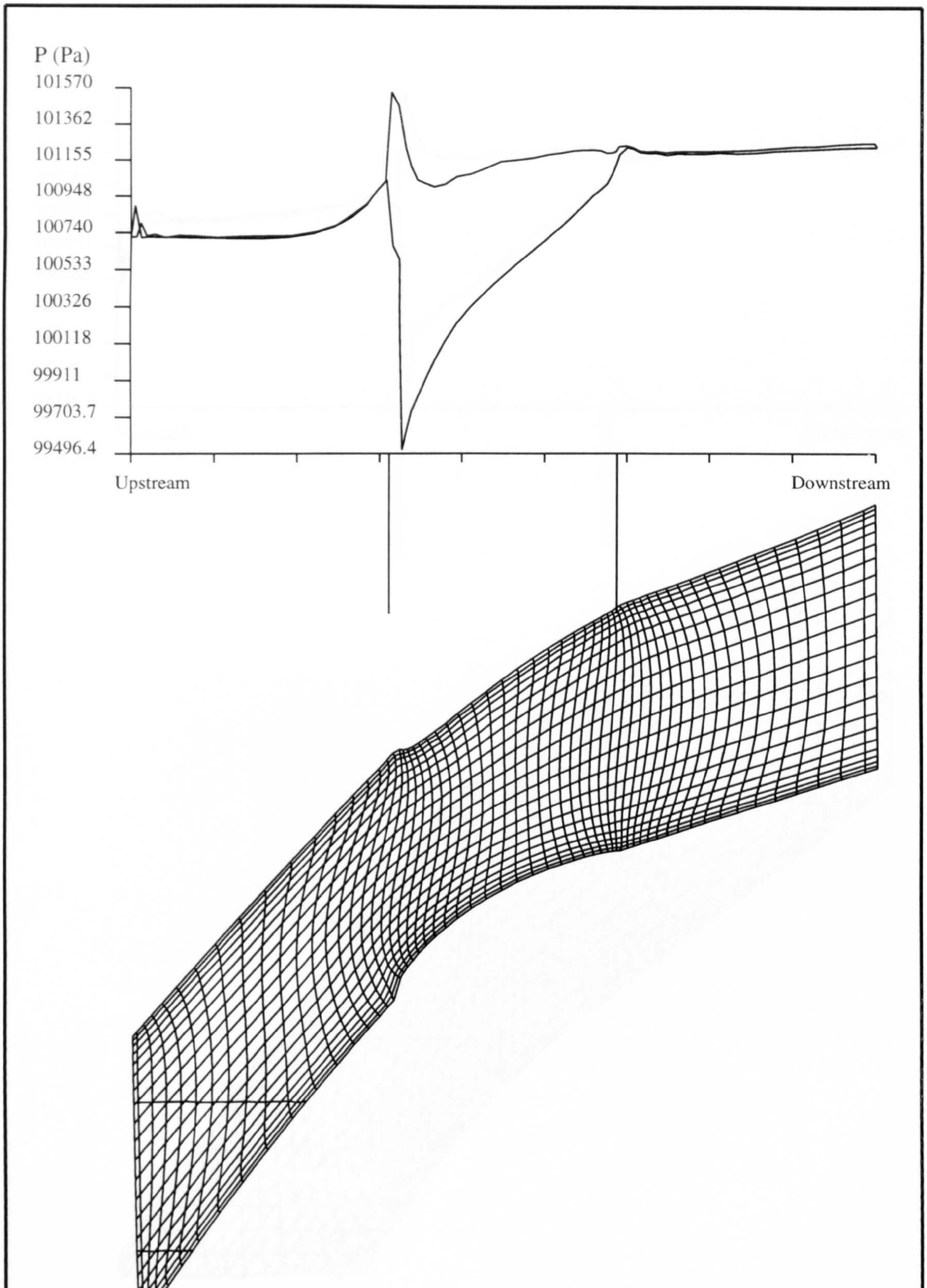

Fig.6-5	Pressure Distribution along the Boundary of the Cut Plane at Mid-span (Tip Clearance=1.2% of Blade Height, Va/Um=0.72)

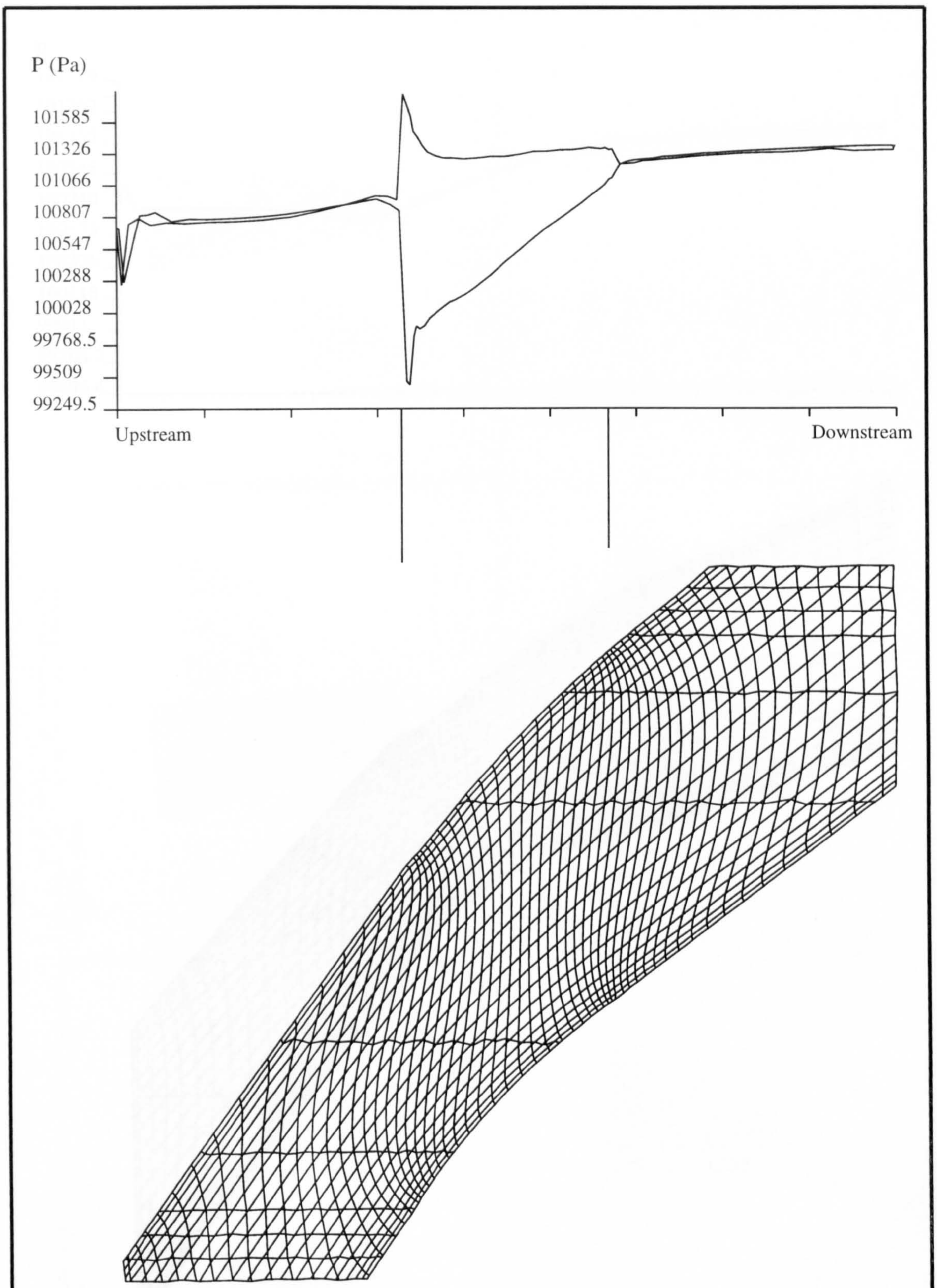

Fig.6-6	Pressure Distribution along the Boundary of the Cut Plane Near the Tip (Tip Clearance=1.2% of Blade Height, Va/Um=0.72)

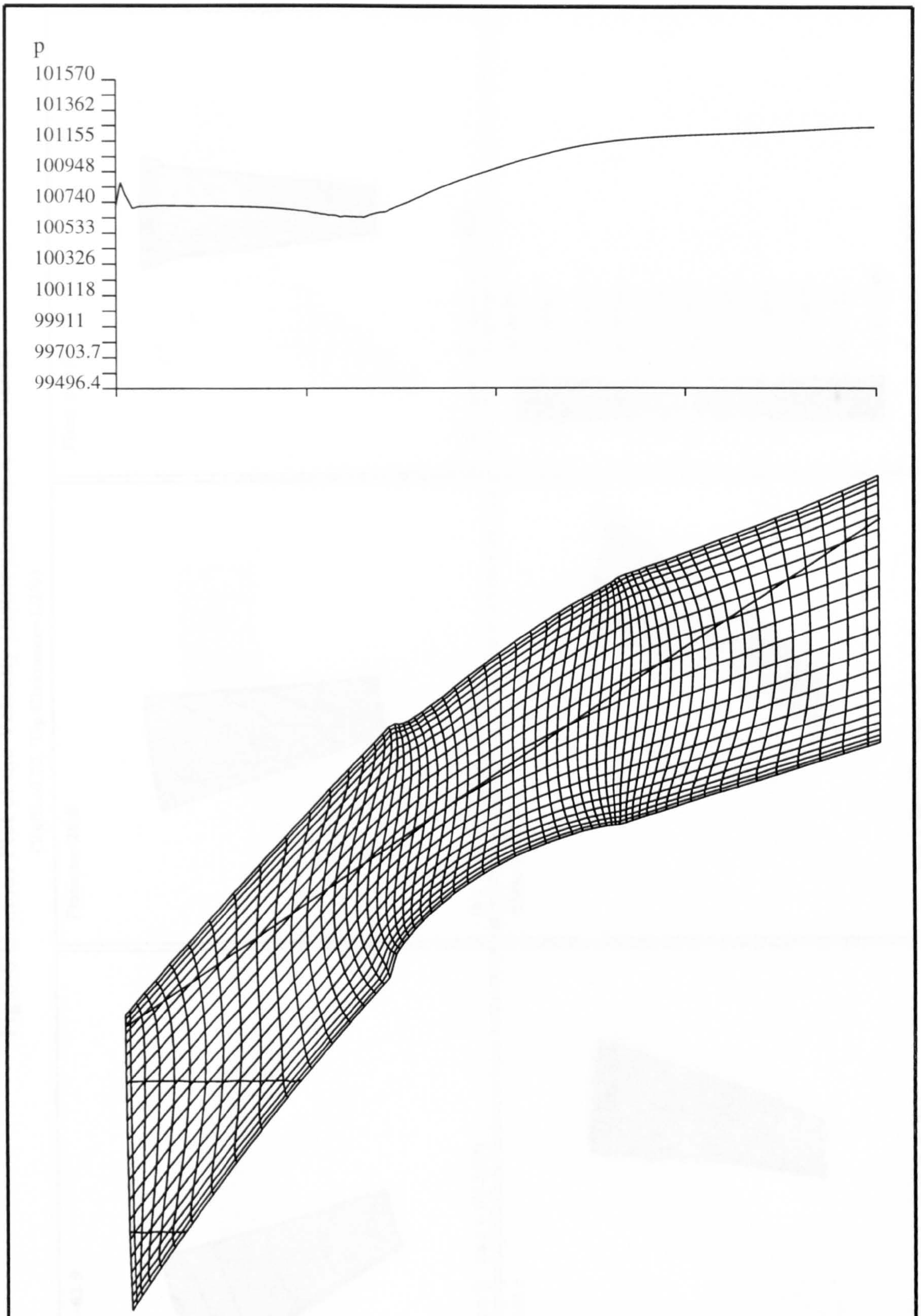

Fig.6-7	Pressure Distribution along the Cut Line Shown (Tip Clearance=1.2% of Blade Height, Va/Um=0.72)

Fig.6-8 Contour Plot of the Velocity Distribution on X-Y Planes

(Va/U=0.72, Tip Clearance=1.2%)

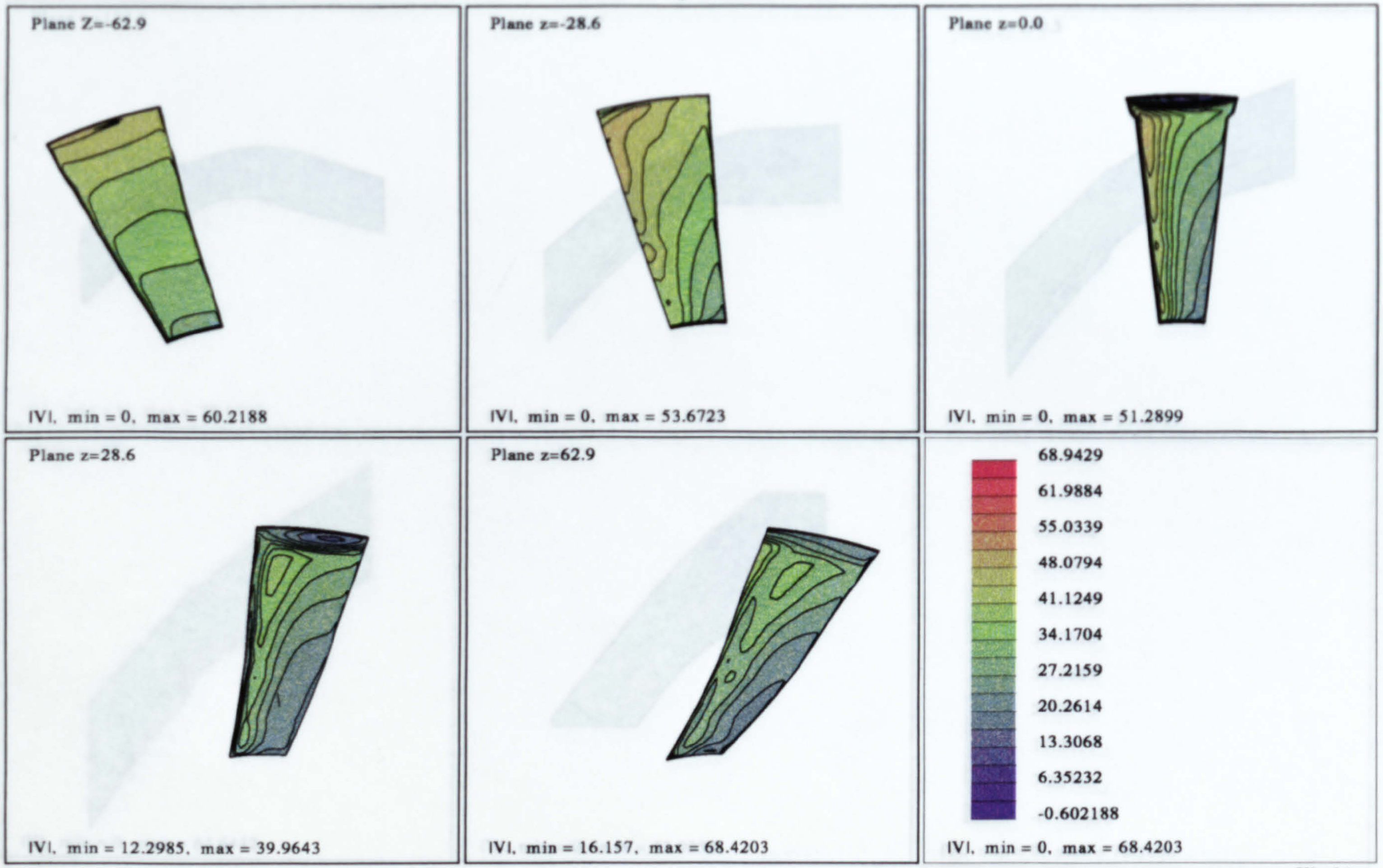

Fig.6-9 Contour Plot of the Velocity Distribution on X-Z Planes

(Va/U=0.72, Tip Clearance=1.2%)

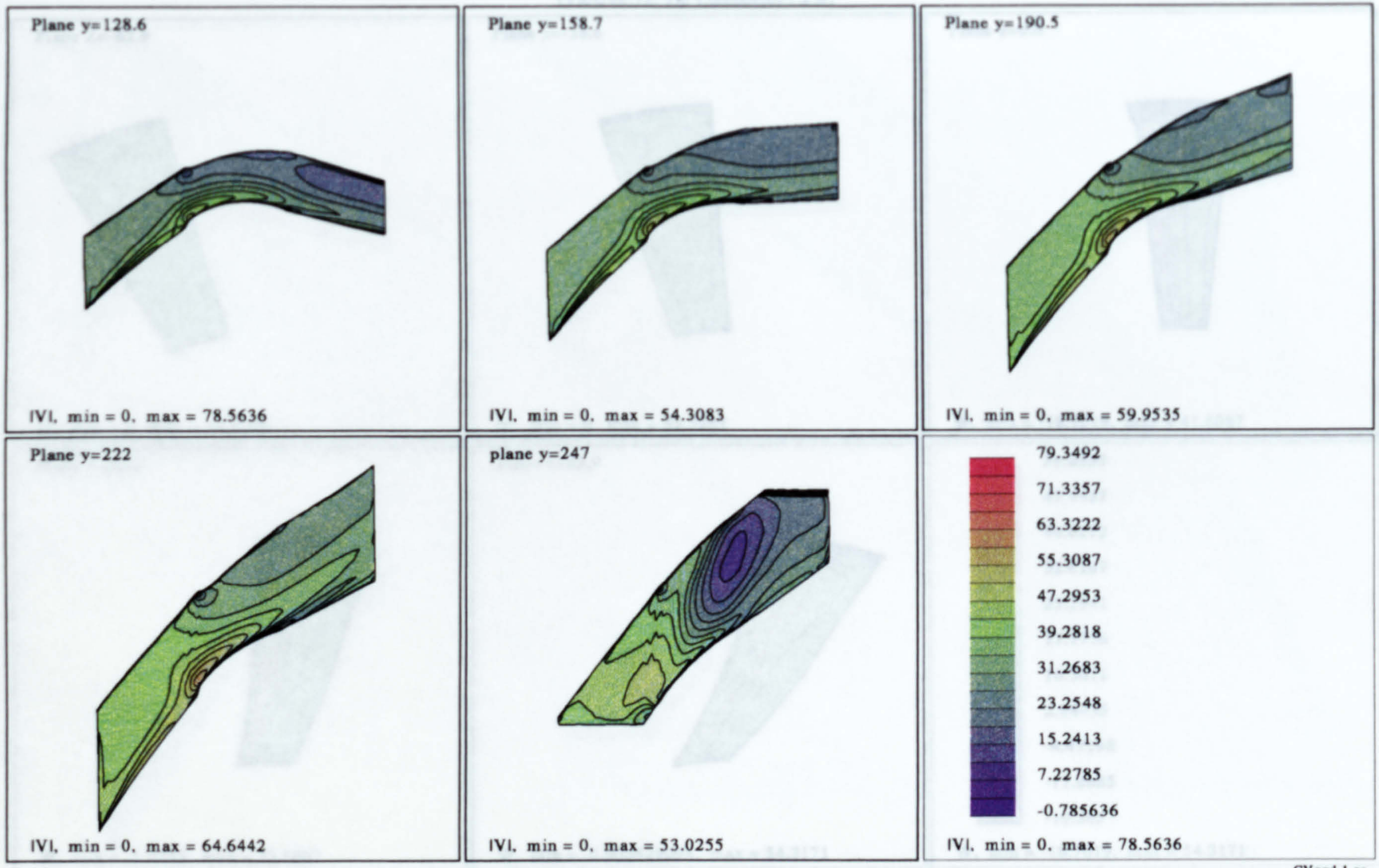

Fig.6-10 Contour Plot of the Axial Velocity Distribution on X-Y Planes

(Va/U=0.72, Tip Clearance=1.2%)

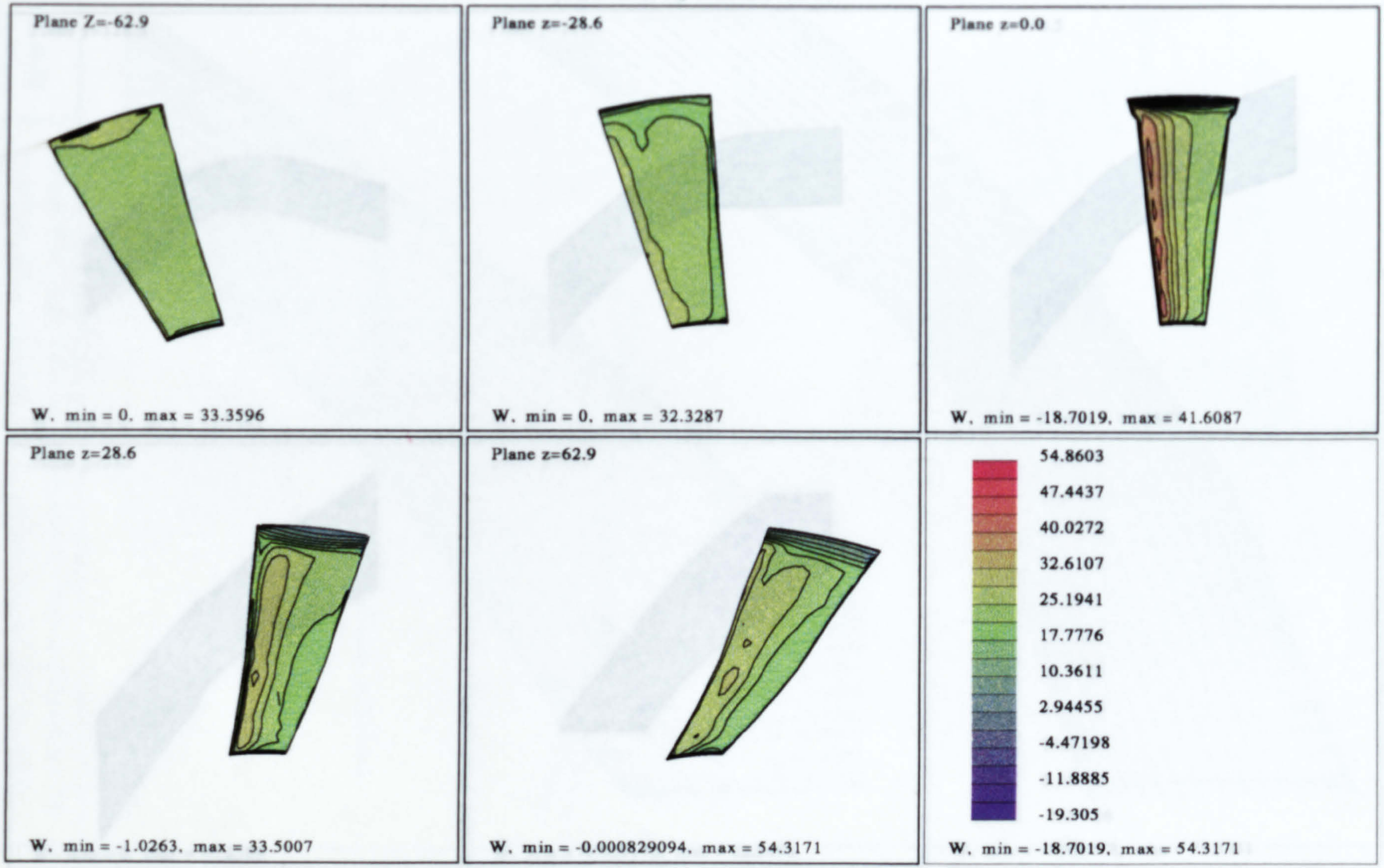

Fig.6-11 Contour Plot of the Axial Velocity Distribution on X-Z Planes

(Va/U=0.72, Tip Clearance=1.2%)

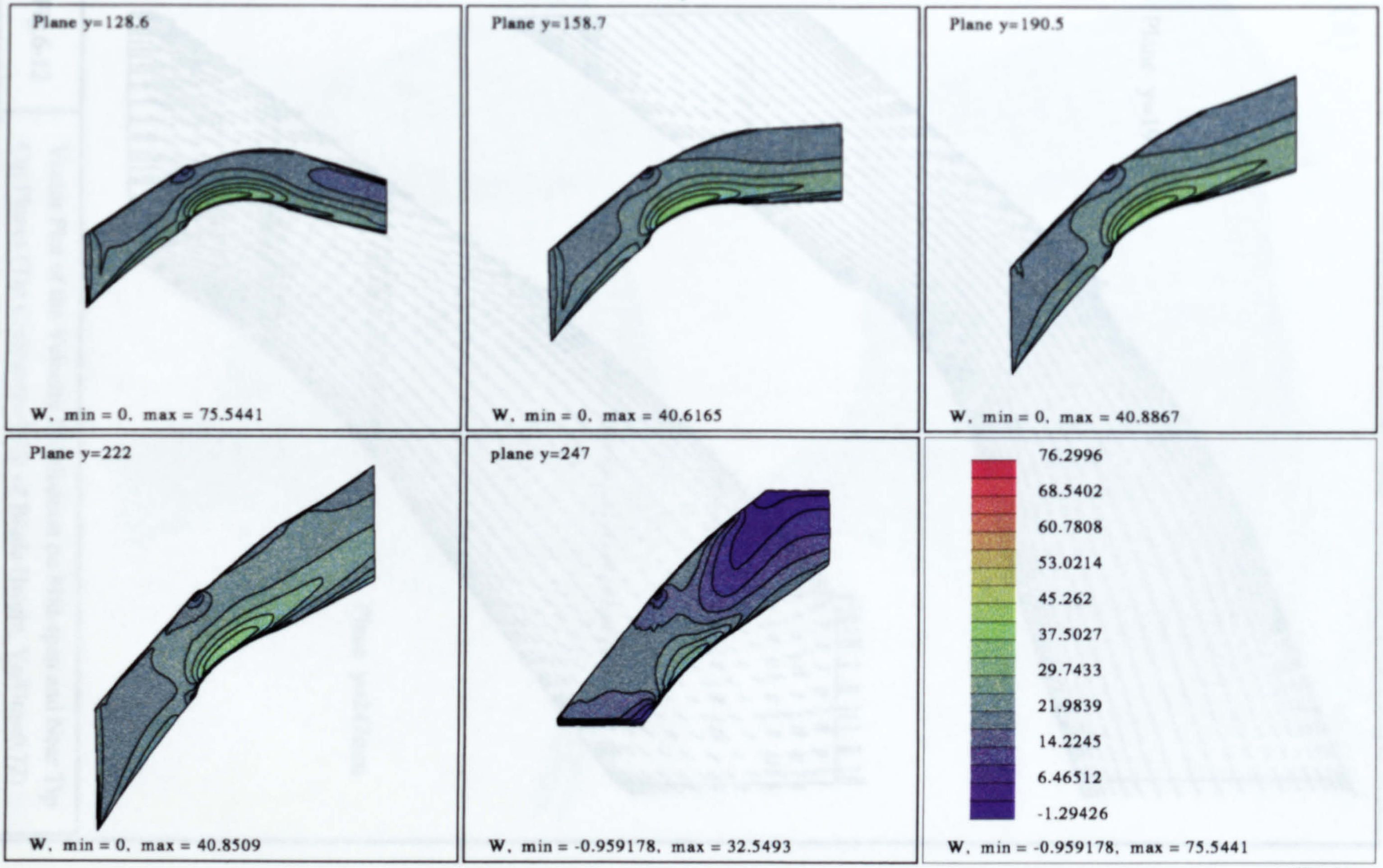

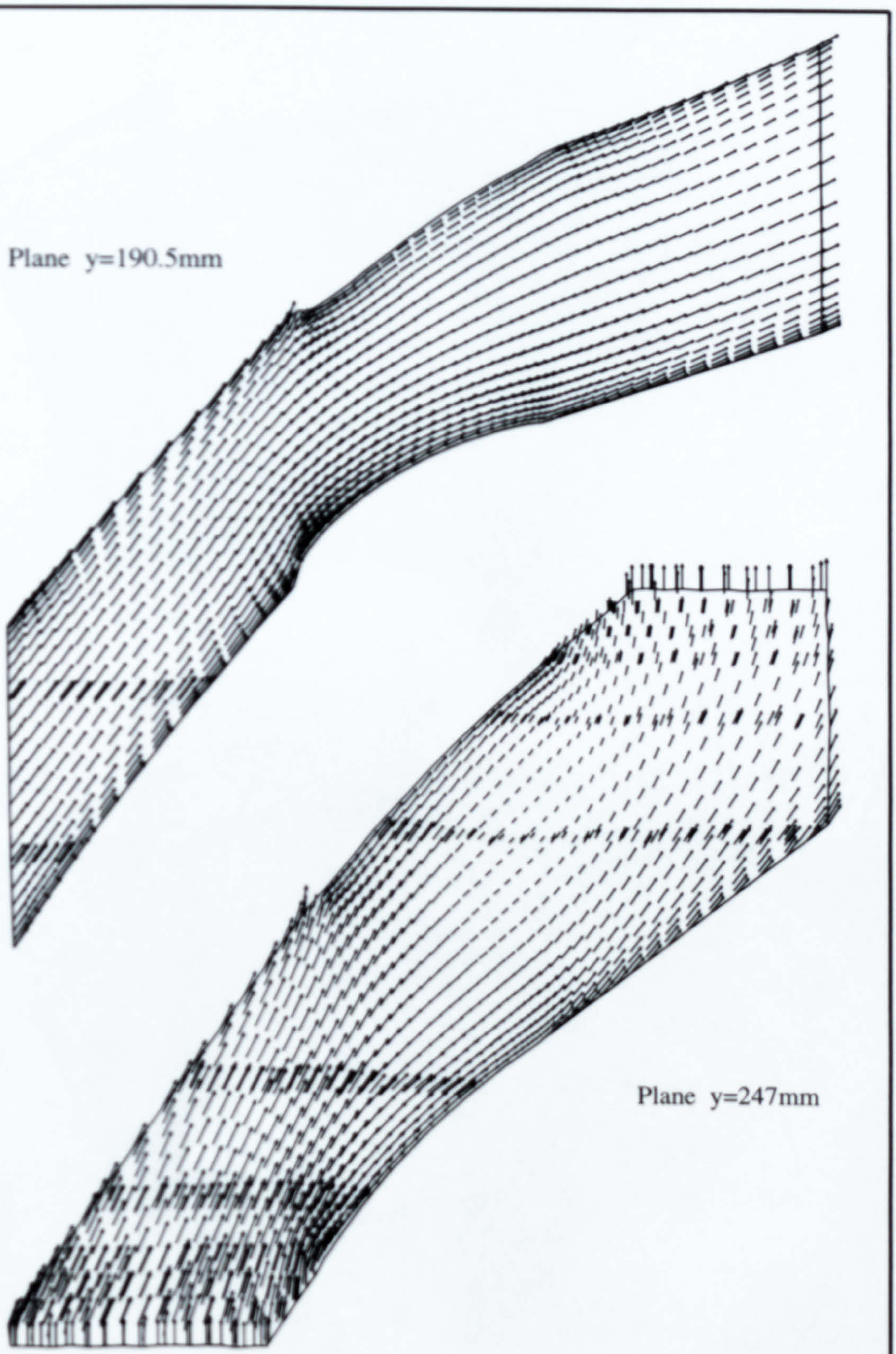

Fig.6-12	Vector Plot of the Velocity Distribution on Mid-span and Near Tip Cut Planes (Tip Clearance=1.2% of Blade Height, Va/Um=0.72)

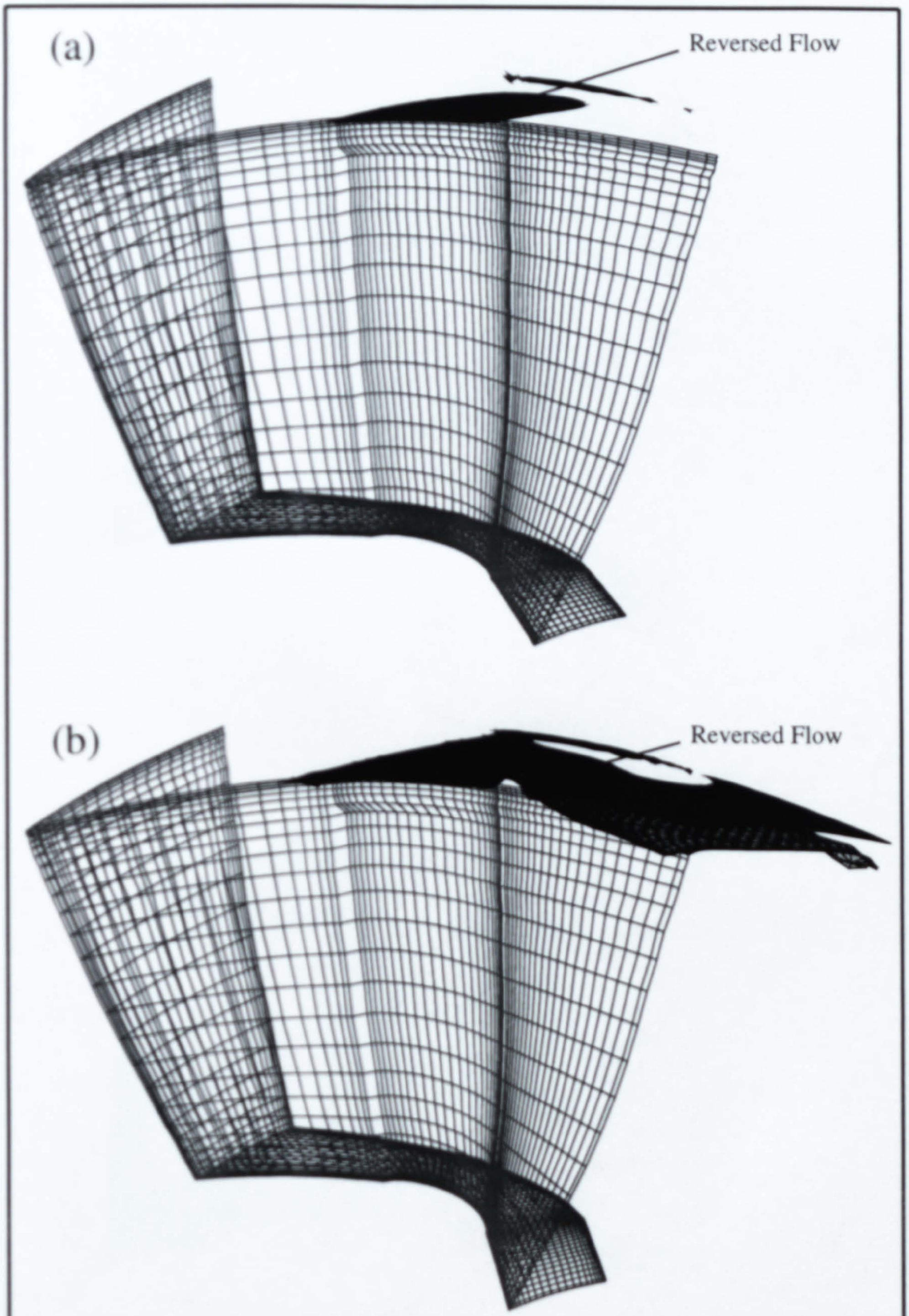

Fig.6-13	Isosurface Plot of Reversed Flow (Va=-5m/s, tip Clearance=1 .2%) (a) Design Point (Va/Um=0.72); (b) Near Stall Point (Va/Um=0 .62)

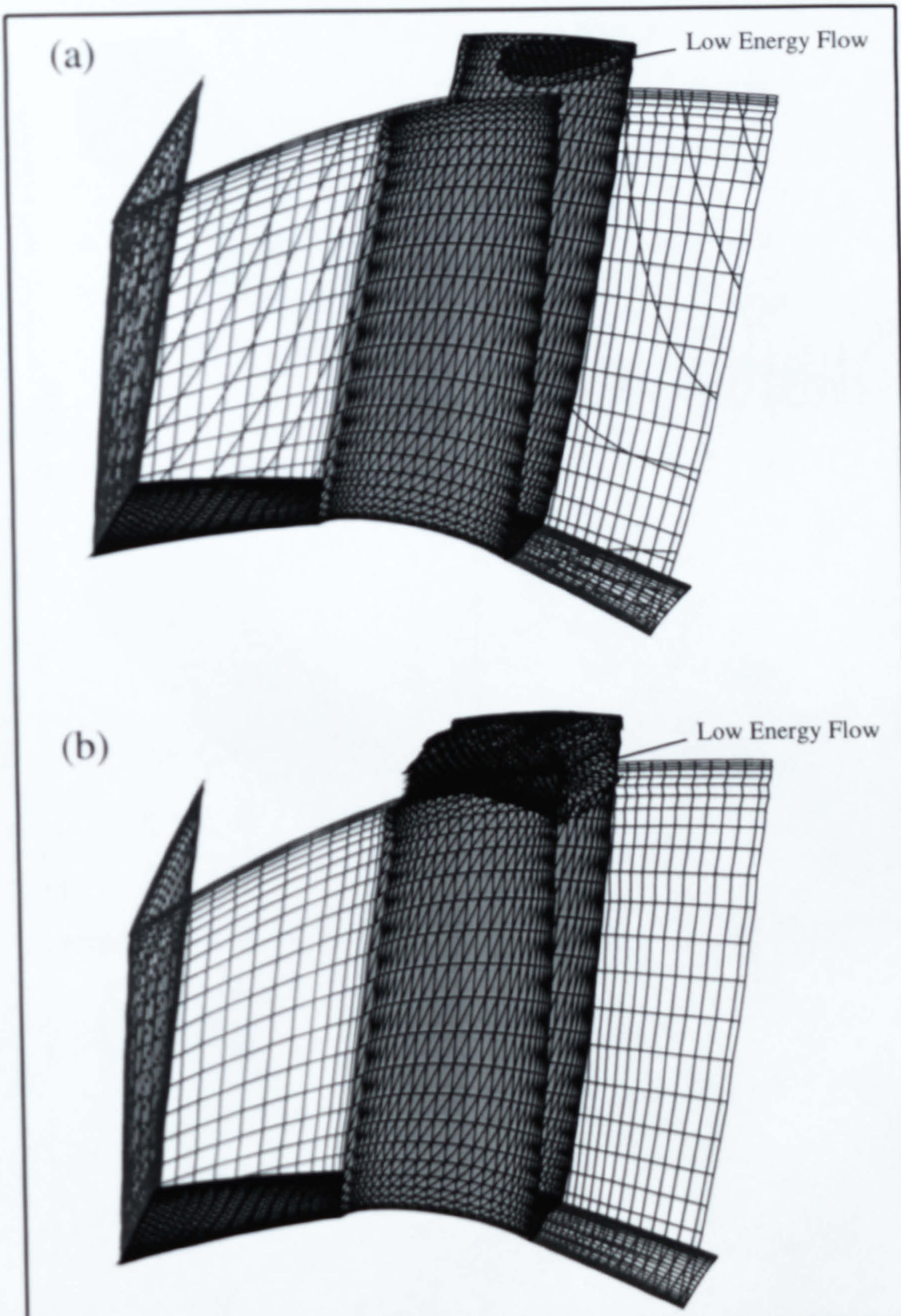

Fig.6-14	Isosurface Plot of Low Energy Flow (V=8m/s, tip Clearance=1.2%) (a) Design Point(Va/Um=0.72); (b) Near Stall Point(Va/Um=0.62)

Fig.6-15 Pressure Contours for Various Tip Clearance (Va/Um=0.72)

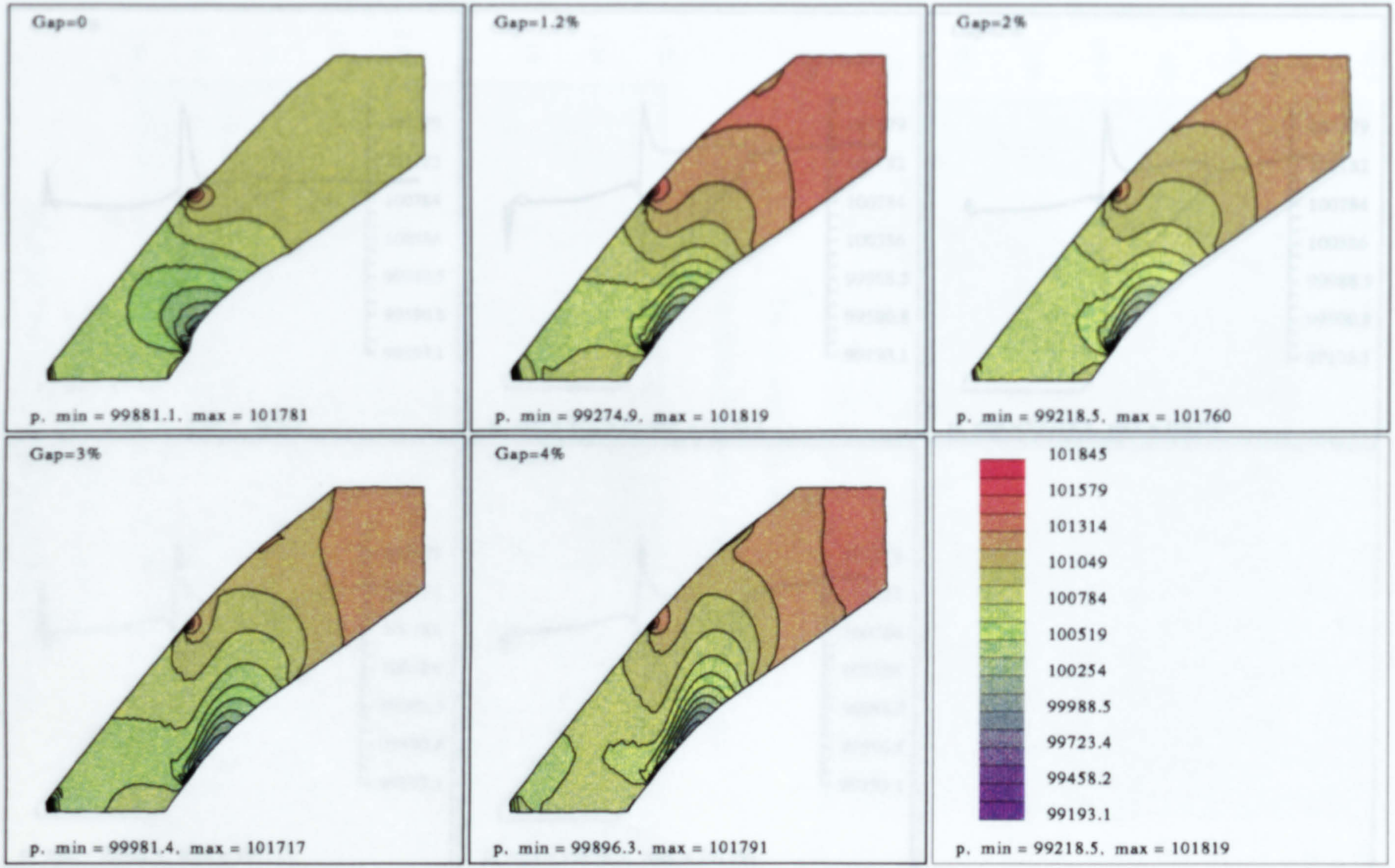

Fig.6-16 Pressure Along the Mesh Boundary for Various Tip Clearance (Va/Um=0.72)

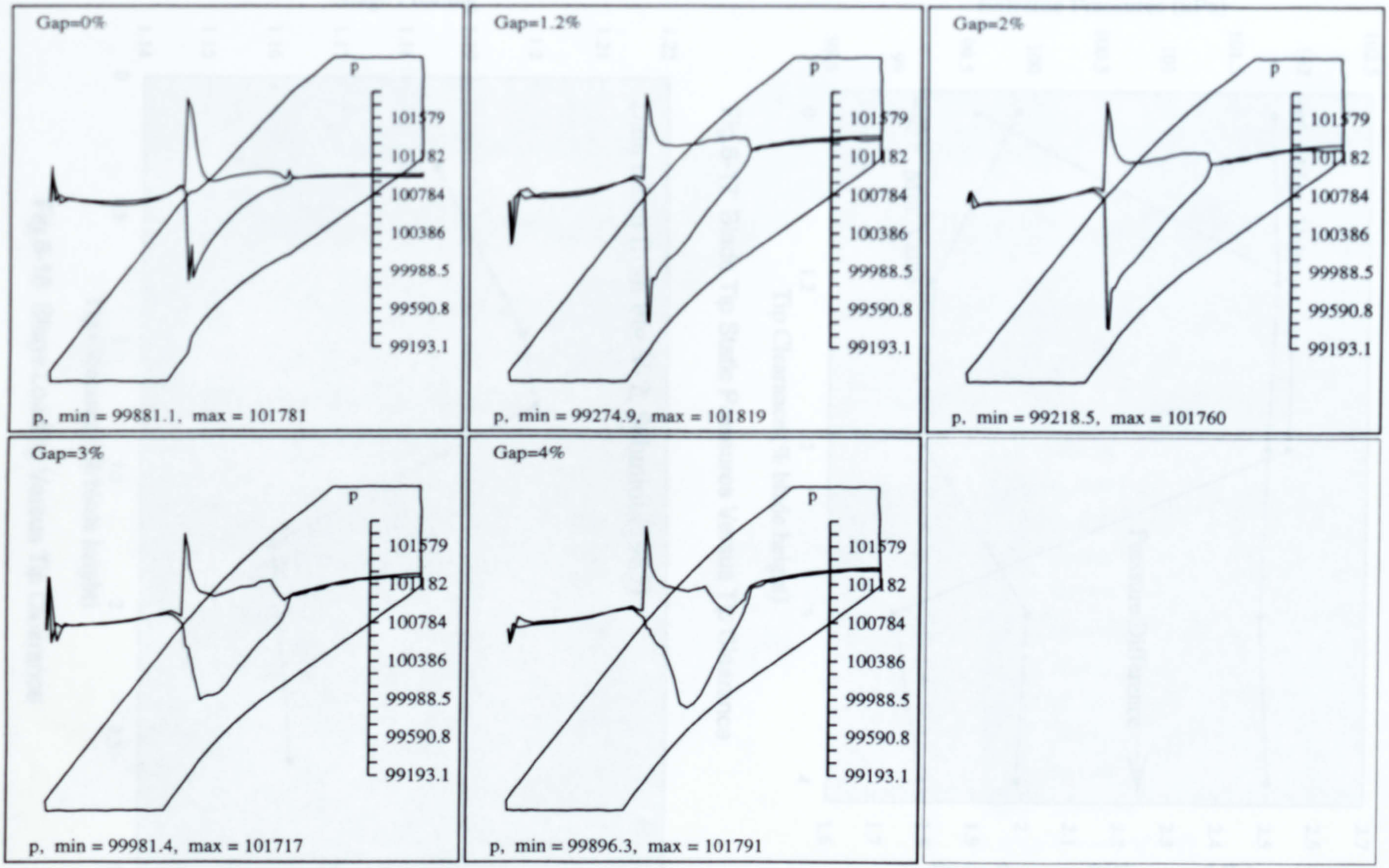

Ptipd3.ps

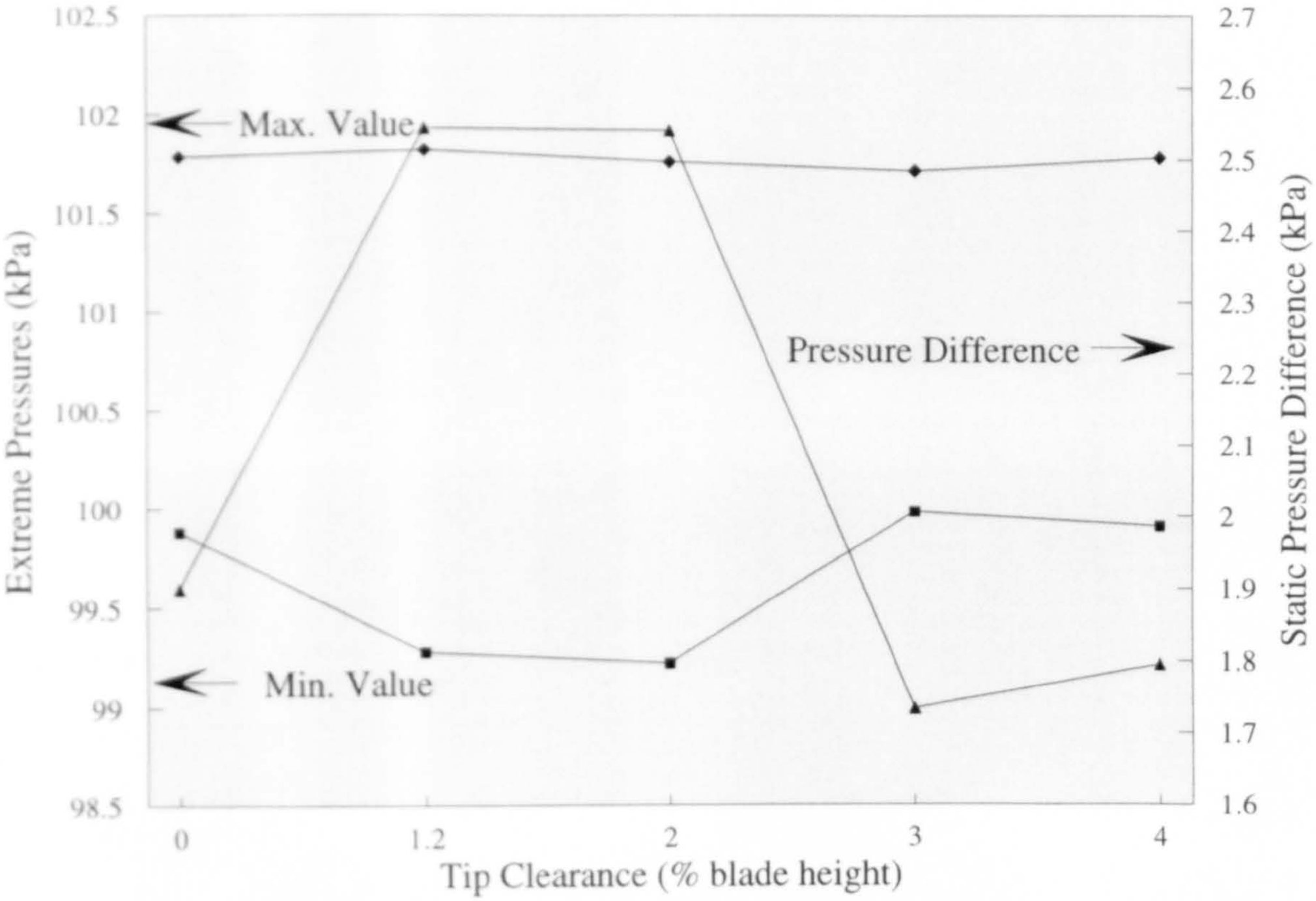

Fig.6-17 Blade Tip Static Pressures Versus Tip Clearance

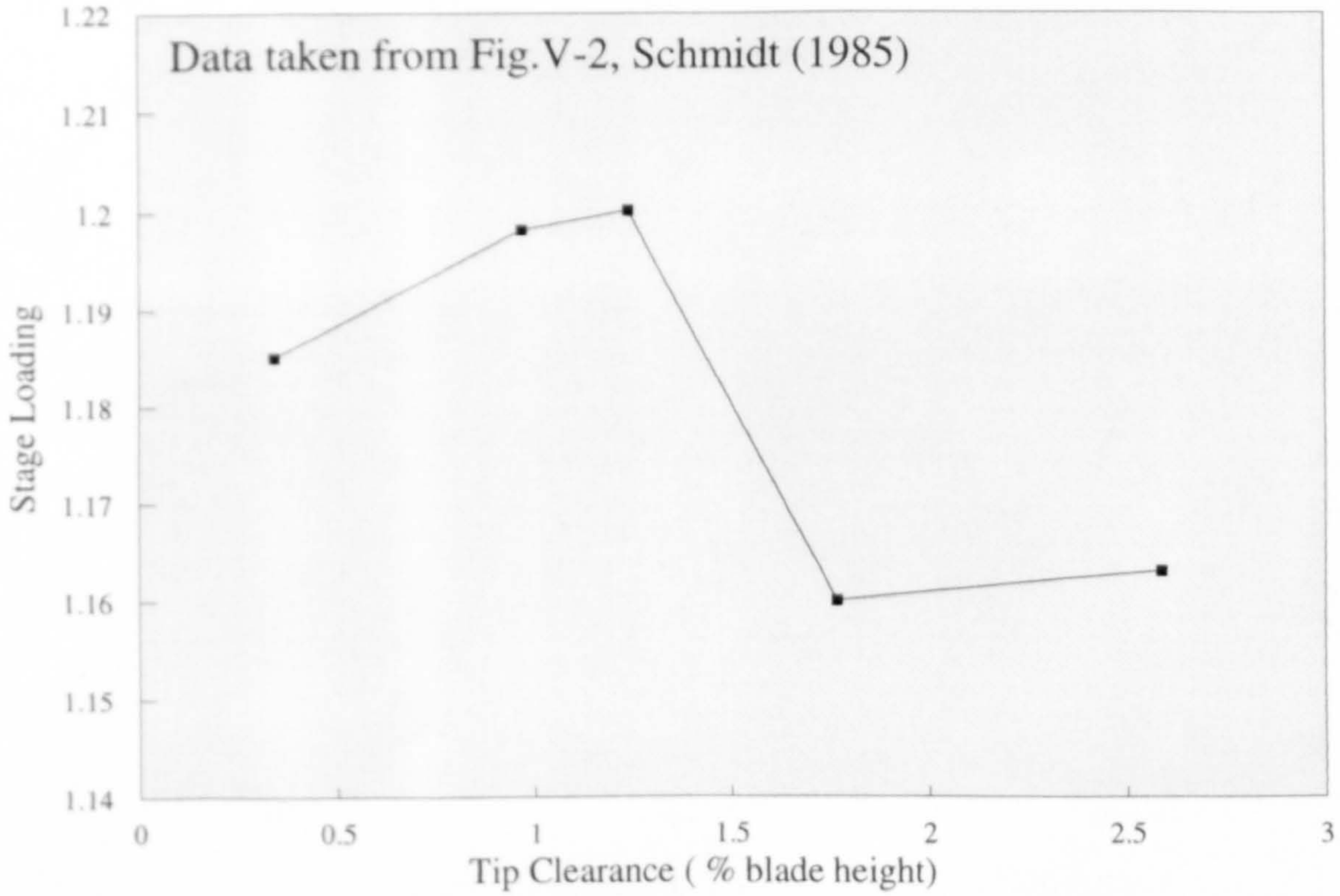

Fig.6-18 Stage Loading Versus Tip Clearance

Fig.6-19 Velocity Contours for Various Tip Clearance (Va/Um=0.72)

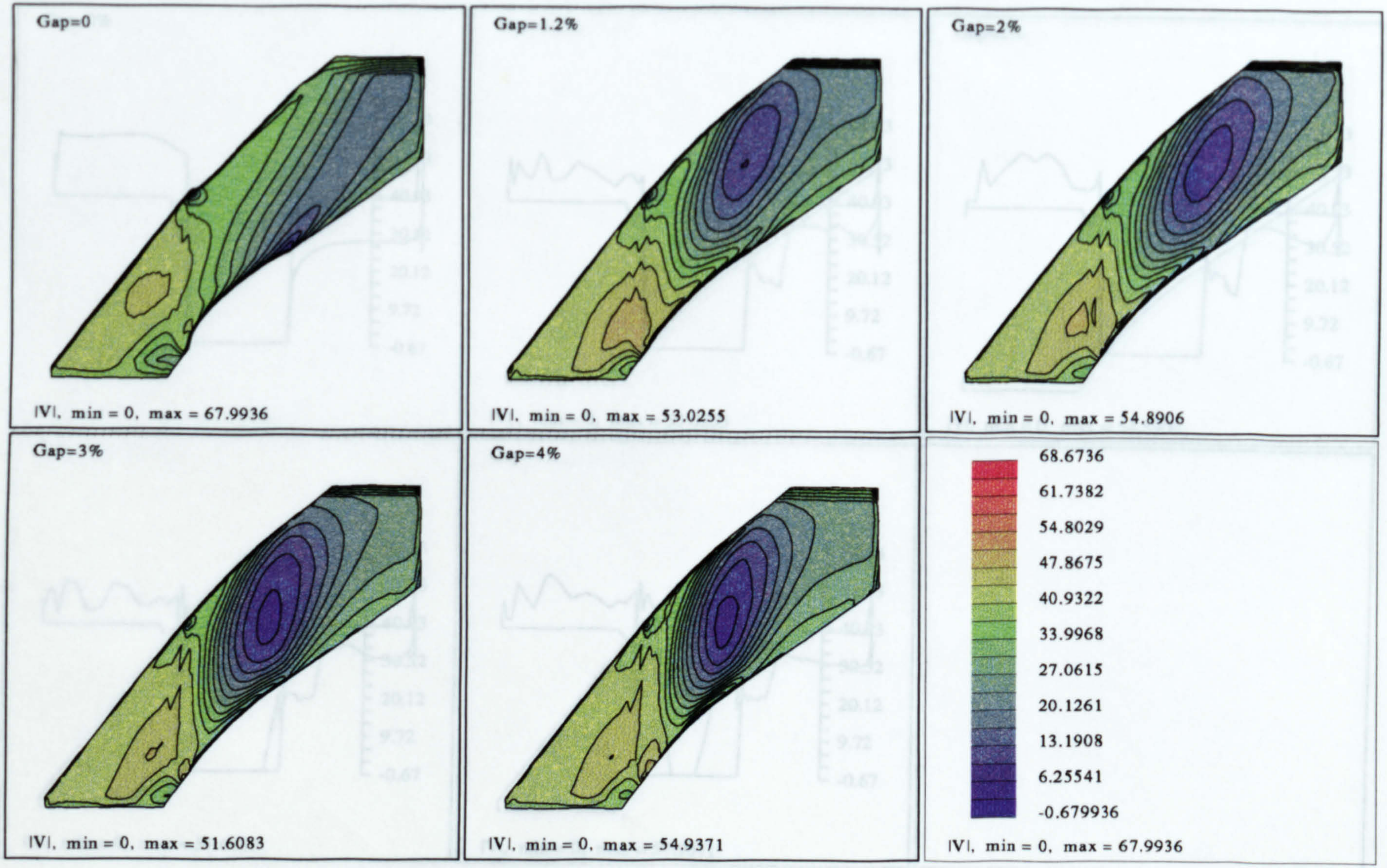

Fig.6-20 Velocity Along the Mesh Boundary for Various Tip Clearance (Va/Um=0.72)

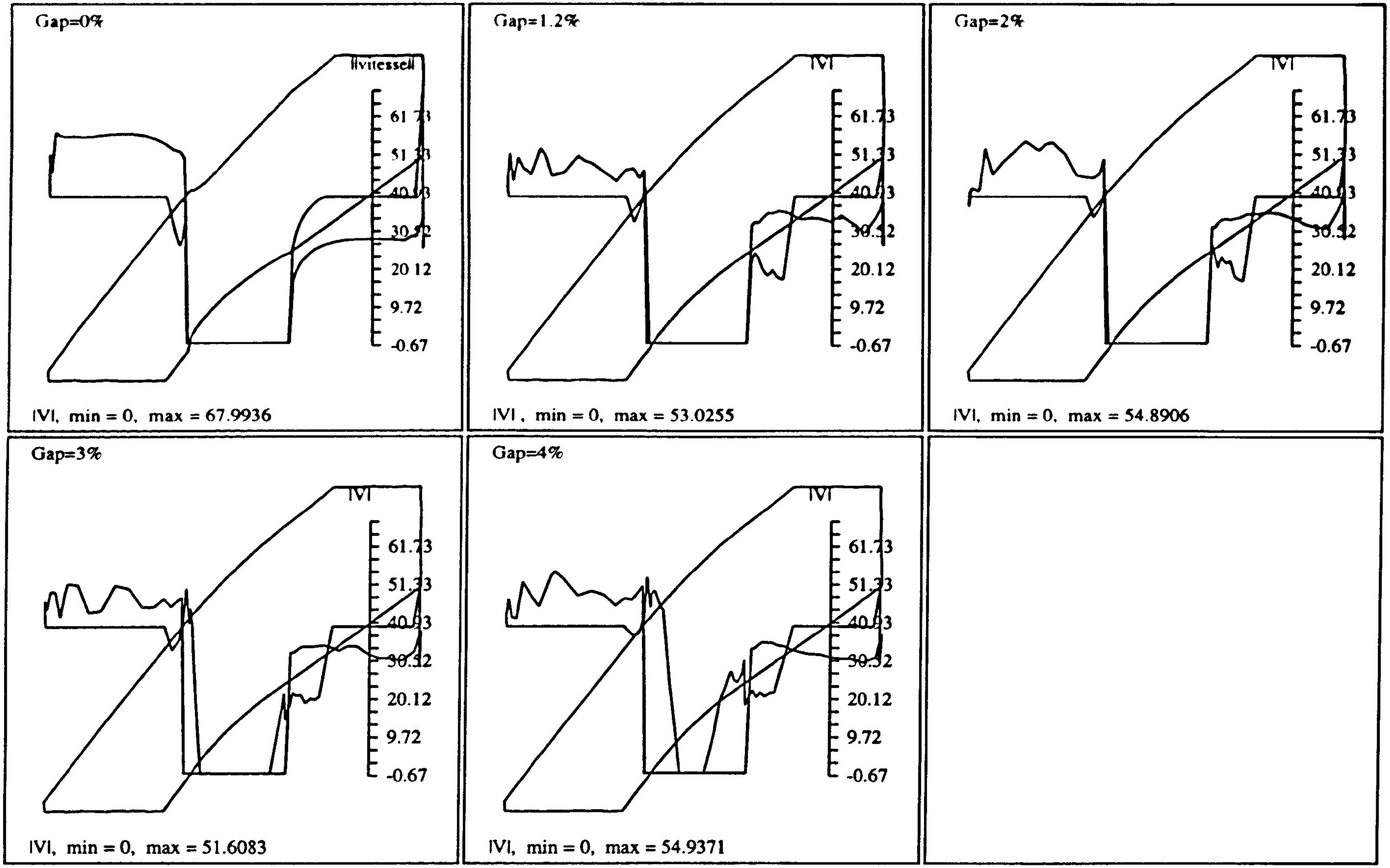

Vtipd3.ps

Fig.6-21 Velocity Vectors for Various Tip Clearance (Va/Um=0.72)

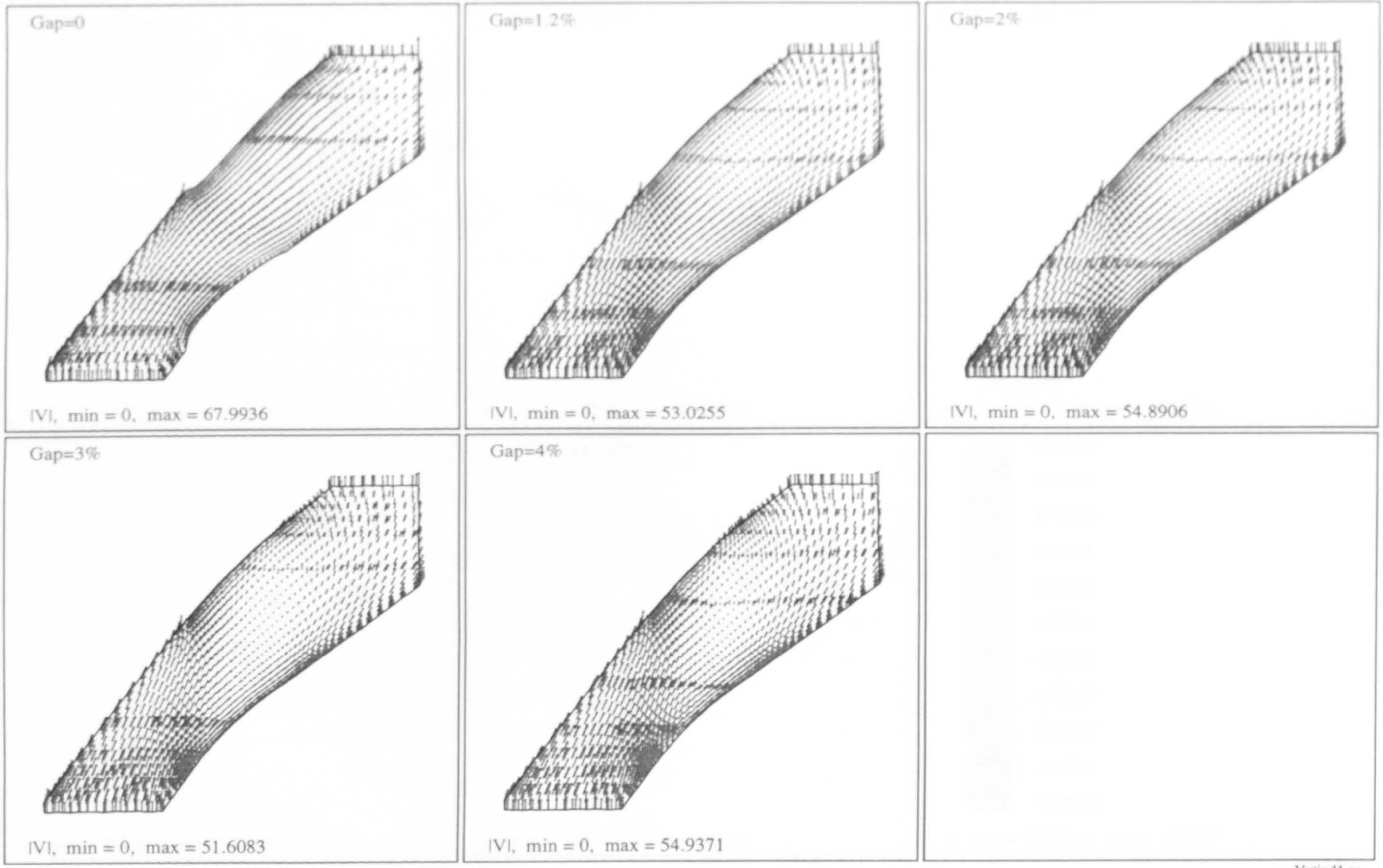

Fig.6-22 Pressure Contours for Various Tip Clearance (Va/Um=0.66)

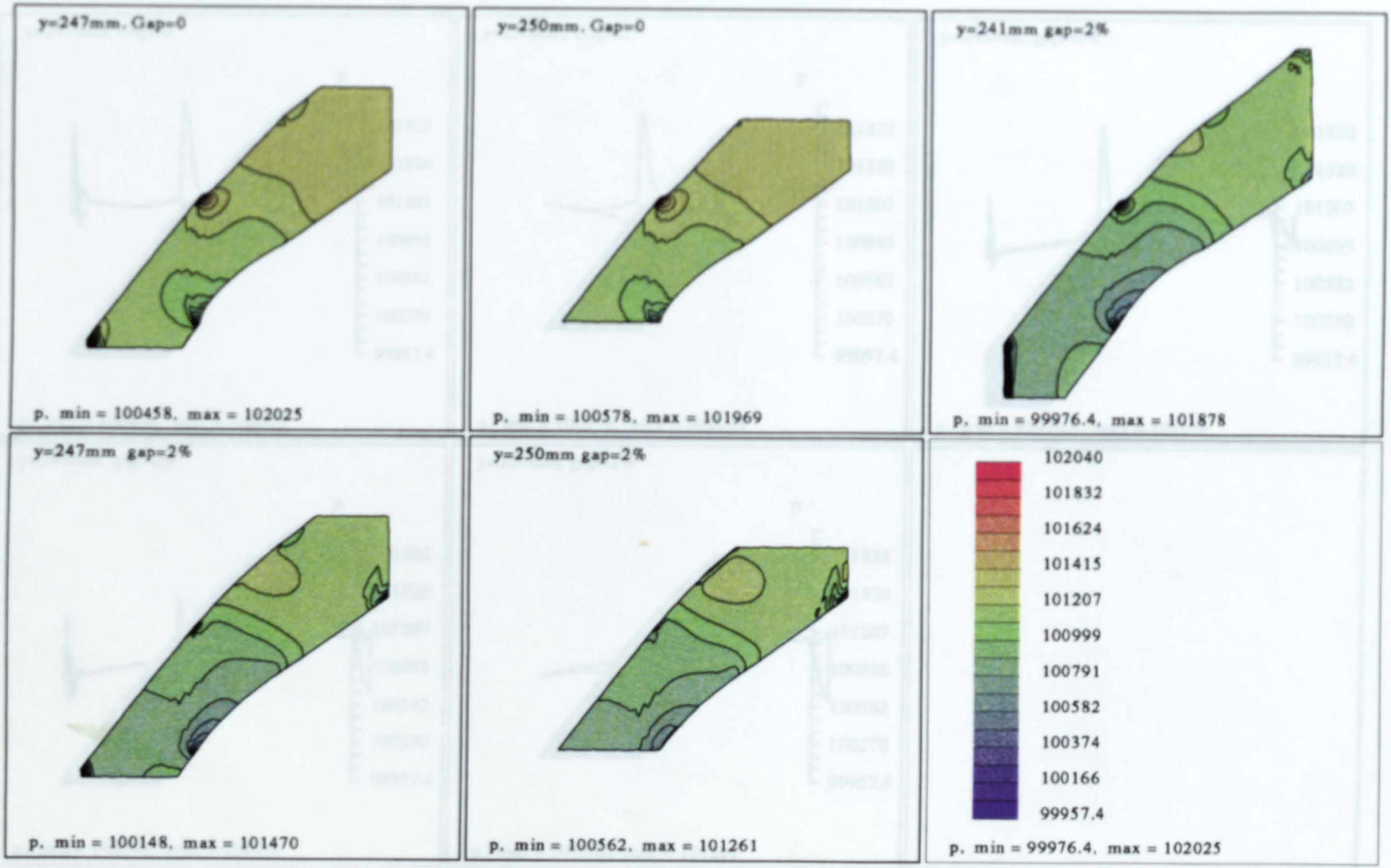

Fig.6-23 Pressure Along the Mesh Boundary for Various Tip Clearance (Va/Um=0.66)

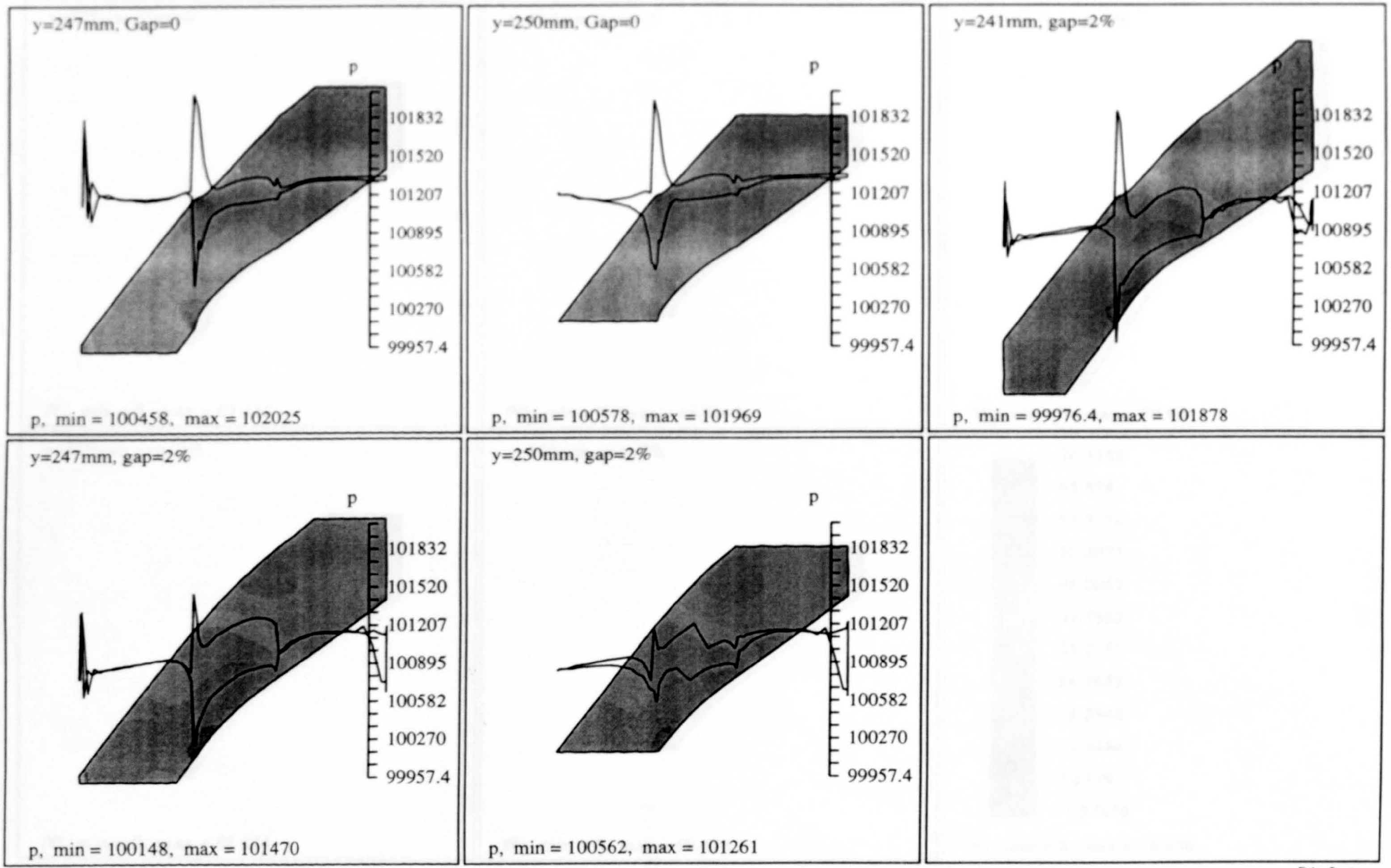

Ptips2.ps

Fig.6-24 Velocity Contours for Various Tip Clearance (Va/Um=0.66)